Department of Chemical Engineering

Investigating novel biopolymeric nanostructures for drug delivery

Hazim Jasim Mohammed Haroosh

This thesis is presented for the Degree of

Doctor of Philosophy

of

Curtin University

October 2014

DECLARATION

To the best of my knowledge and belief this thesis contains no material previously published by any other person except where due acknowledgement had been made.

This thesis contains no material which has been accepted for the award of any other degree or diploma in any University.

Signature: _____

Date: _____

ABSTRACT

In recent times, drugs loaded into nanocomposite fibre mats have gained significant attention due to their good structural stability, reduced toxic side-effects, enhancement of healing effectiveness and higher efficiency of drug encapsulation compared to other drug delivery carriers. This study created novel electrospun hybrid nanocomposite fibre mats from a variety of materials: poly(lactic acid) (PLA) with poly(ε-caprolactone) (PCL); PLA and PCL embedded with halloysite nanotubes (HNTs); and PLA and PCL embedded with magnetic nanoparticles (MPs), with the aim of finding a material combination that could maintain the steady release of a hydrophilic drug from this hydrophobic polymer system. The main purpose of this work is to holistically understand the influences of the solvent system, solution electrical conductivity, solution viscosity, polymer blend ratio, PCL concentration and PCL molecular weight on the nanofibre diameters, porosity and degree of crystallinity, which are considered as important parameters in the control of drug release. The research mainly concentrated on studying the impact of adding pure MPs, impure MPs, unmodified HNT and HNT modified with 3-aminopropyltriethoxysilane (ASP) on the morphology, structure, crystallinity, thermal properties, connecting bonds and drug release kinetics of nanocomposite fibre mats. This study also took into account the effect of the interaction between the drugs (tetracycline hydrochloride TCH and Indomethacin IMC) and the PLA: PCL polymer blend on the drug release rate. Additionally, the mechanism of drug release was investigated by fitting five mathematical models, including zero order, first order, Higuchi, Ritger-Peppas and Zeng models, to the experimental drug release data.

Increasing the molecular weight and PCL concentration enhanced the solution viscosity and created bead-free nanofibrous structures, especially at a blending ratio of 1:1 for PLA: PCL. The nanofibres produced from a chloroform: methanol solvent were larger in diameter and better aligned in their fibrous structure compared with counterparts from a DCM: DMF solvent. The crystallinity (X_c) increased when the concentration of high molecular weight PCL increased, especially at a blend ratio of 1:1; whereas, using low molecular weight PCL led to a sharp decline in X_c and melting temperature (T_m) of PCL, and a noticeable increase in the crystallisation temperature (T_c) of PLA within the blend

compared with high molecular weight PCL. Furthermore, the rapid evaporation of methanol solvent led to a reasonable decrease in X_c and T_c when compared to DMF solvent. There was better miscibility between PLA and PCL within their blends, particularly in the case of using PLA: 15% PCL at a blend ratio of 1:1 and dissolved in the chloroform: methanol system.

Adding HNT to PLA: low molecular weight PCL blend hindered the homogeneous dispersion of HNT in the solution. The nanofibre diameters did not noticeably change when increasing the amount of HNTs from 1 to 2 wt%/v owing to the low solution viscosity, which is opposite to what was obtained from embedding HNT into PLA: high molecular weight PCL. Moreover, PLA: high molecular weight PCL composites embedded with modified HNT-ASP showed moderately enhanced HNT dispersion, leading to less agglomeration and decreased average fibre diameters compared to unmodified HNTs. Adding HNT-ASP to the blends led to a reasonable decline in X_c and there were also slight decreases in the glass transition temperature (T_g) of PCL, and the T_c and T_m of PLA within the composites. Furthermore, the infrared spectra confirmed a reduction in HNT agglomeration when embedding HNT-ASP into PLA: PCL nanofibres.

The embedding of pure MPs raised the solution viscosity and supported better MP dispersion compared to adding impure MPs, which led to a significant decline in the average fibre diameter as a result of a significant viscosity reduction. Embedding impure MPs generated unique cell structures that were observed for the first time in this study. Pure MPs led to decreases in the X_c and T_g of PCL, as well as the T_c of PLA; whereas, impure MPs caused overall increases in the above-mentioned thermal parameters, except for the undetected T_m of PLA. The infrared spectra showed that impure MPs considerably affected chemical bonds and confirmed the effective embedding of MPs into the composites.

The addition of the drug indomethacin (IMC) did not alter nanofibre diameters as opposed to what resulted from adding another model drug, tetracycline hydrochloride

(TCH). Thermal properties, such as T_g and T_m of PCL within the blends, and X_c were reduced when loading both TCH and IMC. The biodegradation rate was accelerated by decreasing the PCL concentration and also by embedding MPs into the composites. Loading TCH into HNT-ASP and then adding this mixture into PLA: PCL solution produced a nanocomposite system that reduced the drug release rate and overcame the weakness of the interaction between the polymer and drug, which was in contrast to the behaviour of PLA: PCL blend solution embedded with pure MPs. There was good agreement between the acquired experimental data on drug release kinetics and the Ritger-Peppas and Zeng models in description of the mechanisms of drug release.

ACKNOWLEDGEMENTS

First and foremost, all glorification and gratefulness are due to Allah, the Creator, (praise be to Him) who granted me this rare opportunity and gave me the capability and knowledge to proceed successfully. I am fully sincere and faithful to his bounties.

This thesis would not have been possible without the encouragement and enthusiasms of my supervisor distinguished Professor Moses Oludayo Tadé, Dean of Engineering – Curtin University, Western Australia. From the depths of my heart, I acknowledge him for his always positive approach during all stages of this research. I would like to convey my appreciation to my co-supervisor Dr. Yu Dong for his countless guidance and support during my study. Their constant help and direction are really supportive, particularly in the difficult times of performing my PhD study. I would like to extend my sincere gratitude to my associate supervisor Dr. Gordon Ingram for his enormous help and insistence. I want also to thank my associate supervisor Dr. Deeptangshu Chaudhary for his supportive supervision in the early stages of this research. I extend my sincere gratitude to Professor Hongwei Wu for the assistance as the chairman of thesis supervisory committee.

My research would not have been completed without the tremendous supports from the technical staff. I would also like to extend my sincere appreciation to Karen Haynes, John Murray, Jason Wright, Jimmy Xiao Hua, Araya Abera and Roshanak Doroushi in engineering lab. I wish to thank Ms. Elaine Miller and Dr. Cat Kealley from the Department of Medical Imaging and Applied Physics as well as Prof. Shin-ichi Yusa from University of Hyogo- Japan for their technical assistances. I would like to say thanks also to all the kind staff in Chemical Engineering, especially Jann Bolton, and Tammy Atkins.

While conducting my research, I had to work sometime all day, evening and holidays. This may cause some inconvenience for my wife and kids (Mustafa, Rusul and Abdullah). I would like to thank them for their supports during this study. I should also be thankful for my great parents, brothers, sisters and parents-in-law who helped me a

lot during any stages of my life and as well my uncle, Saeed Ahmad for his marvellous support during my studies.

I would like to make particular thanks to my sponsor, Iraqi ministry of higher education, for offering a full PhD Scholarship. Finally, I wholeheartedly thank Curtin University for providing me this opportunity to complete my research goal at this stage of my career.

BIOGRAPHY AND PUBLICATIONS

Brief Biography

Hazim received his B.Sc. degree in July 1999 and M.Sc. degree in May 2002 in Chemical Engineering from Tikrit University, Iraq. He has worked in the State Company for Drug Industries and Medical Appliances, Samara (SDI), Iraq, since November 2002. He has hands-on experience in quality control and management, project planning and environmental impact assessment. He was the Director of the Wastewater Treatment Department, and was also appointed as the Assistant Chief Engineer. He is a member of the Iraqi Engineers Association. He commenced his PhD studies in January 2010 in the Chemical Engineering Department at Curtin University. He has been working as a Tutor since 2012, for Engineering Foundations: Design and Processes 100 at Curtin University. In addition, He was also involved in the Workshops for Engineering Foundations: Principles and Communications 100, as well as for Engineering Materials 100.

Journal Papers

1- **Haroosh, H. J.,** Dong, Y. and Lau, KT. (2014). "Tetracycline hydrochloride (TCH) loaded drug carrier based on PLA: PCL nanofibre mats: experimental characterisation and release kinetics modelling." *Journal of Materials Science*, 49: 6270-6281.

2- Dong, Y., Ghataura, A., Takagi, H, **Haroosh H. J.,** Nakagaito, A., Lau, KT. (2014). "Polylactic acid (PLA) biocomposites reinforced with coir fibres: Evaluation of mechanical performance and multifunctional properties". *Composites Part A*, 63: 76-84.

3- Dong, Y., Mosaval. T., **Haroosh H.J.**, Umer, R., Takagi, H., and Lau, KT. (2014). "The potential use of electrospun PLA nanofibers as alternative reinforcements in an epoxy composite system". *Journal of Polymer Science Part B: Polymer Physics,* 52(9): 618–623.

4- Albetran, H., **Haroosh, H. J.**, Dong, Y., Prida, V., O'Connor, B., and Low, I. (2014). "Phase transformations and crystallization kinetics in electrospun TiO2 nanofibers in air and argon atmospheres". *Applied Physics A*, 116(1)**:** 161-169.

5- **Haroosh, H. J.,** Dong, Y. and Ingram, G. D. (2013). " Synthesis, morphological structures and material characterization of electrospun PLA:PCL/magnetic nanoparticle compositesfor drug delivery." *Polymer Science Part B-Polymer Physics*, 51(22): 1607-1618.

6- Azman, N., Siddiqui, S., **Haroosh, H.**, Albetran, H., Johannessen, B., Dong, Y. and Low, I. (2013). Characteristics of x-ray attenuation in electrospun bismuth oxide/ poly-lactic acid nanofibre-mats. *Journal of Synchrotron Radiation*, 20(5): 741-748.

7- Dong, Y., Thomas, B., **Haroosh, H. J.**, Lau, K., and Takagi, H. (2013). "Analysis in the material characterisation of electrospun poly(lactic acid)/ halloysite nanotube composite fibres based on Taguchi design of experiments: fibre diameter, non-intercalation and nucleation effects." *Applied Physics A: Materials Science & Processing*, 112(3): 747-757.

8- **Haroosh, H. J.**, Dong, Y., Chaudhary, D. S., Ingram, G. D. and Yusa, S. (2013). "Electrospun PLA: PCL composites embedded with unmodified and 3-aminopropyltriethoxysilane (ASP) modified halloysite nanotubes (HNT)." *Applied Physics A: Materials Science & Processing*, 110(2): 433-442.

9- **Haroosh, H. J**., Chaudhary, D. S., and Dong, Y. (2012). "Electrospun PLA/PCL fibers with tubular nanoclay: Morphological and structural analysis." *Journal of Applied Polymer Science*, 124(5): 3930-3939.

10- Dong, Y., Chaudhary, D., **Haroosh**, **H.,** and Bickford, T. (2011). "Development and characterisation of novel electrospun polylactic acid/tubular clay nanocomposites." *Journal of materials science*, 46(18): 6148-6153.

Conference Papers

1- Dong, Y., Marshall, Y., and **Haroosh, Hazim J.** 2014. Processing-structure-property relationship for electrospun poly lactic acid (PLA)/halloysite nanotube (HNT) composite mats. ACCM-9, October 15-17, 2014. Suzhou-China (Oral presentation).

2- **Haroosh, Hazim J.,** and Dong, Y. 2014. Evaluation of Electrospun Nanofibrous Structures for Drug Release Application. Chemeca 2014 - Processing Excellence; Powering Our Future, 28 September - 1 October 2014. Perh - Western Australia (Oral presentation).

3- Umer, R., Li, Y., Dong, Y., **Haroosh, Hazim J.**, and Liao, K. 2014. Processing and Mechanical Characterization of Glass Fiber Reinforcements using GO Nano Particles. The 12th International Conference on Flow Processing in Composite Materials (FPCM 12), The University of Twente, Enschede, the Netherlands, 14-16 July 2014. (Poster).

4- **Haroosh, Hazim J**. and Dong, Y. 2013. Electrospun Nanofibrous Composites to Control Drug Release and Interaction between Hydrophilic Drug and Hydrophobic Blended Polymer Matrix. Proceedings of ICCM 19th –The 19th International Conference on Composite Materials, July 28- August 2, 2013. Montreal (Canada) (Oral presentation).

5- Dong, Y., Ghataura, A., and **Haroosh, Hazim J**. 2013. Mechanical, Thermal and Biodegradable Properties of Polylactic Acid (PLA)/ Coir Fibre Biocomposites. Proceedings of SMN 2013– 4th International Conference on Smart Materials and Nanotechnology in Engineering, July 10- 12, 2013. Gold Coast, (Australia) (Oral presentation).

6- Dong, Y., Mosaval, T., and **Haroosh, Hazim J**. 2013. A Novel Epoxy/Electrospun PLA Nanofibre Composite Material: Fabrication and Characterisation. Proceedings of SMN 2013– 4th International Conference on Smart Materials and Nanotechnology in Engineering, July 10- 12, 2013. Gold Coast, (Australia) (Oral presentation).

7- Albetran, H., **Haroosh, Hazim J**., Dong, Y. and Low, I. M. 2013. Effect of Doping on In-Situ Crystallization and Crystal Growth in Electrospun TiO_2 Nanofibres", Paper ID# ICACC-S7-014-2013, The 7th International Symposium on Nanostructured Materials and Nanocomposites at The 37th International Conference and Expo on Advanced Ceramics and Composites (ICACC'13), January 27- February 1, 2013. Daytona Beach, Florida, (USA) (Oral presentation).

8- Dong, Y., Bickford, T., and **Haroosh, Hazim J**. 2012. Statistical Design of Experiments for Electrospun Poly(lactic acid) (PLA)/Halloysite Nanotube (HNT) Composites in Response to Fibre Diameter and Thermal Properties. Proceedings of (ACCM-8) - The 8th Asian-Australasian Conference on Composite Materials, November 6 – 8, 2012. Kuala Lumpur (Malaysia) (Oral presentation).

9- **Haroosh, Hazim J** and Dong, Y. 2012. Electrospun PLA/PCL/MPs Nanofibrous Hybrid Composite Structures for Sustained Drug Release. Proceedings of ECCM 15th - The 15th European Conference on Composites Materials, June 24-28, 2012. Venice (Italy), European Society for Composite Materials. (Oral presentation).

10- Dong, Y., Mathew, R., Chaudhary, D., Bickford, T. and **Haroosh, Hazim J**. 2011. Flexural Properties and Morphological Structures of Epoxy Composites Reinforced with Platelet and Tubular Nanoclays, in Amal, R. and Gomes, V. and Chen, V. (ed), CHEMECA 2011 "Engineering A Better World", September 18-21, 2011. Sydney: Engineers Australia. (Oral presentation).

11- John, J., Chaudhary, D., and **Haroosh, Hazim J**., Guagliardo, P., and Yusa, S. 2011. Drug Release from Magnetically Aligned Bionanocomposite in Amal, R. and Gomes, V. and Chen, V. (ed), CHEMECA 2011 "Engineering A Better World", September 18-21, 2011. Sydney: Engineers Australia. (Oral presentation).

12- **Haroosh, Hazim J**., Chaudhary, D., and Ingram, G. 2011. Effect of Solution Concentration and co-Solvent Ratio on Electrospun PEG Fibers, in Amal, R. and Gomes, V. and Chen, V. (ed), CHEMECA 2011 "Engineering A Better World", September 18-21, 2011. Sydney: Engineers Australia. (Poster).

13- **Haroosh, Hazim J**., Chaudhary, D., and Dong, Y. 2011. Effect of Solution Parameters on Electrospun PLA/PCL Fibers, in Amal, R. and Gomes, V. and Chen, V. (ed), CHEMECA 2011 "Engineering A Better World", September 18-21, 2011. Sydney, NSW: Engineers Australia. (Poster).

14- **Haroosh, Hazim J**., Chaudhary, D., and Yusa, S. 2011. Effect of Halloysite on Electrospinning of PLA/ PCL Nanofibres, in Amal, R. and Gomes, V. and Chen, V. (ed), CHEMECA 2011 "Engineering A Better World", September 18-21, 2011. Sydney, NSW: Engineers Australia. (Oral presentation).

15- Dong, Y., Chaudhary, D., **Haroosh, Hazim J**., Sharma, V., and Thomas, B. 2011. Functionally Electrospun PLA/tubular Clay Nanocomposites for the Potential Application of Drug Delivery, in D. Bhattacharyya, R. J. T. Lin, T. S. Srivatsan (ed), Nineteenth International Conference on Processing and Fabrication of Advanced Materials (PFAM XIX), January 14 2011, pp. 836-846. Auckland, New Zealand: The University of Auckland, Auckland (New Zealand) (Oral presentation).

16- **Haroosh, Hazim J**., Chaudhary, D., Dong, Y., and Hawkins, B. 2011. Electrospun PLA : PCL/ Halloysite Nanotube Nanocomposites Fibers for Drug Delivery, in D. Bhattacharyya, R. J. T. Lin, T. S. Srivatsan (ed), Nineteenth International Conference on Processing and Fabrication of Advanced Materials (PFAM XIX), January 14 2011, pp. 847-858. Auckland, New Zealand: The University of Auckland, Auckland (New Zealand) (Oral presentation).

Thesis

1- **Haroosh, Hazim J**. Estimation of Heavy Metals in Samarra Drugs Factory Wastewater and Determination of Proper Treatment. M.Sc. of Chemical Engineering, 30th, May, 2002, University of Tikrit.

TABLE OF CONTENTS

LIST OF FIGURES

LIST OF TABLES

ABBREVIATIONS, NOMENCLATURES and NOTATIONS

PLA	Poly(lactic acid)
PCL	Poly(ε-caprolactone)
HNT	Halloysite nanotubes
ASP	3-aminopropyltriethoxysilane
MP:	Magnetic nanoparticles
DCM:	Dichloromethane
DMF	Dimethylformamide
$CHCl_3$	Chloroform.
MeOH	Methanol
TCH	Tetracycline hydrochloride
IMC	Indomethacin
PBS	Phosphate buffer solution
LMW	Low molecular weight
HMW	High molecular weight
M_u	Concentrations of drug in solution
M_t	Amount of drugs released
M_∞	Initial amount of drug
m	Initial weight of mat
m_1	Weight of mat after degradation
K_0	Zero-order release constants
K_1	First-order release constants
K_H	Higuchi release constants
K_R	Ritger-Peppas release constants
n	The diffusion exponent in the Ritger-Peppas model.
ΔG	Difference in the free energies of the free and bound states of the drug in the nanofibres.
K_{on}	Rate constant of association
K_{off}	Rate constant of disassociation

A/V	Surface area-to-volume ratio of the nanofibre mat.
k	Rate constant
D	Diffusion coefficient of the drug
l	Thickness of the shell
SEM	Scanning electron microscopic
TEM	Transmission electron microscopy
XRD	X-ray diffraction
DSC	Differential scanning calorimetry
FTIR	Fourier transform infrared spectroscopy
GPC	Gel permeation chromatography
wt%/v	The percentage of weight-to-volume
d	d-spacing
θ	Diffraction position
λ	Wavelength
L	Crystallite size
B	Complete width at half maxima of the crystalline peak in radians.
T_g	Glass transition temperature
T_c	Crystallisation temperature
T_m	Melting temperature
X_c	Degree of crystallinity

Chapter 1
Introduction

1.1. Background

Nanotechnology is a cutting-edge interdisciplinary area that combines the study, control, management and assembly of diverse nanoscaled elements into materials, methods and apparatuses of enormous interest and creative potential. This promising field has possible applications in various areas of the worldwide application system, including power, transportation, health, manufactured consumer goods and agriculture (Kumbar et al., 2008). Nanotechnology deals with synthetic and natural formations on the nanoscaled level, specifically in the range of 1 nm to1µm (Qi et al., 2010). Fibres fabricated from polymers are employed for a variety of purposes from fabrics to composite reinforcements (Deitzel et al., 2001). Diverse approaches have been developed in recent years to produce nanoscaled level structures for many applications. Several fabrication techniques are used, such as phase separation, self-assembly and electrospinning (Kontogiannopoulos et al., 2011). Among these methods, electrospinning is a flexible polymer processing method to produce nanofibres in which a flow of a polymer melt or solution is charged in a high voltage electric field, leading to the formation of polymer jets. These jets are driven out from the droplet surface and drawn in the direction of a collecting plate (Ji et al., 2006a). Recently, electrospinning has been developed for various uses in a number of diverse research areas such as biomaterials, energy, filtration media (Bosworth and Downes, 2012), nanosensors, cosmetics, protecting clothes, separation, and fuel cells (Li et al., 2012). Furthermore, the electrospun non-woven mats with nano/microfibres can be also applied in the biomedical field, for example as drug delivery carriers (Yan et al., 2012), materials for wound dressing, tissue repair replacements and tissue engineering scaffolds due to their biodegradability, fibre physical properties, biocompatibility and high fibre surface area to volume ratio (Jiang et al., 2005). Among these applications, electrospun mats demonstrate the great potential as drug carriers in that they facilitate drug delivery to the target area in the human body for wound therapy and cancer treatment (Song et al., 2012). Polymers may possess certain properties that can cater specific criteria for the

design of appropriate drug delivery systems (Bermudez and Grau, 2011). In drug delivery from polymer nanofibres mats, it is believed that the dissolution speed of the drug macromolecules is increased by raising the surface area to volume ratio of the drug-loaded nanofibres mats and the drug. Moreover, drugs can be easily loaded into the polymeric carriers by employing the electrospinning method, which differs from universal encapsulations, which involve a number of preparation difficulties (Cui et al., 2006). Nanofibres have been effectively electrospun from diverse polymer systems like polymer blends, co-polymers like poly(lactic-co-glycolic acid), high performance polymers, biopolymers and organic polymers such as ribonucleic acid and starch. The electrospinning method can facilitate and shape different morphologies such as continuously aligned and randomly distributed nanofibres (Chowdhury and Stylios, 2011). Nanofibres are ultrafine solid fibres which are promising nanomaterials due to their huge surface areas per unit volume, flexibility, absorbency (Cai et al., 2011) and tiny porous areas (Subbiah et al., 2005). Continuous nanofibres can be achieved by adjusting the polymer solution and electrospinning parameters, which in turn control the formation of polymer fibres on a collector (Evcin and Kaya, 2010; Thompson et al., 2007). Consequently, the consideration of the processing conditions, structure, morphology and solution properties are important for engineering polymer nanofibres to achieve end-user requirements for different applications (Inai et al., 2005).

Nanoparticles are able to be incorporated into biomolecules during various synthesis methods, such as complementary recognition, covalent coupling, electrostatic binding, and physical adsorption. They can be tailored to accomplish particular intracellular objectives in particular areas (Goldberg et al., 2007). Nanocarriers of different geometries and compositions including liposomes, polymeric nanoparticles, solid lipid particles, micelles, nanofibres, and core-shell nanofibres have been used as carriers for drug delivery (Zeng et al., 2011).

Nanocomposite fibres have gained a significant attention owing to their continuously improving optical, electronic, electrical and chemical characteristics. The applications of these materials are not limited to defence and safety areas, but also include filtration

membranes, microelectronics appliances, structural strengthening, energy production, and biomedical engineering (Zhang et al., 2009). In recent years, using a polymer as a carrier and controller for drug delivery systems has become very popular due to the enhancement of healing effectiveness and decrease in toxic side-effects (Xie and Buschle Diller, 2010). Drug release has been an essential subject in the area of drug delivery for a long time. Novel materials with increasing complication and more functions have been fabricated for the improvement of drug delivery apparatus with progressive work in materials science and engineering. In the area of controlling drug release, both natural and synthetic polymers have been employed broadly to increase bioeffectiveness and assist medical applicability. Drug release is the method in which drug molecules travel from the primary location in the polymeric system to the environment (Fu and Kao, 2010). In order to obtain controlled drug release, different dosages have been manufactured by employing biodegradable polymers such as nanoparticles, microspheres, millirods and films (Tiwari et al., 2010). In addition, the interaction between drug and carrier is important to manage a sustained drug release (Zeng et al., 2011). Many benefits from using electrospun polymer nanofibres have been identified compared with other dosage forms. Therapeutic composites can be simply loaded into the carrier polymers by means of the electrospinning technique. The drug release system can be adapted by adjusting the material composition and morphology of the nanofibrous mats (Huang et al., 2006).

1.2 Research motivation

1.2.1 Knowledge gap in electrospinning and drug delivery

Poly(lactic acid) (PLA) and poly(ε-caprolactone) (PCL) have been used widely in the biomedical engineering area due to their excellent properties of biodegradability and biocompatibility, and also their soft texture, suitable morphology and light weight. In general, to fabricate biopolymers into nanofibres during electrospinning is usually not easy because of the mixed effects between the electrospinning parameters, which makes investigating the effect of these parameters on the nanofibres really challenging (Biber et al., 2010). Furthermore, the key factors that hinder the electrospinning solution are often the solution viscosity, molecular weight, and solution concentration, as well as the

insufficient evaporation of solvents leading to fusing of the electrospun nanofibres on the collector.

Development of a new composite nanofibre system for the effective loading and sustained release of drugs is still faced with great challenges (Qi et al., 2010). The control of electrospinning parameters to obtain fibres with the desired morphology, crystallinity and molecular structure has yet to be achieved (Ribeiro et al., 2011). The drug dosing decreases significantly over a short time owing to burst drug release at the beginning of release (Im et al., 2010a). Since PCL with high crystallinity easily restricts the mobility of drug molecules, they tend to stay on the fibre surfaces. In addition, PCL has apparently slower degradation than other aliphatic polyesters owing to its hydrophobic nature and high crystallinity. Besides, the addition of PLA with low crystallinity can accelerate fibre degradation. Loading a hydrophilic drug (tetracycline hydrochloride, TCH) into hydrophobic polymers (PLA and PCL) will lead to drug deposition outside of the nanofibres and will subsequently cause a burst release due to the weak interaction between them. Furthermore, the chemical interaction between the polymer and drug is able to hinder the crystallisation process of the drug in the nanofibres, which may generate a sustained drug release in the crystalline state.

1.2.2 Significance of the current study

The current study aims to develop new electrospun hybrid nanocomposite systems, including PLA: PCL, PLA: PCL/ halloysite nanotubes - 3-aminopropyltriethoxysilane (HNT-ASP) and PLA: PCL/ magnetic nanoparticles (MPs), to benefit the sustained release of hydrophilic drugs with hydrophobic polymers. Such a PLA: PCL based composite system could help to achieve balanced crystallinity with the possible benefit of steady drug release. The specific objective of this study is to understand the effects of the solvent system, solution electrical conductivity, solution viscosity, PCL concentration and PCL molecular weight on the nanofibre diameters, porosity and degree of crystallinity, which are regarded as important factors in the control of drug release. Moreover, due to its low pH value, the PLA degradation components can damage tissues. Blending PCL with PLA can decrease that effect as PCL is gradually

degraded and does not form the same acidic environment as PLA. The addition of HNTs can reduce that effect due to the hydroxide groups in the HNT structure (Touny et al., 2010). The current work has particularly focused on studying the effect of the embedded MPs and HNTs on morphology, structure, crystallinity, thermal properties, connecting bonds and drug release of hybrid nanocomposites. The blend viscosity is an important factor for HNT and MP dispersion within the polymer blend in the electrospinning process. The current work has promoted nanofibre quality without any bead defects or non-fibrous structures by controlling the crystallinity level of the PLA: PCL blend. Furthermore, HNT agglomeration may be reduced by using the ASP modifier, having benefits for future drug release applications. The study also examined the drug release kinetics by fitting the release data to five mathematical models including zero order, first order, Higuchi, Ritger-Peppas and the newly developed Zeng model to help understand the mechanism of drug release.

1.3 Research contributions

This thesis makes significant contributions to understanding PLA: PCL nanocomposites and drug release phenomena as follows:

- Fabricating a variety of nanofibres with diameters ranging from one micron down to a few nanometers with a particularly large surface area to volume ratio was achieved. Such extremely small nanofibres were suitable for tailoring different biomedical application requirements. The small nanofibre diameter allowed the drug release to be achieved more quickly, which is beneficial for some wound healing applications. Alternatively, the nanofibre mat is able to offer the protection to certain bioactive substances, like growth genes, which need to be sheltered for some time to accelerate wound healing in the early stages.

- It took into consideration understanding the effect of three co-solvents (dichloromethane (DCM): N,N, dimethylformamide (DMF), chloroform: methanol and chloroform: acetone), PLA: PCL solution viscosity, electrical conductivity of the solution, blend ratio of PLA to PCL, molecular weight of

PCL and PCL concentration as vital parameters for the successful production of uniform nanofibre mats. Additionally, a clear explanation was given for their influences on the nanofibre diameters. For some of them, a clear overview was presented for their impacts on the morphological structures, thermal properties and the degree of crystallinity of the fabricated composites.

- The investigations of PLA: PCL/ HNT nanocomposites resulted in a new drug delivery system with sustained release for a range of applications. Both unmodified HNTs and HNTs modified with 3-aminopropyltriethoxysilane were utilised to improve the HNT dispersion in the solution. The infrared spectra of nanocomposites provided insight for identifying the successful embedding of HNT-ASP into nanofibres relative to unmodified HNTs due to the pre-modification leading to reduced agglomeration behaviour.

- A new study investigating the effects of the purity of synthesised magnetic nanoparticles (Fe_3O_4) on the structure, morphology, crystallinity, thermal properties and the interaction between MPs and PLA: PCL polymer blend was performed. TCH release was accelerated by adding MPs to the blend. One of the application possibilities is the direct delivery of a drug to the target area of the body by using an external magnetic field.

- Electrospun nanofibre mats can be cut to any dimension and be applied typically for skin and wound therapeutic purposes or for other types of drug release. The goals for the development of nanofibre composite/drug systems are that they dramatically improve patient compliance and therapeutic activity, minimize the toxic side-effects of drugs through extended dosing, with the ability to avoid being rapidly taken up by the reticuloendothelial system, and target the drug to specific sites.

- Electrospun nanofibrous hybrid composite structures were successfully created for carrying a therapeutic compound, like TCH and indomethacin (IMC), with

the potential use for medical applications. The material system provided useful information on how constituents of hybrid composites influenced the surface morphology that controlled drug release. Loading a hydrophilic drug (TCH) into HNT-ASP and hydrophobic polymers (PLA and PCL) was observed to enhance drug release and to overcome the weak interaction between the polymer and the drug.

- Release kinetics data have been successfully fit to five mathematical models, which are categorized as zero order, first order, Higuchi, Ritger-Peppas and Zeng models. Typical characteristics were clearly revealed and excellent agreement was obtained between the experimental data and the Ritger-Peppas and Zeng models for the drug release kinetics.

1.4 Thesis outline

The thesis is structured into eight chapters as summarised below and in Figure 1-1:

Chapter 1 presents an introduction about the project consisting of background information about the research growth in electrospinning, nanofibres, nanocomposites and drug delivery. Moreover this chapter demonstrates a current knowledge gap, and presents the significance of the current study and its research contributions.

Chapter 2 covers an extensive literature review on progress, existing findings and knowledge gaps in electrospinning, biopolymers, blending polymers, nanofibres, nanocomposites and drug delivery areas.

Chapter 3 reports on the material selections for PLA, PCL, HNT, synthesised MP, TCH, IMC, solvents and modifiers. It explains the research methodology, which includes the electrospinning setup, blending of PLA: PCL, nanofibre fabrication, embedding of HNT and MPs, drug incorporation and release, and drug release kinetics, and finally the analytical characterization techniques. These include scanning electron microscopy (SEM), transmission electron microscopy (TEM), X-ray diffraction (XRD), Fourier transform infrared spectroscopy (FTIR), differential scanning calorimetry (DSC), UV-

vis spectrophotometer (UV), gel permeation chromatography (GPC), energy dispersive spectroscopy (EDS), viscometry and electrical conductivity testing.

Chapter 4 presents the initial investigation, which is pertinent to determining the appropriate polymer concentration, blending ratio, molecular weight, viscosity and co-solvents to obtain uniform electrospun nanofibres, controlling the crystallinity level, and adjusting blend solution viscosity prior to embedding HNTs and MPs.

Chapter 5 employed the obtained results from *Chapter 4* by embedding two different concentrations of unmodified HNTs and HNTs modified with 3-aminopropyltriethoxysilane (ASP) into two different concentrations of the PLA: PCL blend (namely 9% and 15% wt%/v of PCL). The effect of modified and unmodified HNTs on nanocomposite morphology, solution viscosity, thermal properties, degree of crystallinity and interaction level between HNTs, ASP and the biopolymers was investigated.

Chapter 6 utilised the findings obtained from *Chapter 4* by embedding three different concentrations of synthesised pure and impure MPs into the PLA: 15% PCL mixture (which was proven by *Chapter 5* to give better nanoparticle dispersion than PLA: 9% PCL). The effect of pure and impure MPs on nanocomposite morphology, solution viscosity, electrical conductivity, thermal properties, degree of crystallinity and interaction level between HNTs and the biopolymers was investigated.

Chapter 7 reports an application and test of drug release and nanofibre biodegradation, which uses results obtained through *Chapters 4*, *5* and *6*. The effect of drug type (TCH and IMC) and drug (TCH) concentration on the nanofibre mat morphology, solution electrical conductivity, thermal properties, degree of crystallinity, drug release, biodegradation, and release kinetic models was examined.

Chapter 8 summarise the main conclusions and presents a number of recommendations for future work respectively.

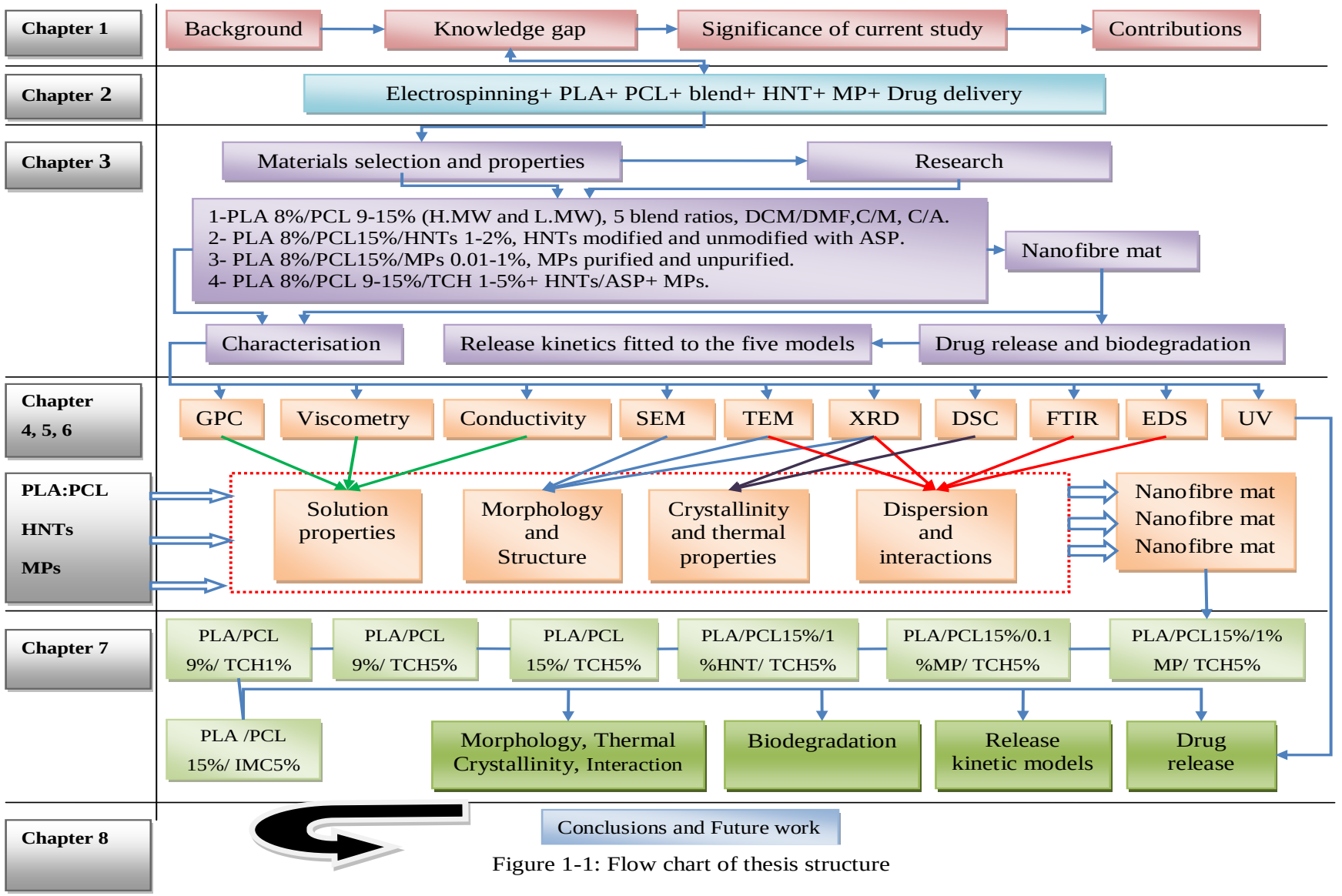

Figure 1-1: Flow chart of thesis structure

Chapter 2
Literature Review

2.1 Electrospinning

Nanofibres can be created by diverse techniques such as wet spinning, drawing, template synthesis, electrospinning (Ribeiro et al., 2010), phase separation and self-assembly (Ma et al., 2005). However, the majority of these methods cannot well control the orientation and the diameter of the fibres for certain polymers. Electrospinning has been established to be a brilliant technique for the production of small diameter fibres down to the nanoscale level for a broad range of polymeric materials (Jiang et al., 2006; Jian et al., 2008). Electrospinning is a combination of two processing methods, namely electrospraying and spinning (Agarwal et al., 2008). This technique has a number of attractive qualities, such as comparatively high fabrication rate, being reasonably inexpensive, the ability to produce fibres with large surface area to volume ratios (Singh et al., 2009; Zhang et al., 2007b), and applicability to several varieties of polymers. Polymer micro/nanofibres have been electrospun from different types of polymers, such as textile fibre polymers, proteins, conventional polymers, biodegradable and biocompatible polymers, and peptides (Jiang et al., 2004). Micro/nanofibres have widespread applications due to their good properties (Karim and Yeum, 2010), for example fibre-strengthened plastics, light and solar sails, plant pesticides, biomedical needs, mirrors in space, protective clothing for chemical and biological safety, catalyst supports (Kim et al., 2010), filtration (Charernsriwilaiwat et al., 2010), membranes for gas separation, water treatment, protein refinement (Meng et al., 2012) and military defensive clothing (Jiang et al., 2004). Electrospinning is an efficient, convenient and versatile method for creating reliable ultrafine fibres from polymer solutions, and it has been the subject of growing interest during recent years. It offers a promising technique to manufacture continuous fibres with diameters ranging from nanometres to microns (Han et al., 2009; Hadjiargyrou and Chiu, 2008). Fibre length could reach thousands of kilometres in a short period of time (Chowdhury and Stylios, 2011).

The initial patent for the electrospinning method was published as early as 1934, and in 1964 (Zong et al., 2002a). However, the manufacturing of polymeric nanofibres by this

method has not been well performed until recent times (Jian et al., 2008; Frenot and Chronakis, 2003). The method is comparatively simple, flexible, speedy, and efficient, resulting in adjustable surface morphologies and superior mechanical properties of the fibres produced (Kontogiannopoulos et al., 2011; Dong et al., 2013). Electrospun fibrous structures have potential biomedical applications such as sutures, cardiac grafts, wound dressings, artificial blood vessels (Sonseca et al., 2012), nerve guidance conduits, bone regeneration materials, vascular grafts (Liu et al., 2012), tissue engineering scaffolds, implants and systems for drug delivery control (Ribeiro et al., 2011). Electrospun polymer fibres are of particular importance to the field of tissue engineering and drug delivery because they have a number of benefits such as achieving high drug loadings, comparatively simple drug entrapment through the fabrication method, stability and protection of drug, drug burst control, high surface area to volume ratio, which improves drug release, and special morphologies that can be managed during fabrication (He et al., 2006; Natu et al., 2010). Additionally, the benefits from this technique are to decrease the drug's side effects and to improve the drug's bioavailability. This fabrication technique is extremely interesting in biomedical applications, especially for drug-delivery systems, because nanofibres can allow site-specific drug delivery in the body, and maybe one or more drugs can be encapsulated straight into the fibres as well (Wei et al., 2010).

The setup of an electrospinning system typically consists of four main components as shown in Figure 2-1. These include a grounded collecting plate, a pump, a spinneret and a high-voltage power supply (Qian et al., 2010; Dong et al., 2014b). When a charged polymer solution is ejected from the spinneret, a Taylor cone is created with the aid of an external electric field. At that time, the surface tension of solution droplets is balanced with the electric field (Bosworth and Downes, 2012; Sung et al., 2012; Demir et al., 2002). A little jet is driven out from the droplet surface and drawn in the direction of the collecting plate, towards the electrode of opposite polarity, across an air gap when the affected electric field is high enough to overcome the surface tension, (Sung et al., 2012; Chew et al., 2006). In addition, the jet is stable and does not break up into droplets of beads as expected for a solution conical thread. This is attributed to the polymer

solution's viscosity and the presence of polymer chain entanglements (Duzyer et al., 2011). Moreover, the solvent in the jet stream steadily evaporates as the jet spreads in the direction of the collecting plate, and the resulting product is a non-woven micro/nanofibre mat (Zhang et al., 2012). The morphology, fibre diameter and mat thickness can be manipulated by various solution parameters, such as solution concentration, viscosity, electrical conductivity and surface tension, or process parameters, including electric field strength and distance between the spinneret and the collecting plate (Liang et al., 2007; Cui et al., 2010; Yu et al., 2012).

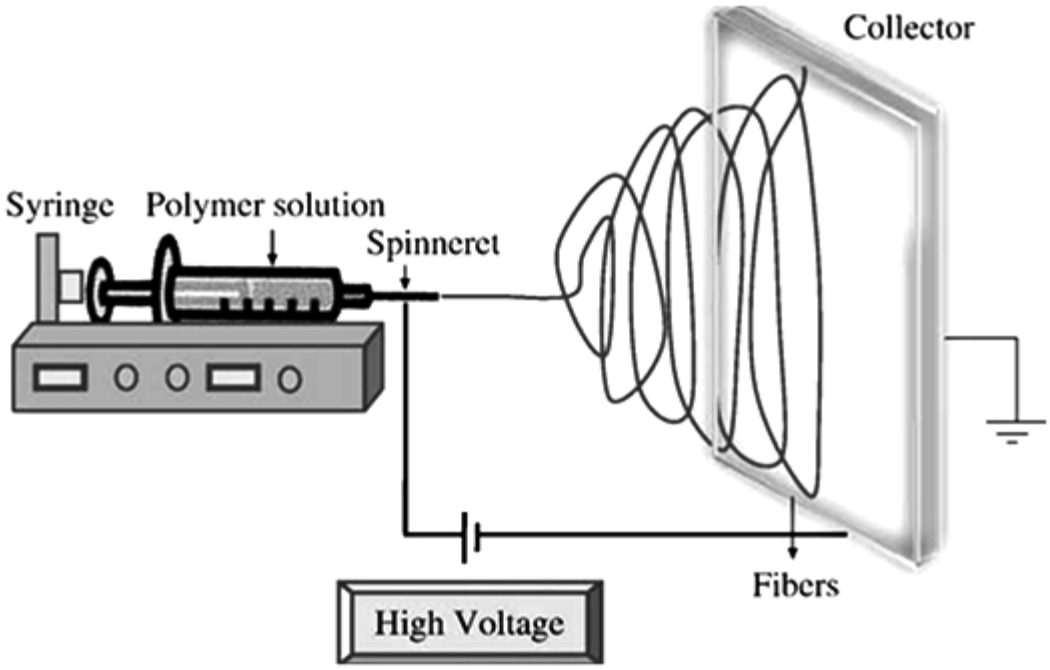

Figure 2-1: A typical electrospinning apparatus (Bhardwaj and Kundu, 2010).

2.2 Natural and synthetic polymers

In the last decade, various studies have demonstrated the use of biodegradable polymers as helpful vehicles for drug delivery (Kim et al., 2004). Polymers offer of different fields and wide range of using in scope of biological and drug-delivery systems (Goldberg et al., 2007). A diversity of biocompatible non-biodegradable or biodegradable polymeric materials is employed for drug delivery. The selection of the polymer is dictated by the necessities of the particular application (Kenawy et al., 2002). Biodegradable polymers

are excellent candidates for some applications in the biotherapeutic field due to their degradation without side-effects, their biocompatibility, and good mechanical properties (Wei et al., 2010). The US Food and Drug Administration (FDA) has approved biocompatible nanofibres for medical applications and for specific purposes. For example, those applications consist of wound healing devices, tissue repair and materials appropriate for controlled drug release. For those structures, the morphology is a significant characteristic, because of adsorption processes that take place at the boundary of the biofibres and the physiological surroundings (Buschle-Diller et al., 2007). Naturally produced biodegradable polymers have been fabricated into micro/nanofibres, such as hyaluronic acid, dextran, collagen, silk protein, elastin, chitosan and their blends. The poor mechanical properties of these natural materials and theirstructure loss in aqueous sources (Tiwari et al., 2010) are significant factors that limited and prevented them from being applied in drug delivery systems and tissue engineering (Cui et al., 2010). A limited number of natural biopolymers has been effectively electrospun compared with synthetic polymers owing to their poor processability (Li et al., 2006). Biodegradable hydrophobic polymers normally have excellent mechanical strength relative to natural biopolymers (Jiang et al., 2004). Aliphatic polyesters, including of poly(lactic acid) (PLA), poly(lactide-co-glycolide) (PLGA), poly(glycolic acid) (PGA), poly-DL-lactide-poly(ethylene glycol) (PELA) and poly(ε-caprolactone) (PCL) are biodegradable polymers that have been employed in biomedical industries (Lee et al., 2003b). This is mostly due to their biocompatibility and the flexibility present in terms of degradation ability and mechanical properties, which allow investigators to modify these polymers for particular applications (Cui et al., 2006). Suitable drug release kinetics can be achieved by manipulating the selected polymer and polymer matrix properties, such as enhancing the degradation speed and swelling ratio of the polymer matrix (Cao et al., 2010). Table 2-1 summarizes the various types of biopolymers that have been electrospun by different researchers and their applications. These biocompatible materials may find use in many applications such as wound dressing, tissue scaffolds or drug delivery vehicles (Wang et al., 2012).

Table 2-1: Different polymers used in electrospinning and their applications.

Polymer	Solvent	Fibre diameter (nm)	Application	Reference
PEG-PLA	Chloroform	600-730	Wounds	(Xu et al., 2010)
PEO	Water	200	Drug delivery	(Im et al., 2010)
PLGA-PVA	HFIP	400-700	Tissue engineering	(Samani et al., 2010)
PVA-alginate	Doubly distilled water	50-500	_	(Islam, 2010)
(PLGA) - collagen	HFIP	150-650	Wound dressing	(Liu et al., 2010a)
(PLGA)	DMF	260-360	Drug delivery	(Kim et al., 2004)
PDLLA	Methanol: Chloroform	220-830	Drug delivery	(Xie and Buschle Diller, 2010)
HA-Collagen	FA: HFIP	50-400	Tissue engineering	(Hsu et al., 2010)
PELA-HPCD	DCM :DMSO	700-780	Drug delivery	(Xie et al., 2010)
Eudragit® L 100-55	Ethanol:DMAc	360-1950	Drug delivery	(Shen et al., 2011)

2.2.1 Poly(lactic acid) (PLA)

PLA is a biodegradable polymer produced from sustainable materials (Fowlks and Narayan, 2010), mostly from starch, sugarcanes, wheat and sugar beets (Chow et al., 2012; Dong et al., 2014a). It is a promising biodegradable material source to decrease the solid waste disposal problems (Wang et al., 2006b). PLA is a biodegradable

polyester derived from α-hydroxy acids with good mechanical properties and several possible applications (Wang et al., 2012; Picciani et al., 2010), such as a dialysis medium, matrix for tissue engineering, biodegradable sutures, agricultural products, drug-delivery systems, food packaging and consumer products (Lim et al., 2008). Depending on the relative ratio of PLA backbone chains produced during chemical syntheses, PLA can be either semicrystalline or amorphous. PLA can be obtained by lactic acid condensation or through ring opening polymerization of a cyclic lactide dimer (Jandas et al., 2011). Figure 2-2 shows the chemical structure of PLA (Wang et al., 2010b).

PLA has attractive properties, including easy processability, ability to be dissolved in common solvents (Deng et al., 2007), sustainability, good biocompatibility, reasonably good optical properties (Lim et al., 2008), moderate thermal plasticity and suitable mechanical properties relative to petroleum-based polymers (Kim et al., 2003; Li et al., 2012). Additionally, it has been generally used as a system for drug release control. There are several reasons for PLA to be well recognized. First, PLA is biocompatible and degrades to form nontoxic monomers for biomedical application (Haroosh et al., 2012). It undergoes scission to monomeric units of lactic acid in the body, which is naturally in the carbohydrate metabolism (Lv et al., 2008; Kim et al., 2010). However, using PLA in this way is not effective because it produces an initial burst release of drug at the commencement of healing (Kim et al., 2010), as well as having brittleness and slow crystallization (Chow et al., 2012; Bhatia et al., 2007). In addition, PLA degradation is harmful to local tissues (Touny et al., 2010) due to its low pH value (Xu et al., 2010). The second reason is that when used in oral drugs, the polymer matrix protects drugs and proteins from the negative environmental conditions (Romero-Cano and Vincent, 2002). There are some advanced ways to enhance PLA usage, which consist of loading fillers or using blending method (Chow et al., 2012).

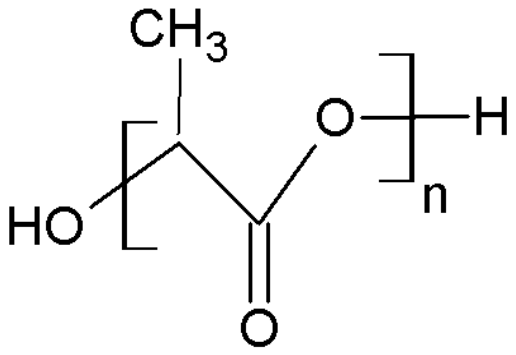

Figure 2-2: Chemical structure of poly (lactic acid) (Wang et al., 2010b).

2.2.2 Poly(ε-caprolactone) (PCL)

Poly(ε-caprolactone) (PCL) is a hydrophobic and semi-crystalline polymer (Kenawy et al., 2009), so it usually is employed for enhancing elasticity (Lee et al., 2003b). It is well-known for its acceptable drug permeability and good biocompatibility (Huang et al., 2006). A local acidic environment is not generated when PCL degrades. This advantage, along with its moderately low cost, places PCL as a good candidate for biomedical applications (Kenawy et al., 2009; Luong-Van et al., 2006). Among a variety of polymers, PCL has a molecular structure of five nonpolar methylene groups and one comparatively polar ester group as shown in Figure 2-3. It can be used in several biomedical applications such as scaffolds and bone renewal (Qin and Wu, 2012). The presence of the aliphatic ester bond that can undergo hydrolysis makes the polymer degrade in the body (Kweon et al., 2003) and the resulting materials can be both metabolized through the tricarboxylic acid cycle and removed straight via renal secretion (Sun and Downes, 2009). Furthermore, PCL is a slowly degraded biopolymer compared with many other counterparts such as PLA because of its semi-crystalline nature (Huang et al., 2006). Moreover, it is not harmful to local tissues such as poly(lactide-co-glycolide) (PLGA) or PLA. The chains of PCL polymer degrade to low molecular weight nontoxic products when they accompany by simultaneous drug release (Hamoudeh and Fessi, 2006). However, some disadvantages have been identified from using PCL in biomedical applications. For instance, the hydrophobicity and semi-crystalline nature of PCL polymer restricted its practical application (Fu and Kao, 2010;

Li et al., 2008). Furthermore, the insufficient mechanical properties of PCL and its poor porosity restrict its applications in hard tissue engineering and drug delivery, respectively. PCL based composites were generally investigated to overcome these shortcomings; these included PCL/ collagen and PCL/ gelatin electrospun nanofibre composites (Meng et al., 2010). Moreover, Kenawy et al. (2009) demonstrated drug release from PCL fibres and also the period of fibre degradation. The process of degradation primarily takes place by the diffusion of water into the fibres, and then by random hydrolysis fragmentation of the fibres, and lastly by broader hydrolysis accompanied by diffusion, metabolism, and phagocytosis. Hydrolysis is influenced by the hydrophilicity of the polymer, the pH value of the release environment and the crystallinity of the polymer (Kenawy et al., 2009). Furthermore, Natu et al. (2010) showed that PCL fibres absorbed water steadily, which was attributed to the semi-crystalline and hydrophobic fibres hindering water penetration within the fibre. For example, the fibres that created from high molecular weight PCL did not demonstrate approximately any mass loss (0.45%) whereas, mass loss of PCL was obvious just after the molecular weight reaches 10,000 g/mol (Natu et al., 2010).

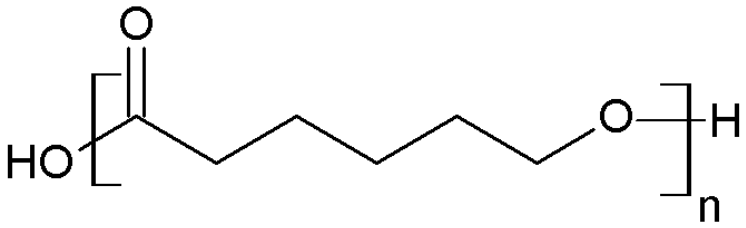

Figure 2-3: Chemical structure of polycaprolactone (PCL) (Han et al., 2010).

2.3 Polymer blending

Polymer blending is usually employed to build up novel materials because of the property variation that can be gained by suitable blending of individual components (Kenawy et al., 2002; Dhandayuthapani et al., 2010). The matrix properties, such as swelling, hydrophobicity and mechanical strength, can be modified just by adjusting the composition (Jiang et al., 2004). Polymer blending represents an extremely helpful technique for the development or adjustment of the physicochemical properties of

polymeric materials (Picciani et al., 2009). A number of polymer blends can be created that are extremely different from the individual polymers, showing unusual properties. The miscibility of elements is a significant property of a polymer blend because it influences the mechanical properties, the degradation, morphology, and the permeability. The blends are physical combinations of structurally diverse polymers that network using secondary forces, such as charge transfer complexes for single polymer combinations, hydrogen bonding and dipole–dipole forces, without covalent bonding (Islam, 2010). The efficiency of blending process can be reorganized in terms of enhanced elasticity of the polymeric solution, which is frequently traced to enhanced entanglement density (Wang et al., 2010d). Biodegradable hydrophobic polymers normally have good mechanical strength but with weak cell affinity; whereas hydrophilic polymers have good cell affinity but little mechanical strength, especially in the swollen and degradation conditions. Blending biodegradable hydrophilic and hydrophobic polymers will avoid the limitations of the pure materials. However, hydrophobic polymers and hydrophilic polymers have greatly different intrinsic properties, and blending them to form a uniform structure is not easy to achieve (Cui et al., 2009). Moreover, about 24 h after blending, separation of the polymer phases occurs. Therefore, to minimize this phase separation problem, the blend solutions need to be electrospun immediately after their blending (Srikar et al., 2008).

Various studies have been conducted into the electrospinning of blended polymers, especially those composed of biocompatible and biodegradable materials. Zhang et al. (2005) showed that the approach of blending synthetic polymers, and occasionally bio-artificial polymeric materials, with gelatine has been commonly studied by investigators. They have shown that blending is a feasible approach that provides a compromise solution for overcoming the shortcomings of synthetic and natural polymers. Additionally, it reduces the potential problem of cytotoxin, due to employing a chemical cross-linking reagent. This technique creates a novel biomaterial with suitable biocompatibility and enhanced the chemical and mechanical properties of the biopolymeric matrix. The incorporating of the hydrophobic polymer PCL with the hydrophilic polymer gelatin offers a reliable way to release gelatin protein molecules

from the blending matrix (Zhang et al., 2005). In addition, Han et al. (2009) found that blending poly(trimethylene carbonate) PTMC with PCL at a blending ratio of 5:5 resulted in dissolved and swollen fibres in the solution. This was because amorphous PTMC is more hydrophilic than the semi-crystallised PCL, which increased the porosity on the film surface. Therefore, high PTMC content in the fibres results in raising water absorption, leading to fibres dissolving quickly in the release solution. They also found a higher PCL ratio prevented the blend fibres from swelling to some extent (Han et al., 2009). Another study demonstrated that increasing the ratio of PTMC to PCL led to decreased fibre diameter with acceptable fibre morphology (Han et al., 2010). According to Zhang et al. (2006), when blending the water-soluble polymer poly(ethylene glycol) (PEG) with PCL and protein, fluorescein isothiocyanate-conjugated bovine serum albumin (fitcBSA) to produce nanofibres by a normal electrospinning technique, they have shown evidence of beaded fibre morphologies even though they used established processing conditions. The determined fibre diameters of core-shell-structured PCL-r-fitcBSA/PEG were slightly bigger than those of PCL/ PEG / fitcBSA blends (Zhang et al., 2006).

The blending of poly(L-lactic acid) (PLA) with other polymers has received significant attention recently and is deemed one of the most innovative materials built up from renewable resources (Picciani et al., 2010). According to Kim et al. (2003), PLA-based multi-component blends containing lactide (a hydrolytic catalyst) and two connecting materials (triblock copolymer PLA-b-PEG-b-PLA and low molecular weight random copolymer PLGA) were combined and employed in electrospinning. The data revealed that the biodegradation speed of the electrospun scaffolds was adjusted with different material compositions, which displayed steady mechanical properties in aqueous conditions. Those matrixes were appropriate for some biomedical applications, such as prevention of post-operative adhesions and scaffolds for tissue engineering (Kim et al., 2003). In another study, fibres of different blending ratios of PEG in poly (DL-lactide) PDLLA were fabricated by the electrospinning method. The degradation patterns of the PEG/ PDLLA matrix changed from bulk degradation to surface erosion with the

decrease of the PEG content in the composites. During the creation of crystal sections of PEG in the fibre matrix, the dimensional shrinkage was lowered (Cui et al., 2010).

The mechanical properties of electrospun fibrous mats are influenced by the properties of fibre structure and each polymer in the blend (Yao et al., 2007). Studies on blends of hyaluronic acid HA and gelatin GE have indicated that GE can provide HA with protein properties to enhance the cell attachment, and blends of HA-GE have a potential application in tissue mending. The reason for incorporating GE was to enhance the electrospinning processability and to provide the fibrous mats with protein characteristics (Li et al., 2006). In addition, it was found that the decrease in surface tension of the spinning solutions was achieved when GE was added to HA to improve the processability (Xu et al., 2009). Furthermore, blending chitosan and alginate produced a hydrogel because of complications of the polyelectrolytes. Several parameters of the polysaccharides and their solutions were significant factors in the formation of polyelectrolyte complexes. Those parameters were molecular weight, pH value and the ratio of chitosan to alginate. The nanofibres including alginate and chitosan were less swelling in an aqueous environment compared to those composed only of water-soluble alginate because the chitosan was not water-soluble. The swelling ratio increased as the quantity of chitosan decreased (Jeong et al., 2010). Moreover, the addition of poly(D,L-lactide-co-glycolide) PLGA materials to the collagen enhanced the mechanical strength of electrospun nanofibres (Liu et al., 2010a). A differential scanning calorimeter (DSC) was used to evaluate the miscibility between dextran and PLGA in the electrospun composite membranes. The composite fabric membranes were in a two-phase system because the glass transition temperature (T_g) of dextran did not change by blending with PLGA (Jiang et al., 2004).

Many other studies have been conducted into electrospun blended polymers. For instance, electrospun fibres imitating the extracellular matrix for tissue engineering were prepared from blending collagen with chitosan and from blending PLA with chitosan. A vehicle for drug controlled release was developed from electrospun nanofibres by blending gelatin with PVA, and more recently, a potential application for wound

dressings was investigated using electrospun fibre mats from mixing gelatin with PLLA. Moreover, the incorporating of PLCL into collagen fibres improved proliferation and cell adhesion (Samani et al., 2010). The cell attachment, proliferation and extracellular mat secretion were enhanced by blending PLGA with collagen, which were indicated to be related to the ratio of collagen in the composite scaffold (Cui et al., 2010). In another study, the synthetic polymer PVA was blended with alginate to overcome the poor electrospinnability of alginate solutions. Furthermore, the nanofibres of polymer blends showed improvement in the mechanical properties with the addition of alginate compared to electrospun PVA alone (Islam, 2010).

2.4 Nanoparticles and nanocomposites

Polymer nanocomposites incorporating nanoparticles have attracted great attention due to their tailored properties (Fowlks and Narayan, 2010; Noor Azman et al., 2013) and unique structures, which might not be accomplished in conventional composites (Du et al., 2008). This material system has been studied for many applications because of their inexpensive manufacturing, simple processability, remarkable electrical, thermal (Lee et al., 2003a), optical, (Sonseca et al., 2012) and magnetic properties, and antibacterial activities, as well as excellent substrate adhesion (Zhang et al., 2009). It is hypothesised that the interfacial interactions between the polymer and embedded inorganic particles are significant factors in the final performance of nanocomposites. The interfacial interactions between inorganic particles and the matrix of the polymer generally consist of covalent bonds, vander Waals force, ionic bonds and hydrogen bonds. To improve the interfacial interactions of such nanocomposites, various approaches were developed to modify the matrix properties. Up to now, novel effective approaches to enhance the interfacial interactions in nanocomposites are still and important research area (Du et al., 2008). Moreover, the final properties of the composites are determined by several critical factors including the dispersion of nanoparticles in the matrix and the interfacial bonding between the matrix and inorganic particles (Liu et al., 2009c; Schmidt, 2005).

Composite inorganic – organic materials with polymers are produced when two or more different materials are blended on a nanoscale level to achieve unique characteristics

resulting from a synergy between the two chemical components. Furthermore, interactions between organic materials and inorganic layered materials (such as Zn-Al layered double hydroxide) are attractive, particularly in the examination of guest-host interactions and their potential in a variety of technical and manufacturing applications. Moreover, syntheses of these hybrids are achieved by direct intercalation of inorganic components into polymers or by pre-intercalation of their monomers. This will establish a novel method to construct new polymer-inorganic nanoscale assemblies (Lappas et al., 2005) with high porosity (Meng et al., 2012). Nanofillers such as nanosilica, carbon nanotubes, calcium carbonate nanoparticles and layered silicates have been widely examined. Usually, polymer-inorganic nanocomposites with good properties are characterized by strong interfacial interactions and good dispersion at the nanoscale level (Jia et al., 2009). Zhang et al. (2008) showed that the encapsulation of inorganic nanomaterials with polyaniline resulted in many interesting nanocomposites. So far, several methods have been explained to produce nanocomposites by using coated inorganic nanomaterials with polyaniline such as nanobelts and silicate clays in in-situ oxidative polymerization, as well as nanoparticles and nanotubes in gamma radiation-induced chemical polymerization or electropolymerization. Some of the chemical and physical properties of these materials differ from those of the pure polymers, and they also differ from each other in many properties such as permeability and toughness (Zhang et al., 2008).

Increasing both shear viscosity and extensional viscosity is very effectively achieved by means of dispersions of nanoparticles such as clay silicates into the polymer, which are generally due to the interactions between the nanoparticles and between the polymers and the nanoparticles (Wang et al., 2010d). There are diverse feasible techniques for fabricating hybrid inorganic-organic fibres, such as electrospinning, coating, and blending (Liu et al., 2008c). Electrospinning of dispersed nanoparticles in the polymer is an efficient approach to create a fibre with diameters at the nano to micro level from polymeric solutions at low concentrations (Wang et al., 2010d; McCullen et al., 2007). However, hard nanoparticles hinder polymer chain interactions by increasing their distance (Tsioptsias et al., 2010). The electrospinning method has been used for

fabricating fibre mats based on biodegradable polymers and inorganic-polymer nanocomposite materials (Tsioptsias et al., 2010). Particles embedded in the nanocomposite sustain an additional homogeneous charge density in the whipping instability generated via electrospinning (McCullen et al., 2007). In addition, nanocomposite fibres electrospun after dispersing nanoparticles into the polymer demonstrated improved mechanical properties. For instance, electrospun polymeric PMMA nanocomposite fibres displayed an improved thermal stability compared with fibres produced just from PMMA (Wang et al., 2010d). Furthermore, poly(hydroxybutyrate) (PHB), poly(butylene succinate) (PBS) and PLA are generally employed as biodegradable polymers and their thermal and mechanical parameters can be significantly enhanced by incorporating different inorganic or organic particles (Matusik et al., 2011).

2.4.1 Halloysite nanotubes (HNTs)

The interaction between clay minerals and organic polymers to produce novel hybrid materials has attracted more interest in the past decade. The varied characteristics of nanocomposites, such as thermal properties, electrical properties, electrochemical properties and mechanical properties, can be efficiently tailored by a suitable selection of synthesis conditions and initial materials. The properties of prepared nanocomposites are basically different from the properties of pure polymer or nanoclay components. This is because of the diverse types of polymer and clay interactions that occur at a molecular level (Matusik et al., 2011). Halloysite nanotubes (HNT) as nanoparticles for polymer reinforcement purposes have been a focus of research recently. HNT belong to the kaolin group of clay minerals, with a composition of $Al_2Si_2O_5(OH)4.nH2O$, which naturally has the structure of multilayer inorganic nanotubes (Qi et al., 2010). Dehydrated halloysite (interlayer spacing d_{001}=7 Å) corresponds to n = 0, while hydrated mineral halloysite (d_{001}=10 Å) forms when n = 2. HNTs show a hollow tubular formation as the main morphology (Carli et al., 2011). Wrapping clay layers around onto themselves to form hollow tubes over suitable geological conditions will result in highly this unusual meso/macroscopic superstructure (Yuan et al., 2008). HNTs are aluminosilicates with a mainly tubular form at the nanoscale level and the surface of

HNTs is composed of siloxane and a few hydroxyl groups (Chew et al., 2006). This indicates that HNTs have a high dispersion characteristics compared to other natural silicates such as kaolinite and montmorillonite (MMT), and have the ability to create hydrogen bonds (Du et al., 2008; Liu et al., 2008b). Additionally, a majority of HNTs are rolled multi-wall nanotubes (Rooj et al., 2010). The structure of a HNT is revealed in Figure 2-4.

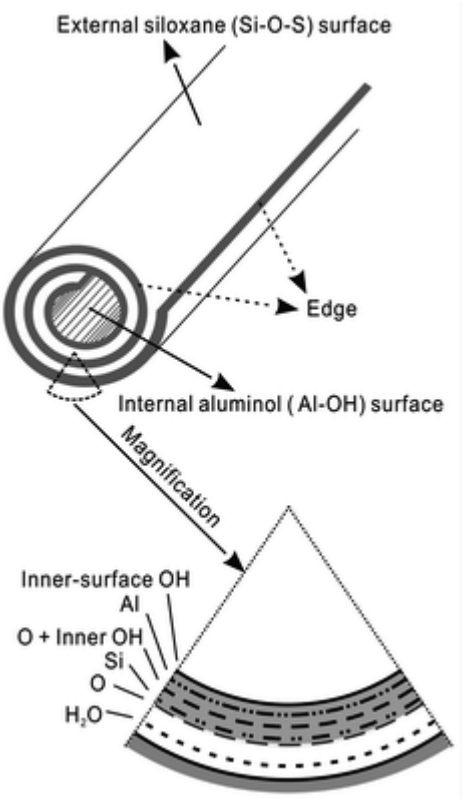

Figure 2-4: Schematic diagrams of HNT structure (Yuan et al., 2008).

HNTs from diverse sources differ in size and the usual dimension of halloysiteranges from 300 to 1500 nm in length, 15 to100 nm for the inner diameter and 40 to 120 nm for the outer diameter (Liu et al., 2009b). HNTs are useful in various applications, such as cosmetics, catalyst carriers, ceramics and drug delivery, due to their unusual shape and geometry, surface properties and chemical structure (Jia et al., 2009). HNT is appropriate for the carrier of a range of materials due to its extremely large halloysite

lumen diameter (Yuan et al., 2008). Figure 2-5 is a schematic diagram of the HNT crystalline structure.

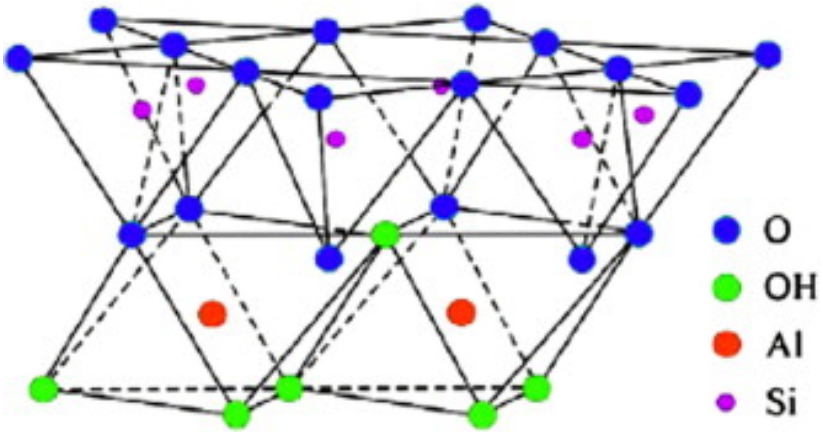

Figure 2-5:Crystalline structure of HNTs (Rooj et al., 2010).

HNTs work as nanofillers embedded within polymer matrices. It has been found that the natural inorganic nanotubes have significant reinforcement and influence on many polymers such as polypropylene, linear low density polyethylene epoxy resin, nylon (Jia et al., 2009), natural rubber (Carli et al., 2011) and polyvinyl alcohol to enhance the thermal and mechanical properties of the composites (Ismail et al., 2008, Guo et al., 2009a). In addition, Liu et al. (2007) mentioned that nanocomposite films could be produced from dispersed HNTs in polyvinyl alcohol PVA solution, which is attributed to the hydrogen bonding between the hydroxyl groups of PVA and surface silanols of the HNT. They showed that, as a result of the strong hydrogen bonding between the HNT particles, HNTs re-aggregated after that and this aggregation influenced the properties and structure of the composite film (Liu et al., 2007). Jia et al. (2009) demonstrated that HNTs without the surface enhancement offered poorer dispersion and weak interfacial combination in rubber due to low compatibility with the rubber macromolecules. They mentioned that the surface enhancement of HNTs must be performed to enhance the dispersion of HNTs in rubber film and improve the interactions between the rubber film and HNTs (Jia et al., 2009). According to Qi et al. (2010), the incorporation of HNTs into the poly(lactic-co-glycolic acid) PLGA fibres did not affect significantly the morphology of the fibres; whereas the fibre diameters obtained by incorporating HNTs in PLGA were slightly larger than those obtained for pure PLGA fibres. They proposed

that HNTs are promising drug carriers. They stated that by mixing the drug with HNTs using the eletrospinning method, a novel drug delivery system with sustained-release properties may be developed for a variety of applications in pharmaceutical areas and tissue engineering (Qi et al., 2010).

2.4.2 Magnetic Particles (MPs)

Among a range of multiple-use composite materials, those with electrical and magnetic properties are appropriate candidates for a wide range of applications such as magnetic transporters for microwave absorbers, biofuel cell membranes, electromagnetic equipment applications and biomedical applications (Bayat et al., 2011; Kyung Sung et al., 2011). Moreover, magnetic materials frequently show numerous attractive properties such as transparency, solubility and low density, allowing them to be used as components of superior electronic devices (Schlueter et al., 2010). Magnetic particles are typically manufactured from maghemite, cobalt ferrite ($CoFe_2O_4$) and magnetite (Fe_3O_4) (Yang et al., 2006). Magnetite Fe_3O_4 has been widely investigated and employed among the magnetic nanoparticles for bioscience applications due to its simplicity of synthesis, good biocompatibility and large saturation magnetization (Lin et al., 2009; Haroosh et al., 2013b) . Moreover, Fe_3O_4 shows very little toxicity, so that it can be well accepted in the human body (Yang et al., 2006). Magnetic particles can be employed in a variety of medical systems because of their desirable magnetic properties that are unavailable in other materials. These magnetic nanoparticles are also potentially helpful in various fields such as data storage, sensors, (Sung et al., 2012), purification separation, magnetic resonance imaging, enzyme immobilization, immunoassay, drug delivery, and hyperthermia treatment (Hamoudeh and Fessi, 2006). Magnetic nanoparticles tend to agglomerate to reduce their energies owing to their high surface area to volume ratio. Many studies have suggested overcoming this difficulty by using a stabilizer, such as steric polymers and electrostatic surfactants (Kyung Sung et al., 2011). For example, adding oleic acid was able to stabilize magnetite precipitate, as it works as a surfactant to prevent magnetic particle agglomeration by producing a hydrophilic surface (Timko et al., 2006).

Various methods have been implemented to manufacture polymer – magnetic particle hybrids, such as solvent evaporation, emulsion polymerization, suspension polymerization, micro emulsion polymerization, dispersion polymerization and solvent diffusion (Zhang et al., 2007a; Hamoudeh and Fessi, 2006). However, these techniques are complex and it is hard to tailor the physical and chemical properties of the polymer magnetic composites. So far, the techniques to prepare magnetic polymer composites are still under investigation for novel applications (Guo et al., 2009b). In addition, there are a variety of feasible techniques for fabricating polymer magnetic particle hybrids, such as coating, blending, and electrospinning (Liu et al., 2008c). Direct drug delivery to the target region of the body is one of the possible strategies that may be achieved with drug-enabled MPs and external magnetic fields (Zavisova et al., 2007) as shown in Figure 2-6.

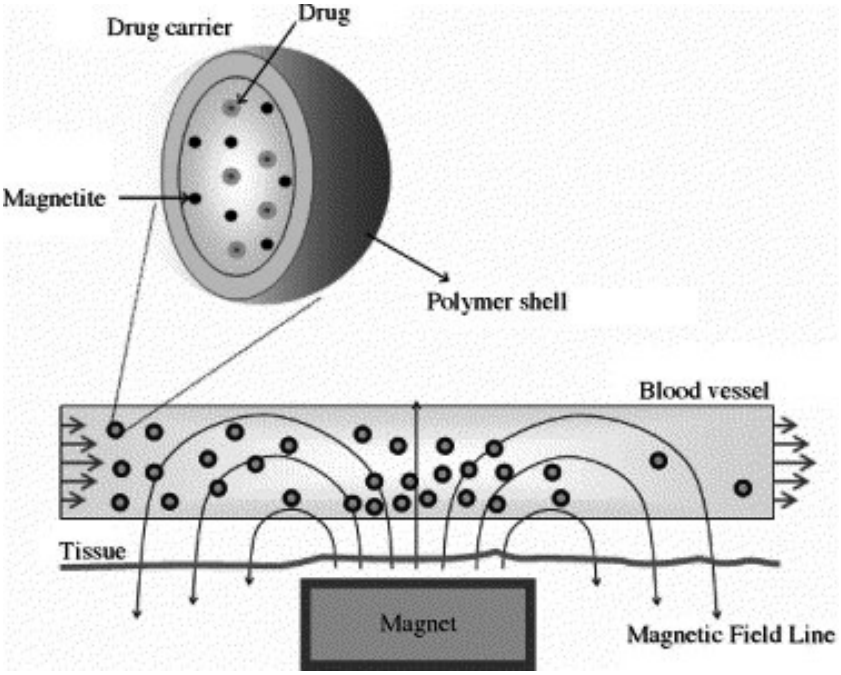

Figure 2-6: The mechanism of the drug delivery to a target area with the assistance of magnetic nanoparticles (Yang et al., 2006).

Magnetic nanocomposites such as nanowires, nanotubes, and nanofibres have lately gained prominence as they demonstrate a number of unique properties that are not shown by their bulk materials, in addition to having high processability, versatility, and

cost-effectiveness (Wang et al., 2010a). The aim of manufacturing such nanocomposites is to achieve the homogeneous dispersion of magnetic nanoparticles inside the polymeric structures by selecting an appropriate method for fabricating the nanofibres (Kyung Sung et al., 2011). Manufacturing nanofibres based on magnetic polymer hybrids from a variety of polymers with specific mechanical properties is still not easily achieved. In addition, the ability to electrospin a range of polymer magnetite nanocomposites has not been methodically studied (Wang et al., 2010a). Lin et al. (2009) developed a simple method to create Fe_3O_4 nanoparticles encapsulated in polyvinyl pyrrolidone PVP nanofibres by the electrospinning technique, and investigated their magnetic characteristics and structures (Lin et al., 2009). The electrostatically driven instability rises in magnitude because the electric field force increases in the electrospinning process, which causes the jet to undergo more whipping leading to the reduction of fibre diameter (Chowdhury and Stylios, 2011). Moreover, the effect of Fe_3O_4 in increasing the electrical conductivity is ascribed to its catalytic influence. Schmidt (2005) synthesized a core-shell hybrid, using magnetite (Fe_3O_4) as the inorganic core because of its paramagnetic behaviour and a polymeric shell was provided as a stabilizing coating, which gave the preparation a stable particle dispersion. This type of dispersion of magnetic particles has been called a ferrofluid: it behaves as a liquid with flow performance and physical properties being manipulated by external magnetic fields (Schmidt, 2005). Wang et al. showed a combined method of electrospinning with in-situ composites of Fe_3O_4/ PVA nanofibres. They found that the Fe_3O_4 nanoparticles were stabilized by PVA to prevent agglomeration in the electrospun composite nanofibres (Liu et al., 2008a). Yang et al. (2007) hypothesized the mechanism for the formation of parallel fibres by magnetic electrospinning (MES) as shown in Figure 2-7. The mechanism is that fibres with magnetic particles are considered to act as a thread charged with magnetic dots and connected through a viscoelastic source. They illustrated the main aspects to the effective fabrication of well-aligned fibrous arrays by MES including a suitable magnetic field, the magnetized polymeric solution, and appropriate gap size between the two magnets. The magnets they used were made of a ferromagnetic oxide mineral and were insulators. The results confirmed that the

magnetic field is the driving power that induces the fibres to align into parallel collections (Yang et al., 2007b).

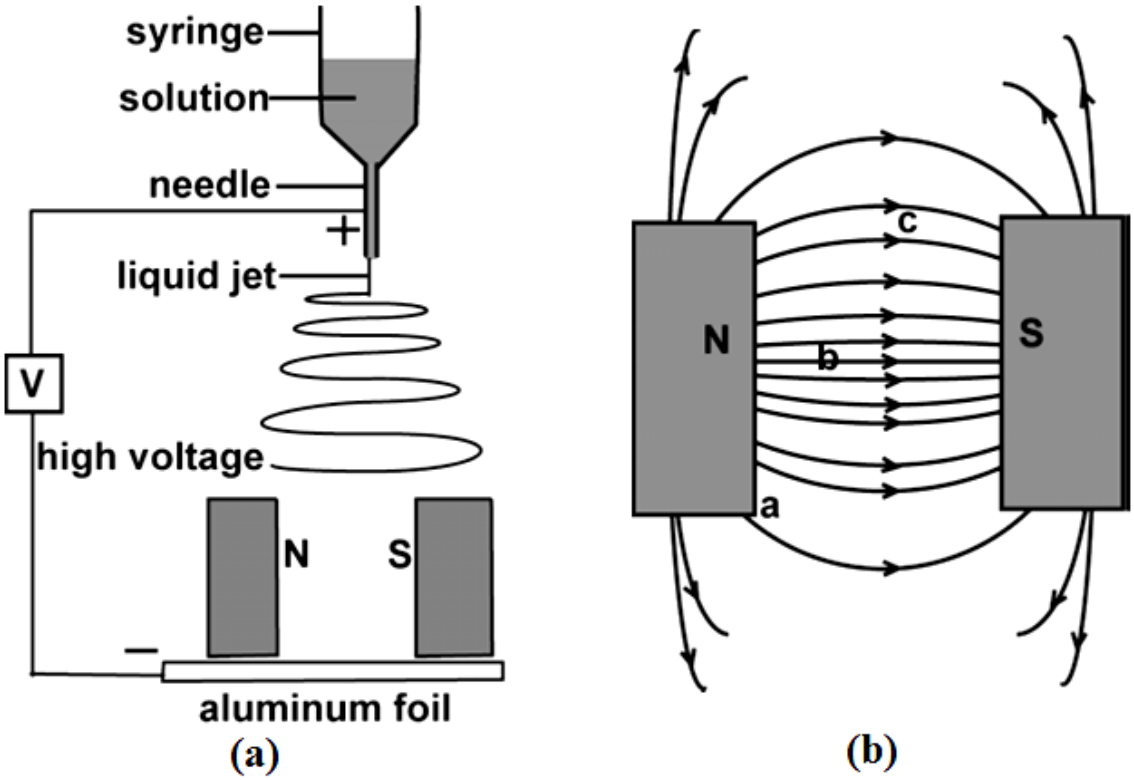

Figure 2-7: (a) clarification of the system for magnetic electrospinning (MES), (b) illustration of magnetic field strength between the two magnets (Yang et al., 2007b).

In addition, vertical anisotropy is revealed in magnetic chains built up using a high magnetic field. Magnetic nanoparticles re-orient themselves to align along their axis with the applied field during solvent vaporization (Sharma et al., 2010b).

2.5 Parameter effects

Electrospinning is a complex process that can be affected by either the processing parameters or solution characteristics (Ji et al., 2006; Zhang et al., 2005). The properties of nanofibres and their morphology heavily rely on the properties of the solution and the electrospinning parameters (Liao et al., 2011). The electrical and mechanical properties of electrospun fibre matrixes are related to the resulting fibre diameter. A decrease in the

fibre diameter will lead to an increase in the mechanical strength and fibre density while the porosity decreases accordingly (Dhakate et al., 2011; Duzyer et al., 2011). Moreover, the fibre size and material morphology influence the hydrophobic behaviour of polymers (Chen et al., 2009). Solution parameters, such as concentration of the solution, the viscosity of the solution, surface tension (Arumugam et al., 2009, Liu et al., 2009a), and molecular weight of the polymer, affect the chain entanglement of the polymer (Ribeiro et al., 2010). Moreover, solvent properties, such as dielectric properties, solubility, boiling point and the solvent volatility, play a significant role in the electrospinning process. In addition, processing parameters can also affect fibre manufacturing these parameters include geometry of the needle tip, voltage, distance between collector and needle tip, the solution feed rate and fibres collector (Ribeiro et al., 2011). Furthermore, environmental parameters, such as the type of atmosphere, humidity, temperature and pressure, could have some impact. The examination of polymeric fibres produced by electrospinning and the consideration of the connection between molecular structure and properties of these electrospun fibres are a challenge (Heydarkhan-Hagvall et al., 2008). The investigation of the effect of the parameters on the electrospun fibresis in fact quite challenging due to interactions between the parameters (Biber et al., 2010). Among a range of electrospinning parameters, the solution concentration (Yao et al., 2007), the viscosity, electrical conductivity of solution (Kim et al., 2008), polymer molecular weight and use solvents (Buschle-Diller et al., 2007) are the most influential variables that control the morphology and fibre diameter. Many studies have been undertaken into manipulating all these electrospinning parameters to achieve desired crystallinity, fibre diameter, molecular structure, and morphology (Ribeiro et al., 2011, Wang et al., 2006a).

2.5.1 Polymer viscosity

The solution viscosity is a significant parameter that affects the fibre morphology since it is connected with chain entanglement (Alipour et al., 2009; Lee et al., 2010). The number of beads created in the mat and the fibre diameter decrease when the viscosity of the solution is reduced (Chen et al., 2010). The viscosity of the polymer solution must be within a certain range that permits effectual polymer chain entanglement so as to

accomplish the arrangement of uniform fibres (Verreck et al., 2003b). When the solution viscosity is low, that can lead to the formation of nanoscale beads instead of long fibres because the Coulombic forces have a tendency to stretch the jet and control the viscoelastic forces that resist the jet breakup. So, low viscosity assists in a fast breakup of the charged polymer jet at smaller distances (Chuangchote et al., 2009). At moderate viscosity, the viscoelasticity produced by chain entanglements increases as a result of an increased number of polymer chains per unit volume of polymer solution. As a result, the charged polymer jet cannot completely break up into beads (Jiang et al., 2004). At high solution viscosity, there is a larger number of chain entanglements which are required to formation a steady jet in order to compensate for the influence of the surface tension which reduces jet sizes (Spasova et al., 2007; Sharma et al., 2010a). During the electrospinning process, the equilibrium between the electrostatic repulsion, viscoelastic strength, and surface tension is found to be important to control the fibre uniformity. In addition, high quality fibres can be achieved by balanced forces which can shape and maintain a Taylor cone. Otherwise, considerable bead formation will occur when the jet at the spinning tip is unstable (Zhang et al., 2009).

According to Alipour et al. (2009), the shear viscosity of poly(vinyl alcohol) (PVA) and N-[(2-hydroxy-3-trimethylammonium)propyl] chitosan chloride (HTCC) blend solutions increases with a decrease in the HTCC amount. At a constant applied electrical field, a drop off in the average fibre diameter was observed. This finding was attributed to solution conductivity and viscosity, which are significant parameters that influence the electrospun fibre morphology and spinnability of the solution. Pure HTCC solutions with a concentration between 10 and 12 wt%/v were unsuitable, and just beads were formed on the target plate collector. This was due to the low viscosity of HTCC solution, which prevents the creation of a steady drop at the needle tip (Alipour et al., 2009). Gu et al. (2009) mentioned that the transfer from bead structures to elongated fibre morphology resulted from a relationship between the solution viscosity and surface tension. When the solution concentration decreases, the viscosity of the polymer solution can be expected to decrease (Gu et al., 2009). Moreover, Homayoni et al. (2009) showed that chitosan solution with a molecular weight of 1095000 g/mol dissolved in glacial

acetic acid (AcOH) solvent resulted in an excessive viscosity solution, which prevented the solution jet from being elongated in the electrical field during electrospinning. This difficulty was not solved even by altering the electrospinning parameters and the produced solution arrived on the collector as droplets (Homayoni et al., 2009). Arayanarakul et al. (2006) demonstrated that the addition of 0.5 wt%/v Sodium Dodecyl Sulfate (SDS) into poly(ethylene glycol) (PEG) solution decreased the solution viscosity. The data showed that the viscosity increased from about 338cP at 7 wt%/v SDS to about 476 cP at 0.5 wt%/v SDS. In general, the decrease in the viscosity of the electrospun solution leads to the decrease of fibre diameters (Arayanarakul et al., 2006). Cui et al. (2009) found that the viscosity of the blended poly(ethylene glycol) PEG and poly(DL-lactide) PDLLA at the same concentration dropped with the addition of a large amount of PEG, resulting in smaller fibre diameters. However, there were no electrospun fibres formed when the blend contained 60 wt%/v PEG owing to the low solution viscosity resulting from blending a high ratio of low molecular weight PEG (Cui et al., 2009).

2.5.2 Material concentration

The polymer concentration plays one of the most important roles in controlling fibre diameter in the electrospinning process (Pham et al., 2006; Xie and Buschle Diller, 2010) because of the polymer chain entanglements necessary for effective electrospinning and the quantity of solvent to be removed during processing (Wang et al., 2005). The polymer solution concentration is an important factor in the formation of beads, bead-fibre structures and fibre mats (Macossay et al., 2007; Beachley and Wen, 2009). A high solution concentration with an appropriate viscosity is vital for effective fibre formation (Um et al., 2004). However, at extremely high solution concentrations, the electric force cannot overcome the surface tension and the large viscosity of the solution, leading to the collapse of steady jet flow. Conversely, at low solution concentrations, the polymer chains are not adequately entangled to form nanofibers (Wang et al., 2005). Additionally, the quick evaporation of the solvent at higher concentrations decreases spinningas a smaller amount of solvent needs to be removed in the same time, leading to large fibre diameters (Heydarkhan-Hagvall et al., 2008).

Thinner fibres can be produced at low concentrations and the solvent needs a longer time to be removed from the fibres (Jiang et al., 2004). Thicker fibres can be generated at high concentrations and solvent removal is achieved by the time they arrive at the target, resulting in the prevention of further fibre elongation (Duzyer et al., 2011). When the solution concentrations are excessively high, it could be difficult to produce fibre structures due to their high viscosity. The Taylor cone angle of a polymer jet decreases with decreasing the solution concentration (Hsu et al., 2010). The appropriate solution concentration is the key factor in the formation of a steady and continuous charged jet, which is important to exceed the extensive molecular entanglements (Qin and Wu, 2012). When enough chain entanglement is present in the solution, fibres are can be steadily produced (Chen et al., 2010; Liao et al., 2011). A collapse from electrospinning to electrospraying takes place for solutions with a concentration lower than the entanglement concentration, and this produces beads on the collector due to the capillary unsteadiness at the end of the jet (Wang et al., 2010b).

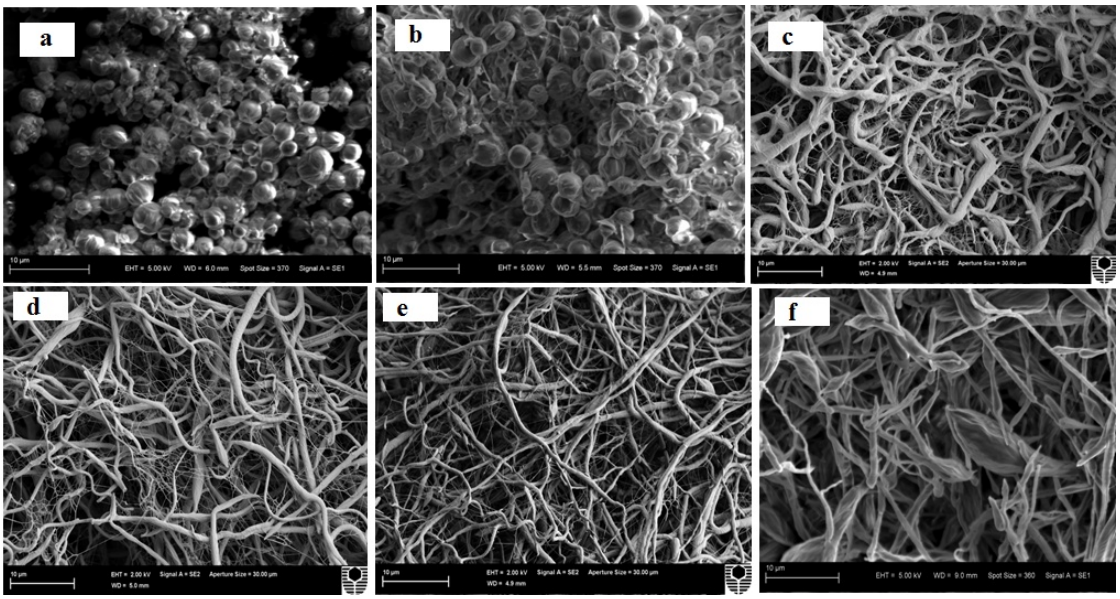

Figure 2-8: SEM micrographs of electrospun PEG fibres using various PEG concentrations: (a) 15%, (b) 20%, (c) 25%, (d) 30%, (e) 35% and (f) 40%. The scale in the micrographs is 10 µm (Haroosh et al., 2011).

From our previous study, Figures 2-8a and b show that using PEG at concentrations of 15 and 20%, respectively, led to the formation bead structures. This is because there is a lower limit to the polymer concentration and viscosity that must be exceeded for successful electrospinning. After all, extensive molecular entanglements are prerequisites for the formation of a stable and continuous charged jet. On the other hand, Figures 2-8c, d and e demonstrate that increasing the PEG concentration to 25, 30 and 35%, respectively, leads to the formation of fibrous structures. Figure 2-8f, shows that when the PEG concentration reaches 40%, the large fibres have inhomogeneous diameters within the mat (Haroosh et al., 2011). Wang et al. (2005) mentioned that a low concentration of hyaluronic acid (HA) of about 2wt%/v cannot facilitate electrospinning because of low viscosity, which means fewer polymer chain entanglements and a large amount of solvent. As a result of this, they showed it is difficult to fabricate tiny fibres just by dropping the polymer concentration (Wang et al., 2005). Spasova et al. (2007) reported that solutions with three various concentrations (5, 7 and 9%) by blending PLLA with PEG were electrospun to produce fibres. It was found that decreasing the solution concentration led to decreasing the average fibre diameter (Spasova et al., 2007). According to Chen et al. (2009), blending of chitosan with collagen at a low polymer solution concentration(less than 4%) makes beads even by varying the applied voltage and the distance between the tip of the needle and the collector. Surface tension influences were dominant with dropping polymer concentration and beaded fibres were created (Chen et al., 2009). Puppi et al. (2010) observed that by increasing the polymer concentration for PLGA the gap between beads on the fibres became bigger and the bead formation moved from round to spindle-shaped, and when the concentration of PLGA was 20wt%/v homogeneous fibres were obtained (Puppi et al., 2010). Dhandayuthapani et al. (2010) demonstrated that at low chitosan concentrations of 4 and 5wt%/v, a nonhomogeneous mat with many beads was created even when the voltage was changed from 10 to 25 kV. This was due to the low viscosity of the polymer solution. Conversely, they mentioned that the flow properties of the solution are affected when the polymeric concentration is very high. Therefore it is necessary to maintain an optimum concentration for the occurrence of chain entanglement (Dhandayuthapani et al., 2010).

2.5.3 Molecular weight of polymers

The selection of a polymer with appropriate molecular weight is essential in electrospinning, especially when used for the control of degradation rate and drug release from the electrospun fibre mat (Ignatious et al., 2010; Cao et al., 2010). When the polymer is dissolved in the solution, it may degrade if stored for a long time and the molecular weight of the polymer will drop quickly in due course (Cantón et al., 2010). When a high electrical voltage is applied, small droplet formation occurs for jets of low molecular weight solution (Gu et al., 2009; McKee et al., 2004). Blending polymers with lower molecular weight decreases the viscosity of the solution without reducing the concentration (Um et al., 2004). Duzyer et al. (2011) evaluated the impact of the polymer molecular weight on electrospun poly(ethylene terephthalate) (PET) fibre mats and their mechanical properties as a function of the linear velocity of the collecting drum They reported that the polymer molecular weight and mechanical properties of the electrospun PET fibre mats were associated with the linear velocity of the collecting drum (Duzyer et al., 2011). According to Chuangchote (2009), low molecular weight poly(vinyl pyrrolidone) PVP at a higher concentration showed slightly smaller fibre diameter than higher molecular weight PVP. The electrospinning of low molecular weight PVP produced flat and non-uniform fibre mats compared with high molecular weight PVP. They attributed this to the charged jet from the high molecular weight PVP being elongated through bending instability, which is less than that from the low molecular weight PVP (Chuangchote et al., 2009). Liu et al. (2009) electrospun different molecular weights of Poly[(lactic acid)-co-(glycolic acid)] PLGA nanofibres at fixed process conditions, such as an applied voltage about 20 kV and flow rate around 1 mL/h. For lower molecular weight PLGA (15000 g/mol), bead structures were observed, resulting from the low viscosity of the polymer solution. Finer fibres beside many bead structures were also observed when the molecular weight was increased to 28000 g/mol. Additional increase in the molecular weight of PLGA to 45000 g/mol could produce small spindle structures with some fibres. When the molecular weight was 57000 g/mol or higher, homogeneous fibrous mats were formed (Liu et al., 2009a). Srikar et al. (2008) mentioned that low molecular weight poly(methylmethacrylate) PMMA at concentration 15 wt%/v could not be electrospun due to its low viscoelasticity, which

affects the spinnability. In addition, the data obviously pointed out the significant influence of molecular weight on the drug release speed. The effect of initial polymer concentration on drug release speed is considerably weaker than the influence of the molecular weight (Srikar et al., 2008). According to Wang et al. (2010), the low molecular weight polymer PEG-b-poly(α-hydroxyoctanoic acid) PEG-PHOA with a small degree of polymerization is not suitable for electrospinning apparently due to its low viscosity. As a result, researchers often use PEG-PHOA as a modifier in the electrospinning process by blending it with high molecular weight poly(ethylene glycol)-b-poly(L-lactide) PEG-PLLA. In addition, by incorporating a small amount of low molecular weight polymer with a high molecular weight polymer, fibre degradation and captured drug release from the fibre might be well controlled (Wang et al., 2010c).

2.5.4 Conductivity

It is well recognized that solution conductivity is one of the most significant factors controlling fibre diameter and distribution (Meng et al., 2010; Arumugam et al., 2009). The decrease in the solution electrical conductivity influenced the splitting of the charged jet in the electrostatic field. Usually, when the electrical conductivity increases, the additional electric charges are carried by the electrospinning jet. As a result, higher elongation powers are inflicted to the jet over the electrical filed (Liu et al., 2010b). The droplet of polymer solution at the needle, which is connected to an electrical pole, converts the solution into a Taylor cone (Meng et al., 2010). When the tensile strength becomes higher than the droplet surface tension, a solution jet will be ejected from the droplet. It undergoes a stretching process (Chen et al., 2010) and whipping in the atmosphere. Finally, after the solvent has evaporated, the jet is converted into a fibre on the collector. Hence, a high solution electrical conductivity holds a large charge leading to greater tensile force which enhances jet splitting and stretching, leading to small fibre diameters (Alipour et al., 2009). However, a broader jet is ejected by large tensile force leading to larger fibre diameters at high solution flow rate (Zamani et al., 2010). When the fibres are too thin due to high electrical potentials of the solutions, the fibres could break down due to their low mechanical strength, which may not sustain the weight of

the fibres along the distance between the needle tip and the collector (Yang et al., 2007b).

The addition of ions can increase the electrical conductivity of the solution and also the fibre diameter is affected by the ions' size. For example, potassium and phosphate ions have bigger radii than sodium and chloride ions (Zong et al., 2002b; Zong et al., 2002a). A high mobility in response to an external electric source can be achieved when ions have smaller atomic radii with a higher charge density. Furthermore, many studies have shown that the final fibre diameter is affected by incorporating salts into the polymeric solution and that different types of salts have diverse effects (Zong et al., 2002b). The incorporation of a small amount of salt increases the charge density in the split jets. The use of salt is reported to have strong effects on the morphology of electrospun fibres, thus altering the fibres from a bead structure to a uniform structure, and also decreasing the nanofibre diameters (Charernsriwilaiwat et al., 2010). For instance, the addition of an organic salt such as pyridiniumformate (PF) into the polymer solutions led to a decreased amount of bead formation in the fibre mats due to the significantly increased conductivity of the solutions (Arayanarakul et al., 2006). The use of salts in polymer solutions is a well-recognized technique to enhance solution spinnability. For example, the fibre diameter of polyhydroxybuterovalerate (PHBV) was decreased from a range of 1–4 µm to less than1µm when organosoluble trialkylammonium chlorides were added to the polymer solution. In addition, to show electrostatic repulsions, NaCl has been dissolved in the polymer solutions of polyelectrolyte (Arumugam et al., 2009). On the other hand, there was an increase in fibre uniformity and solution conductivity when NaCl and $CaCl_2$were employed in a polymeric solution of poly(2-acrylamido-2-methyl-1-propanesulfonic acid) (Arumugam et al., 2009). However, Jeong et al. (2010) found that a high amount of PEO demonstrated much lower conductivity, which can lead to uniform electrospun nanofibres (Jeong et al., 2010). Moreover, Beachley and Wen (2009) found that the surface charge density of the solution jet and the conductivity of the solution have increased by using additional NaCl salt in the PCL solution. When a rotating drum was employed for the collecting device, incorporating salts into the polymer solutions decreased bead formation and fibre diameter. The researchers

mentioned that a low concentration of NaCl added to the polymer solution did not produce any considerable differences in fibre length, uniformity, or diameter (Beachley and Wen, 2009). Nevertheless, Arayanarakul et al. (2006) observed that incorporating a small quantity of inorganic salts such as NaCl, LiCl, KCl, $MgCl_2$, and $CaCl_2$ into the PEO solution gave rise to the formation of non-uniform structures with beaded fibres, except for NaCl. Increasing the salt concentration in PEO solution produced films of fused fibres with occasional attendance of the salt crystals. Furthermore, the moderately low hygroscopicity of NaCl compared with the other salts could be the reason for the result with the PEO solution since NaCl is the only salt that produced fibrous structures. By incorporating filler molecules, like ionic salts and drugs, the conductivity of the spinning solution can be changed and this influences the fibre diameter (Arayanarakul et al., 2006).

2.5.5 Solvents

Appropriate choice of solvent is one of the main factors in producing electrospun polymer fibres and for incorporating drugs into the fibres for use as a drug delivery system (Shen et al., 2011). The solvent system plays a vital dual role during electrospinning. The first role is dissolving the polymer molecules. This is essential for the polymer solution being able to form an electrified polymeric jet. The second role is carrying the molecules of dissolved polymer into the fibre collector to synthesise fibre mats. This allows solvent molecules to quickly vaporize from the polymer fibres. Thus, successful electrospinning can also depend upon the selection of a suitable solvent system (Hsu et al., 2010; Han et al., 2010). Generally, there are various solvent parameters which have a considerable effect on the electrospinning technique such as the dielectric constant of the solvent (Saraf et al., 2009) and polymer solubility in the solvent (Abdul Rahman et al., 2010). The evaporation is affected by many factors such as the initial solution concentration, the solvent boiling point and the charged jet size (Cui et al., 2009). The solvent dielectric constant affects the electrospun fibre diameter and morphology. The bead size and the fibre diameters decrease for high dielectric constant solvents. For example, when the dielectric constant of solvents increased, the diameter of PMMA hollow fibres was reduced slightly, but the hollow wall thickness of

fibres was considerably reduced from 700 to 180 nm. High dielectric constant leads to reduced fibres diameters due to a high repulsive force in a thin jet lead to splitting resulting in more thinning of the jet (Lee et al., 2010). Additionally, acids can serve as the co-solvent or solvent, and sometimes they are used to enhance the solution conductivity. For example, formic and acetic acid were employed as solvents for gelatin and chitosan, respectively; whereas camphorsulfonic acid and HCl were used in small amounts in the solutions as co-solvents (Arumugam et al., 2009).

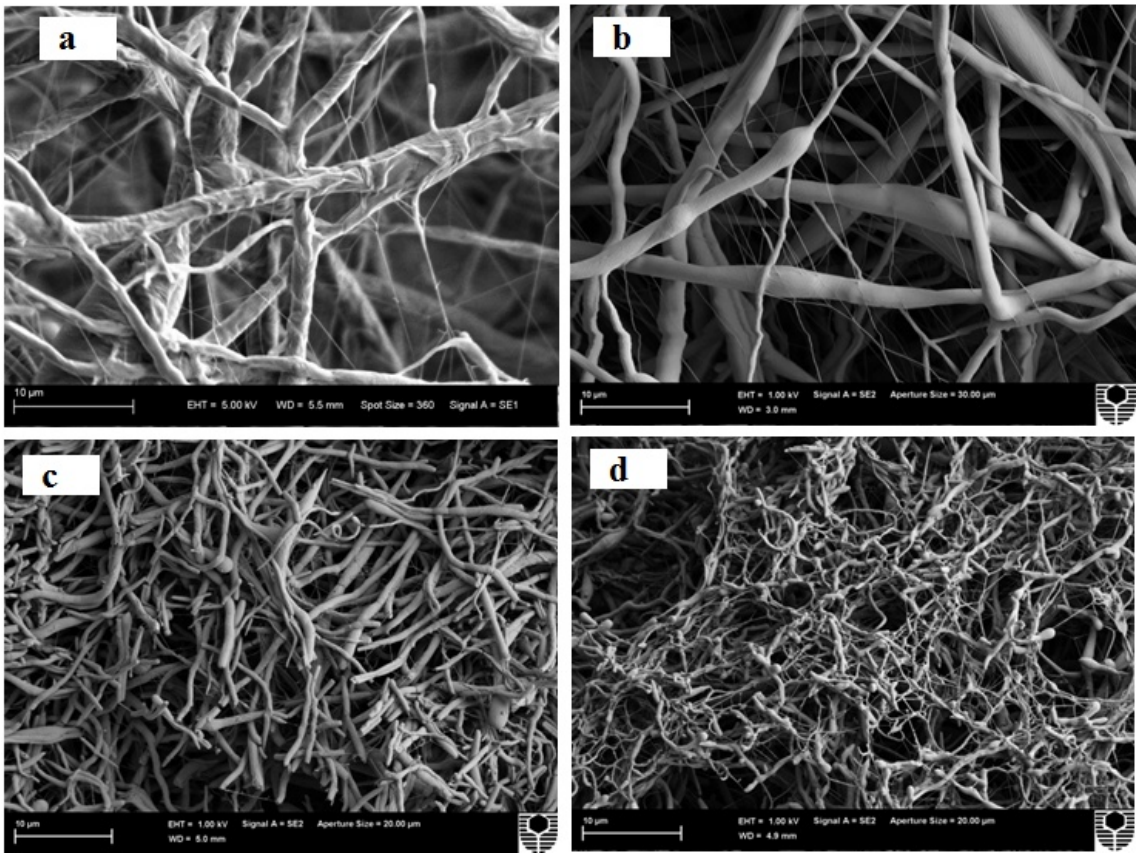

Figure 2-9: SEM micrographs of electrospun PEG fibres for 35% PEG concentration and various ratios of chloroform: methanol: (a) 1:0, (b) 3:1, (c) 1:1 and (d) 1:2. The scale in the micrographs is 10 µm (Haroosh et al., 2011).

From our previous study, Figures 2-9a to d show the effect of various ratios of chloroform to methanol. When the chloroform to methanol ratio was 1:0 (i.e. pure chloroform), a uniform fibre structure with a large average diameter of 870 nm was produced. By increasing the amount of methanol to give a chloroform: methanol ratio of

3:1, the average large fibre diameter decreased to 703 nm. Further increasing the amount of methanol to a 1:1 ratio resulted in broken fibres, and the average fibre diameter also decreased to 395 nm. When the ratio of chloroform to methanol was reduced even further to 1:2, fibres were produced with some beads, and the average fibre diameter was reduced to 301 nm (Haroosh et al., 2011). In Qian et al. (2010) work, they studied the dissolving ability of PMMA to create electrospun fibres. The low boiling point solvents such as dichloromethane (CH_2Cl_2) at 40°C and chloroform ($CHCl_3$) at 62°C facilitate rapid evaporation following jet splitting, leading to the production of fibres with internal pores. In addition, they showed that solidification is considerably influenced by the volatilities of the solvents. The relatively low solvent volatility of the electrospun PMMA fibres also affected the fibre morphology. The quite high molecular weight of the 1,1,1,3,3,3-hexafluoro-2-propanol (HFIP) solvent that was used to dissolve the PMMA polymer caused incomplete evaporation of the solvent while producing fibres (Qian et al., 2010). Jiang et al. (2004) demonstrated partial aggregation of the fibres when they reached the collecting plate due to the low volatility of dimethyl sulfoxide (DMSO) as a considerable quantity of the solvent stayed on the fibres (Jiang et al., 2004). Another study revealed that when tetrahydrofuran (THF) was used as a solvent for polystyrene (PS), the PS fibres created an unexpected half hollowed spherical arrangement. Furthermore, the quantity of beads on the fibre mats were controlled by changing the ratio of dimethylformamide (DMF) to THF (Arayanarakul et al., 2006). The surface tension and volume fraction dropped with increasing the DMF ratio, but the dielectric constant and solution conductivity increased (Lee et al., 2003b, Zamani et al., 2010). According to Shen et al. (2011), the solution remained for a longer period in a jet state due to the lower evaporation of N,N-dimethylacetamide (DMAc). That low evaporation led to thin fibres because it permitted the solution to undergo a longer drawing period under the electrical voltage in the instability area (Shen et al., 2011). However, Kim et al. (2008) demonstrated that the majority of fibres were broadly interconnected because of the DMF, which had a slow evaporation rate, and that fibre interconnection was reduced by decreasing the DMF ratio. They showed that a stable nanofibre mat with an average diameter of 198 ± 45 nm was achieved when the hyaluronic acid (HA) concentration was 10 wt% and the NaOH: DMF volume ratio was

4:1 (Kim et al., 2008). Furthermore, the incomplete evaporation of solvents from dilute polymer solutions is associated with bead formation in electrospinning. For example, it is found that low concentrations of DMF solution of a polyurethaneurea created a fibre-bead morphology and that the created beads were attributed to low polymer solution viscosity and solvent evaporation (Verreck et al., 2003b). It is believed that the high dielectric constant of water produces ultrafine fibres with an extremely thin diameter, but the very high surface tension of water affects the solution jet and in many cases hinders the generation of fibres by forming spherical beads. The reduction of surface tension can be achieved by mixing water with solvents that have lower surface tension. One study reported that uniform fibres could be achieved by raising the ethanol ratio for a water-ethanol co-solvent in a poly(ethylene oxide) (PEO) solution, which is attributed to the decrease in the surface tension of the solution (Chuangchote et al., 2009). Another study mentioned that hyaluronic acid (HA) dissolves in water quickly, but it does not dissolve in the majority of organic solvents. Therefore, a water-ethanol co-solvent was employed to dissolve HA so as to increase the evaporation rate and to reduce the surface tension of the HA solution, which in turn could produce electrospun fibres without beads (Li et al., 2006).

2.6 Drug delivery

The use of biodegradable polymers as carriers for drug had established various applications in biomedical areas (Cui et al., 2006). The major benefit of this system is that biodegradable polymers in the delivery systems do not need to be removed from the body at the end of the healing time because they degrade into physiologically occurring compounds that are easily emitted from the body (Im et al., 2010b). In addition, this system has some benefits, like non-toxic degradation in the body, and sustained release of encapsulated drugs (Yang et al., 2007a; Han et al., 2009), and it does not cause bad effects in the surrounding tissue (Liu et al., 2010a). Due to the increased surface area of the carrier and drug, the speed of drug uptake by the human body could be enhanced with reduction of size of the carrier and drug assembly. Therefore, drug delivery systems have been built up by employing polymeric materials in the shape of micelles, nano/microparticles and hydrogels. In addition, a broad range of polymers, fabrication

systems, and polymer processing methods have been investigated in various geometries for loading drug molecules into delivery media (Cui et al., 2006). Recently, the incorporation of drugs into electrospun nanofibres has gained attention because this system has good structural stability and higher efficiency of drug encapsulation than other drug delivery media (Haroosh et al., 2014). Generally, the chemical and physical properties of diverse drugs influence the ability for loading them into fibres (Xu et al., 2010). The drug release from nanofibre mats can be controlled by the modulation of fibre morphology, polymer composition, dosage amount, and drug loading method. The large surface area to volume associated with electrospun fibre mats permits solvent evaporation (Kim et al., 2010), giving the loaded drug a limited period to recrystallise, with the preference to form amorphous dispersion (Qi et al., 2010). The nanofibre's porous structure and extremely small diameter also assist efficient drug release (Jannesari et al., 2011).

Hence, this system offers site-specific drugs delivery from the scaffold into the body (Kenawy et al., 2002) and could be applicable in wound therapeutics and treatments for skin (Verreck et al., 2003b). In the wound therapeutic field in cooperation with topical delivery systems, biocompatibility with the nature of the drug release is significant for successful treatments (Verreck et al., 2003b). In addition, in wound healing, it is used to avoid the decomposition of a labile compound in harsh surroundings, and also to carry a drug in a sustained method (Zhang et al., 2006).

Loading a drug into the polymer solution influences solution properties such as viscosity, surface tension and conductivity. Moreover, the position of the drug inside electrospun fibres affects the release characteristics (Buschle-Diller et al., 2007). The fundamental requirement for controlled release drug treatment includes the delivery of a fixed quantity of drug in a particular time span. The benefit of drug release methods is to enhance the efficiency of drug treatment. This enhancement is able to increasing the therapeutic activity compared to the intensity of side effects, reducing dosage of drug needed through the healing, or eliminating the requirement for the particular drug (Xu et al., 2008). Drug release from polymer mats could happen by different mechanisms such

as drug diffusion within the polymer, mat erosion and sometimes by both mechanisms. This release is influenced by a range of aspects like carrier morphology, drug physicochemical properties, crystallinity, molecular weight, drug–nanofibre mat interaction and polymer composition (Zamani et al., 2010). It is very difficult to predict the mechanism leading to the drug release kinetics from biodegradable polymers due to the variations in polymeric properties through degradation, and interfusion between permeability and diffusivity of the drug with time (Puppi et al., 2010). Polymer fibres are able to offer drug release at fast, immediate or slow speeds, depending on the polymer carriers employed and any incorporated stabilizers (He et al., 2006). Furthermore, the interaction between carrier (polymer) and drug plays an important role in controlled drug release (Zhang et al., 2006). This chemical interaction can block the crystallization of the drug in the nanofibres and may establish constant drug release in crystalline state (Natu et al., 2010). Hydrophobic drugs including clindamycin, ciprofloxacin, and cephalexin can be simply incorporated with hydrophobic polymers. However, hydrophilic drugs cannot be embedded into hydrophobic polymers due to weak interactions between them, and thus the drug release rate may not be controlled (Xu et al., 2010). Table 2-2 outlines some of the previous studies into electrospun systems for drug release applications.

Table 2-2: Some of the previous studies into electrospun systems for drug-release applications.

Electrospun mat	Drug	Reference
PVP	Ketoprofen	(Yu et al., 2010)
PLLA	Clarithromycin	(Wei et al., 2010)
PEO	Rhodamine	(Kim et al., 2010)
PDLLA	Tetracycline and chlorotetracycline	(Xie and Buschle Diller, 2010)
PLGA	Mefoxin	(Kim et al., 2004)
PEG-PLA	Doxorubicin hydrochloride	(Xu et al., 2008)
PEG-PLLA	Ibuprofen	(Wang et al., 2010c, Cantón et al., 2010)
PELA-HPCD	Hydroxycamptothecin	(Xie et al., 2010)
Gelatin	Centellaasiatica-herbal extract	(Sikareepaisan et al., 2008)
Cellulose acetate	Vitamin A and E	(Tungprapa et al., 2007)

Natu et al. (2010) noticed that drug dissolution was the predominant mechanism of drug release. Fibres with low drug loading presented sustained release in contrast to high drug loading which had a burst release. Those drug crystals in the fibre shell and even in the fibre core were not completely encapsulated and were immediately released (Natu et al., 2010). Verreck et al. (2003) have reported the applicability of electrospinning for poorly soluble drugs for transdermal and oral delivery. They mentioned that a poorly soluble drug, itraconazole, was loaded into hydroxypropylmethylcellulose (HPMC) by using dichloromethane with ethanol as co-solvents for the drug and polymer. The amount of itraconazole to the polymer played an important role on the drug release from the nanofibre mats. In addition, it was found that the drug presented in the amorphous form from the thermal analysis data (Verreck et al., 2003a). Cantón et al. (2010) has shown achievement of gradual release of Ibuprofen from biodegradable nanofibres of wound dressings without affecting wound healing. A biodegradable dressing is extremely attractive for the healing of this kind of wound because it does not need to be removed after wound healing (Cantón et al., 2010). Liu et al. (2010) mentioned that collagen/

PLGA nanofibre group was obviously quicker than those of the gauze group and the commercial dressing group in wound healing and drug delivery areas. The electrospun nanofibre mats might begin to rapidly signal the pathway and draw fibroblasts to the dermis layer that can excrete vital extracellular mat components such as collagen and growth factors to mend injured tissue (Liu et al., 2010a).

2.7 Summary

In summary, electrospinning has been recognized to be a sophisticated method for manufacturing ultrathin micro/nanofibres using a broad range of polymeric materials or composites. There has been a significant increase in the study of electrospun fibres in the drug delivery field in recent years. Due to their biocompatibility, degradation without side effect and good mechanical properties, biodegradable polymers are excellent candidates for a number of applications in biomedical fields (Wei et al., 2010). A biodegradable polyester polymer PLA has some attractive properties, including easy processability, biocompatibility, degradation to form nontoxic monomers and the ability to be dissolved in common solvents (Deng et al., 2007). In addition, the monomeric units of lactic acid split up in the human body, and are naturally in the carbohydrate metabolism (Kim et al., 2010). These properties made PLA very suitable for various biomedical purposes. However, the efficiency of using PLA fibre as a drug carrier is too low because it is associated with burst drug release at the commencement of healing (Kim et al., 2010) and with its brittleness and slow crystallization (Chow et al., 2012). In addition, the degradation of PLA mat is harmful to local tissues (Touny et al., 2010) because of its low pH value. On the other hand, PCL degrades slowly compared with PLA (Huang et al., 2006). Moreover, it is not harmful to local tissues because it does not form an acidic environment like PLA. However, the slow degradation, poor porosity and semi-crystalline nature of PCL inevitably limits its usage in drug delivery. PCL with high crystallinity easily restricts the mobility of drug molecules so they tend to stay on the fibre surfaces. Polymer blends show extremely unusual properties compared with individual polymers. Electrospinning is not a straightforward technique because it is affected by both the processing parameters and the solution properties (Zhang et al., 2005). The nanofibre properties and morphology thus effectively depend on the solution

properties and the parameters of electrospinning. Investigating the effects of the parameters on the electrospun fibres is challenging owing to the interaction between the solution and processing parameters (Biber et al., 2010). Among the electrospinning parameters, the solution concentration (Yao et al., 2007), viscosity, electrical conductivity (Wei et al., 2010), polymer molecular weight and choice of solvent (Buschle-Diller et al., 2007) are the most effective variables to control fibre morphology and diameter. To manipulate electrospinning parameters, many studies need to be carried out in order to achieve the desired crystallinity, fibre diameter, molecular structure, and morphology (Ribeiro et al., 2011).

Controlled drug delivery systems have received great attention in the last decades (Kenawy et al., 2009). Electrospun nanofibre drug carriers have been highly considered, as this system presents good structural stability and a higher efficiency of drug embedding than other drug delivery carriers. The drug release from fibre mats can be controlled by changing the polymer composition, drug loading method, dosage amount, and morphology. Hydrophobic drugs can be efficiently embedded in hydrophobic polymers. However, hydrophilic drugs cannot be embedded into hydrophobic polymers due to weak interactions between them, and the drug release rate cannot be controlled (Xu et al., 2010). Polymer nanocomposites have attracted significant interest due to their unique structures and customisable properties, which cannot be achieved by normal materials (Liu et al., 2008b). HNTs have a high dispersion characteristics compared to other natural silicates, and also have the ability to produce hydrogen bonding (Du et al., 2008). HNTs are useful in various areas because of their unusual geometric form, surface properties and chemical formation (Jia et al., 2009). Magnetic nanoparticles Fe_3O_4 have low toxicity and are acceptable in the human body (Yang et al., 2006). Due to their high surface area to volume ratio, Fe_3O_4 nanoparticles tend to agglomerate with each other to reduce their energy. So far magnetic nanoparticles-polymer system are still under investigation for novel applications (Guo et al., 2009b).

Chapter 3
Materials, Methodology, and Characterisation

3.1 Materials

3.1.1 Biopolymers

Two different types of hydrophobic polymers (PLA and PCL) were selected for the purpose of blending them together and using the resulting mixture in electrospinning experiments. PLA and PCL are both polyesters where the monomers are related by having the same ester functional group.

3.1.1.1 Poly(lactic acid) (PLA)

Poly(lactic acid) (PLA) is a compostable polymer obtained from sustainable sources, mostly from corn, sugar beets, sugarcanes and wheat. PLA belongs to the group of aliphatic polyesters obtained from α-hydroxy acids (Lim et al., 2008; Fowlks and Narayan, 2010). Despite PLA having limitations of brittleness and low degree of crystallinity, it is still widely used due to its biocompatibility, sustainability, ability to be formed into a fabric and biodegradability (Chow et al., 2012). PLA 3051D pellets were supplied by NatureWorks, USA and used without any purification. The detailed specifications are shown in Table 3-1.

Table 3-1: Physical and thermal properties of PLA.

Product	Molecular weight	Colour	Melting temperature T_m	Glass transition temperature T_g
PLA (3051D)	93,500 g/mol	White	145-155°C	55-65°C

3.1.1.2 Poly(ε-caprolactone) (PCL)

PCL is a hydrophobic, semi-crystalline polyester, which makes it degrade slowly and have a low porosity. The aliphatic polyester bond undergoes biodegradation in vivo without generating a local acidic environment and toxicity. The biodegradation is due to the vulnerability of its aliphatic ester bond to hydrolysis (Sun and Downes, 2009; Kweon et al., 2003). Low molecular weight PCL (MW = 33,000 g/mol) was purchased from Daicel Chemical Industries Ltd, Japan, while high molecular weight PCL (MW = 80,000 g/mol) was obtained from Sigma-Aldrich. Both were used without any purification. The properties are detailed in Table 3-2.

Table 3-2: Physical and thermal properties of PCL.

Product	Molecular weight	Colour	Melting temperature T_m	Glass transition temperature T_g
PCL	80,000 and 33,000 g/mol	White	≈ 60°C	≈ –60°C

3.1.2 Nanoparticles

Nanocomposite technology is used to tailor material properties to be suitable for specific applications by incorporating nanoparticles into polymers (Lee et al., 2003, Fowlks and Narayan, 2010). Two different kinds of nanoparticles, Halloysite nanotubes (HNT) and Magnetic nanoparticles (MPs), which have different compositions, shapes, sizes and properties, have been incorporated into PLA: PCL blends for the purpose of the enhancement of their performance capabilities.

3.1.2.1 Halloysite nanotube (HNT) and 3-aminopropyltriethoxysilane

The halloysite nanotubes (HNTs) belong to the kaolin group of clay minerals, with a composition of $Al_2Si_2O_5(OH)_4.H_2O$. They disperse well and have the ability to form hydrogen bonds. The HNT elemental composition (wt %) is listed as follows: SiO_2, 49; Al_2O_3, 34.8; Fe_2O_3, 0.35; TiO_2, 0.12; Na_2O, 0.25; MgO, 0.15 (Ismail et al., 2008). The dimensions of HNT are about 300–1500 nm in length, 15–100 nm for the inner diameter

and 40–120 nm for the outer diameter (Carli et al., 2011). The halloysite nanotubes were obtained from Imerys Tableware Limited, New Zeal and 3-aminopropyltriethoxysilane (ASP) $H_2N(CH_2)_3Si(OCH_3)_3$ was used as modifier for the HNT and was purchased from Sigma-Aldrich Ltd.

3.1.2.2 Magnetic nanoparticles (MPs)

Magnetic nanoparticles (Fe_3O_4) were employed to synthesize nanocomposites for biomedical applications because they have good biocompatibility and low toxicity that can be well accepted in the human body (Yang et al., 2006). Additionally, these Fe_3O_4 nanoparticles were selected owing to their comparatively higher stability in air than metal nanoparticles, as well as because they can carry more charges (Zhang et al., 2009).

Pure MPs and Impure MPs were synthesized in the laboratory by using iron sulphate, iron nitrate, sodium hydroxide, and lauric acid. All these materials were purchased from Sigma-Aldrich Ltd.

3.1.3 Solvents

Choosing a suitable solvent system is essential for the success of electrospinning. Dichloromethane (DCM), dimethylformamide (DMF), chloroform, acetone and methanol were used as solvents. They were purchased from Sigma-Aldrich Ltd and were used without any purification. The detailed properties of the solvents are shown in Table 3-3. Phosphate buffer solution (PBS) acted as a medium of drug release and was also purchased from Sigma-Aldrich Ltd.

Table 3-3: Properties of solvents used in the electrospinning method (Bhardwaj and Kundu, 2010).

Solvent	Dielectric constant	Boiling point (°C)	Density (g/ml)	Surface tension (mN/m)
Chloroform	4.8	61.6	1.498	26.5
Acetone	21	56.1	0.786	25.2
DCM	9.1	40	1.326	27.2
DMF	38.3	153	0.994	37.1
Methanol	33	64.5	0.791	22.3

3.1.4 Drugs

3.1.4.1 Tetracycline hydrochloride (TCH)

TCH ($C_{22}H_{24}N_2O_8 \cdot HCl$, MW=480.9 g/mol) is hydrophilic antibiotic drug and was chosen as a model drug. It was purchased from Sigma-Aldrich Ltd and used without any purification. The chemical structure is revealed in Figure 3-1.

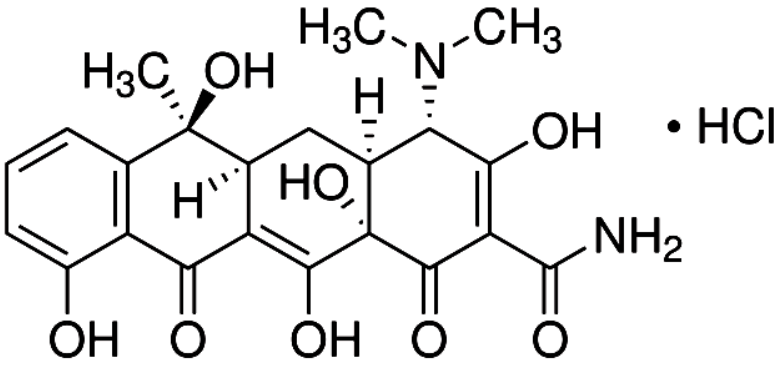

Figure 3-1: Chemical structure of model antibiotic drug TCH (tetracycline hydrochloride) (Buschle-Diller et al., 2007).

3.1.4.2 Indomethacin (IMC)

IMC ($C_{19}H_{16}ClNO_4$, MW=357.79 g/mol) is hydrophobic non-steroidal anti-inflammatory drug and was chosen as another model drug. It was purchased from Sigma-Aldrich Ltd and used without any purification. The chemical structure is given in Figure 3-2.

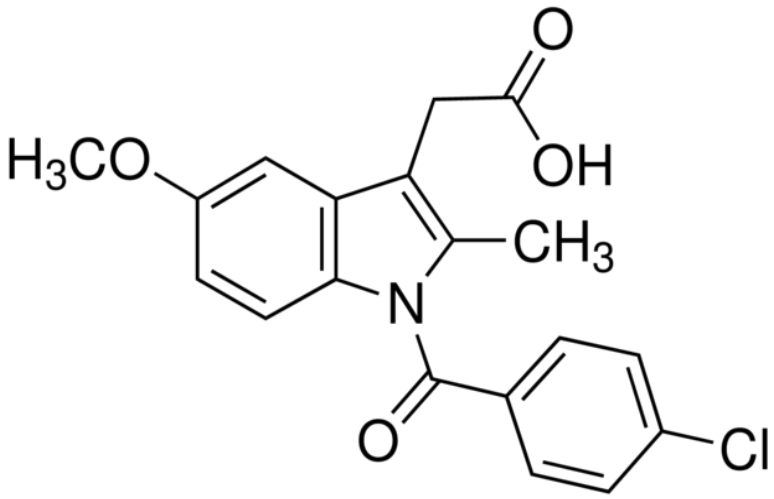

Figure 3-2: Chemical structure of model drug IMC (Indomethacin) (Chennamaneni et al., 2012).

3.2 Research methodology

3.2.1 Processing techniques

Solution variables such as viscosity, solution concentration and electrical conductivity play very important roles in the electrospinning technique. In addition, they have a great impact on fibre diameters and the degree of crystallinity. For this reason, the focus of this study was on the solution parameters, while the process parameters remained constant for all experiments.

3.2.1.1 Electrospinning rig setup

The electrospinning rig consists of four main components including a ground collector, a Fusion 100 syringe pump (Chemyx Inc., Stafford, TX, USA) to automatically control the solution flow, a spinneret and the positive electrode of a ES30P–5Whigh voltage

power supply (Gamma High Voltage Research, Ormond Beach, FL, USA), as illustrated in Figure 3-3.

During the electrospinning process, the solutions were ejected using a 10 ml syringe pump with a 20G metallic needle (0.584 mm in inner diameter). The flow rate of polymer solution was set at 2 ml/h, and the applied positive voltage setting was in the range of 25–28 kV. The electrospinning process was carried out at 24ºC. The resulting fibres were collected on a flat aluminium foil sheet covering a mesh collector. The distance between the needle tip and the collector was 13 cm. The thickness of fibre mats ranged from 300 to 500 µm.

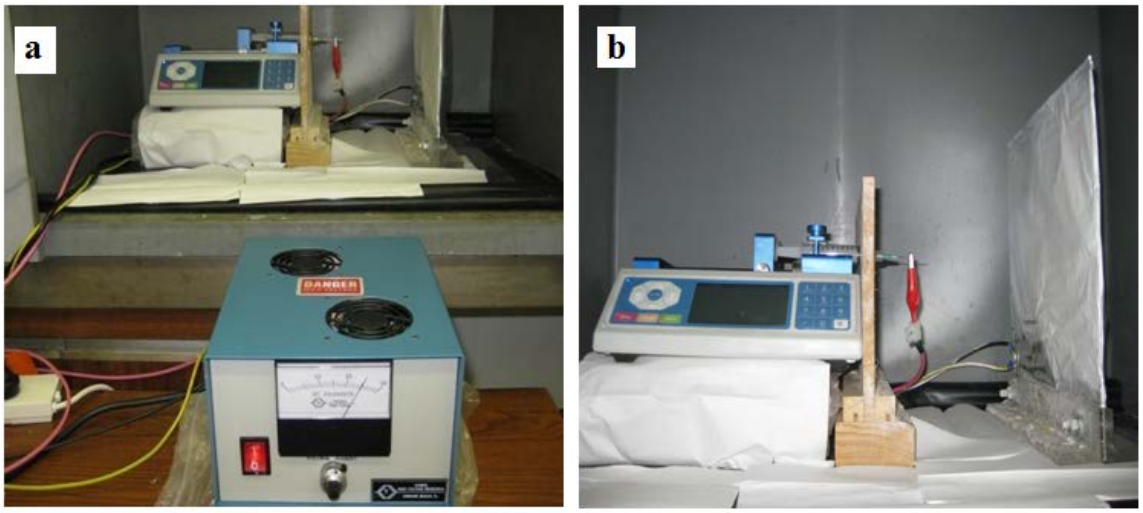

Figure 3-3: Laboratory-scale electrospinning apparatus (a) a wider shot of the voltage suppler, pump, needle and collector and (b) a closer shot of the pump, needle and collector.

3.2.1.2 Polymer solution preparation and blending

Electrospinning was carried out using an 8wt%/v solution of PLA mixed with one of three PCL solutions: 9 wt%/v high molecular weight (HMW) PCL solution, 15wt%/v high molecular weight PCL solution and 15wt%/v low molecular weight (LMW) PCL solution. The PLA and PCL solutions were mixed at different blending ratios of 1:0, 3:1, 1:1, 1:3 and 0:1 v/v with three solvents, namely a DCM: DMF mixture blended at 3:1

v/v, a chloroform: methanol mixture blended at 2:1 v/v and a chloroform: acetone mixture blended at 2:1 v/v, as summarised in the Table 3-4. The mixing took place at room temperature in a bench top orbital shaking incubator for about 3 h.

Table 3-4: The material formulations.

No.	Polymer composition(wt%/v)	PLA to PCL blend ratio (v/v)	Co-solvent type and composition (v/v)
1	8%PLA: 15% HMW PCL	(1:0),(3:1),(1:1),(1:3) and (0:1)	DCM: DMF (3:1)
2	8%PLA: 15% LMW PCL	(1:0),(3:1),(1:1) and (1:3)	DCM: DMF (3:1)
3	8%PLA: 15% HMW PCL	(1:0),(3:1),(1:1) and (1:3)	Chloroform:Methanol (2:1)
4	8%PLA: 15% LMW PCL	(1:0),(3:1),(1:1) and (1:3)	Chloroform:Methanol (2:1)
5	8%PLA: 15% LMW PCL	(1:0),(3:1),(1:1) and (1:3)	Chloroform:Acetone (2:1)
6	8%PLA: 9% HMW PCL	(1:1)	Chloroform:Methanol (2:1)

3.2.1.3 Halloysite nanotube (HNT) solution preparation, modification and loading

In order to modify HNT by using ASP, 2 ml of ASP was initially dissolved in 30 ml of chloroform: methanol co-solvent. About 2 g of HNT powder was added to the ASP solution and the suspension was sonicated for 1 h at room temperature. The suspension was then heated at 120°C for 6 to 8 h by using a magnetic stirrer coupled with a hot-plate. The deposited HNT-ASP in the resulting mixture was filtered and thoroughly washed twice with chloroform: methanol, and then dried for 24 h at 120°C to ensure the removal of all solvents. Meanwhile the unmodified HNT were sonicated separately in the chloroform: methanol solvent for 1 h and the suspension was then heated and dried using the same method as for the modified HNT. Different HNT contents were added at

1wt%/v and 2wt%/v to the polymer solution (8 wt%/v of PLA blended with 15 wt%/v solution of PCL at a 1:1 volume ratio) and were mixed and sonicated for additional 2 h.

3.2.1.4 Magnetic particles (MPs) synthesis and loading

Iron sulphate ($FeSO_4$) and iron nitrate ($Fe(NO_3)_3$) were dissolved in deionised water to make an aqueous solution with molar ratio 2 Fe(III) to 1 Fe(II). Under vigorous stirring for 1 hour at 80°C, 1 molar solution of NaOH was added dropwise to achieve a solution with pH =12. A black precipitate formed, indicating the presence of magnetite. The black precipitate was dried without any purification to get impure MPs. To produce pure MPs, 1 ml of lauric acid was added to the solution to coat the MPs then the precipitate was centrifuged and washed with deionised water several times. Finally, the powders were dried.

The pure and impure MPs were added at 0.01, 0.1 and 1wt%/v to the polymer solution (8 wt%/v of PLA blended with 15 wt%/v solution of PCL at a 1:1 volume ratio), mixed using ultrasonication for 2 h and then the solutions were used in electrospinning.

3.2.1.5 Drug preparation and loading to electrospun fibrous mats

For the purpose of the drug release study, TCH was added to the mixture of different polymer and nanocomposite solutions. Firstly, 1 and 5wt% of TCH (calculated according to the weight of polymer) was dissolved in methanol using an orbital shaking incubator and then it was mixed with the blended polymer solution (8 wt%/v of PLA mixed with 9 and 15 wt%/v PCL at blending volume ratio of 1:1).

Secondly, 5wt% of TCH was mixed with 0.1and 1 wt%/v of pure MPs for 2 h in methanol by using the ultrasonication method and then added to the polymer solution (8 wt%/v of PLA blended with 15 wt%/v solution of PCL at a 1:1 volume ratio).

Thirdly, 5wt% of TCH was combined with 1 wt%/v of modified HNT for 2 h to make HNT adequately dispersed in the TCH by using methanol as a solvent and an incubator for the mixing process. After that, the TCH/HNT was blended with the polymer solution

(8 wt%/v of PLA blended with 15 wt%/v solution of PCL at a 1:1 volume ratio). Figure 3-4 shows a variety of mixtures containing TCH used in the electrospinning experiments.

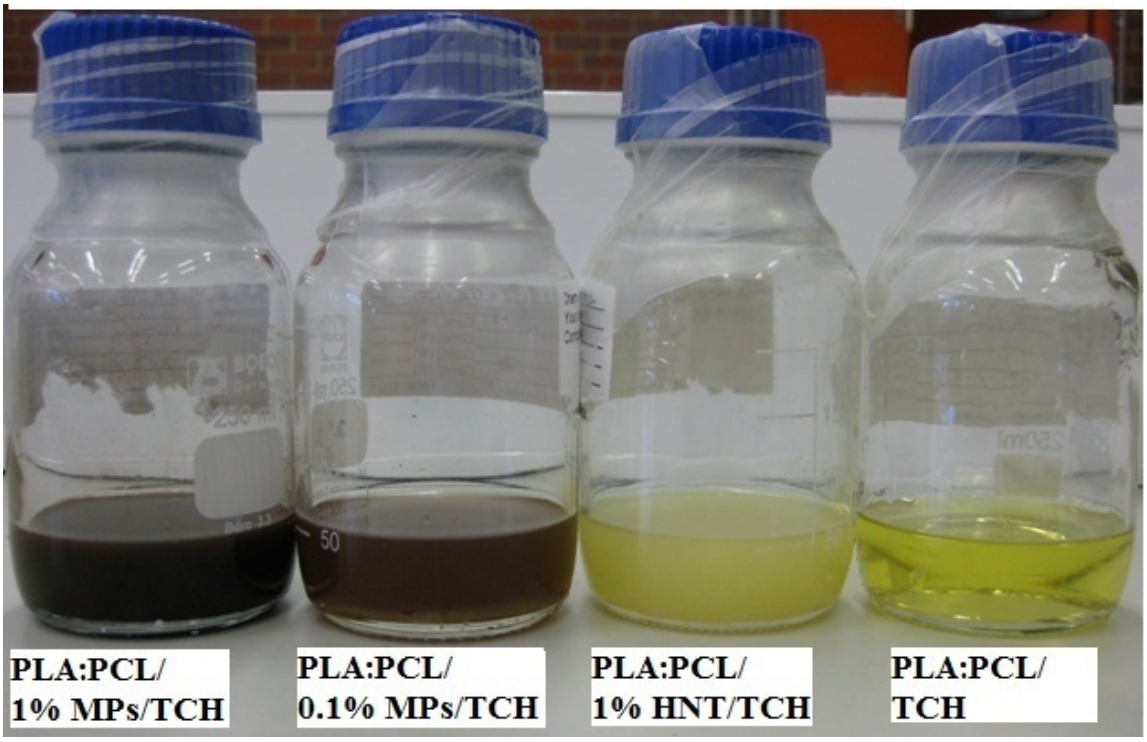

Figure 3-4: Hybrid composite solutions with TCH drug.

IMC at 5wt% was dissolved in methanol using an orbital shaking incubator and then mixed with the blended polymer solution (8 wt%/v of PLA mixed with 15 wt%/v PCL at blending volume ratio of 1:1), as summarised in the Table 3-5.

Table 3-5: The material formulations with drug.

No.	Polymer composition (wt%/v)	PLA to PCL blend ratio (v/v)	Co-solvent type and composition (v/v)	Drug type and concentration (wt/wt)
1	8%PLA: 9% HMW PCL	(1:1)	Chloroform:Methanol (2:1)	1% TCH
2	8%PLA: 9% HMW PCL	(1:1)	Chloroform:Methanol (2:1)	5% TCH
3	8%PLA: 15% HMW PCL	(1:1)	Chloroform:Methanol (2:1)	5% TCH
4	8%PLA: 15% LMW PCL	(1:1)	Chloroform:Methanol (2:1)	5% IMC
5	8%PLA: 15% HMW PCL/ 0.1% MP	(1:1)	Chloroform:Methanol (2:1)	5% TCH
6	8%PLA: 15% HMW PCL/ 1% MP	(1:1)	Chloroform:Methanol (2:1)	5% TCH
7	8%PLA: 15% HMW PCL/ 1% HNT-ASP	(1:1)	Chloroform:Methanol (2:1)	5% TCH

3.2.1.6 In vitro drug release study

A drug-loaded fibre mat sample (2 × 2 cm) was incubated in a rotary shaker at rotor speed 100 rpm during the drug release study at 37°C in 20 ml of PBS (pH=7.4). After the required incubation time for drug release, the sample was transferred to 20 ml of fresh buffer solution and the released TCH and IMC amounts in the buffer solution were determined. The amount of drug was measured over 10 day release tests.

A standard release curve was obtained by measuring different concentrations of TCH/PBS and IMC/PBS solution with the aid of a UV-vis spectrometer at 360 nm and 319 nm respectively. The slope and intercept of the line provide a relationship between absorbance and concentration:

$$Y = intercept + slope\ M$$

where Y is the absorbance and M is the concentration. The unknown concentrations of drug in solution (M_u) were determined from the standard absorbance curves, using the slope and intercept, for the measured value of the absorbance (Y_u). The estimation used the following equation:

$$M_u = (Y_u - intercept) / slope$$

The percentage of the released drug was calculated from the primary weight of the drug (TCH and IMC) included in the electrospun mat. The cumulative amount of drug released from the nanofibre mat was calculated by the following equation:

$$Cumulative\ quantity\ of\ drug\ released\ (\%) = (M_t/M_\infty) \times 100$$

where M_t is the amount of drugs released up to time t and M_∞ is the initial amount of drug within the electrospun fibres. Three release tests were conducted for each electrospun fibre mat and the average data were recorded.

3.2.1.7 In vitro biodegradation of nanofibre mats

For in vitro degradation studies, the nanofibre mats with thickness ranging from 300 to 500 µm were sliced into 2 × 2 cm samples. They were measured to get the initial weight (m) and were put into an incubated rotary shaker at rotor speed 100 rpm during the biodegradation study at 37°C in 15 ml of PBS (pH=7.4) for the required incubation time.

The nanofibre mats were removed at each designated incubation period and washed with deionised water. The nanofibre mats dried under vacuum at 37°C until they reached a constant weight (m_1). The percentage of mass loss was determined by the equation below:

$$\textit{Percentage mass loss} = ((m - m_1)/m) \times 100$$

3.2.1.8 Release kinetics

The kinetics of TCH and IMC release from the nanofibre mats were determined from the curves of % release (M_t/M_∞) against time *t*. The experimental drug release data were fitted to five mathematical models for drug release kinetics (Cai et al., 2011), including the zero order, first order, Higuchi, and Ritger-Peppas models,and the recently-developed Zeng model (Zeng et al., 2011). These models are shown below:

1. Zero order model

$$M_t/M_\infty = K_0 t$$

2. First order model

$$M_t/M_\infty = 1 - \exp(-K_1 t)$$

3. Higuchi model

$$M_t/M_\infty = K_H t^{1/2}$$

4. Ritger-Peppas (power law) model

$$M_t/M_\infty = K_R t^n$$

5. Zeng model

$$M_t/M_\infty = K_{off}/(K_{on}+K_{off}) \times (1 - e^{-K_S t}) + K_{on}/(K_{on} + K_{off}) \times (1 - e^{-K_{off} t})$$

where K_0, K_1, K_H, and K_R are the zero-order, first-order, Higuchi, and Ritger-Peppas release constants, respectively, while *n* is the diffusion exponent in the Ritger-Peppas model. In the Zeng model, K_{on} is the rate constant of association, K_{off} is the rate constant of disassociation, and $K_S = Ak/V$ where (A/V) is the surface area-to-volume ratio of the

nanofibre mat and k is the rate constant. Here, $k = DK/l$, where D is the diffusion coefficient of the drug, K is the partition coefficient of the drug between the shell and the core, and l is the thickness of the shell.

3.3 Characterisation

Morphology and structure characterization of nanocomposite fibres is essential to understand the effect of nanoparticles and drug within the nanocomposites, as well as to understand the drug release mechanism from nanofibre mats, which may help todevelop drug delivery systems. Various characterization methods, including scanning electron microscopic (SEM),transmission electron microscopy (TEM), X-ray diffraction (XRD), differential scanning calorimetry (DSC), Fourier transform infrared spectroscopy (FTIR), viscometry, electrical conductivity measurement, gel permeation chromatography (GPC) and UV-vis spectrophotometry, were performed on some typical mat samples. The specific arrangements and investigation conditions are explained in the following subsections.

3.3.1 Scanning electron microscopy (SEM)

SEM was carried out to investigate the morphological structures of nanofibre mats when blending PLA with PCL and incorporating HNTs, MPs and drug (TCH) with the blending polymers. SEM employs a focused beam of high energy electrons to produce a diversity of signals at the solid specimens' surface (Bozzola, 1992). The signals that are received from the interaction between the nanofibres and electrons are reformatted to form microscopic images.

The morphology of electrospun nanofibres was studied via an EVO 40XVP scanning electron microscope from Zeiss (Germany) at an accelerating voltage of 5 kV. Before SEM observation, the samples were sputter-coated with platinum. Fibre diameter was calculated from the SEM images by using an image analysis tool in the Zeiss Smart SEM software. For each sample, measurements were made with a minimum of 150 fibres from multiple scanned SEM images and at a rate 15 fibres per image.

3.3.2 Transmission electron microscopy (TEM)

Transmission electron microscopy was utilized to examine the morphology of HNT and MP dispersion within the nanofibres in order to confirm the XRD data. TEM is a broadly utilized characterization method for solid materials. In contrast to SEM, the beam of TEM electrons is transmitted through a thin sample of the material and assists in revealing the detailed structures that are embedded within the material (Williams and Carter, 2009).

The nanofibre mat was embedded in Araldite® epoxy resin. The following method was used to control the homogeneity and distribution of the fibres in the mat sample: a $1\times1\times1$ cm^3 volume of epoxy was polymerized for 24 h, then the fibre mat was macerated in epoxy solution and placed on the solid pre-polymerized epoxy, and subsequently the composite was re-polymerized. The composite was sectioned into 100 nm layers using a diamond knife with a Leica EM UC6 microtome, and the sections were later mounted onto carbon grids. The TEM observations were performed using a JEOL 2011 at an accelerating voltage of 200 kV to study the dispersion level of HNT and MP within the composite fibre mats.

3.3.3 X-ray diffraction (XRD)

X-ray diffraction (XRD) allows phase identification of the crystalline material structure, including degree of crystallinity, crystallite size, and structural changes.XRD measurements of prepared samples were performed in a Bruker Discover 8 X-ray diffractometer (Germany) operated at 40 kV and 40 mA using Cu-Kα radiation that was monochromatised with graphite sample monochromators in a 2θ range from 5° to 40° with a scanning rate of 0.05°/s. The *d*-spacing (*d*) corresponding to the silicate XRD peak was determined from Bragg's equation:

$$n\lambda=2d\sin\theta$$

where θ is the diffraction position, λ is the wavelength, which is 1.54 Å for a Cu target, and *n* is an integer. The crystallite size (*L*) was calculated from the Scherrer relation:

$$L = K\lambda / (B\cos\theta)$$

where B is the complete width at half maxima of the crystalline peak in radians and K is the shape factor of the average crystallite. The crystallinity was determined by applying the area integration method from diffracted intensity over the range of 2θ data from 8° to 27° (Ning et al., 2007).

3.3.4 Differential scanning calorimetry (DSC)

DSC is a common thermo-analytical technique that is used to understand effects of heating and cooling on polymer behaviour and also study a polymer's thermal transitions (Menczel et al., 2009). This technique was employed to determine the impact of changing the PCL concentration, blending ratio of PLA to PCL, embedding of HNTs, embedding of MPs and the addition of drugs on the thermal properties of the composites. Thermal analysis was performed using a DSC6000 from PerkinElmer (USA) with Cryofill liquid nitrogen cooling system. Approximately 10mg of fibre mat was sealed in aluminium pans and its thermal behaviour was analysed during heating between 30°C and 200°C with a ramp rate of10°C/min for PLA nanofibres, while samples with PCL were heated from –100°C to 200°C. The glass transition temperature (T_g), crystallisation temperature (T_c) and melting temperature (T_m) were obtained for PLA: PCL nanofibres from analysis of the DSC data.

3.3.5 Fourier transform infrared spectroscopy (FTIR)

FTIR is a method of materials analysis that produces the 'fingerprint' of a material with absorption peaks that match the frequencies of vibrations of the material's atomic bonds. It can identification of different compounds because each material is a unique combination of atoms (Smith, 2009). FTIR was used to investigate the interaction level between biopolymers (PLA: PCL), HNTs, MPs and drugs. It was performed in a Spectrum 100 FTIR Spectrometer from PerkinElmer (Japan). Spectra were recorded in the range between 4000–550 cm^{-1} with 4 cm^{-1} resolution by using an attenuated total reflectance (ATR) technique (Chittur, 1998).

3.3.6 Viscometry and electrical conductivity measurement

Solution viscosity, which is a very important variable that influences nanofibre diameters, was measured by using a Visco 88 portable viscometer from Malvern Instruments (UK). It has a built-in temperature sensor and is supplied with a double gap measuring geometry to provide extra sensitivity when measuring low-viscosity fluids. All the samples were measured under constant temperature of 23°C. The electrical conductivity and pH value of the solution were measured by using a WP-81 Waterproof pH and conductivity meter (TPS, Australia).

3.3.7 Gel permeation chromatography (GPC)

Gel permeation chromatography (GPC) was utilized to find the effect of impurities that accompany the MPs on the molecular weight of PLA: PCL blending. GPC analysis was performed to measure the molecular weight of polymers at 40°C using a Shodex DS-4 pump, one Shodex KF-805L and three KF803L columns connected in series, and a UV detector. Tetrahydrofuran (THF) was used as the eluent at a flow rate of 1.0 ml/min.

3.3.8 UV-vis spectrophotometry

UV-vis spectrophotometry is a method that has been used to identify and measure the organic and inorganic materials in many processes. The amount of TCH present in the release buffer (PBS) was obtained by means of a UV-vis spectrophotometer (JascoV-67) at wavelengths of 360 nm and 319 nm of TCH and IMC respectively.

Chapter 4
Morphological Structures of Electrospun Biopolymers

4.1 PLA: PCL system

Blending polymers is generally an effective strategy for establishing novel materials based on the beneficial properties of each polymer constituent. The mat structure and properties of the blends can be tailored by changing the composition to produce blends with characteristics quite different from those of the pristine or individual polymers. A blended poly(lactic acid) (PLA): poly(ε-caprolactone) (PCL) system may assist in achieving well-balanced crystallinity with the potential advantage of well-controlled drug release. However, the control of electrospinning parameters to obtain better nanofibre quality without any bead defects and also with the desired morphology, crystallinity and molecular structures, has yet to be achieved.

This chapter was designed to investigate the effect of polymeric solution variables such as solution viscosity, polymer molecular weight, polymer concentration, blend ratio of polymers and solvent type. These variables had a substantial and direct impact on fibre diameters, morphological structures, thermal properties and the degree of crystallinity, as well as potentially on the rate of drug release, which will be investigated in Chapter 7. This research work focused on blending high and low molecular weight PCL at 9 wt%/v and 15 wt%/v solution with PLA solution (fixed at 8 wt%/v) at five blending ratios. Various co-solvents, including chloroform ($CHCl_3$): acetone (C_3H_6O), chloroform ($CHCl_3$): methanol (MeOH) and dichloromethane (DCM): N,N, dimethylformamide (DFM) were used for the preparation of PLA: PCL solutions.

4.2 Morphological observations

4.2.1 Effect of PCL molecular weight

Molecular weight is an important parameter in the electrospinning process. Figure 4-1(a) shows that blending PLA with high molecular weight PCL led to homogenous fibres

with an average nanofibre diameter of 814±15 nm. However, by decreasing the molecular weight of PCL no fibrous structure was obtained, Figure 4-1(b). This can be attributed to lowering the required solution viscosity for effective electrospinning due to decreasing the molecular weight. Figure 4-2 shows the viscosity of PLA: 15% PCL solutions dissolved in chloroform: methanol ($CHCl_3$: MeOH). It can be seen that a decrease in the PCL molecular weight led to a significant decrease of solution viscosity.

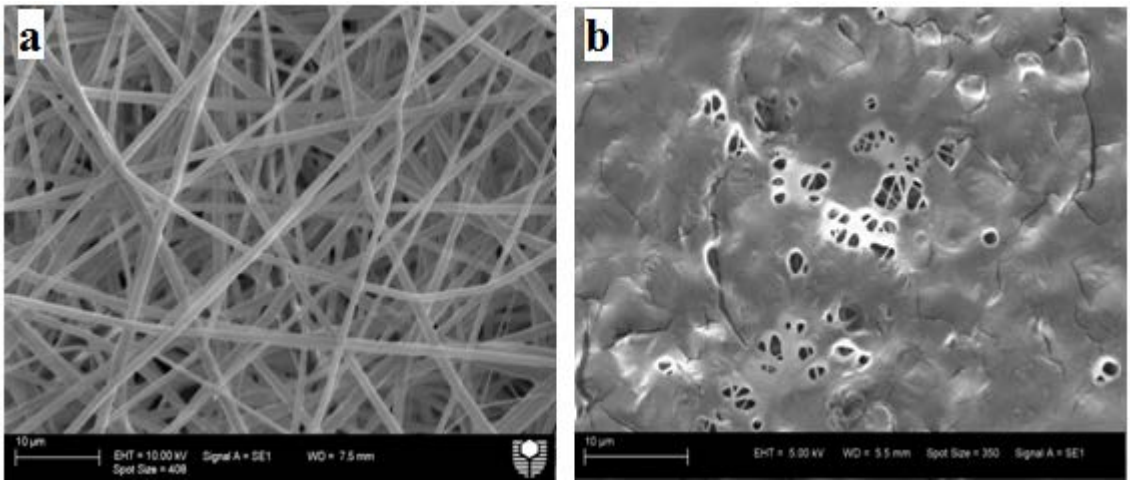

Figure 4-1: SEM micrographs of electrospun PLA: PCL (1:1) fibres using chloroform: methanol as a solvent: (a) high molecular weight 15% PCL and (b) low molecular weight 15% PCL.

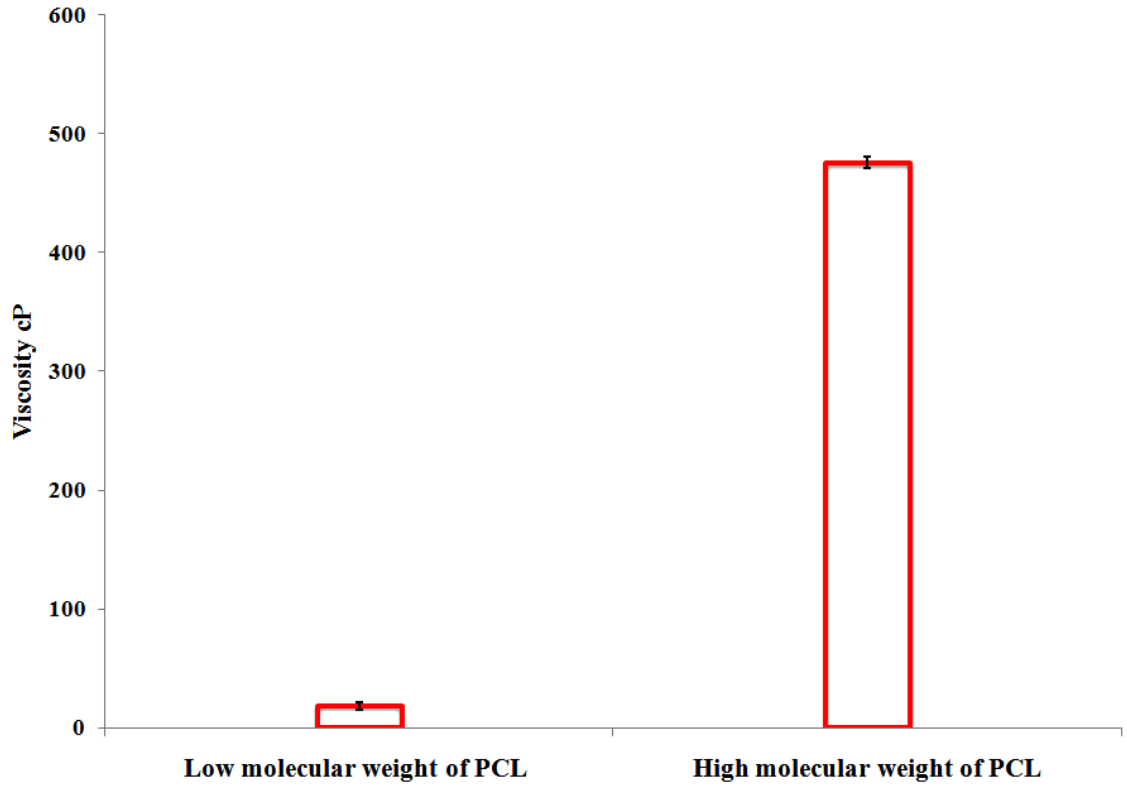

Figure 4-2: Viscosity of 1:1 v/v solutions of PLA with high and low molecular weight PCL dissolved in chloroform: methanol co-solvent.

4.2.2 Effect of PCL concentration

A PLA solution was blended with two different concentrations of high molecular weight PCL solution, namely 9 and 15 wt%/v, at a 1:1 blending ratio using chloroform: methanol solvent and used for electrospinning. These two systems generated a moderately regular fibrous morphology with a number of differences in the fibre diameters and morphology. Figure 4-3 demonstrates that when increasing the PCL concentration from 9 wt%/v to 15 wt%/v, the corresponding average fibre diameter is enlarged from 689±15 nm to 814±15 nm. This finding is ascribed to the increased solution viscosity: from 113 cP for 9 wt%/v PCL to 476 cP for 15 wt%/v PCL, Figure 4-4. It is in good agreement with previous studies that have shown that small fibre diameters result from low solution viscosity (Zamani et al., 2010; Arayanarakul et al., 2006). The increase of solution viscosity is associated with an increase in the number of

molecular entanglements per polymer chain and a low amount of solvent due to the increased solution concentration, which is regarded as an important factor for stable jet formation in compensation for increased surface tension (Spasova et al., 2007).

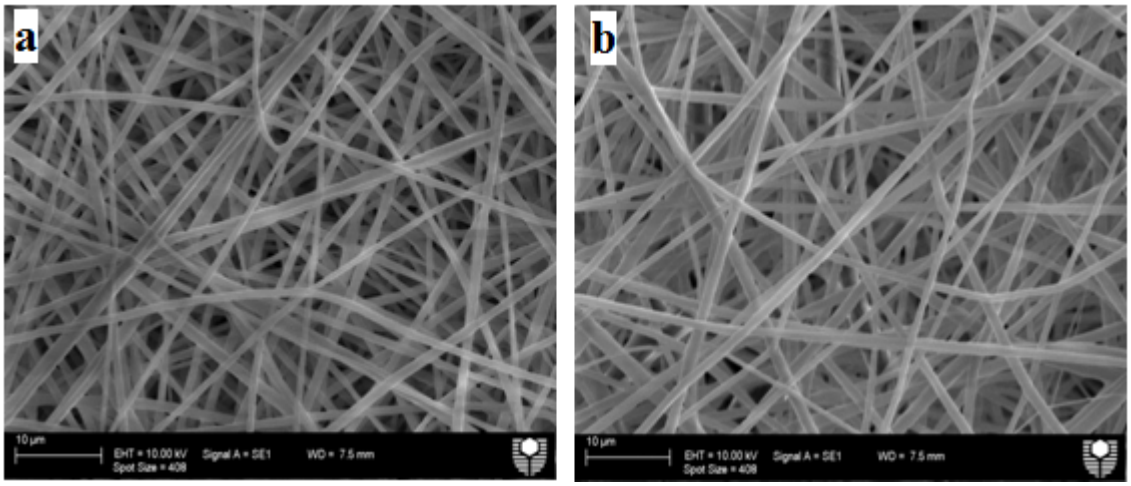

Figure 4-3: SEM micrographs of electrospun 8 wt%/v PLA solution with high molecular weight PCL (a) 9 wt%/v PCL solution, and (b) 15 wt%/v PCL solution.

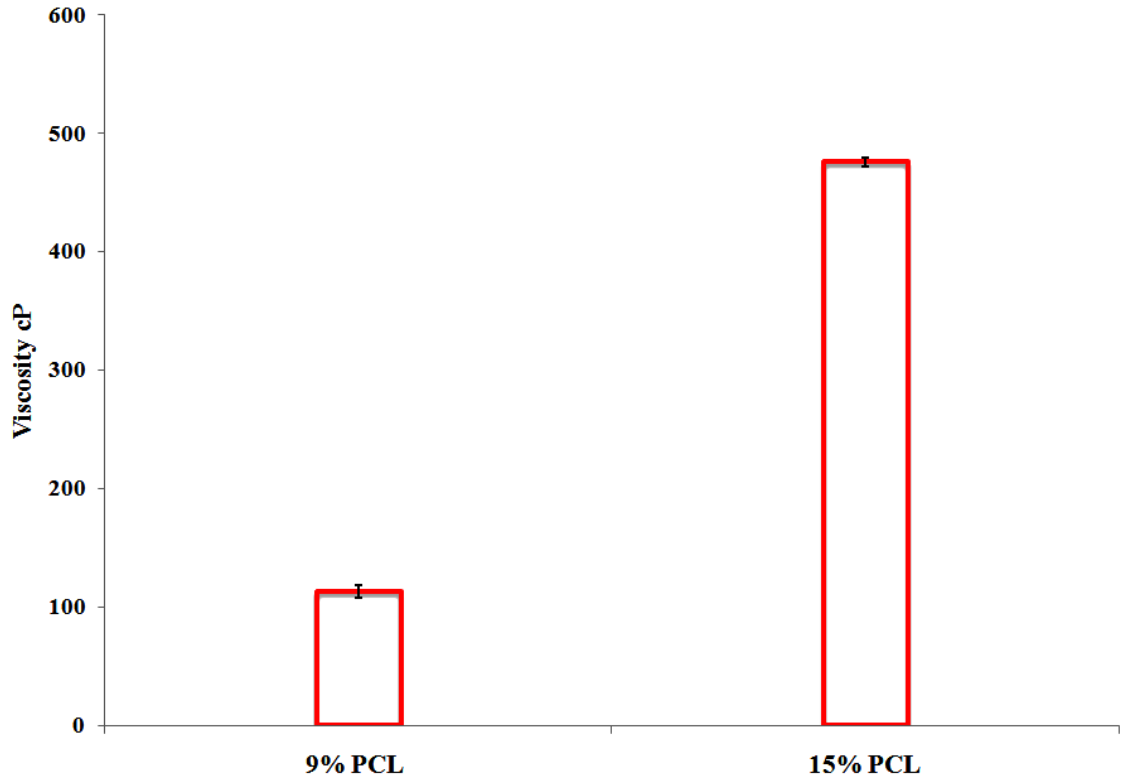

Figure 4-4: Solution viscosity of 1:1 v/v mixtures solutions of PLA with high molecular weight 9 and 15 wt%/v PCL dissolved in chloroform: methanol solvent.

4.2.3 Effect of PLA: PCL blending ratio

Figure 4-5 shows that the use of PLA dissolved in dichloromethane: dimethylformamide (DCM: DMF) produced homogenous fibres with average diameter 450±15 nm. In the first trial set, the high molecular weight PCL concentration was fixed at 15 wt%/v and it was found that for this system the ratio of PLA to PCL of 3:1 facilitated the production of good electrospun fibres with average diameter 553±15 nm, Figure 4-6. However, by increasing the amount of PCL up to a PLA: PCL ratio of 1:1, the average fibre diameters were increased to 610±20 nm, but the fibres produced possessed intermediate quality due to the non-uniform morphology. The increasing trend in the fibre diameter continued up to 744±15 nm with uniform fibrous structures when the PLA: PCL ratio reached 1:3. It was found to be difficult to achieve homogeneous fibres at an even higher PLA: PCL ratio of 0:1 due to the significant increase of the solution viscosity preventing the solution droplets from being elongated into continuous fibres, Figure 4-6. Solution

viscosity plays a significant role in the formation of a greater number of entanglements per polymer chain, which is a precursor to generating a stable jet (Spasova et al., 2007).

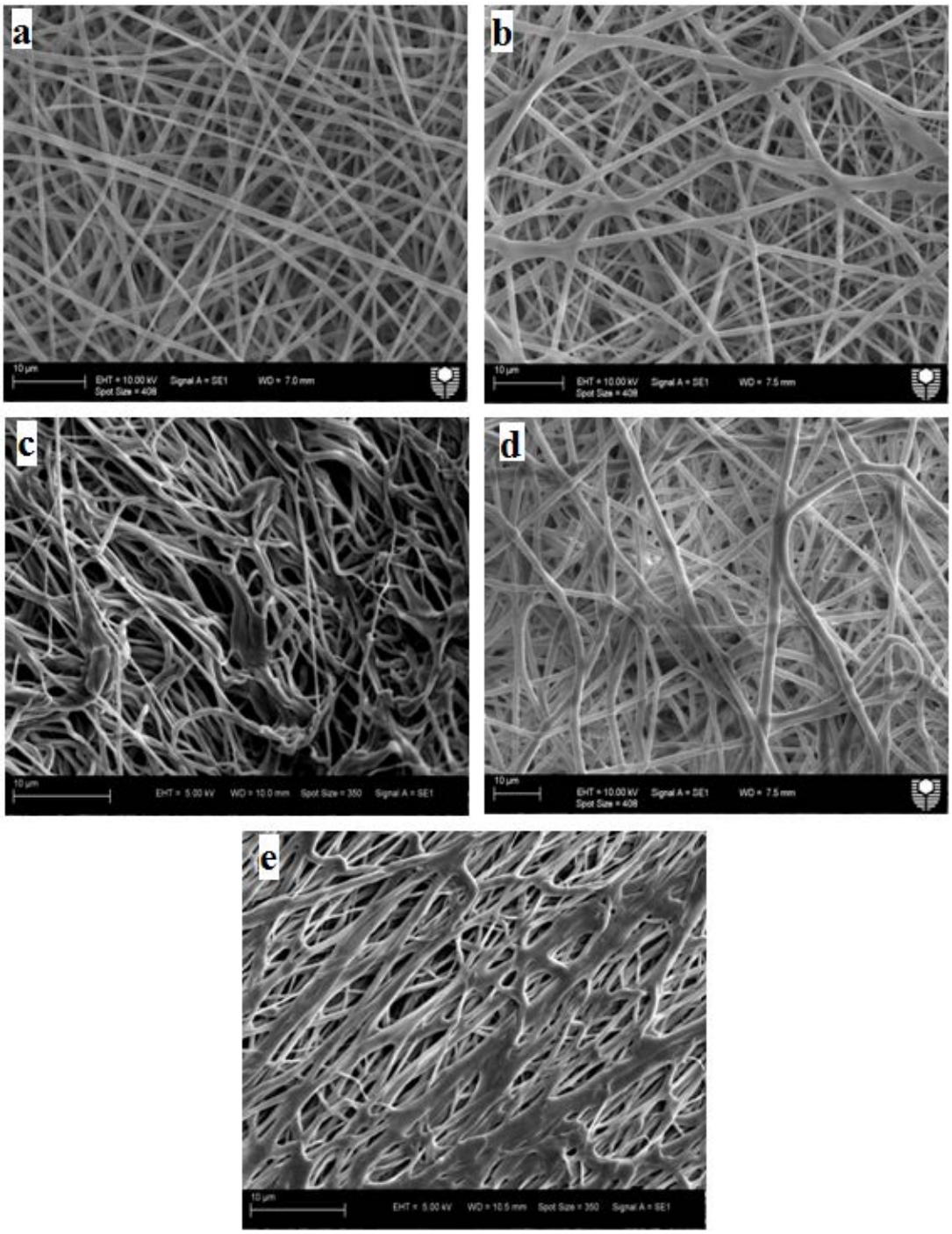

Figure 4-5: SEM micrographs of electrospun PLA: 15% PCL fibres by using DCM: DMF as a co-solvent with different PLA: PCL blend ratios: (a) 1:0, (b) 3:1 , (c) 1:1, (d) 1:3 and (e) 0:1.

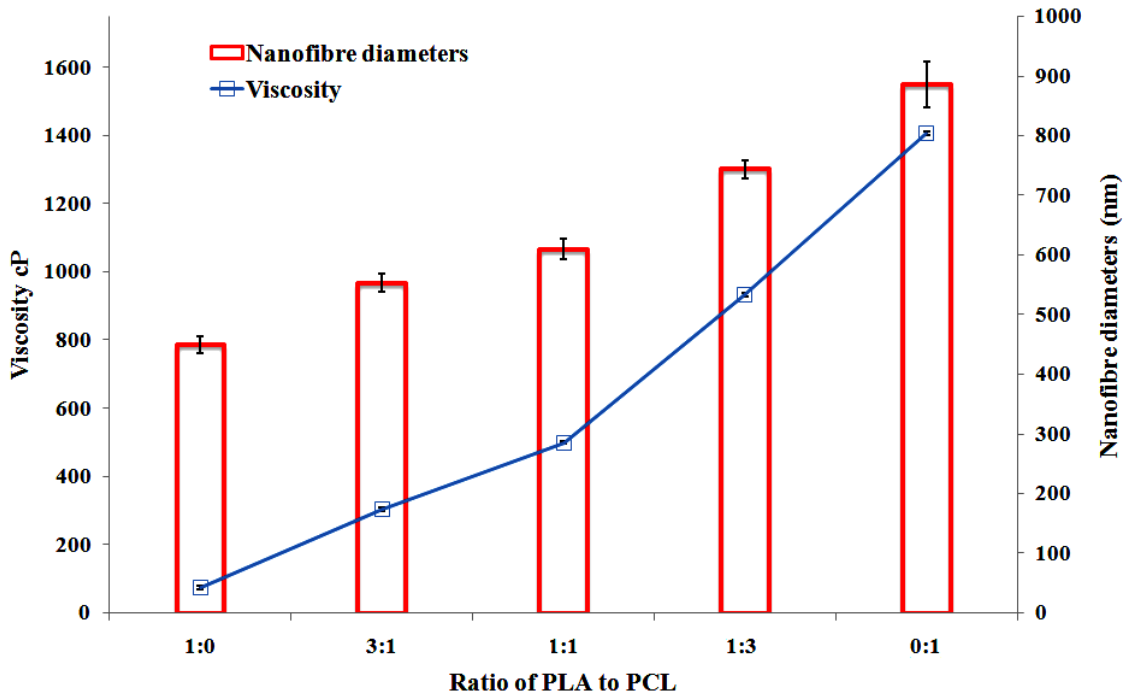

Figure 4-6: Solution viscosity and nanofibre diameters of PLA: high molecular weight 15% PCL solutions dissolved in the DCM: DMF with different blend ratios.

Figure 4-7(a) shows that the low molecular weight PCL concentration was fixed at 15 wt%/v and it was established that for this system a PLA: PCL blend ratio of 3:1 resulted in an average fibre diameter of 490±15 nm, Figure 4-8. This implies that the increase in blend ratio from 1:0 to 3:1 did not considerably affect the fibre diameters within experimental errors. Moreover, increasing the amount of PCL to a blend ratio of 1:1 caused beads and inhomogeneity in the structures, and decreased the average fibre diameter to 250±25 nm, with maximum and minimum diameters of 425 nm and 130 nm, respectively. This indicates that by lowering the solution viscosity, as illustrated in Figure 4-8, the fibre diameter can be reduced, while inhomogeneity occurs to a great extent in the fibre structure. Moreover, the low viscosity leads to quick fragmentation of the charged polymer jet at short distances, which may be a plausible reason for the beads occurring in the electrospinning process. When the amount of PCL was further increased, no visible fibre structures were obtained.

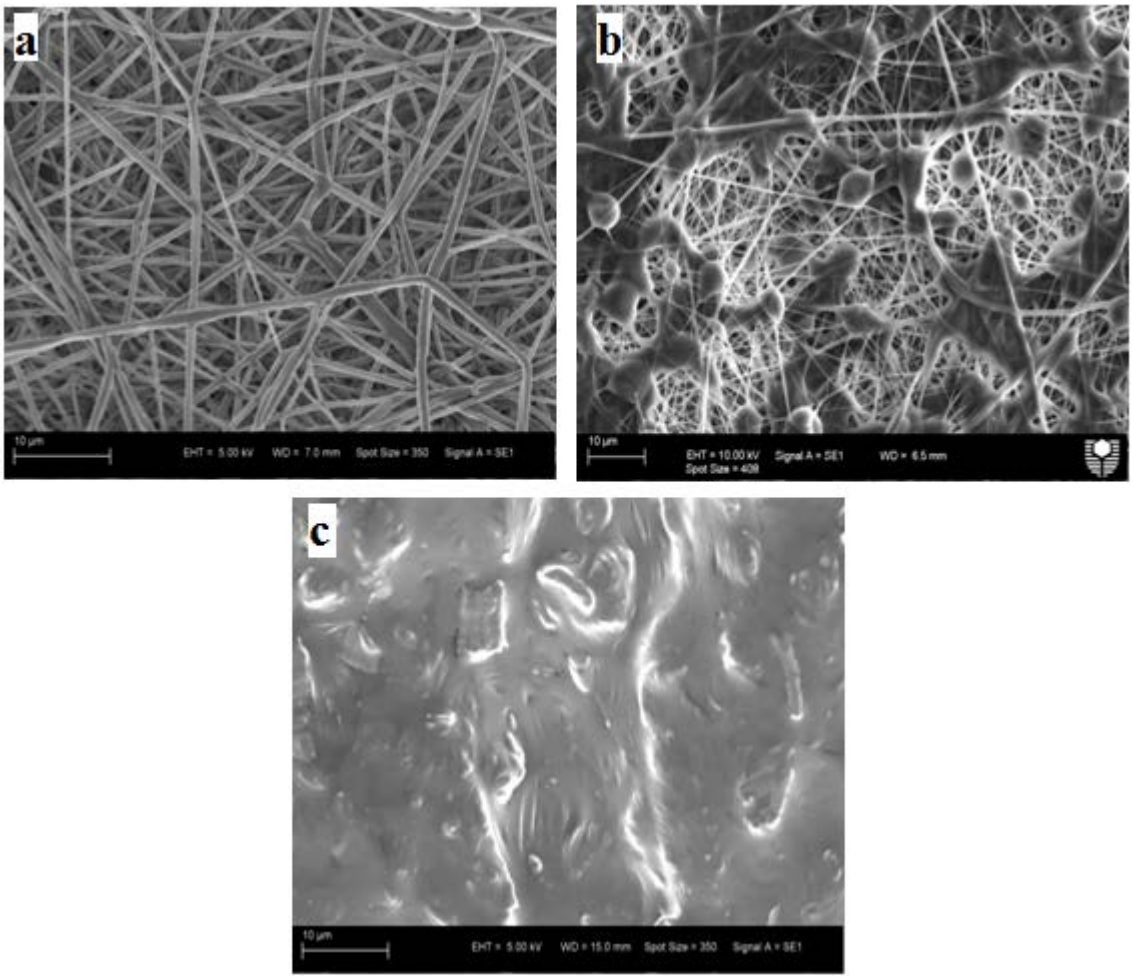

Figure 4-7: SEM micrographs of electrospun PLA: 15% PCL fibres using DCM: DMF as a co-solvent with different PLA to low molecular weight 15% PCL blend ratios: (a) 3:1, (b) 1:1 and (c) 1:3.

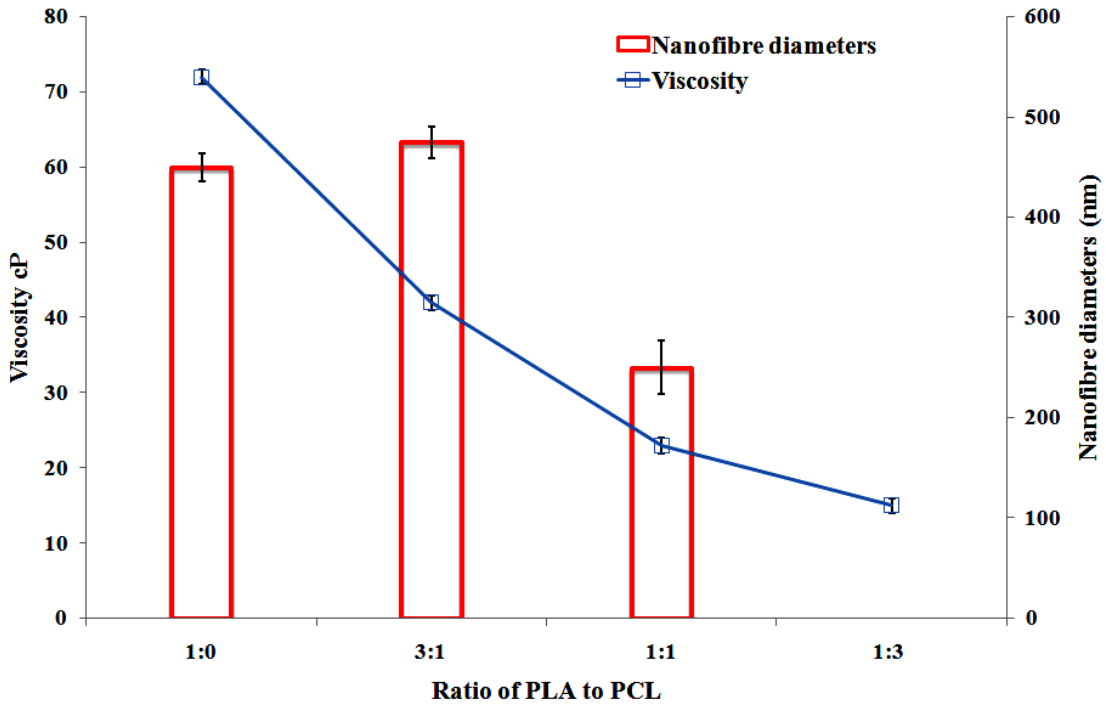

Figure 4-8: Solution viscosity and nanofibre diameters of PLA: low molecular weight 15% PCL solutions dissolved in the DCM: DMF with different blend ratios.

4.2.4 Effect of solvent

The electrospun solvent is also a major determinant which affects the fibre structure. The selection of an appropriate solvent system is crucial for successful material fabrication via electrospinning (Han et al., 2010). Figure 4-9 shows that using PLA dissolved in chloroform: methanol co-solvent produced fibres with the average diameter of 510±15 nm. Increasing the amount of low molecular weight PCL to PLA with the blend ratio of 1:3 produced a mixed fibre-bead structure with average nanofibre diameters of 325±25 nm. Further increasing the PCL: PLA blend ratio to 1:1 resulted in non-fibrous structures, as evidenced in Figure 4-10.

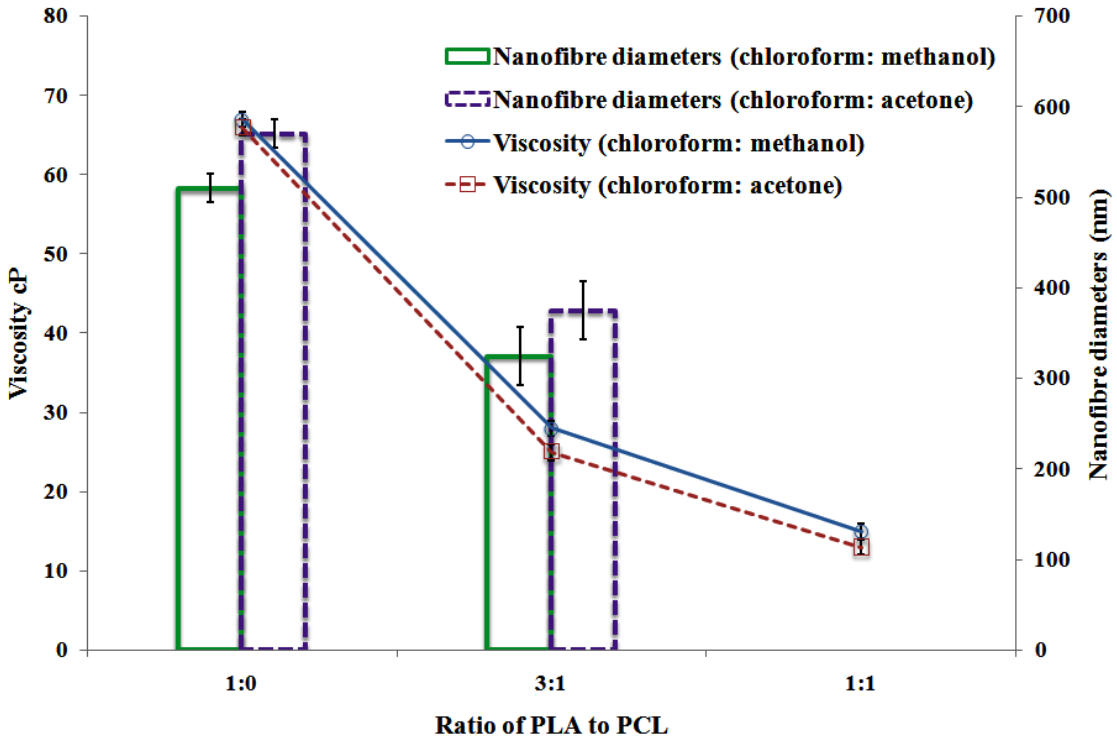

Figure 4-9: Solution viscosity and nanofibre diameters of PLA to low molecular weight 15% PCL solutions dissolved in chloroform: methanol and chloroform: acetone co-solvents with different blend ratios.

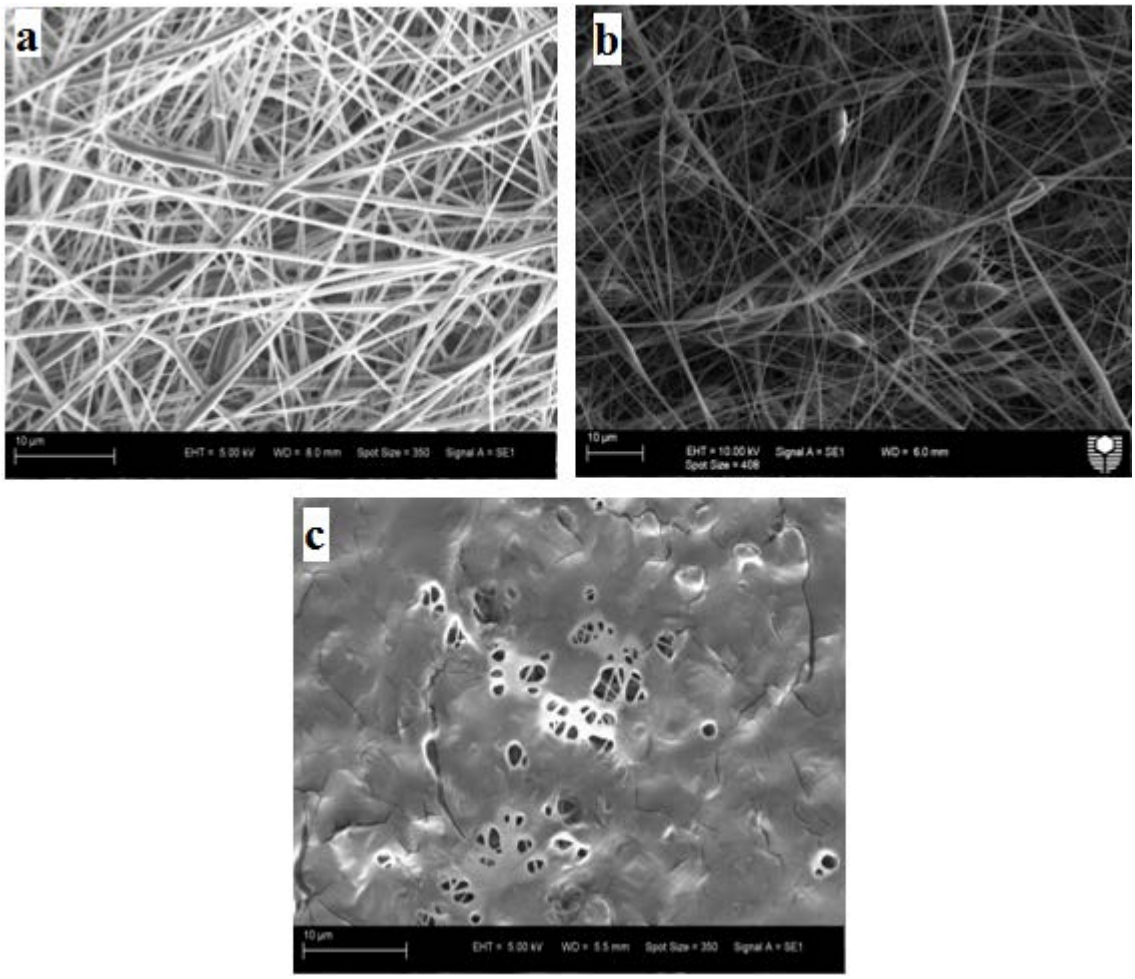

Figure 4-10: SEM micrographs of electrospun PLA: 15% PCL fibres using chloroform: methanol as a co-solvent with different PLA to low molecular weight 15% PCL blend ratios: (a) 1:0, (b) 3:1 and (c) 1:1.

Figure 4-11 demonstrates that electrospun PLA dissolved in chloroform: acetone co-solvent led to nanofibres with an average diameter of 570±15 nm (Figure 4-10). When the amount of low molecular weight PCL with a PLA: PCL blend ratio of 3:1 was used, inhomogeneous fibre structures with a reduced average fibre diameter to 375±30 nm were observed. Additionally, further increasing the amount of PCL led to non-fibrous formations.

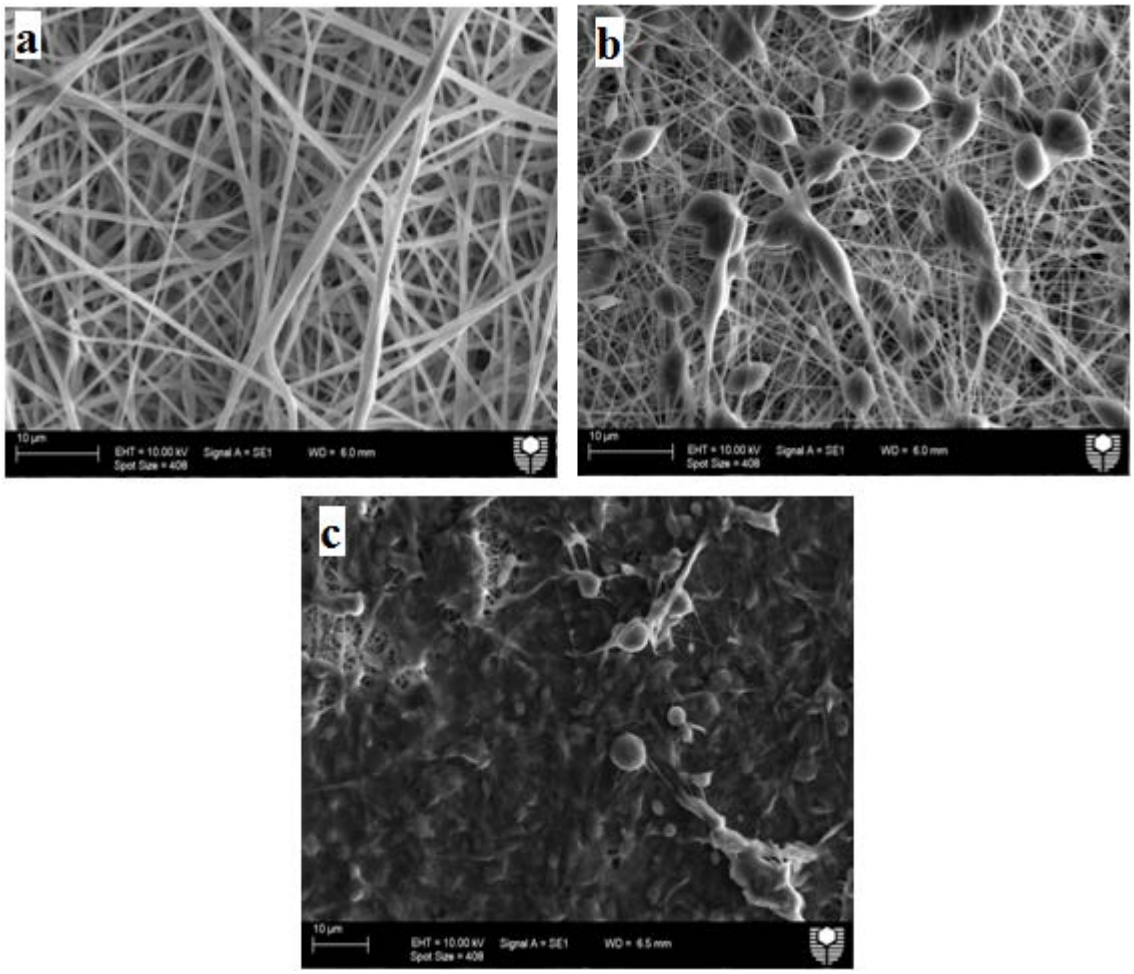

Figure 4-11: SEM micrographs of electrospun PLA: 15% PCL fibres using chloroform: acetone as a co-solvent with different PLA to low molecular weight 15% PCL blend ratios: (a) 1:0, (b) 3:1 and (c) 1:1.

Considering that the solution viscosity is critical in forming fibres, Figure 4-10 demonstrates that the viscosity was significantly reduced by the increasing amount of low molecular weight PCL and its effect on the electrospun fibres was almost the same for all solvent systems. The nanofibres produced from the DCM: DMF co-solvent system were uniform, with smaller fibre diameters, as compared to those obtained from chloroform: methanol and chloroform: acetone systems. This is because the conductivity of DCM: DMF solution is higher than the chloroform: methanol solution, which is, in turn, higher than chloroform: acetone. As a result, increasing the conductivity can

facilitate a uniform charge density, and thus cause higher conductivities to produce smaller nanofibres.

On the other hand, Figure 4-5 shows that PLA with high molecular weight PCL in DCM: DMF produced approximately sinuous fibres especially when the PCL concentration was increased to 15 wt%/v, since the viscosity was significantly increased by the additional high molecular weight PCL (Figure 4-6). The effect on the electrospun fibres was the same, as can be seen with chloroform: methanol co-solvent, Figure 4-3(b). The electrospun fibres formed from the DCM: DMF system for all polymer blend ratios was relatively small as compared to those from the chloroform: methanol system, which can be due to the effect of the solution electrical conductivity. This finding indicates that the choice of a suitable solvent system is also essential in the electrospinning process. Furthermore, the dielectric constant of the solvent and the solubility of polymers in the solvent can significantly influence the structure of the resulting fibres (Abdul Rahman et al., 2010). DMF has a higher dielectric constant (38.3) compared to methanol (33.0), while DCM has a higher dielectric constant (9.1) than chloroform (4.8) (Bhardwaj and Kundu, 2010). Consequently, it can be concluded that enhancing the solution electrical conductivity promotes the first step of manufacturing uniform fibre mats due to their higher charge density. Secondly, at the step of fibre solidification, the volatilities of solvents significantly affect the drying properties and the solidification process. Additionally, the morphologies of electrospun nanofibres are considerably impacted by the rate of solvent evaporation (Qian et al., 2010). Therefore, it was found that unlike methanol, the low volatility of DMF could result in decreased solvent evaporation, leading to wet fibres being received at the collector plate. Additionally, it was found that fibres from the chloroform: methanol co-solvent system produced a better-aligned fibrous structure compared with their DCM: DMF and chloroform: acetone counterparts.

4.3 Crystallinity level and thermal properties

An XRD investigation was carried out to examine the changes in the PCL molecular weight, solvents, PCL concentration and PLA: PCL blend ratio on the degree of crystallinity (X_c). Figure 4-12 demonstrates the XRD patterns for blending PLA with

two concentrations of high molecular weight PCL, 15 wt%/v and 9 wt%/v, respectively. It can be seen that when the PLA and PCL blend had a higher PCL concentration, the diffraction peaks of PLA: PCL at angles of 2θ = 20.11° and 23.2° were detected, which are related to the crystal planes (101) and (200), respectively. They become more prominent as a result of the positive impact of PCL, which contributed to an increased degree of crystallisation for increasing PCL concentration and increasing blending ratio of PLA and PCL to 1:1. It is obvious from Figure 4-13 that the degree of crystallinity obtained from XRD patterns was improved in PLA: 15% PCL at the blend ratio of 1:1 when dissolved in chloroform: methanol, not as has been obtained from PLA: 9% PCL and PLA: 15% PCL at blend ratios of 1:1 and 3:1, respectively. This phenomenon is due to the addition of PCL with a modest degree of crystallinity in place of amorphous phase PLA with low crystallinity. As observed in Figure 4-13, the key finding is that a sharp decline in the degree of crystallinity occurred when low molecular weight PCL was added compared with high molecular weight PCL at the same blend ratio (X_c = 37.95% and 58.84%, respectively). This arises from the dominant effect of the amorphous PLA phase with relatively high molecular on the degree of crystallinity when it was blended with low molecular weight PCL. On the other hand, it is noted that there is a moderate effect on the degree of crystallinity by changing the co-solvents. The use of chloroform: methanol co-solvent reduced the degree of crystallinity to 58.84% compared with 61.59% when DCM: DMF solvent was added. This may be ascribed to the higher evaporation rate of methanol compared to DMF. During electrospinning, the fast evaporation leads to quick solidification, which means that the polymer molecules do not have enough time to be arranged into an appropriate crystal structure.

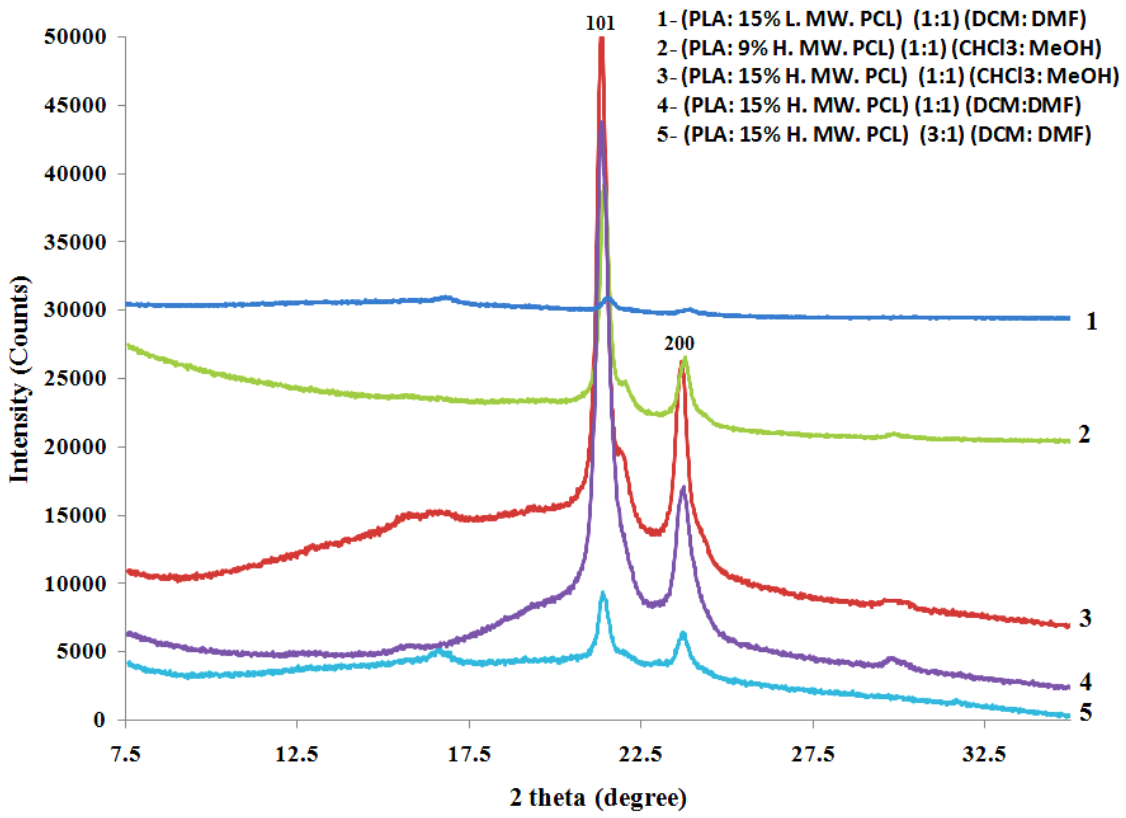

Figure 4-12: X-ray diffraction patterns for selected samples showing the relative position of the intercalation peak due to employing various solvents, PCL concentrations, different PLA to PCL blend ratios, and high and low molecular weights of PCL.

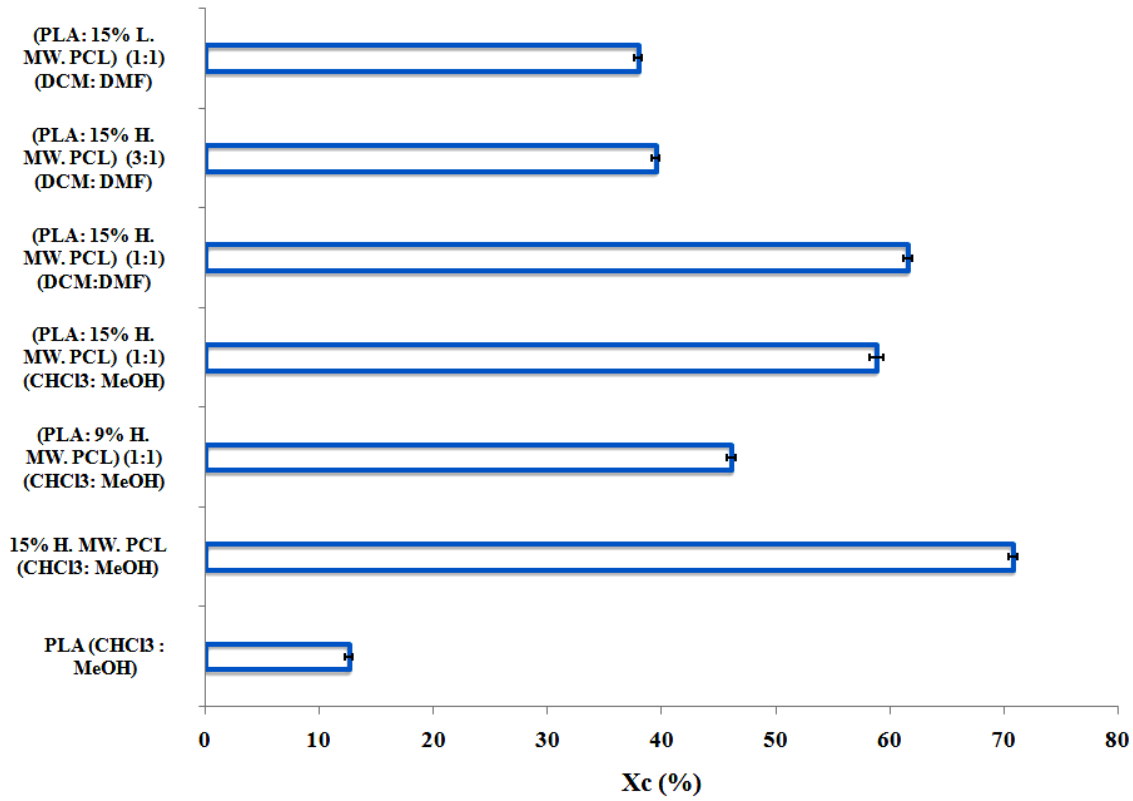

Figure 4-13: Degree of crystallization of PCL: PLA nanofibres created from a variety of solvents, PCL concentrations, different PLA to PCL blend ratios, and high and low molecular weights of PCL.

The thermal behaviour of electrospun fibres was also evaluated in the present work. The DSC results in Figure 4-14 and Table 4-1 show that the crystallisation temperature (T_c) of as-received PLA was higher than that of PLA fibres because the crystallization process can be accelerated by the well-structured PLA molecular chains in fibre-like form. The glass transition temperature (T_g) of PCL within the PLA: PCL blends become higher when the high molecular weight PCL concentration increases from 9 to 15 wt%/v. However, the T_g of PLA within the blends is hardly detected as it has overlapped the melting peak of PCL as shown in Figure 4-14. In addition, the variation of melting temperature (T_m) and T_g values can be attributed to the variation of fibre diameters and also to the electrospinning process, which influences the orientation of the polymer chains (Picciani et al., 2010). With respect to the impact of molecular weight, it can be observed that blending low molecular weight PCL with the PLA leads to the noticeable

increase in the value of T_c of PLA compared with high molecular weight PCL, while there was a significant decrease in the T_m value of PCL within the blend. Whereas with respect to the influence of solvent, the value of the T_c is lower in the case of using chloroform: methanol compared with using DCM: DMF solvent. The reason for this phenomenon is due to the high volatility of methanol, which leads to the preventing of created crystals as a result of rapid solidification. Hence there is no enough time for the relaxation of molecular chains. Moreover, the changes in the values of T_g, T_m and T_c in the case of PLA: PCL blends compared with individually electrospun PLA and PCL fibres, confirm a good miscibility between PLA and PCL within the blend.

Table 4-1: DSC results for PLA, PCL and PLA: PCL blend dissolved in ($CHCl_3$: MeOH) and (DCM: DMF) [a].

Material sample	T_g (°C) PCL	T_m (°C) PCL	T_g (°C) PLA	T_c (°C) PLA	T_m (°C) PLA
PLA (As-received)	-	-	65.2	120.6	152.6
PLA ($CHCl_3$: MeOH)	-	-	64.1	87.2	155.6
15% H. MW. PCL ($CHCl_3$: MeOH)	–58.0	63.1	-	-	-
(PLA: 9% H. MW. PCL) (1:1) ($CHCl_3$: MeOH)	–56.2	62.2	-	81.1	151.6
(PLA: 15% H. MW. PCL) (1:1) ($CHCl_3$: MeOH)	–52.2	63.8	-	84.0	152.5
(PLA: 15% H. MW. PCL) (1:1) (DCM: DMF)	–56.7	63.6	-	85.6	152.7
(PLA: 15% H. MW. PCL) (3:1) (DCM: DMF)	–57.2	62.8	-	81.9	152.4
(PLA: 15% L. MW. PCL) (1:1) (DCM: DMF)	–58.5	56.1	-	87.3	150.5

[a]*Calculations were repeated for three sets of samples. The standard deviation for the T_g, T_c and T_m values was less than 0.5°C.*

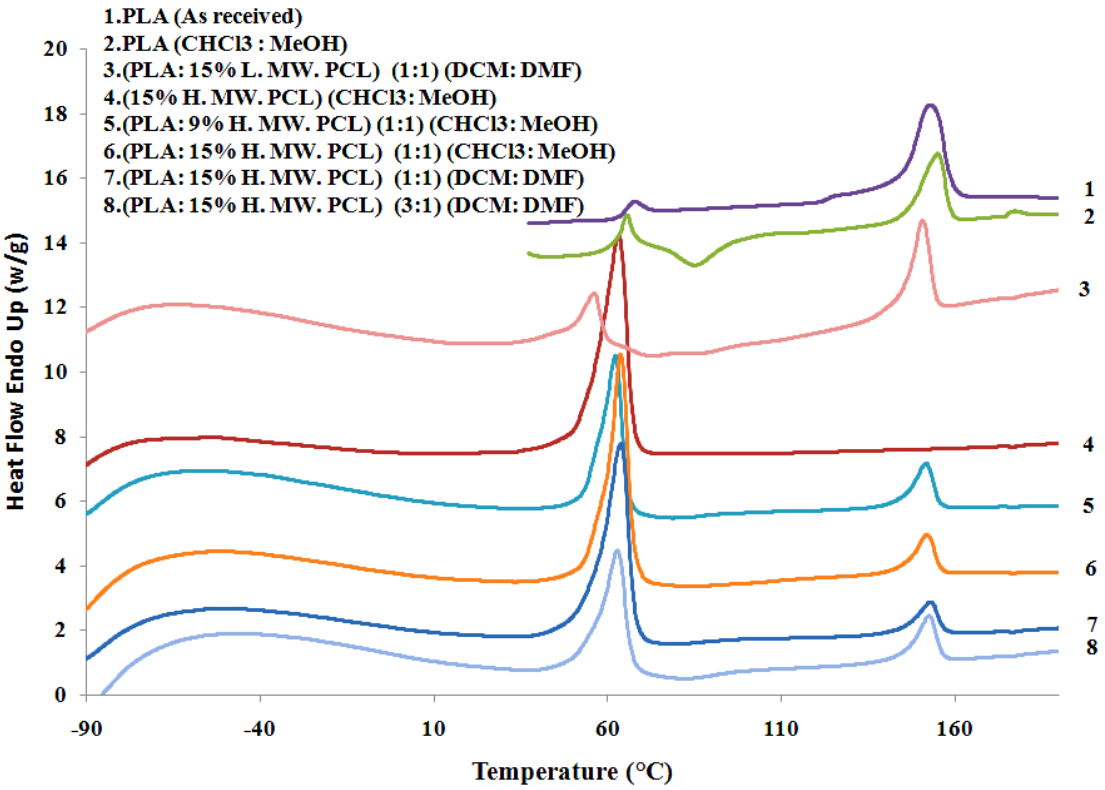

Figure 4-14: DSC thermograms for selected samples.

4.4 FTIR examination

Compositional changes were examined by Fourier Transform Infrared Spectroscopy (FTIR). Figures 4-15(a) and (b) display the FTIR spectra of PLA: PCL blend dissolved in DCM: DMF and chloroform: methanol with 9 wt%/v and 15 wt%/v PCL, different PLA to PCL blend ratios, and high and low molecular weights of PCL. Figure 4-15(a) demonstrates that PLA nanofibres and PCL nanofibres without blending exhibit initially two carbonyl stretching (C=O) bands at 1722 cm^{-1} for PCL and at 1750 cm^{-1} for PLA, respectively. The bands located at 2944 and 2866 cm^{-1} for PCL, and at 2850 cm^{-1} for PLA are assigned to C–H stretching. The peaks at 1456 and 1367 cm^{-1} indicated a C–H deformation of PLA. In addition, many peaks represent C–C and C–O stretching among the range 1240 to 840 cm^{-1} for the PLA and PCL.

In the case of blending PLA with PCL it is evident that the intensity of the carbonyl stretching (C=O) band of PCL decreases as the PLA amount increases in the blend and also when the PCL molecular weight decreases, as seen in samples 1 and 5 from Figure 4-15(b). In addition, FTIR peaks of the carbonyl stretching band have been shifted to higher wave numbers within the blend. This shift was higher (from 1750 to 1757 cm^{-1} for PLA) in the case of using PLA: 15% PCL at a blend ratio 1:1 and dissolved in a chloroform: methanol system. Sample 2 from Figure 4-15(b) suggests better miscibility between PLA and PCL compared with other systems.

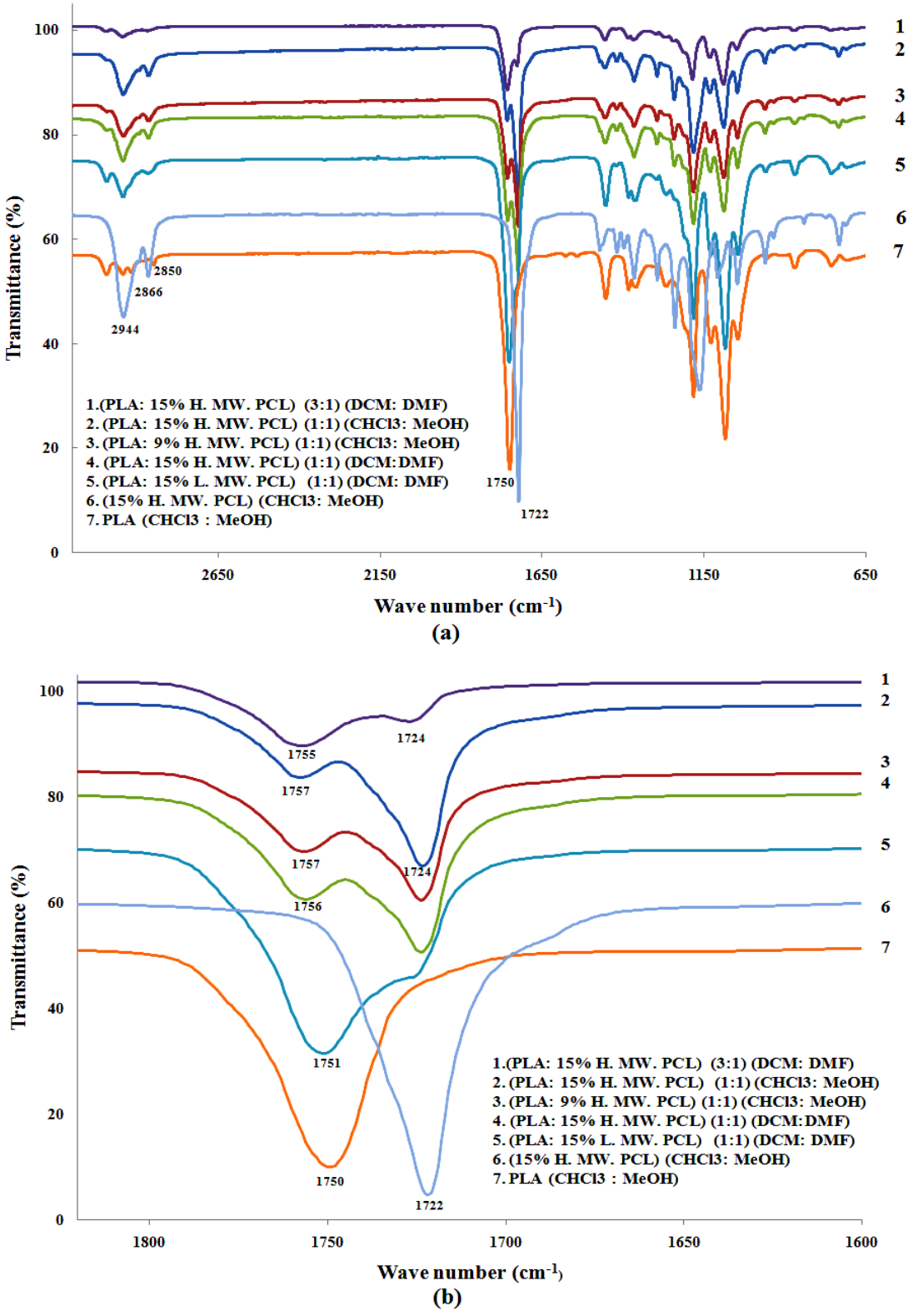

Figure 4-15: FTIR spectra for selected material samples showing the relative FTIR peaks in different ranges: (a) large scale between 3100 and 650 cm^{-1}, and (b) small scale between 1820 and 1600 cm^{-1}.

4.5 Summary

The main finding from this chapter it was that increasing the molecular weight and concentration of the polymeric solution has led to a remarkable improvement in the viscosity values, which in turn results in the formation of bead-free homogeneous nanofibres, especially when the blending ratio was 1:1. The nanofibres produced from the DCM: DMF solvent mixture, for all blend ratios of the polymers, were smaller compared to those created from the chloroform: methanol co-solvent. The nanofibres produced by using the chloroform: methanol co-solvent formed better aligned fibrous structures compared with those based on other co-solvents. The degree of crystallinity (X_c) obtained from XRD patterns increased in the PLA: 15% PCL mixture at a blend ratio of 1:1 when dissolved in chloroform: methanol, which was completely different from those for PLA: 9% PCL and PLA: 15% PCL at blend ratios of 1:1 and 3:1, respectively. Blending low molecular weight PCL with PLA led to a sharp decline in the degree of crystallinity and melting temperature (T_m) of PCL relative to high molecular weight PCL, while there was a noticeable increase in the crystallisation temperature (T_c) of PLA. Furthermore, the rapid evaporation of methanol when using the chloroform: methanol system caused a reasonable decrease in the degree of crystallinity and T_c compared with that for using DCM: DMF. Increasing the PCL concentration from 9 to 15 wt%/v contributed to an enhanced glass transition temperature (T_g) of PCL within the blends. Additionally, the changes in the values of T_g, T_m and T_c in the case of polymer blends compared with the individual PLA and PCL fibres, as well as the shift of the carbonyl stretching band to higher wave numbers, give clear evidence of good miscibility between PLA and PCL within the blends, especially for PLA: 15% PCL at a blend ratio of 1:1 dissolved in chloroform: methanol. This chapter provided structural information on a new material system that could be potentially used as a carrier for nanoparticles and drugs to facilitate good drug release control as presented in the following chapters.

Chapter 5
Biopolymer and HNT Nanocomposites

5.1 PLA: PCL: HNT system

The incorporation of nanoparticles into polymer nanocomposites is an effective approach for tailoring the composite properties and producing unique structures that could not be achieved by normal blending. The properties of fabricated nanocomposites are different from the properties of the poly(lactic acid) (PLA): poly(ε-caprolactone) (PCL) blends or halloysite nanotubes (HNT) individually. This is because of the varied types of PLA: PCL / HNT interactions that happen at a molecular level. Preparation of such nanocomposites is a new way to construct novel polymer-inorganic structures and may be efficiently directed by a suitable selection of synthesis conditions and initial materials. HNTs re-agglomerate when embedded in PLA: PCL blends due to the strong hydrogen bonding between HNT particles. This agglomeration influenced the properties and structure of the composites. HNTs without surface improvement show a much poorer dispersion and low interfacial interactions in the PLA: PCL blend due to their weak compatibility with PLA: PCL molecules in the produced nanocomposite fibres. Such a PLA: PCL based composite system could help to achieve a balanced level of crystallinity with the potential advantage of stable drug release, since PCL with its high level of crystallinity simply restricts the mobility of drug molecules so that they tend to stay around the fibre surfaces. HNT is probably suitable for the accommodation of drugs because of its extremely large halloysite lumen diameter and this may facilitate better control of the drug release process.

In order to facilitate the steady drug release from PLA: PCL nanofibres, this chapter examined the effect of HNT when embedded into PLA: PCL fibres for both high and low molecular weight PCL. The effect of the modifier 3-aminopropyltriethoxysilane (ASP) on HNT was also investigated. ASP directly influences the fibre diameters, morphology, thermal properties, structure and degree of crystallinity, and it may help to delay the fast drug release normally associated with nanofibrous structures. This chapter

focused on blending high molecular weight PCL (9 wt%/v and 15 wt%/v) and PLA (fixed at 8 wt%/v) solutions with HNT at two different concentrations of 1 wt%/v and 2 wt%/v. Both unmodified HNT and HNT modified with ASP were explored in this chapter. Two different PCL concentrations, namely 9 and 15 wt%/v, were chosen in order to evaluate how the blend viscosity affects the nanofibre diameter and degree of crystallinity, which are considered to be two significant factors in the control of drug release. The blend viscosity was a vital factor for HNT dispersion within the polymer blend in the electrospinning process. Additionally, this chapter also concentrated on the effect of using different solvents and blending ratios of PLA: low molecular weight PCL embedded with HNT.

5.2 Morphological observations

5.2.1 Effect polymer blend ratio and solvent on biopolymers containing HNT

Figure 5-1 illustrates that electrospinning PLA and PLA: PCL blends with different blend ratios results in very different behaviour. For example, using PLA: PCL blend of 1:0 in chloroform: methanol with 1 and 2 wt%/v HNT created a good-quality fibre structure with average diameters of 960 and 1050 nm respectively (Figure 5-2). The good fibrous structure is due to the high volatility of methanol, which permits sufficient solvent evaporation before the fibres reach the collector, leading to the creation of the nearly identical fibres. The addition of HNT increased the fibre diameters because HNT increases the solution viscosity. With the addition of HNTs, solution viscosities increase remarkably, especially at a blend ratio of PLA: PCL of 1:0. Increasing the amount of low molecular weight PCL led to heterogeneity in the nanofibrous structure with a configuration of large beads. Whereas, at a blend ratio of 1:1, it was difficult to determine fibre diameters as a result of increasing numbers of beads. Additionally, there was no clear effect of increasing the amount of HNT from 1 to 2 wt%/v on the nanofibre diameters within experimental error. This may be due to the impact of low viscosity, which can hinder and prevent the homogeneous distribution of HNT within polymer blends and also increase the possibility of HNT sedimentation over time during the electrospinning process.

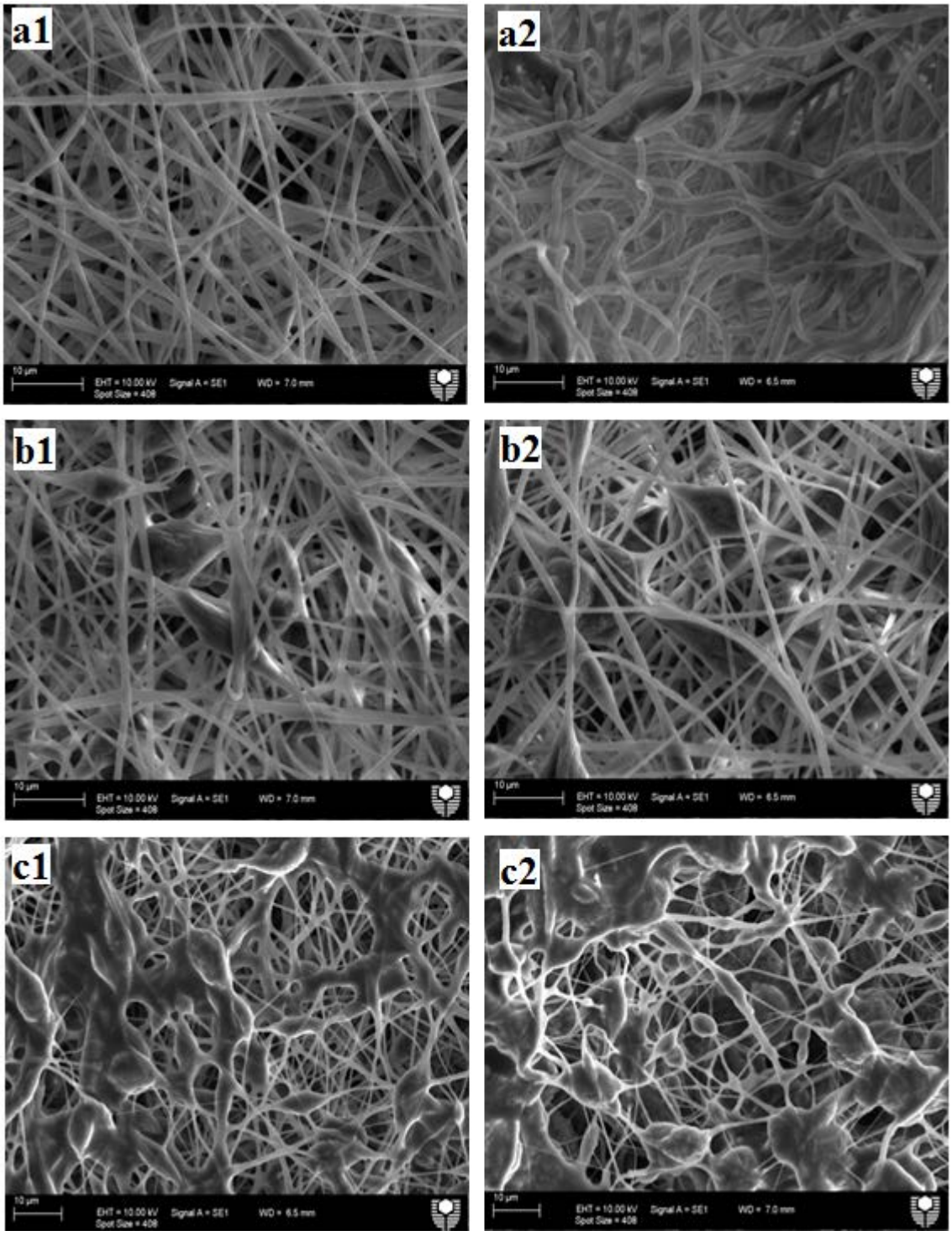

Figure 5-1: SEM micrographs of electrospun PLA: low molecular weight 15% PCL fibres using chloroform: methanol solvent and containing different PLA: PCL blend ratios: (a1) 1:0, (b1) 3:1, and (c1) 1:1 with 1 wt%/v HNT; and (a2) 1:0, (b2) 3:1, and (c2) 1:1 with 2 wt%/v HNT.

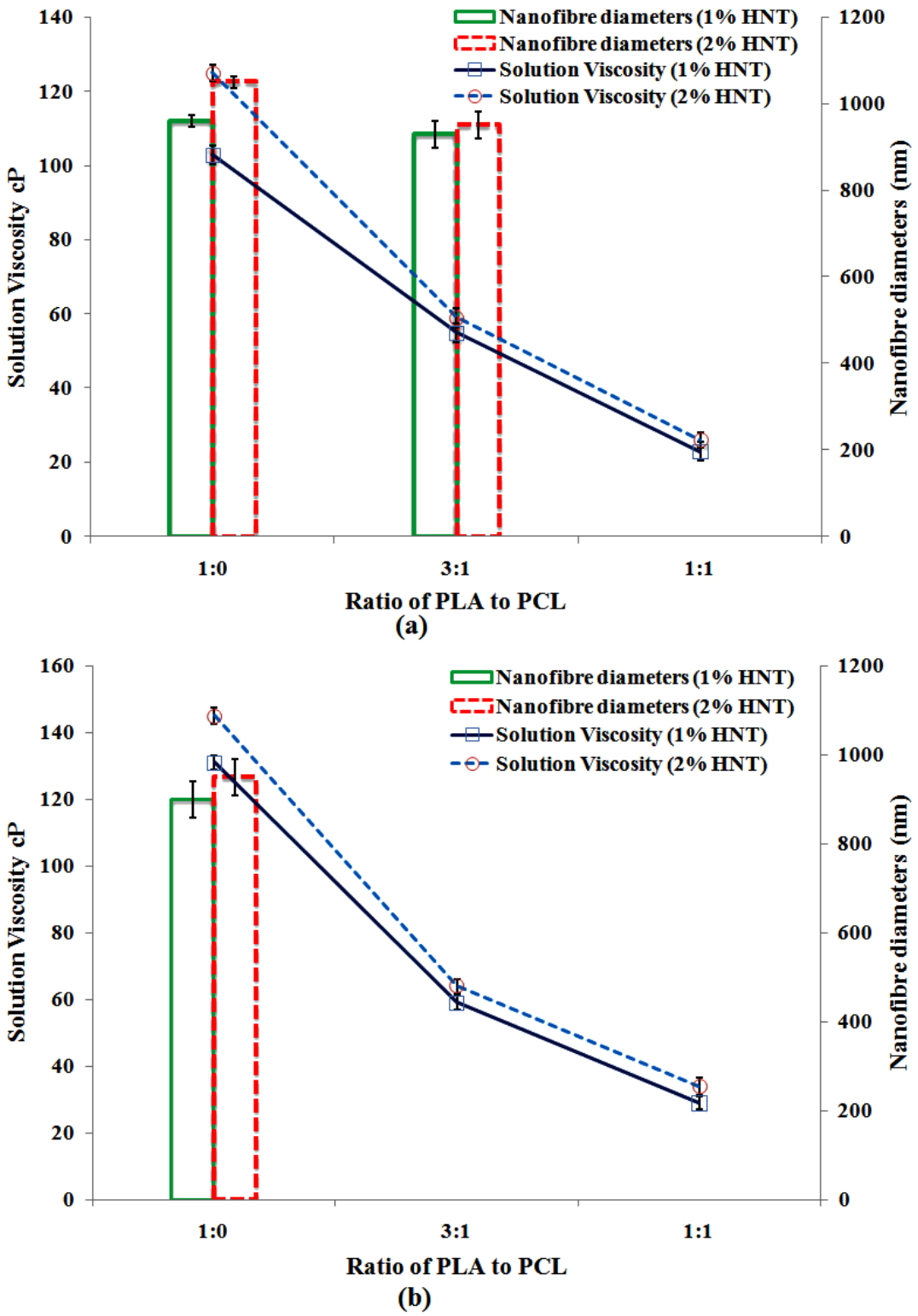

Figure 5-2: Solution viscosity and nanofibre diameters for different HNT concentrations and blend ratios of PLA to low molecular weight 15 wt%/v PCL solutions dissolved in (a) chloroform: methanol solvent and (b) DCM: DMF solvent.

Conversely, as shown in Figure 5-3, electrospun PLA: PCL blended in DCM: DMF with HNT caused beads and inhomogeneities in the structures as compared to nanofibres produced from chloroform: methanol. This phenomenon occurred despite an increase in the solution conductivity. Moreover, an increased amount of HNT from 1 to 2 wt%/v, when added to PLA: PCL at a blend ratio of 1:0 did not affect the fibre diameters within the experimental error. Nevertheless, despite increasing the amount of PCL to blend ratios of 3:1 and 1:1, no clear nanofibrous structure was obtained. The fibre diameter based on the DCM: DMF system was smaller compared to those from the chloroform: methanol system. In the electrospinning process, the low volatility of DMF led to decreased solvent evaporation, resulting in wet fibres on the collector plate. Consequently, the electric potential could not overcome the effect of solvent's low volatility and the slightly increased number of entanglements per polymer chain by increasing solution viscosity, which leads to difficulty in the formation of the jet, causing the bead-fibre structure.

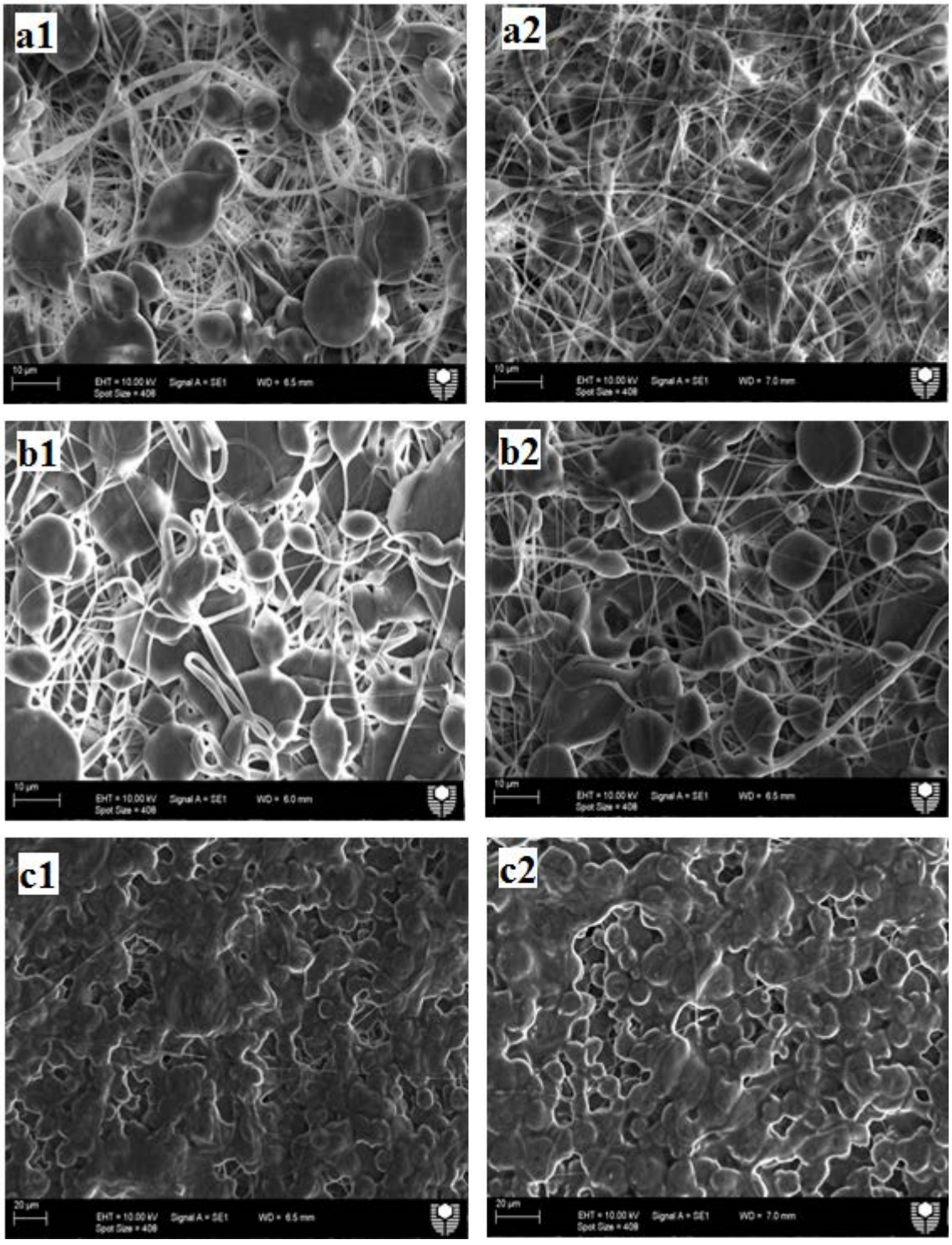

Figure 5-3: SEM micrographs of electrospun PLA: low molecular weight 15% PCL fibres using DCM: DMF solvent and containing different PLA: PCL blend ratios: (a1) 1:0, (b1) 3:1, and (c1) 1:1 with 1 wt%/v HNT; and (a2) 1:0, (b2) 3:1, and (c2) 1:1 with 2 wt%/v HNT.

5.2.2 Effect HNT concentration and HNT type: Unmodified HNT and HNT modified with ASP

To investigate the effect of HNT, the PLA: high molecular weight PCL polymer solution was blended with two different types of HNT, namely unmodified HNT and HNT modified with ASP. In addition, the solution concentration, as reflected by the viscosity of the polymer blends, is an important factor for fibre homogeneity and HNT dispersion within the polymer blend. As can be seen in Figure 5-4, the HNT tended to increase the solution viscosity as expected. Moreover, the embedded HNT frequently created a homogeneous fibrous structure with large diameters compared to those obtained from the corresponding PLA: PCL blends without HNT. Higher HNT amounts also led to larger fibre diameters regardless of the PCL concentration, Figure 5-5. Such an increase in fibre diameters may be ascribed to the dominant effect of solution viscosity on the fibrous structure. This finding is consistent with results obtained recently (Bottino et al., 2013) However, this claim contradicts the finding by Touny et al. (2010), which reported that the addition of HNT was associated with the manufacture of small-diameter fibrous structures owing to the improved electrical conductivity of the solution (Touny et al., 2010).

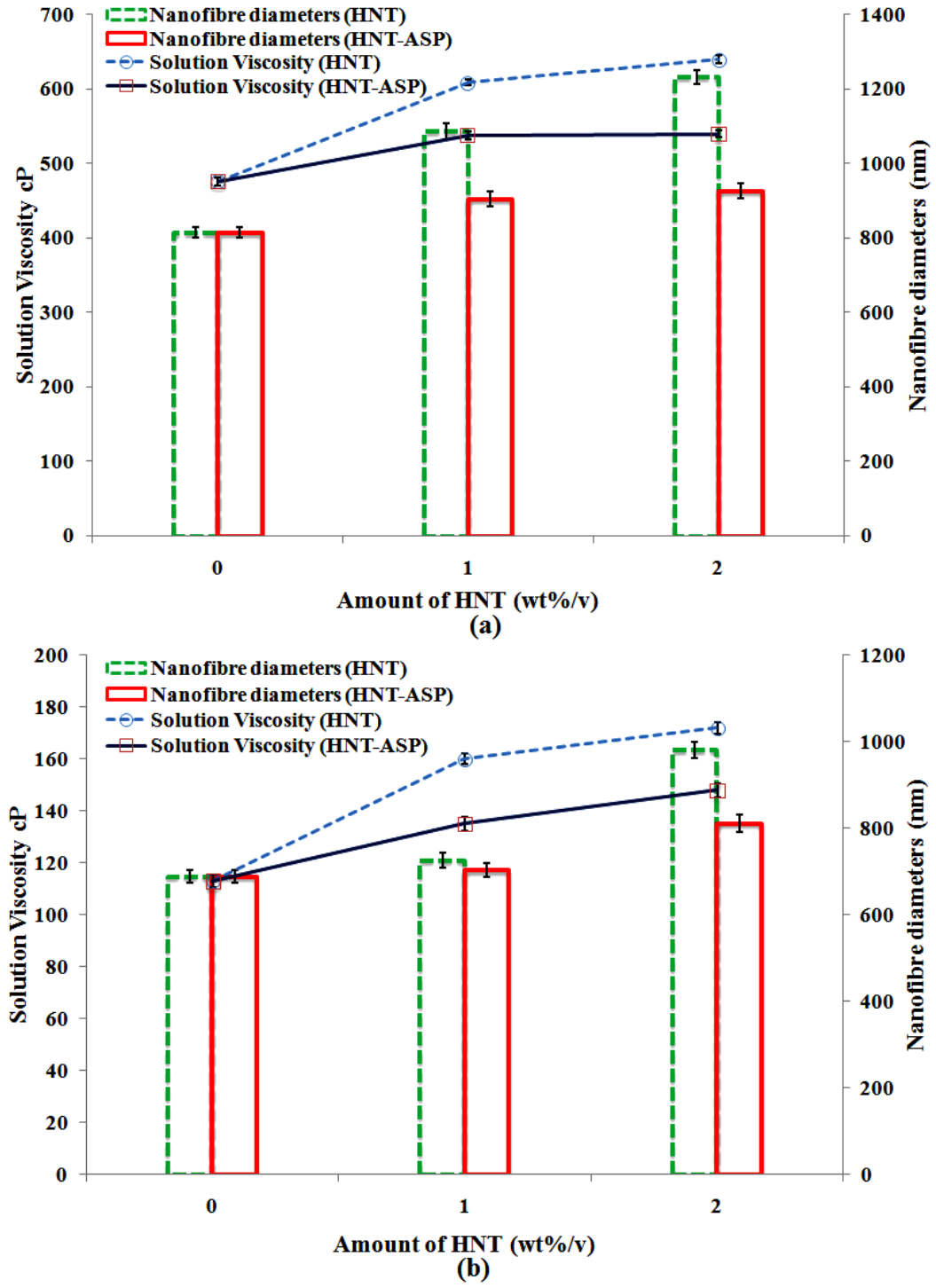

Figure 5-4: Viscosity and nanofibre diameters of 1:1 v/v mixtures of solutions of PLA and high molecular weight PCL dissolved in chloroform: methanol solvent, and blended with unmodified HNT and HNT modified with ASP: (a) 15 wt%/v PCL solution, and (b) 9 wt%/v PCL solution.

From Figure 5-6, it can be seen that the average fibre diameters due to the use of additional 1 and 2 wt%/v of HNT-ASP to form PLA: 15% high molecular weight PCL composites appeared to be virtually unchanged; whereas, there was a reasonable variation in average diameters of the 9 wt%/v PCL counterpart. The explanation for this behaviour could result from the nearly unchanged viscosity of 15 wt%/v PCL composites (538 and 540 cP for 1 and 2 wt%/v of HNT-ASP, respectively). Different from HNT-ASP, there was a reasonable increase in the average fibre diameter when embedding unmodified HNT to 9 and 15 wt%/v PCL composites, as demonstrated in Figure 5-4, owing to an increase of the solution viscosity. This may be also attributed to the increased agglomeration of unmodified HNT, which in turn may possibly lead to an increased solution viscosity. Further, the average fibre diameters produced from the additions of 1 wt%/v unmodified HNT and HNT-ASP to the PLA: 9 wt%/v PCL nanocomposite were unaffected regardless of the obvious variation in the solution viscosity, Figure 5-4(b). The low solution viscosity for 9 wt%/v PCL in comparison with 15 wt%/v PCL may preclude the creation of an HNT suspension and perhaps also lead to HNT sedimentation. In addition, Figure 5-4 demonstrated the dissimilarity in the average fibre diameters between PLA: PCL composites embedded with unmodified and modified HNT-ASP. The difference in average fibre diameter increases with increasing HNT concentration from 1 to 2 wt%/v, which may be understood by the enhanced agglomeration level resulting from increasing the quantity of HNT employed.

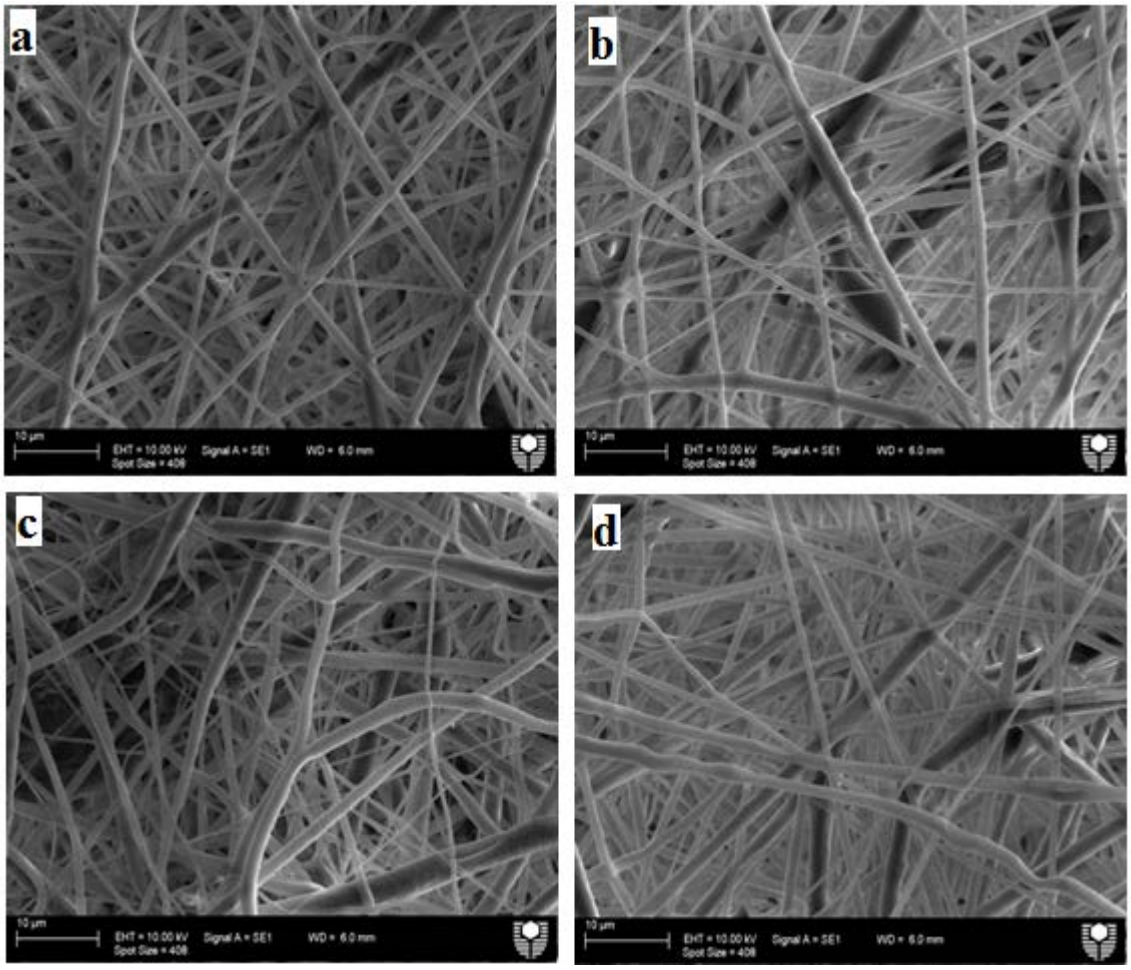

Figure 5-5: SEM micrographs of electrospun PLA: high molecular weight PCL (1:1) fibres using chloroform: methanol solvent and for two PCL concentrations blended with unmodified HNT: (a) 9 wt%/v PCL with 1 wt%/v HNT, (b) 9 wt%/v PCL with 2 wt%/v HNT, (c) 15 wt%/v PCL with 1 wt%/v HNT, and (d) 15 wt%/v PCL with 2 wt%/v HNT.

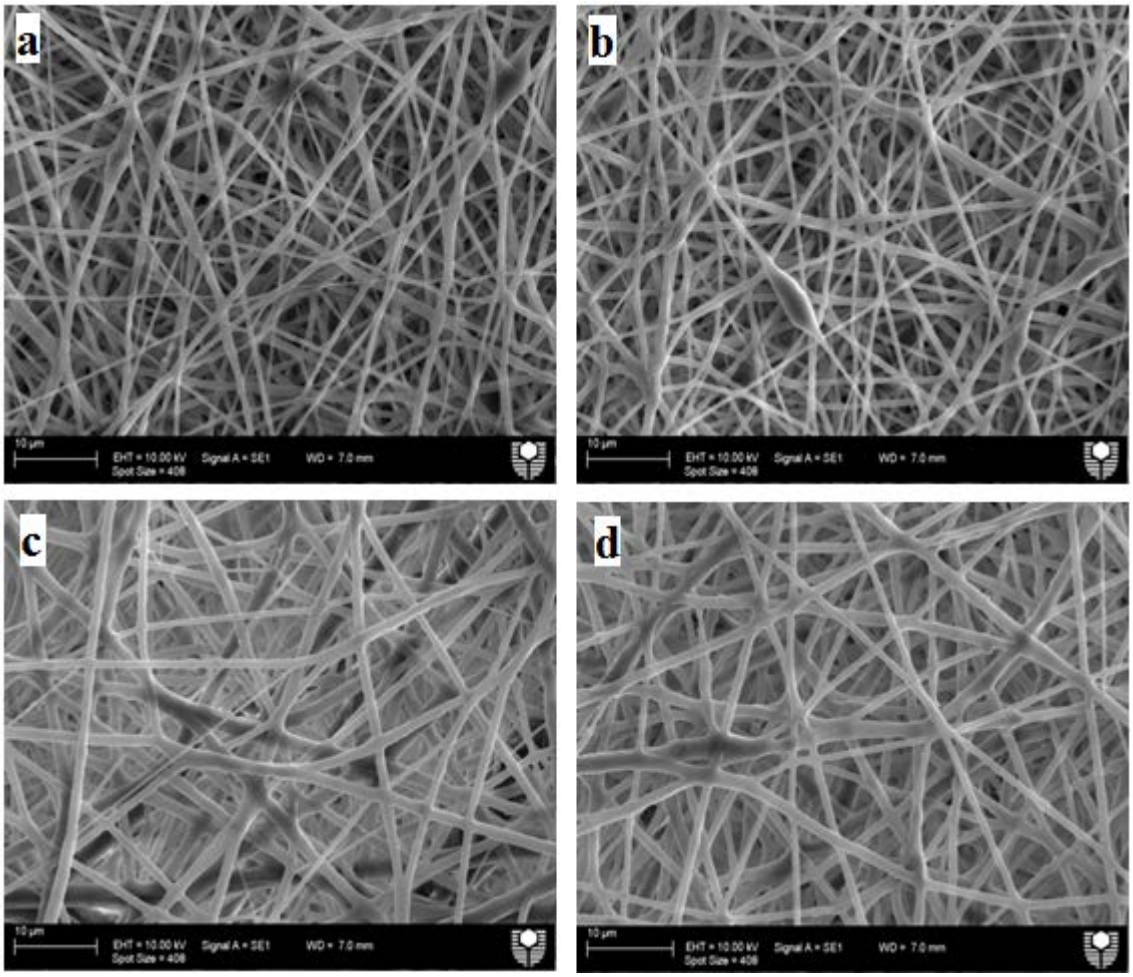

Figure 5-6: SEM micrographs of electrospun PLA: high molecular weight PCL (1:1) fibres using chloroform: methanol solvent and for two PCL concentrations blended with HNT modified with ASP: (a) 9 wt%/v PCL with 1 wt%/v HNT-ASP, (b) 9 wt%/v PCL with 2 wt%/v HNT-ASP, (c) 15 wt%/v PCL with 1 wt%/v HNT-ASP, and (d) 15 wt%/v PCL with 2 wt%/v HNT-ASP.

Figure 5-7(a) shows TEM images of composites embedded with unmodified HNT. It can be seen that several HNT particles have obviously formed agglomerates. HNT aggregated due to strong hydrogen bonding between the filler particles (Liu et al., 2007). In addition, the HNT begins to re-aggregate as a result of the fast solvent evaporation during the electrospinning process, leading to decreased HNT dispersion in the PLA: PCL composites. Even though there is some degree of agglomeration, the TEM image in Figure 5-7(b) illustrates that HNT-ASP are individually better dispersed into the PLA:

PCL blend and epoxy matrices in this composite system as compared to unmodified HNT. As shown in Figure 5-7(a), PLA: PCL rich fibrous structures are created, which are segregated from the HNT and form their special individual skewed fibre clusters. This phenomenon is not noticeable in Figure 5-7(b) for modified HNT with ASP, which proposes that a better interaction could occur between PLA: PCL fibres and HNT-ASP, and an amount of PLA: PCL fibres simply permeate into the hollow configurations of HNT-ASP. It becomes evident that the ASP might facilitate the HNT dispersion to some extent. This is because the modifier ASP tends to react with the shell of HNT throughout the particle interactions, which assists to reduce the sticking problem between the modified surfaces of HNT. The non-homogenous distribution of HNT and PLA: PCL fibres, as clearly depicted in Figure 5-7, might be caused by two processes. Initially, the electrospinning method employed in this work possibly exerts less control on modified fibres, permitting them to become twisted when assembled on the collector. Subsequently, the polymerization of the fibre mat and epoxy resin has a slight impact on the fibre orientation, which is different from injection moulding as usually employed for manufacturing polymer-clay nanocomposites. Because of such processes the TEM images, Figure 5-7 could show both cross-sectional and side views of HNT, which appear as black round dots or cylinders, respectively.

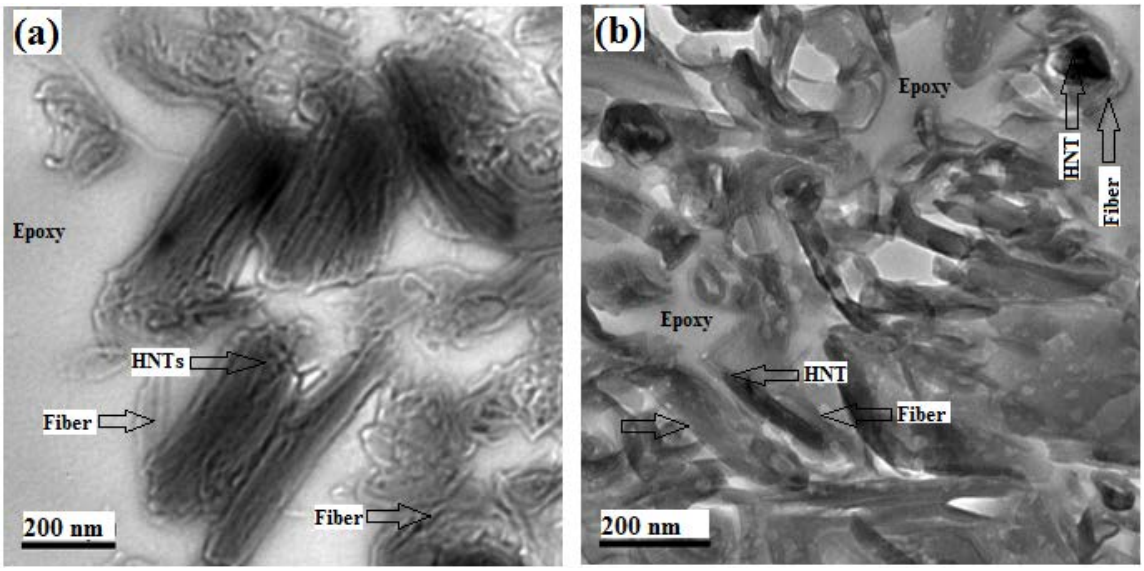

Figure 5-7: TEM images of PLA: 15% PCL composites reinforced with (a) HNT, and (b) HNT-ASP (Haroosh et al., 2013a).

5.2.3 Reaction mechanism of nanocomposites

The ethoxy groups of 3-aminopropyltriethoxysilane (ASP) can hydrolyze, resulting in the formation of SiOH groups, which can form hydrogen bonds with the surface hydroxyl groups. A hydroxyl group can react to a silica surface hydroxyl group or the hydroxyl group of a neighbouring silane molecule to form a siloxane bond. Therefore, the SiOH groups play a critical role in the formation of modified structures on the HNT surface, Figure 5-8.

Grafting occurs between hydrolyzed ASP and the surface hydroxyl groups of HNT, including the aluminol groups at the internal surface of the lumen, which may enhance the drug loading and release delay. Levis and Deasy (2003) mentioned that coating HNT was particularly effective to delay the drug release (Levis and Deasy, 2003). Modification of the HNT external surface will be useful for increasing the interaction with polymers though the HNT contains siloxane and has only a few hydroxyl groups on its external surface, which makes improvement on the inner surface more affective compared to the external surface.

Oligomerization needs high temperatures to some extent to be the dominant process for treating HNT surface. Since the modified HNT-ASP had not been heated to high temperatures during the modification stage, the dominant mechanism will be the direct grafting of ASP to the HNT surface and its preferred modification to control drug delivery compared with oligomerization (Yuan et al., 2008). However, this does not prevent the occurrence of oligomerization by connecting with each other to structure a chain and also connecting with earlier directly grafted ASP. PCL and PLA will be cross-linking with HNT-ASP by creating a hydrogen bond between the carboxylic group of the blending PLA: PCL and the hydroxyl group of the HNT-ASP, as shown in Figure 5-8.

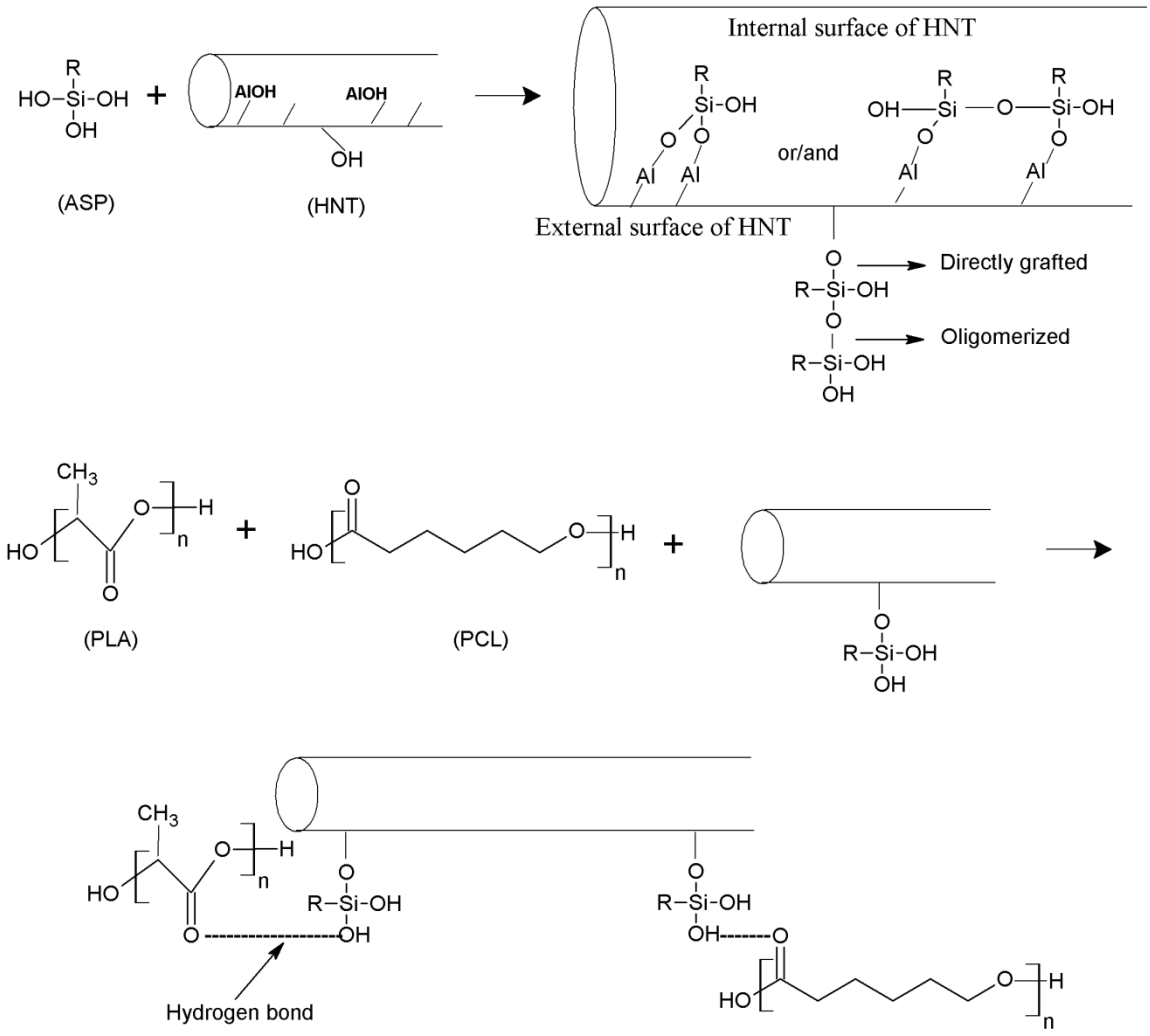

Figure 5-8: Schematic representation of the proposed mechanism of HNT surface modification and formation of cross-linked network between HNT-ASP and PLA: PCL nanofibres.

5.3 Crystallinity level and thermal properties

An XRD examination was employed to investigate the variations in crystallinity owing to the PCL molecular weight, and HNT and HNT-ASP structures, on the electrospun composites formed. Figure 5-9 demonstrates the XRD patterns for blending PLA with high and low molecular weight PCL at 15 wt%/v. It can be observed that when the PLA and PCL blends used high molecular weight PCL, the diffraction peaks of PLA: PCL at diffraction angles of 2θ = 20.11° and 23.2°, corresponding to the crystal planes (101) and (200), respectively, turn out to be more prominent owing to the positive involvement of high molecular weight PCL on the crystallization degree of the blends. It is evident from Figure 5-10 that the degree of crystallinity (X_c) deduced from the XRD patterns also increased for the PLA: 15% high molecular weight PCL as opposed to PLA: 15% low molecular weight PCL, because high molecular weight PCL has reasonable crystallinity compared to amorphous phase PLA with low crystallinity.

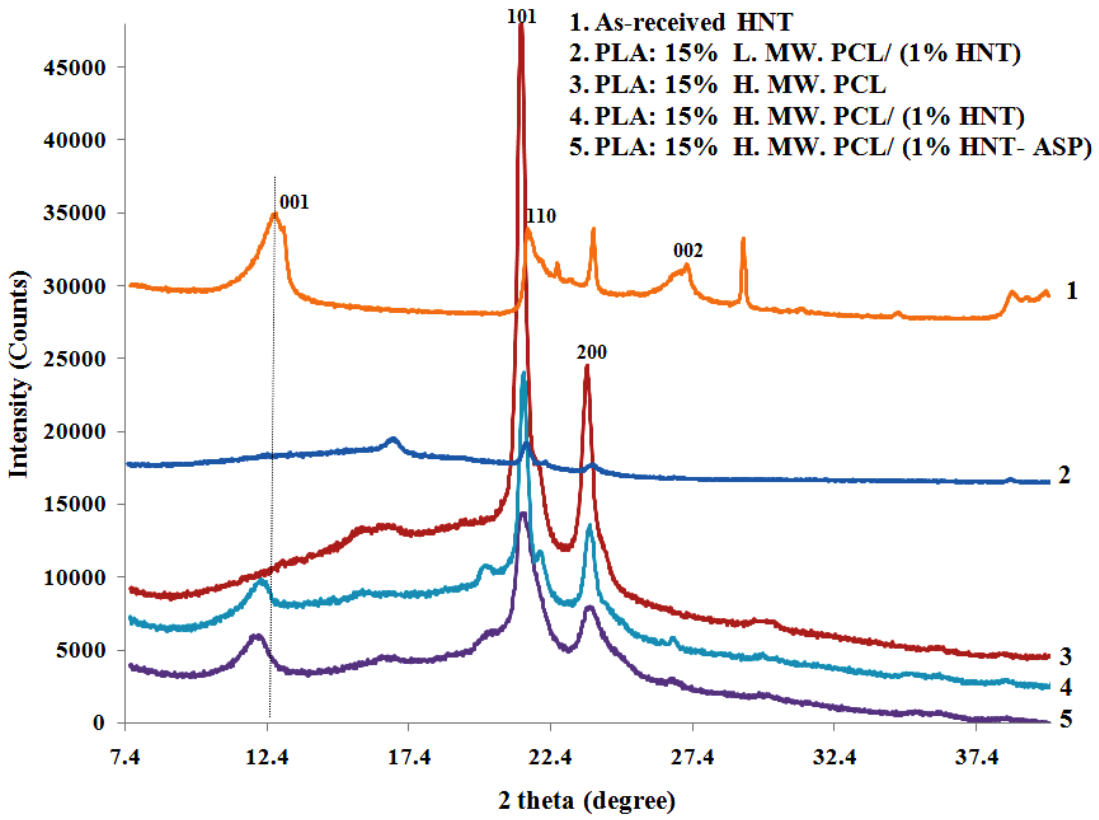

Figure 5-9: X-ray diffraction patterns for selected samples showing the relative positions of the reflection peaks due to the addition of HNT and HNT-ASP in PLA: PCL blends with different molecular weights of PCL.

Figure 5-9 shows the XRD pattern of as-received HNT, with the crystal planes (*hkl*) related to the major crystalline peaks and *d*-spacing as obtained from the DICVOL program in the FullProf software package (Boultif and Louer, 2004). The characteristic XRD peak of as-received HNT was identified at 2θ = 12.44°, in accord with the reflection plane of (001), with *d*-spacing value of 0.72 nm. This HNT basal reflection results from its tubular morphology and small crystal size (*L*) of 21.71 nm calculated from the Scherrer relation (Ning et al., 2007). In addition, further peaks at 2θ = 20.21° and 24.94°, corresponding to the (110) and (002) reflection planes with *d*-spacing values of 0.44 and 0.36 nm, respectively, are revealed in the diffraction pattern of HNT. Moreover, it has been pointed out that the HNT employed in this work is referred to as (7 Å)–halloysite with a dehydrated formation (Dong et al., 2011). It was found from the

database of the EVA program that the peak at 2θ = 8.76° for hydrated particles totally vanishes. Additionally, Figure 5-9 demonstrates the XRD patterns for PLA: 15% high molecular weight PCL composites embedded with 1 wt%/v HNT-ASP and HNT. The data showed that the XRD peaks for HNT-ASP embedded in PLA: PCL nanocomposites appear at 2θ = 12.21°, 19.87° and 23.26° with *d*-spacing values of 0.73, 0.45 and 0.39 nm corresponding to the planes (001), (102) and (111), respectively. The (001) peaks of unmodified HNT and HNT-ASP based on PLA: PCL nanocomposites were smaller and wider compared with the peak of as-received HNT powders, which could correspond to the break-down of bulky HNT agglomerates into sub-micron particles. Furthermore, the (001) peaks were slightly shifted to lower angles of 12.35º and 12.21º for HNT and HNT-ASP based on PLA: PCL nanocomposites compared with that of as-received HNT powders at 2θ = 12.44º. This finding indicates that HNT-ASP based on PLA: PCL nanocomposites possess slightly enhanced dispersion than unmodified HNT based nanocomposites in good accordance with the TEM results in Figure 5-7. A potential explanation could be that the agglomeration tendency is reduced when employing ASP to modify HNT, which could help the HNT-ASP disperse in the PLA: PCL mat with a decreased occurrence of aggregates. The first peak (001) intensities have decreased for unmodified HNT and HNT-ASP based on PLA: PCL nanocomposites when compared to that of as-received HNT, further implying the less well-ordered formation of HNT particles. Since this is verified by the TEM findings in Figure 5-7, it can be said that HNT are present in a partially jumbled and randomly organized distribution. It can be recognized from Figure 5-10 that the embedding of 1 wt%/v HNT to blend polymers decreased the crystallinity of the nanocomposites as opposed to PLA: 15% high molecular weight PCL. Moreover, increasing the amount of HNT to 2 wt%/v led to a further reduction of crystallinity level. The resulting degree of crystallinity is affected by the restricted mobility of the polymer chains, which hinders good crystal growth.

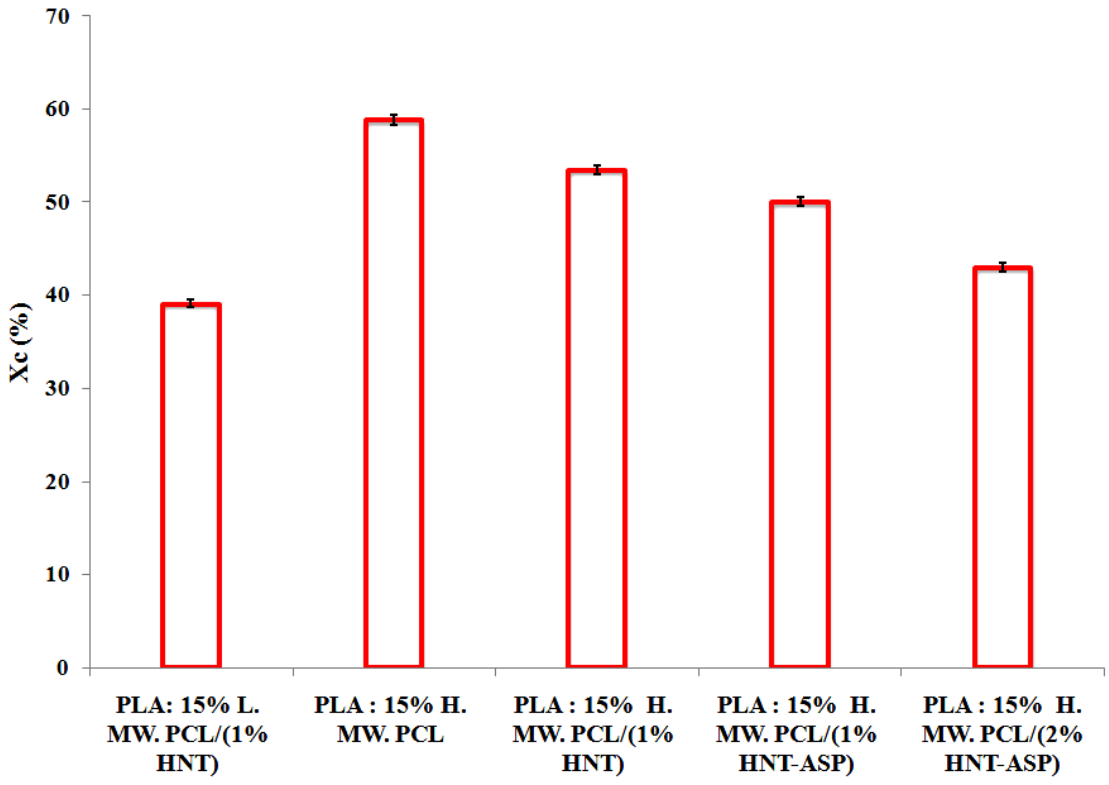

Figure 5-10: Degree of crystallinity (X_c) results for PLA: PCL composites reinforced with HNT and HNT-ASP calculated from XRD data.

The thermal behaviour of electrospun composites was determined in the current work. Data are reported just for the first heating scan. The data from cooling scans were ignored because no DSC peaks were identified due to the cold crystallization nature of PLA (Shibata et al., 2006). As shown in Figure 5-11 and Table 5-1, the glass transition temperature (T_g) and melting temperature (T_m) of PCL within the PLA: PCL/ HNT nanocomposites becomes lower when the PCL molecular weight decreases. However, the T_g of PLA within the blends is difficult to identify owing to its overlapping with the melting peak of PCL. In addition, the presence of 1 wt%/v HNT-ASP in the nanocomposites resulted in reasonable decreases in the values of T_g of high molecular weight PCL and crystallization temperature (T_c) of PLA. Such reductions increased with the addition of 2 wt%/v HNT-ASP, but displayed a more obvious decreasing trend relative to that with unmodified 1 wt%/v HNT. The nucleating agent role of HNT has been demonstrated to promote the heterogeneous nucleation of polymeric molecules, as

confirmed by the decreased value of T_c, particularly in the PLA: 15% high molecular weight PCL nanocomposites embedded with 2 wt%/v HNT-ASP as compared to the polymer blend without HNT.

A small reduction of T_g value occurs in high molecular weight PCL of HNT-ASP based composites compared with unmodified HNT. This finding may result from the decreased crystallinity level and enhanced HNT dispersion as confirmed by the aforementioned XRD results. This has very good implications for the drug loading ability of the nanocomposites, where better dispersion of HNT would be able to accommodate a higher amount of drug molecules within the nanocomposite. The differences in T_m and T_g values might be assigned to the electrospinning processing parameters and resulting dispersed nanofibre diameters, which influence the orientation of polymeric chains (Picciani et al., 2010).

Table 5-1: DSC results for PLA: PCL nanocomposites with unmodified HNT and modified HNT-ASP[a].

Material sample	T_g (°C) PCL	T_m (°C) PCL	T_g (°C) PLA	T_c (°C) PLA	T_m (°C) PLA
PLA: 15% H. MW. PCL	–52.2	63.8	-	84.0	152.5
PLA: 15% L. MW. PCL / (1% HNT)	–62.6	55.0	-	78.4	153.3
PLA: 15% H. MW. PCL / (1% HNT)	–56.5	63.4	-	83.1	152.4
PLA: 15% H. MW. PCL / (1% HNT-ASP)	–58.3	62.8	-	81.1	151.1
PLA: 15% H. MW. PCL / (2% HNT-ASP)	–62.2	59.7	-	74.0	151.1

[a]*Calculations were repeated for three sets of samples. The standard deviation for the T_g, T_c and T_m values was less than 0.5°C.*

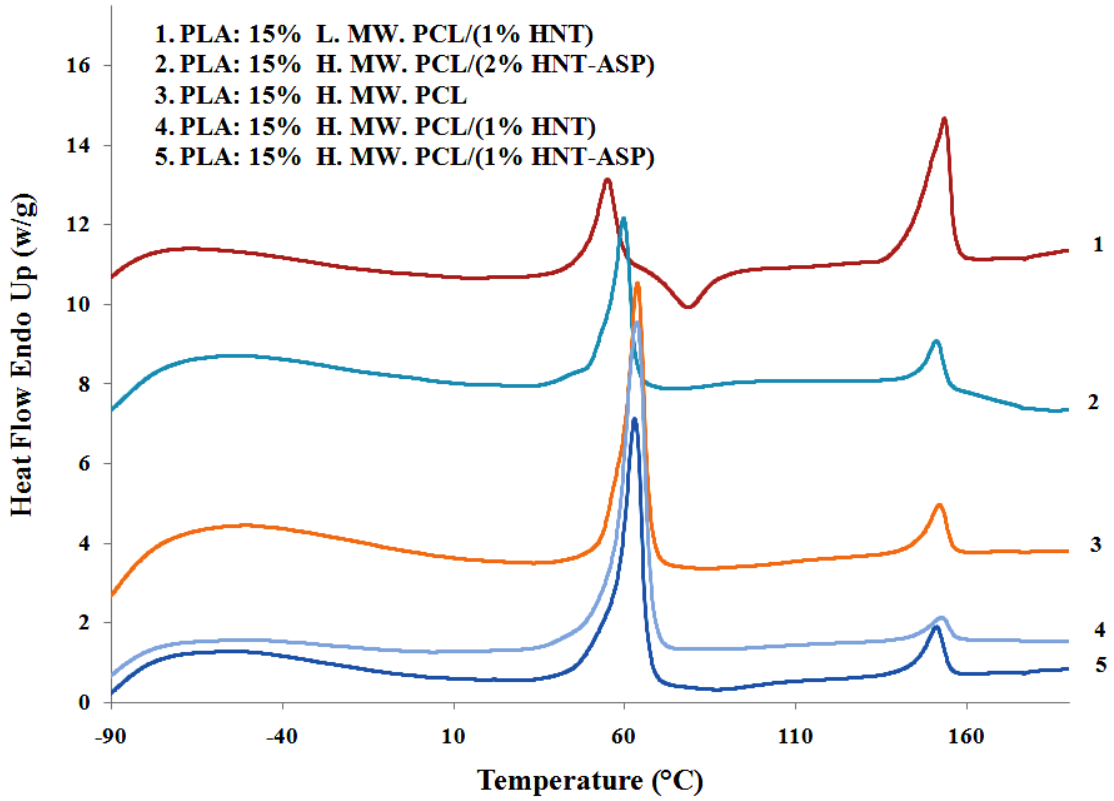

Figure 5-11: DSC thermograms for selected samples including PLA: 15% PCL fibres, PLA: 15% PCL with 1% HNT and 1% HNT-ASP.

5.4 Intermolecular interactions

Fourier transform infrared spectroscopy (FTIR) was employed to explain possible interactions between the HNT and the biopolymers. Figure 5-12 illustrates that PLA: PCL electrospun fibres exhibit two carbonyl stretching (C=O) bands at 1724 cm^{-1} and 1757cm^{-1} for PCL and PLA, respectively. The spectrum of as-received HNT powder shows two intense bands at 3621 cm^{-1} and 3694 cm^{-1}, which are assigned to the O–H group vibration. However, the peaks at 1117 cm^{-1}, 1027 cm^{-1} and 1005 cm^{-1} are associated with stretching of Si–O, and the adsorption peak at 910 cm^{-1} is defined by Al–OH groups. The external surface of HNT is composed of siloxane (Si–O) groups, whilst the internal surface consists of aluminol (Al–OH) groups. Grafting between ASP and HNT occurs by connecting molecules of hydrolyzed ASP straight to the internal and external surface for a fraction of the HNT hydroxyl groups, as shown in the reaction mechanism in Figure 5-8. It comprises the aluminol and silanol groups at edges surface

and the aluminol groups at internal lumen surface, which may enhance the drug loading and delay drug release.

A comparison of the spectra of PLA: PCL, PLA: PCL / HNT and PLA: PCL / HNT-ASP in Figure 5-12 demonstrates that some FTIR peaks have been either moved, have appeared or have totally disappeared. For example, when embedding HNT and HNT-ASP into the PLA: PCL nanocompsites, the single PLA: PCL band at 1184 cm^{-1} has been broadened and moved to lower wave numbers of 1167 and 1179 cm^{-1}, respectively. It is proposed that a moderate contribution of the HNT bands with wave numbers of 1117, 1027 and 1005 cm^{-1} are associated with the stretching of Si–O. Moreover, the peak of PLA: PCL nanocomposites embedded with unmodified HNT disappeared at a wave number of 1130 cm^{-1}, while for PLA: PCL nanocomposites embedded with HNT-ASP a new peak appeared at 913 cm^{-1}. This phenomenon might be the result of the HNT bond recognized at wave number 910 cm^{-1}, which is ascribed to the Al–OH groups. Additionally, the involvement of the surface hydroxyl groups and the O–H group vibration bands at 3621 and 3694 cm^{-1}, also confirm the effective embedding characteristic of HNT-ASP within the PLA: PCL nanocomposite. The infrared spectra of the final composites thus confirm the previous TEM and XRD results.

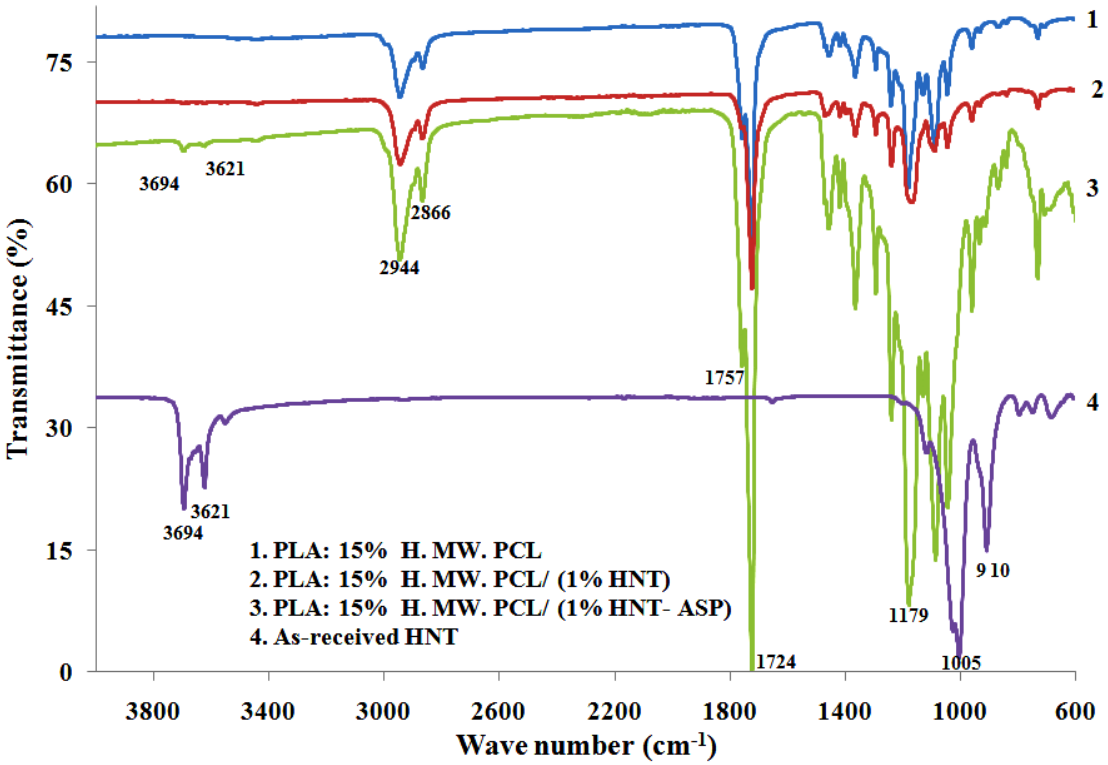

Figure 5-12: FTIR spectra for selected samples including as-received HNT, electrospun PLA: 15% PCL fibres, and PLA: 15% PCL nanocomposites.

5.5 Summary

This Chapter showed that when HNTs were embedded with PLA: low molecular weight PCL, there was no obvious effect on the variation of nanofibre diameters due to the increase of HNT concentration from 1 to 2 wt%/v. This is due to the influence of low viscosity of PLA: low molecular weight PCL solution in reducing the homogeneous distribution of HNTs within the blend solution and also promoting HNT sedimentation during the electrospinning process. In addition, using a DCM: DMF solvent produced beads and inhomogeneity in the structures as compared to nanofibres generated by using chloroform: methanol.

The embedding of HNT into PLA: high molecular weight PCL blends increased the solution viscosity, thus resulting in the occurrence of more homogeneous fibres. The average fibre diameters decreased with the reduction of HNT concentration for both high molecular weight PCL concentrations. The average fibre diameters with HNT-ASP were decreased significantly in comparison to those with unmodified HNT when using 15 wt%/v PCL. Somewhat better dispersion and less agglomeration were achieved for PLA: PCL composites embedded with HNT-ASP compared to unmodified HNT, which has benefits for drug release applications. The low solution viscosity for 9 wt%/v PCL compared with 15 wt%/v PCL reduced the creation of an HNT suspension and led to HNT sedimentation. The current chapter has promoted nanofibre quality without any bead defects or non-fibrous structures by controlling the crystallinity level of the PLA: PCL blend. Moreover, the embedding of HNT-ASP into the polymer blends led to a reasonable decrease in the degree of crystallinity, in addition to small decreases of glass transition temperature of PCL, the crystallization temperature and melting temperature of PLA within the composites. The infrared spectra of the composites proved the effective embedding of HNT-ASP into PLA: PCL nanofibres compared with unmodified HNT due to the modifier ASP minimizing agglomeration.

Chapter 6
Biopolymer and MP Nanocomposites

6.1 PLA: high molecular weight PCL: MP system

Magnetic nanoparticles (Fe_3O_4) are inorganic materials with low toxicity, super-paramagnetic properties, good biocompatibility, easy preparation and better stability in the atmosphere than metal nanoparticles (Zhang et al., 2009). The purpose of this chapter is to ultimately produce a novel electrospun hybrid composite system by mixing PLA: PCL blends with magnetic nanoparticles (MPs), which may be employed with a range of bioactive drugs for wound healing applications. This chapter also provides a holistic evaluation of electrospun PLA: PCL/ MP composites in a systematic manner, from their fabrication to structural analysis and material characterization. Furthermore, MPs have extremely small diameters (20–50 nm) and also have electrical and mechanical properties totally different from HNTs, which may significantly affect the properties of the PLA: PCL blends and the nanofibrous structures produced, and thus result in the alteration of drug release kinetics.

This chapter focused on blending high molecular weight PCL (9 wt%/v and 15 wt%/v) and PLA (fixed at 8 wt%/v) solutions with pure and impure MPs at three different concentrations, 0.01, 0.1 and 1wt%/v. Both pure and impure MPs were synthesized in the laboratory and the chemical reaction suggested for the MP synthesis is expressed in equation (1). Pure and impure MPs were considered in this study because it was desired to assess the effect of the salts present in the impure MPs on the fibre diameter and morphology. It is well known that salts in polymeric solutions enhance their electrical conductivity, which is one of the significant factors in the electrospinning process.

$$FeSO_{4(s)}+2Fe(NO_3)_{3(s)}+8NaOH_{(aq)} \longrightarrow Fe_3O_{4(s)}+Na_2SO_{4(aq)}+6NaNO_{3(aq)} + 4H_2O_{(l)} \quad (1)$$

6.2 Morphological observations

6.2.1 Effect of pure MP concentration

To examine the impact of MPs, the PLA: PCL blend solution was mixed with three different concentrations of pure MPs, 0.01, 0.1 and 1 wt%/v. Figure 6-1 demonstrates that two main processing variables in electrospinning, namely solution viscosity and electrical conductivity, are both enhanced when the pure MP concentration increases from 0 to 1 wt%/v. As seen from Figure 6-2, the embedding of pure MPs in the PLA: PCL blends tends to create homogeneous composite fibrous structures with smaller nanofibre diameters as opposed to electrospun PLA: PCL nanofibres. The average nanofibre diameters are detailed in Table 6-1. It is obvious that the nanofibre diameter decreases sharply from 711 to 583 nm when the pure MP concentration increases from 0.01 to 1 wt%/v, which is much lower than PLA: PCL nanofibre diameter at 814 nm.

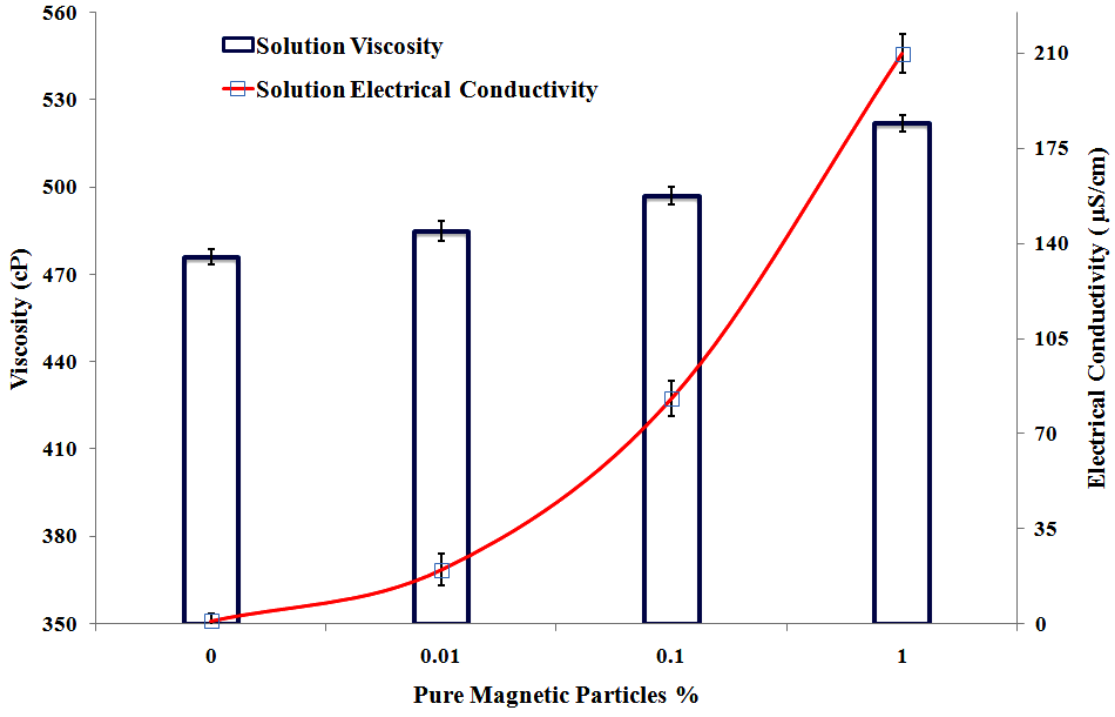

Figure 6-1: Effect of pure MP concentration on viscosity and electrical conductivity of PLA: high molecular weight PCL at a blend ratio of 1:1.

Table 6-1: Summary of the average fibre diameters[a] (nm) for hybrid composites with MPs.

MPs	MP 0%	MP 0.01%	MP 0.1%	MP 1%
Pure	814 (±15)	711 (±15)	685 (±20)	583 (±25)
Impure	814 (±15)	80 (±15)	62 (±15)	51 (±15)

[a]*The numbers in parenthesis are the standard deviations.*

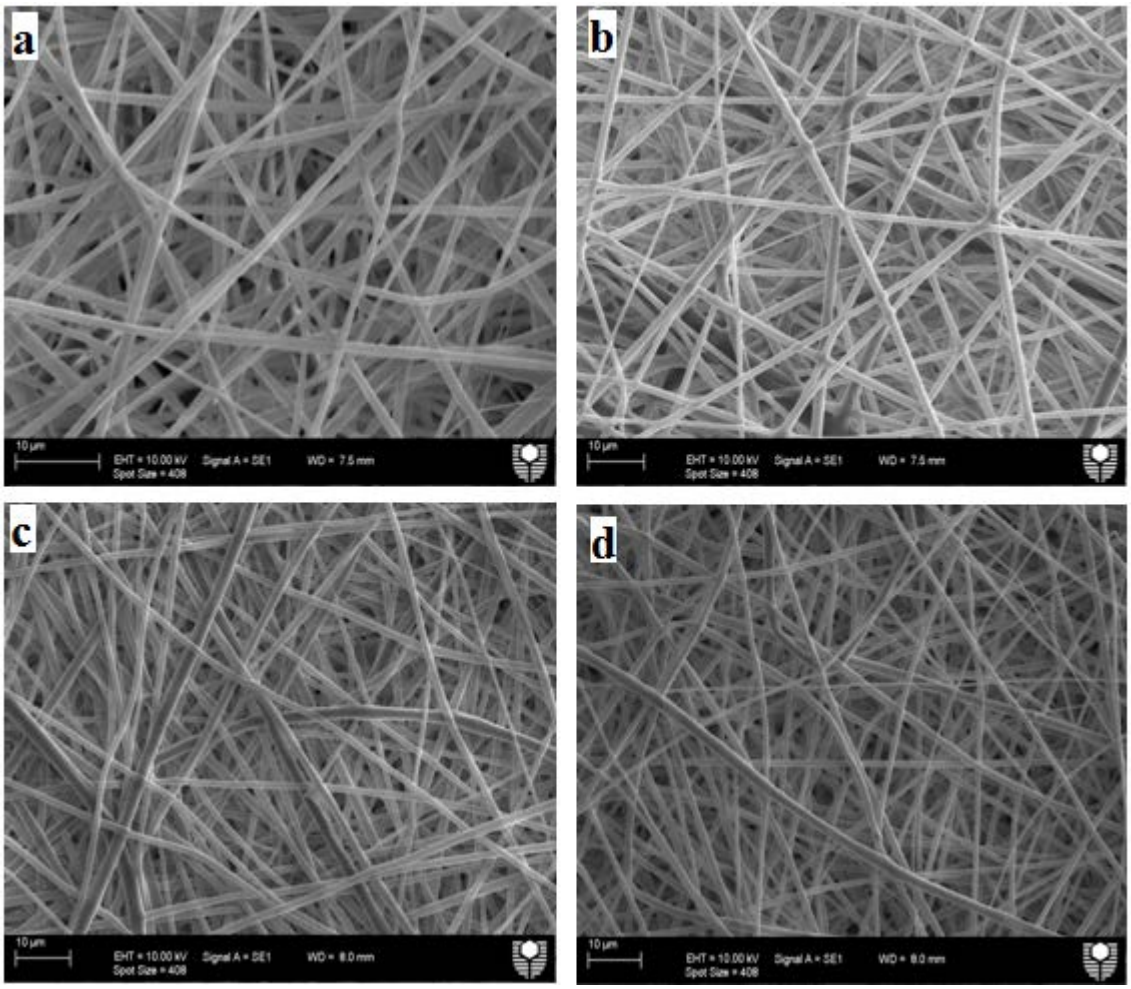

Figure 6-2: SEM micrographs of electrospun PLA: high molecular weight PCL/ pure MP composites: (a) 0 wt%/v MPs, (b) 0.01 wt%/v MPs, (c) 0.1 wt%/v MPs and (d) 1 wt%/v MPs.

It was previously reported that decreasing the solution viscosity resulted in a decrease of the fibre diameter (Ji et al., 2006), whilst a higher electrical conductivity produced electrospun fibres with smaller diameters. The decreased nanofibre diameters found in this study could be ascribed to the predominant effect of the significant increase of electrical conductivity relative to a modest increase of solution viscosity. In terms of the effect of electrical conductivity, as shown in Figure 6-1, an increase in the MP concentration led to an increase in the electrical conductivity, apparently due to the increase of the iron content. As a matter of fact, the increased electrical conductivity inevitably produces more electrical charges that are carried by the electrospinning jet. Consequently, higher repulsive forces are imposed on the jet, which elongate the jet materials into fibrous structures under the electrical field (Zamani et al., 2010). Furthermore, by increasing the electrical conductivity, the draw rate and large draw ratio of the jet in its bending instability area can be increased during electrospinning. Hence, the induced jet path becomes longer and the solution droplets undergo a stretching process. Both higher repulsive forces and greater bending instability could contribute to electrospun fibres with smaller diameters (Lee et al., 2010; Saraf et al., 2009).

6.2.2 Effect of impure MP concentration

PLA: high molecular weight PCL blend solution was mixed with 0.01, 0.1 and 1 wt%/v impure MPs to fabricate electrospun composite nanofibres. As shown in Figure 6-3 and Table 6-1, quite small nanofibre diameters, about one-tenth of those of PLA: PCL blend fibres with pure MPs, were produced with impure MPs. The average fibre diameters decline from 80 to 51 nm when the impure MP concentration increases from 0.01 to 1 wt%/v. This phenomenon might be explained by the dual effect of a sharp decline in solution viscosity and a considerable increase of electrical conductivity caused by increasing the impure MP concentration from 0 to 1 wt%/v. Both solution viscosity and electrical conductivity of PLA: PCL composites with impure MPs are much more sensitive to MP concentration than their counterparts with pure MPs, as shown in Figures 6-1 and 6-4. The solution viscosity suddenly declines from 476 to 13 cP with impure MPs compared to a moderate increase from 476 to 522 cP with embedding pure

MPs. As previously indicated, a significant drop in the solution viscosity and increase in the electrical conductivity inevitably result in reduced nanofibre diameters.

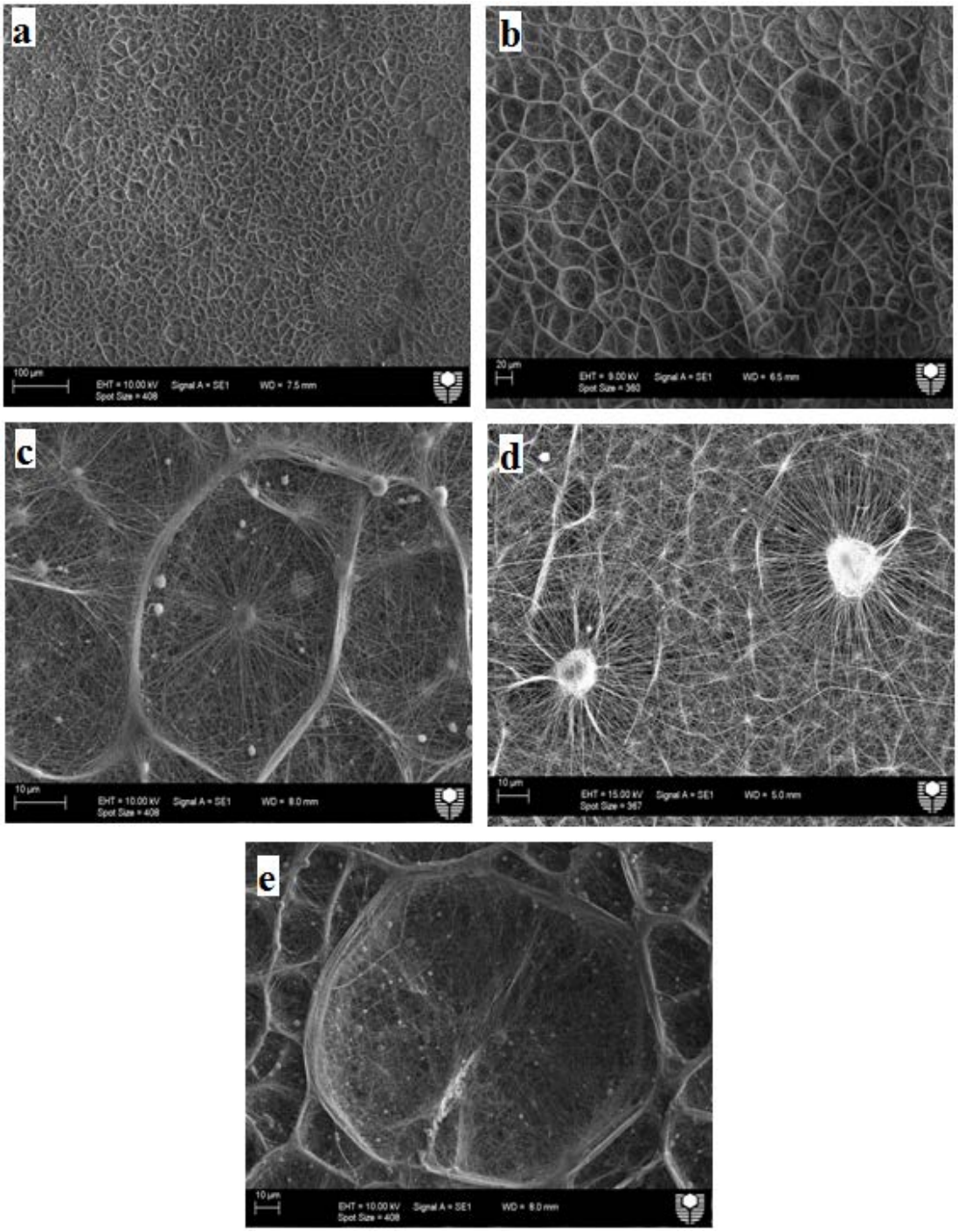

Figure 6-3: SEM micrographs of electrospun PLA: PCL/ impure MP composites: (a) to (c) 0.1 wt%/v impure MPs with micrograph scales 100, 20 and 10µm, respectively; (d) 0.01 wt%/v impure MPs; and (e) 1 wt%/v impure MPs.

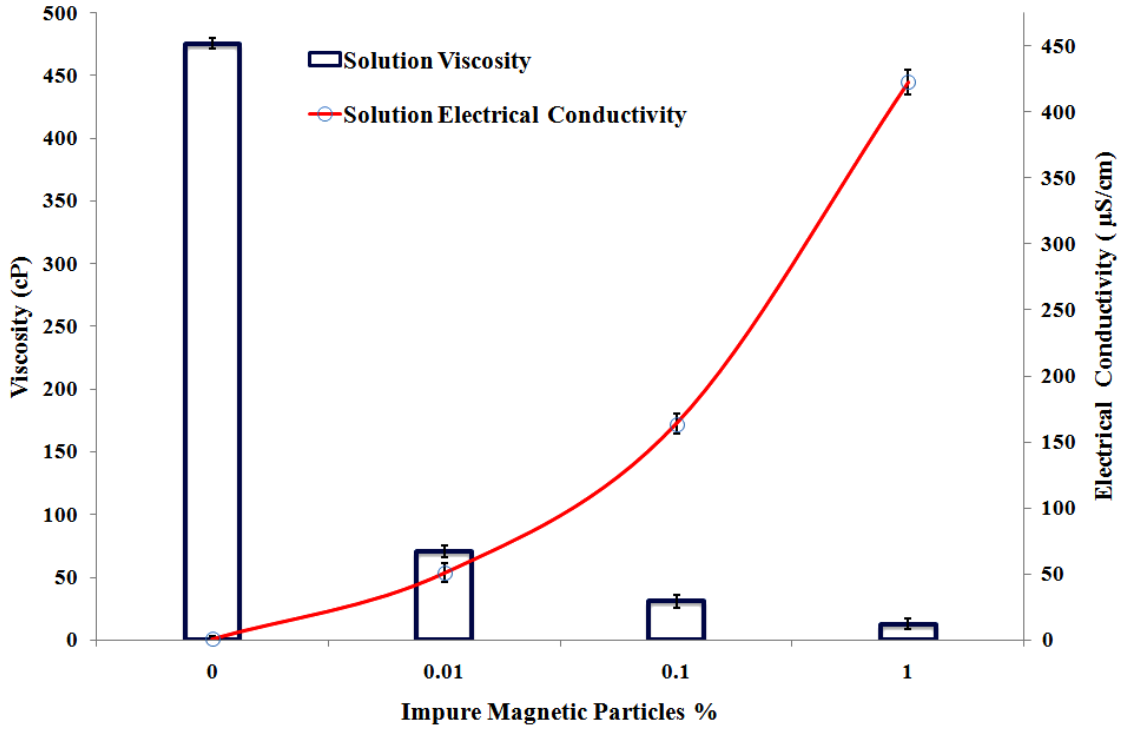

Figure 6-4: Effect of impure MP concentration on solution viscosity and electrical conductivity of the PLA: high molecular weight PCL blend solution.

It is surprising to note that the fibrous structures in Figure 6-3 include nearly 3D spherical cells with rough nuclei diameters ranging between 1 and 10 µm. The fibres radiate away from a central nucleus and these cells became larger and more aggregated with increasing the MP concentration, particularly as revealed in Figures 6-3(c) and (e). Each cell is isolated from other cells by borders, which are shaped from bundles of overlapped fibres. The fibres line up around the nuclei, and more aligned fibres are visible in the central area of nucleus, Figure 6-5. The fibres were found to start to disappear from the nuclei when the MP concentration increased, which could be owing to the rapid decline in the solution viscosity, leading to the creation of tiny-diameter fibres and beads. These unique material structures and behaviour are reported for the first time in this research, and have not been indicated elsewhere in the literature. The nuclei seem to be aggregated MPs produced as a consequence of the low PLA: PCL solution viscosity. For that reason, tiny MPs tend to be easily stirred through the PLA:

PCL solution, which, because of their magnetization, huge surface area and high surface energy, allows them to attract one another and aggregate. The reorientation of MP positions may lead to the alignment of MPs with the applied electrical field after solvent removal during the electrospinning fabrication process.

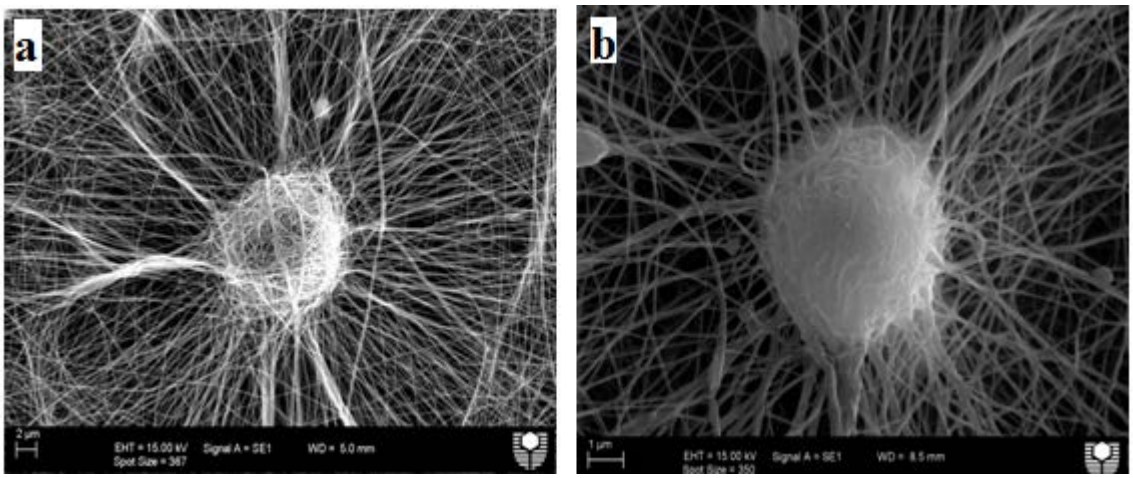

Figure 6-5: SEM micrographs showing the electrospun composite fibres lining up around the nuclei: (a) 0.01 wt%/v impure MPs and (b) 0.1 wt%/v impure MPs.

The sharp decline in the solution viscosity is due to the impurities existing in the untreated magnetic nanoparticles, composed of salts such as sodium sulphate, sodium nitrate and sodium hydroxide. It was indicated in this work that the impurities lead to reduced molecular weight of the PLA: PCL blends, from 84700 g/mol in the neat polymer blend down to 62700, 20200 and 12600 g/mol at three impure MP concentrations of 0.01, 0.1 and 1 wt%/v, respectively, as seen in Figure 6-6. Nonetheless, there was no clear effect of embedding pure MPs on the molecular weight. This decline may be due to sodium sulphate, which can react with the PLA: PCL blend resulting in the break-down of PLA: PCL molecular chains into smaller fragments. In addition, when sodium nitrate loses an oxygen atom, it causes the formation of sodium nitrite, which reduces the polymerization rate, and in turn contributes to a decrease of the molecular weight for polymer blends (Detrembleur et al., 2002). Moreover, the OH group reacts with the ester bonds to produce intermediate degradation polymers, after which further break-down of the initial products into fractions with lower molecular

weights occur (Makino et al., 1986). It was noticed that the pure MPs did not influence the pH value of PLA: PCL solution. However, impure MPs increase the pH values of the solution to 12.11, 12.32 and 12.76, when embedding 0.01, 0.1 and 1 wt%/v impure MPs, respectively. These are in contrast to the pH value of 6.88 for the PLA: PCL blend without MPs. Such a phenomenon might be ascribed to the hydrogen bonding being disturbed through the depolymerisation process, which can increase the pH value, decrease molecular weight and improve the polymer solubility, in good agreement with a previous comparable finding for chitosan polymer (Mao et al., 2004). Impure MPs produce non-uniform fibrous structures with cell aggregation and tiny fibre diameters, making them unsuitable for the drug release application as opposed to pure MPs.

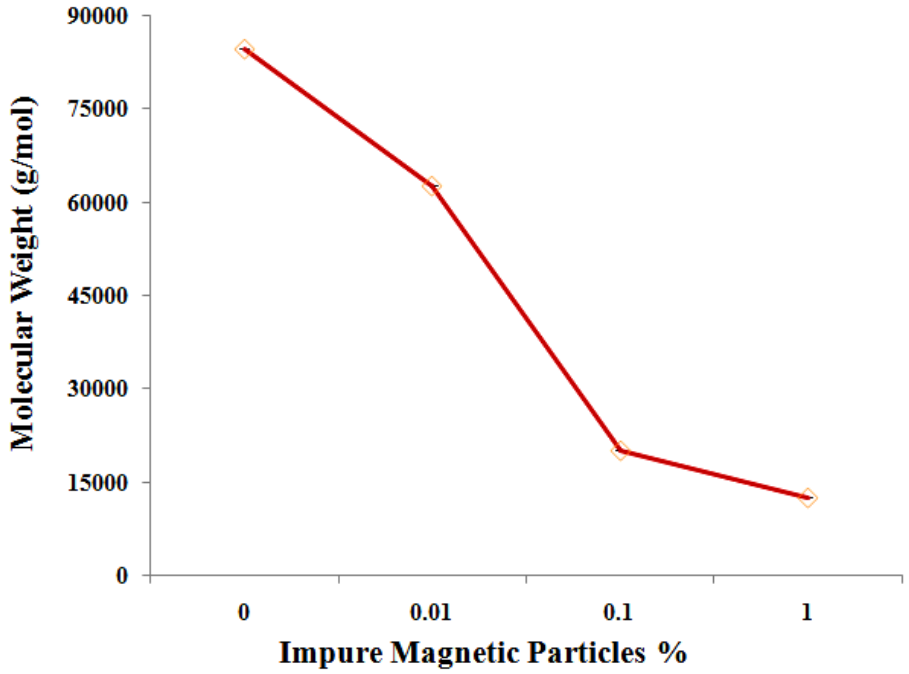

Figure 6-6: Effect of impure MP concentration on molecular weight of PLA: PCL blend.

6.3.3 Pure and impure MP dispersion

The impure MPs dispersed inside the electrospun PLA: PCL composite nuclei within the epoxy matrices were examined by TEM due to the relatively large nuclei diameters that hinder the identification of impure MPs by energy dispersive spectroscopy (EDS). Pure MP dispersion was investigated by SEM. Moreover, the elemental compositions of the impure and pure MPs were confirmed by EDS. Figure 6-7(a) illustrates a TEM image and an EDS spectrum of the morphological structures for 0.1 wt%/v impure MPs. Clearly, most impure MPs aggregate inside large nuclei, which is in good agreement with the previous SEM results. The average diameters of impure MPs are about 15–35 nm according to image analysis based on counting 200 particles from eight TEM images. As shown in the EDS spectra of the nuclei, the peaks of Fe and O elements suggest that the hybrid nanocomposite contained Fe_3O_4. The presence of Na shows the mixture has impure MPs, resulting in the reduced molecular weight of the PLA: PCL blend. The peak of the C element is associated with the PLA: PCL nanofibres. Figure 6-7(b) shows an SEM image and an EDS spectrum of the nanofibrous structures for 1 wt%/v pure MPs. Obviously, some pure MPs aggregate inside nanofibres. As indicated in the EDS spectrum of the aggregated particles (specified in circuits), the peaks of Fe and O elements confirm that the PLA: PCL nanocomposite contained only Fe_3O_4 without any impurities.

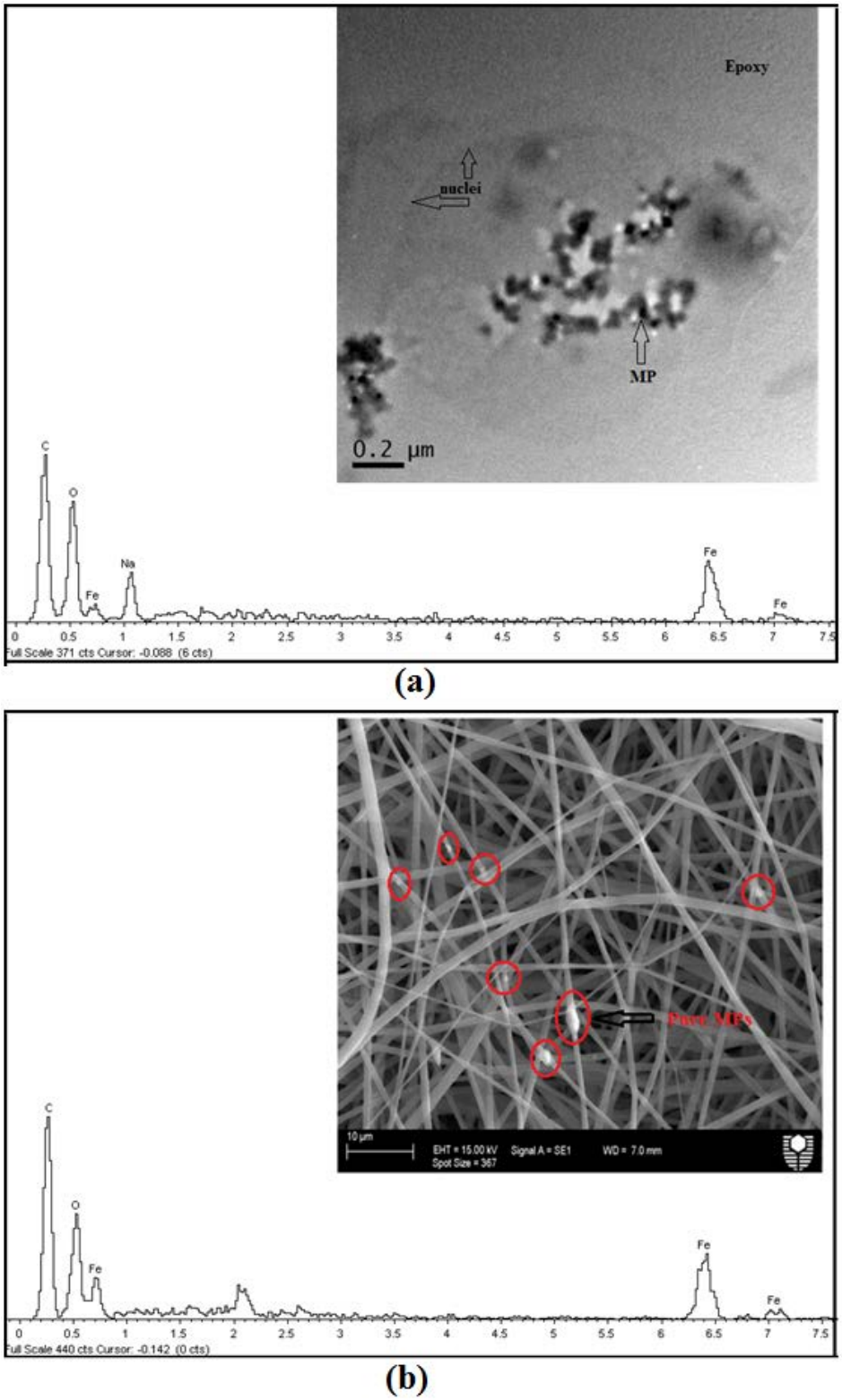

Figure 6-7: (a) typical TEM image and EDS spectra of epoxy/ PLA: PCL fibres embedded with impure MPs, and (b) SEM image and EDS spectra of PLA: PCL fibres embedded with pure MPs.

6.3 Crystallinity level and thermal properties

The crystalline structures of MPs are reported in Figure 6-8(a), with XRD patterns acquired from pure and impure MPs. The peaks were labelled with the XRD reflection, and the crystal planes (*hkl*) corresponding to the main crystalline peaks were detected in the DICVOL program of the FullProf software (Boultif and Louer, 2004). Pure MPs possess the same pattern as that of crystalline magnetite, which includes six diffraction peaks: (220), (311), (400), (422), (511) and (440) identified at 2θ = 30.1, 34.3, 43.1, 53.4, 57.2and 63.2°, respectively. Their corresponding *d*-spacing values are 0.29, 0.25, 0.21, 0.17, 0.16 and 0.14 nm accordingly, in good accordance with those of typical magnetite (Fe_3O_4). As for impure MPs, there were other diffraction peaks (112) and (202) detected at 2θ = 39.2 and 41.5°, which indicates the existence of sodium carbonate (Na_2CO_3) present as an impurity. This component may have been created when impure MPs were synthesized. Sodium hydroxide (NaOH) is in contact with atmospheric air and adsorbs CO_2toform Na_2CO_3 when added dropwise to the MP solution, as shown in equation (2):

$$2NaOH_{(aq)} + CO_{2(g)} \longrightarrow Na_2CO_{3(aq)} + H_2O_{(l)} \qquad (2)$$

Additionally, it seems that the high peak labelled (220) and (002) at 2θ = 30.1º essentially consists of two overlapping peaks for impure MPs. The average crystal size (*L*) of MPs based on the Scherrer relation is on the order of 20±5 and 40±5 nm for pure and impure MPs, respectively.

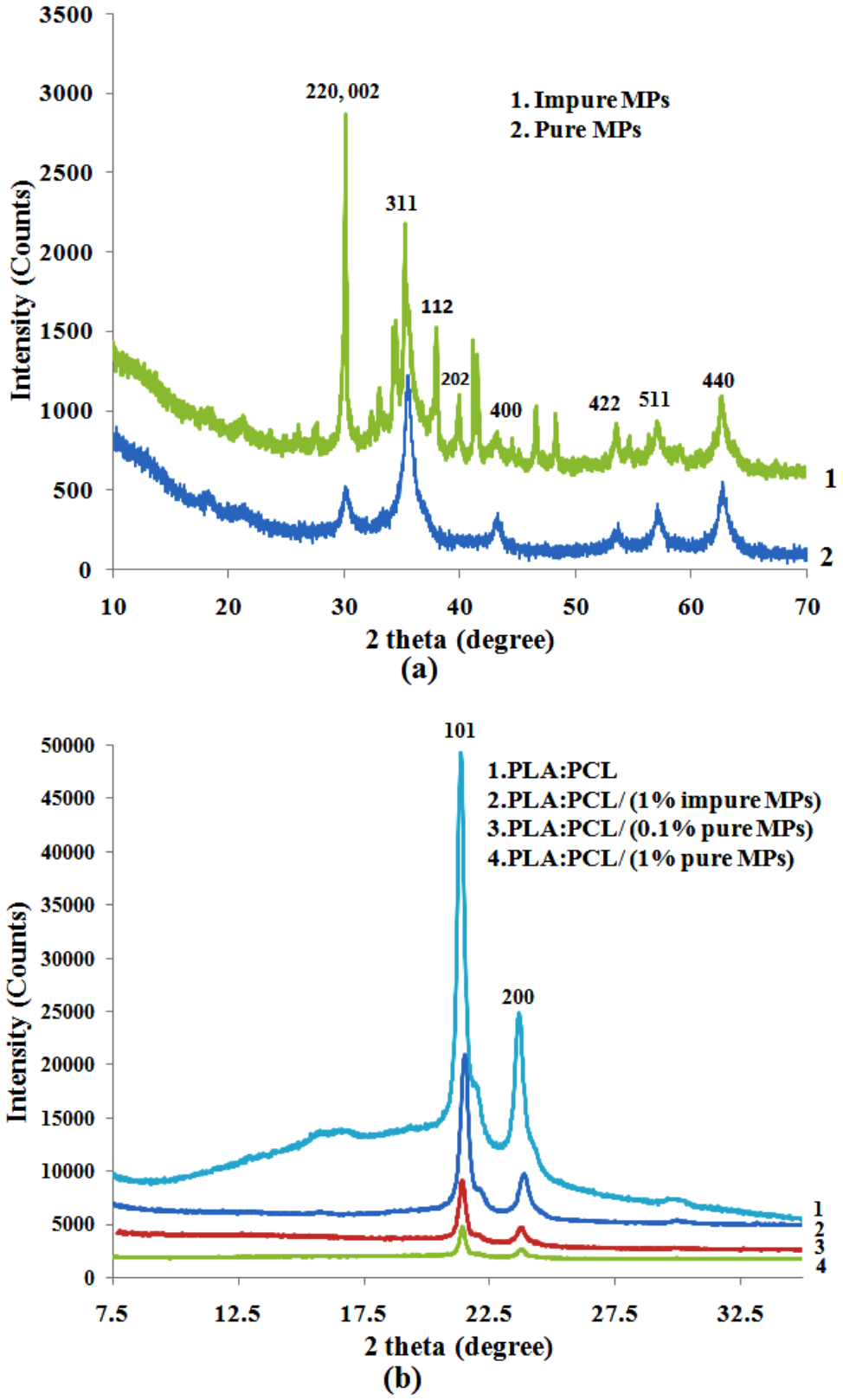

Figure 6-8: XRD patterns for selected materials showing the relative positions of the diffraction peaks: (a) impure and pure MPs, and (b) PLA: PCL/ MP composites.

Figure 6-8(b) also shows the XRD patterns for PLA: PCL/ MP composite fibres with 1 wt%/v impure MPs, and 0.1 and 1 wt%/v pure MPs. Generally the XRD patterns have two diffraction peaks (101) and (200) without any considerable difference in the peak position, which signifies that the addition of MPs has very minor impact on the alteration of the crystalline structures in the composite nanofibres.

The XRD data were employed to detect the degree of crystallinity in Figure 6-9. It has been recognized that the degree of crystallinity of PLA: PCL/ MP composites reduces considerably when increasing the pure MP concentration. Such a decreasing trend might be explained by the abundant nucleation cores that create a proliferation of tiny crystallites leading to a low degree of overall crystallinity (Lee et al., 2003). The crystallinity decreases more remarkably when pure MPs are simultaneously embedded at particle concentrations from 0 to 1 wt%/v. MPs seem to greatly accelerate the nucleation process. Accordingly, this phenomenon results in a shorter period for the disentanglement of molecular chains. The associated degree of crystallinity is usually caused by the restricted mobility of polymer chains, which hinders good crystal growth.

On the contrary, the embedding of impure MPs gives rise to an increase in the degree of crystallinity on account of the impurities that can decrease the molecular weight of the PLA: PCL blends. As a result of the low molecular weight, the short polymer chains could be mainly crystallized through the electrospinning process, as opposed to the highly entangled chains of the high molecular weight blends, leading to more amorphous phases. Besides, molecular rearrangements through the solidification process can be hindered by the longer polymer chains, resulting in lower mobility and greater intermolecular entanglement (Suwa et al., 1973).

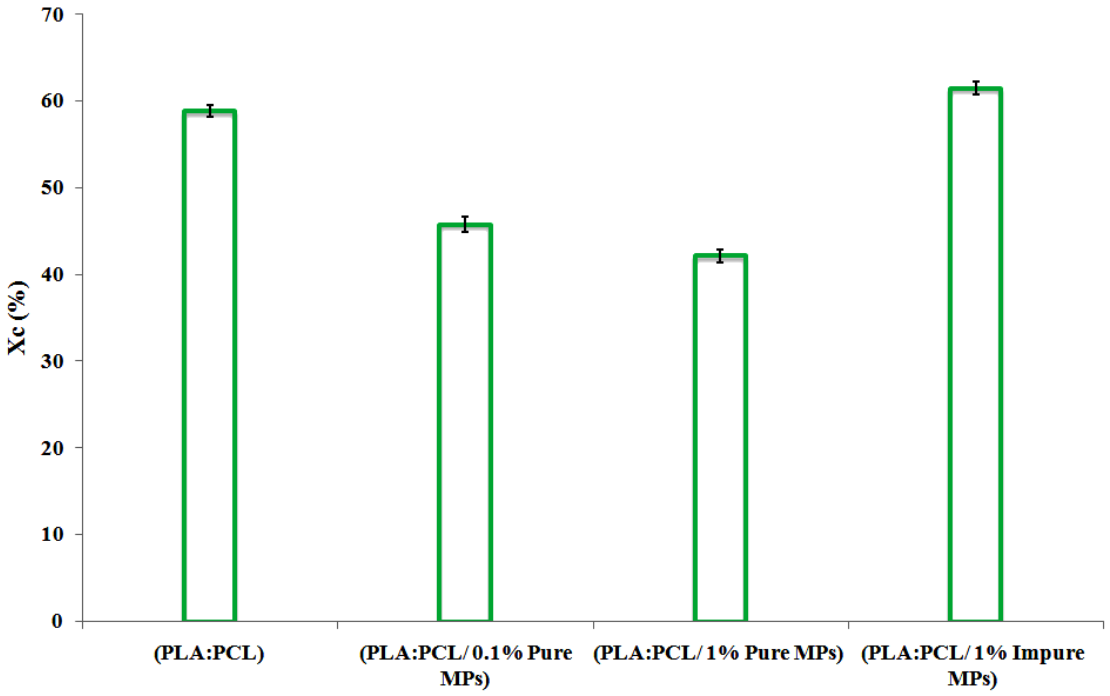

Figure 6-9: The degree of crystallinity X_c for PLA: PCL blends and PLA: PCL based composite fibres with pure and impure MPs. The X_c values were calculated from XRD data.

Table 6-2: DSC results for PLA and PLA: PCL based composite fibres with pure and impure MPs[a].

Sample	T_g (°C) PCL	T_m (°C) PCL	T_c (°C) PLA	T_m (°C) PLA
PCL (fibres)	–58.0	63.1	-	-
PLA: PCL	–52.2	63.8	84.0	152.5
PLA: PCL (0.1% pure MPs)	–53.0	61.5	82.7	151.7
PLA: PCL (1% pure MPs)	–58.2	62.2	81.6	151.5
PLA: PCL (1% impure MPs)	–53.2	63.1	88.0	-

[a]*Calculations were repeated for three sets of samples. The standard deviation for the T_g, T_c and T_m values was less than 0.5°C.*

The DSC thermal properties of electrospun composite nanofibres are revealed along with those of neat PCL fibres and PCL: PLA blends in Figure 6-10 and Table 6-2. The

glass transition temperature (T_g) of PCL within the fibre composites decreases noticeably, and there was a slight decline in the melting temperature (T_m) of both PLA and PCL when increasing the MP concentration from 0 to 1wt%/v. The decrease of T_g is assigned to the effect of incorporation of magnetite particles having an anisotropic character, in good accordance with previous work (Kumar et al., 2000). Furthermore, the electrospinning process and resulting fibre diameters can also affect the directional mobility of the polymer chains, leading to a difference in T_g (Picciani et al., 2010). The added MPs in PCL: PLA have been found to slightly decrease the crystallisation temperature (T_c) of PLA. The role of MPs in promoting the heterogeneous nucleation of polymer molecules has not been substantially demonstrated, which could be assigned to the low MP concentration. The T_g of PLA within the blend is hard to detect because it overlaps with the melting peak of PCL.

The embedding of impure MPs into the PLA: PCL blend leads to a remarkable enhancement in the T_c value of PLA, while there were no significant alterations to the T_g and T_m of PCL, which is attributed to the significant decline in the molecular weight of the polymer blends. This influence of impure MPs on the molecular weight was much greater on PLA as opposed to PCL. The major explanation is that the quantity of PCL was approximately double that of PLA in the blend. It also lies in the comparatively low crystallinity of PLA, which undergoes a more rapid process of ester hydrolysis compared with PCL. This can cause an increased concentration of ester groups easily attainable in the PLA (Pitt et al., 1981). As a result, the impurities associated with MPs are able to react faster with PLA, which could lead to more complexity in the T_m behaviour of PLA.

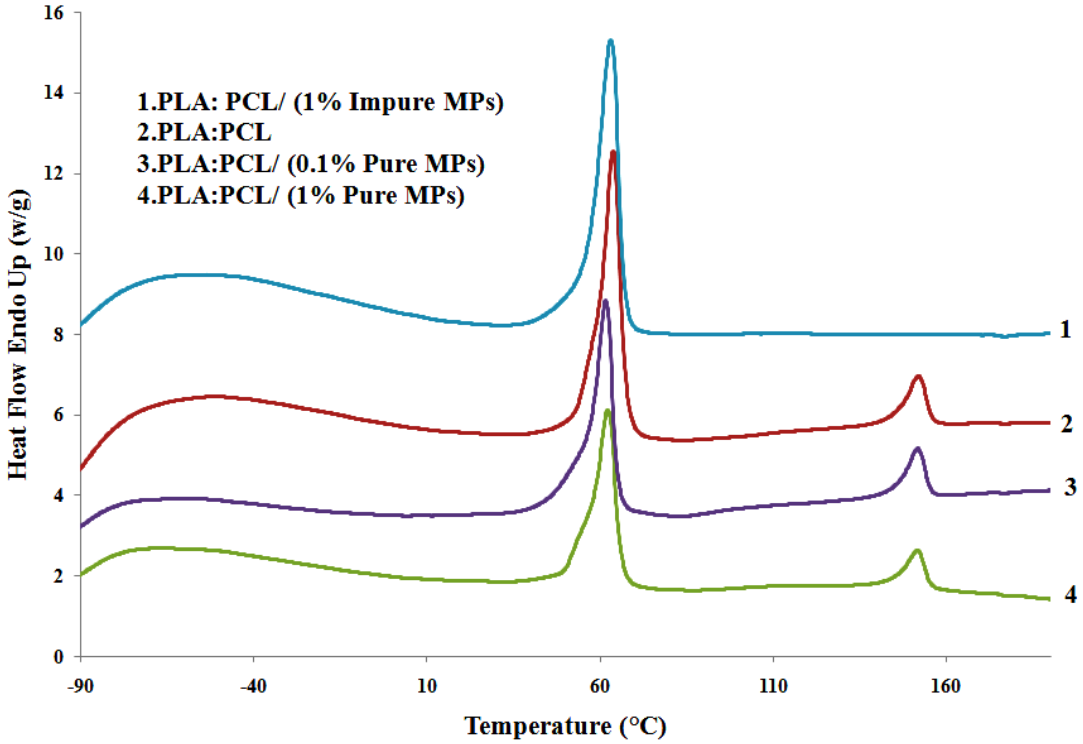

Figure 6-10: DSC thermograms for selected material samples.

6.4 Intermolecular interactions

Fourier transform infrared spectroscopy (FTIR) was utilized to explain interactions between the MPs and the PLA: PCL biopolymers. As displayed in Figure 6-11(a), the IR spectra of MPs show bands in the low frequency region between 1050 to 550 cm^{-1} owing to the absorption band of Fe–O. For pure MPs, the band present at 1636 cm^{-1} is related to water deformation, whereas the peak at 3200 cm^{-1} is associated with the O–H bond, which arises from the hydroxyl group of lauric acid. For impure MPs, new bands occur at 1424 and 1156 cm^{-1}, which are allocated to inorganic nitrates and sulphates. Additionally, there are some shifts in Fe–O bands possibly due to differences in the particle sizes of pure and impure MPs. The surface bond force constant increases when the size of MPs becomes very small, resulting in the reorganization of electrons on the particle surface because of the destruction of many bonds between the surface atoms (Khan, 2008).

Figure 6-11(b) illustrates the FTIR spectra of PLA: PCL and MPs embedded in the PLA: PCL based composites. PLA: PCL nanofibres at 1757cm^{-1} for PLA and 1724 cm^{-1} for PCL show initially two carbonyl stretching (C=O) bands. The spectra of PLA: PCL, PLA: PCL/pure MP composites and PLA: PCL/impure MP composites display a range of different phenomena including shifting, appearance or complete disappearance of peaks. The single PLA: PCL band at 1184cm^{-1} is broadened and shifted to lower wave numbers of 1179 and 1175 cm^{-1} when incorporating pure and impure MPs, respectively, into the PLA: PCL blends. In addition, the existence of the Fe–O band at 583 cm^{-1} confirms the successful embedding of characteristic bands of PLA: PCL and MPs in the infrared spectra of the final composite nanofibres. Moreover, the peaks of PLA within the PLA: PCL blends happen at both 1757 cm^{-1} and 1088 cm^{-1}, which reflect the carbonyl stretching C=O band and the C–O stretching band, respectively. These peaks disappeared when impure MPs were embedded. It can be established that there is a considerable interaction between the PLA: PCL blends and impure MPs owing to the impurities associated with the MPs as previously characterized. Such a result supports the findings from the DSC data that indicate a greater impact of impure MPs on PLA compared to PCL.

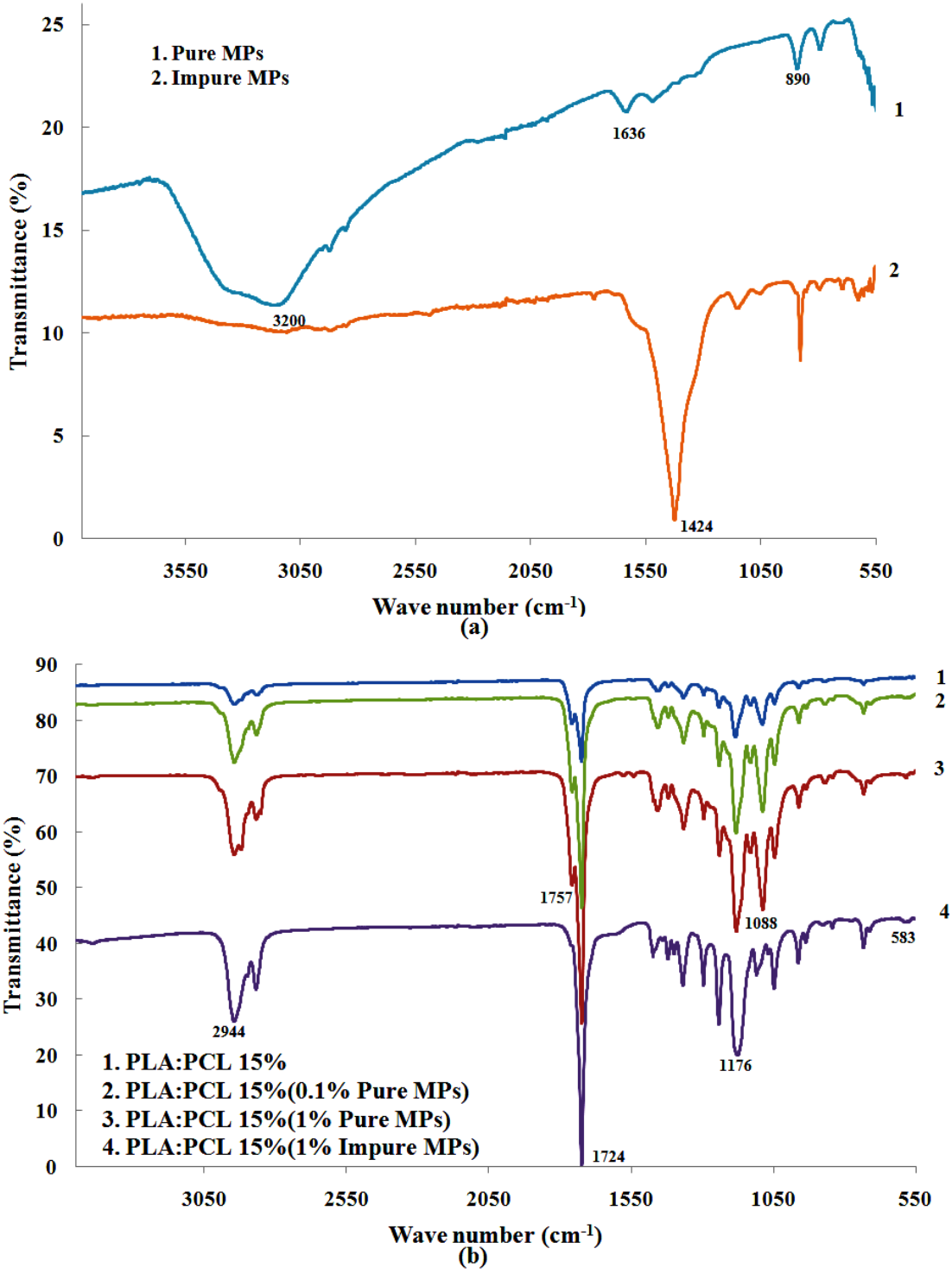

Figure 6-11: FTIR spectra for selected material samples showing the relative FTIR peaks: (a) pure and impure MPs, and (b) PLA: PCL based composites with pure and impure MPs.

6.5 Summary

The main finding from this chapter it was that increasing the pure MP concentration can decrease the average fibre diameter, and this trend was more significant for impure MPs. This effect was associated with two important properties, namely electrical conductivity and solution viscosity, of the PLA: PCL blends. The dispersion of pure MPs was enhanced in the PLA: PCL nanofibre structures relative to impure MPs. Impure MPs created non-uniform fibrous structures with tiny fibres, making them inappropriate for the drug release application. However, the configuration of these novel cell structures has not been observed before in the literature. The employment of pure MPs and impure MPs leads to completely different thermal properties. The degree of crystallinity and the T_g of PCL are reduced when pure MPs are embedded with the PLA: PCL blends. On the contrary, adding impure MPs increases the degree of crystallinity with a modest increase in the melting temperature of PLA. The infrared spectra of electrospun composite nanofibres have confirmed the successful embedding of MPs into their structure. Impure MPs are shown to considerably influence the C=O and C–O bonds of PLA.

Chapter 7
Drug Release

7.1 Drug delivery

Electrospun nanofibres loaded with drugs have good structural stability and higher efficiency of drug encapsulation than other drug delivery systems. Adding a drug into the polymer solution affects solution properties. The drug release from nanofibre mats can be managed by the modified fibre morphology, polymer composition, dosage quantity, and drug loading procedure. The interaction between polymer and drug plays a significant role in controlled drug release. It is very challenging to understand well the mechanism leading to the drug release kinetics from biodegradable polymers.

Based on the findings in previous chapters, fives selected nanofibres mats (PLA: 9% PCL), (PLA: 15% PCL), (PLA: 15% PCL/ 0.1% MPs), (PLA: 15% PCL/ 1% MPs) and PLA: 15% PCL/ 1% HNT-ASP) were investigated as carriers for therapeutic compounds tetracycline hydrochloride (TCH) and indomethacin (IMC) with potential uses in medical applications. These material systems infused with 1 wt% and 5 wt% of TCH and 5 wt% of IMC were analysed and discussed in terms of their morphological structure, crystallinity level, thermal properties and constituent interactions, which can affect drug release and nanofibre degradation. Drug release experiments were also performed. Moreover, the release kinetic data were fitted to five mathematical models, which are classified as zero order, first order, Higuchi, Ritger-Peppas and Zeng models.

7.2 Morphological observations

7.2.1 Effect of TCH concentration

Figure 7-1 shows that using PLA: 9% PCL with blending ratio 1:1 dissolved in chloroform: methanol co-solvents produced uniform nanofibres with an average diameter of 689 nm. On the other hand, the addition of 1 and 5 wt% TCH into the polymer blends facilitates the reduction of fibre diameter as compared to their counterpart without TCH as shown in Figure 7-2. The electrical conductivity is

enhanced remarkably when the TCH concentration increases from 1 wt% to 5 wt%. The additional cationic drug TCH increases the solution conductivity as compared to the solution without TCH, Figure 7-2. Electrical conductivity plays a dominant role in determining fibre morphology. In contrast, when the TCH was added to a polymer blend solution, there was no impact on the viscosity. As a matter of fact, the increased electrical conductivity inevitably produces more electric charges that are carried by the electrospinning jet, which could contribute to electrospun fibres with smaller diameters (Lee et al., 2010; Saraf et al., 2009).

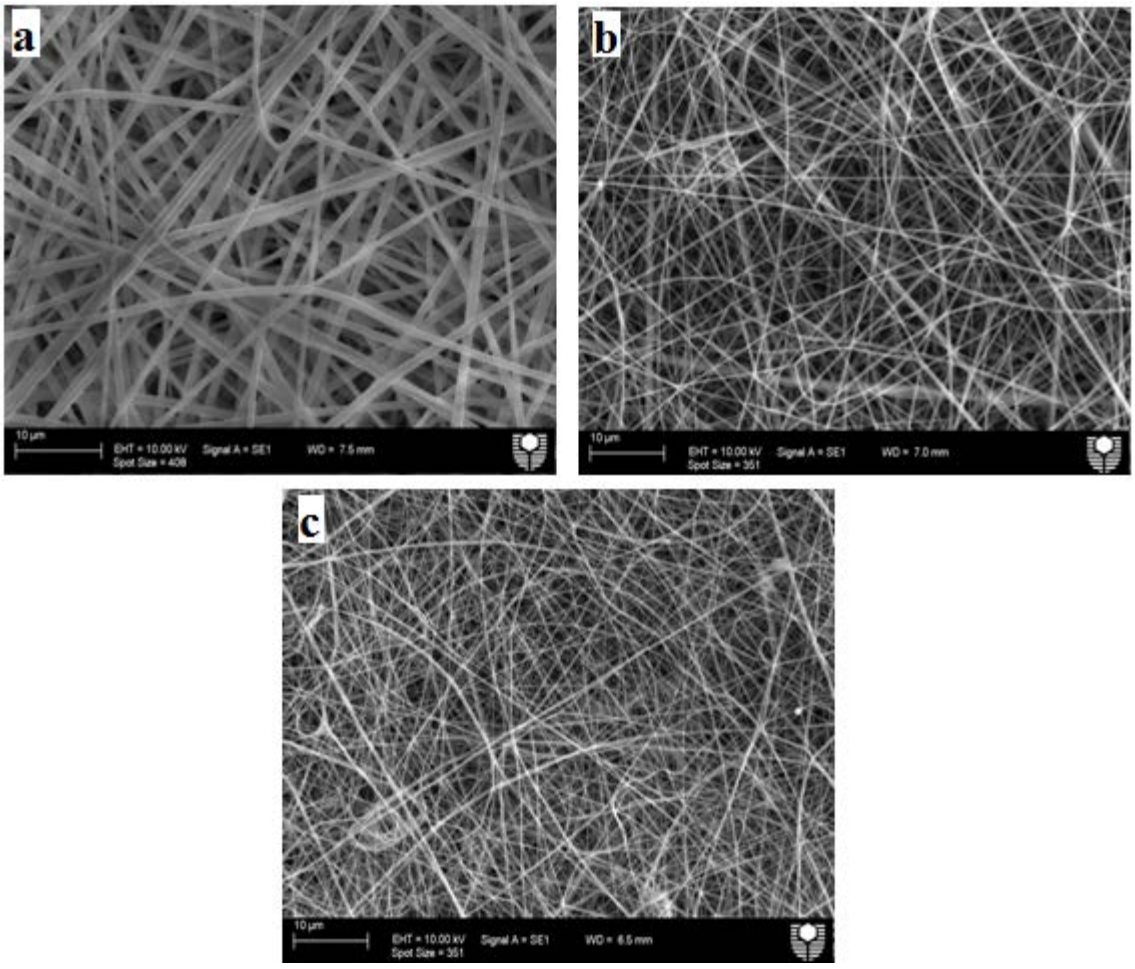

Figure 7-1: SEM micrographs of electrospun PLA: 9% PCL nanofibres using chloroform: methanol as a solvent: (a) without TCH, (b) 1wt% TCH, and (c) 5 wt% TCH.

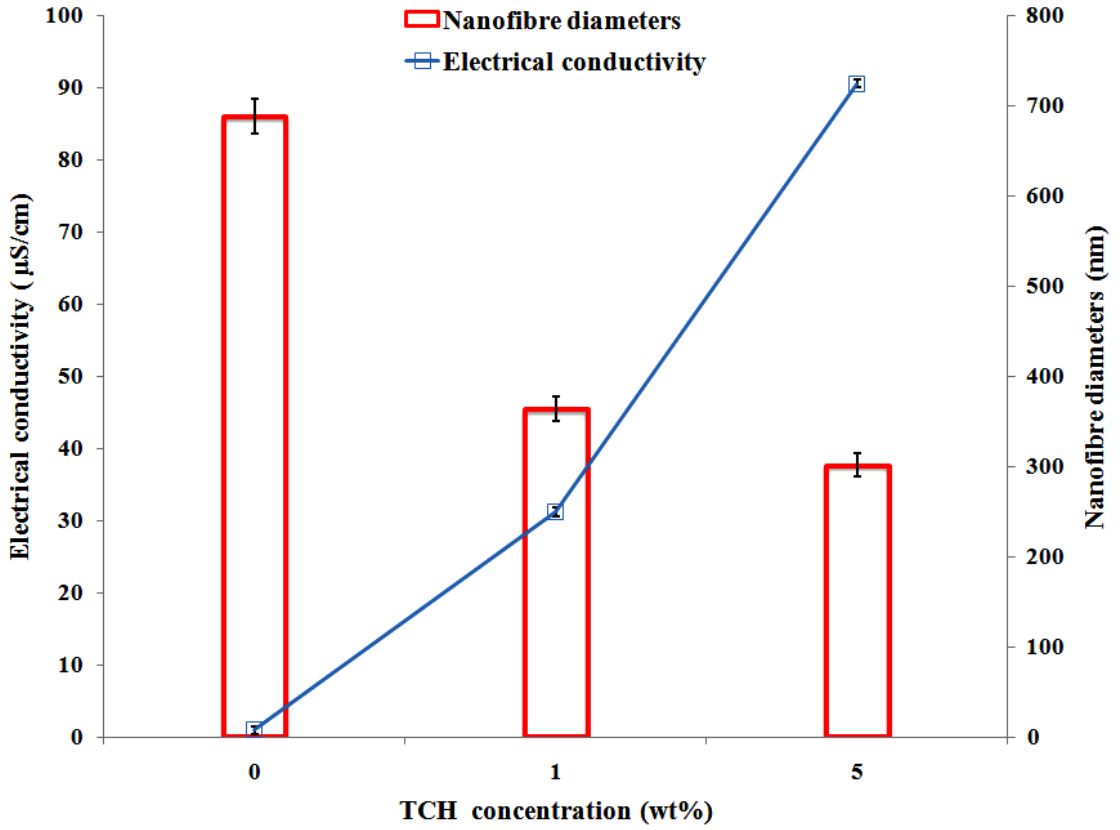

Figure7-2: Effect of TCH concentration on the electrical conductivity of PLA: 9% PCL solution and average nanofibre diameters.

7.2.2 Effect of drug type (IMC and TCH)

To investigate the effect of drug type, the PLA: PCL polymer solution was blended with two different drugs, namely Indomethacin (IMC) and TCH, at a 5 wt% concentration. Figures 7-3 and 7-4 demonstrate that IMC produced a uniform fibrous structure with large diameters compared to TCH. There was no remarkable change of nanofibre diameter with the addition of IMC compared with PLA: PCL nanofibres. The explanation for this phenomenon is that the addition of IMC into the PLA: PCL solution did not appear to significantly affect the electrical conductivity, Figure 7-4. This result agrees well with a previous finding (Nyström et al., 2010). Nevertheless there was a significant increase in the electrical conductivity when using TCH.

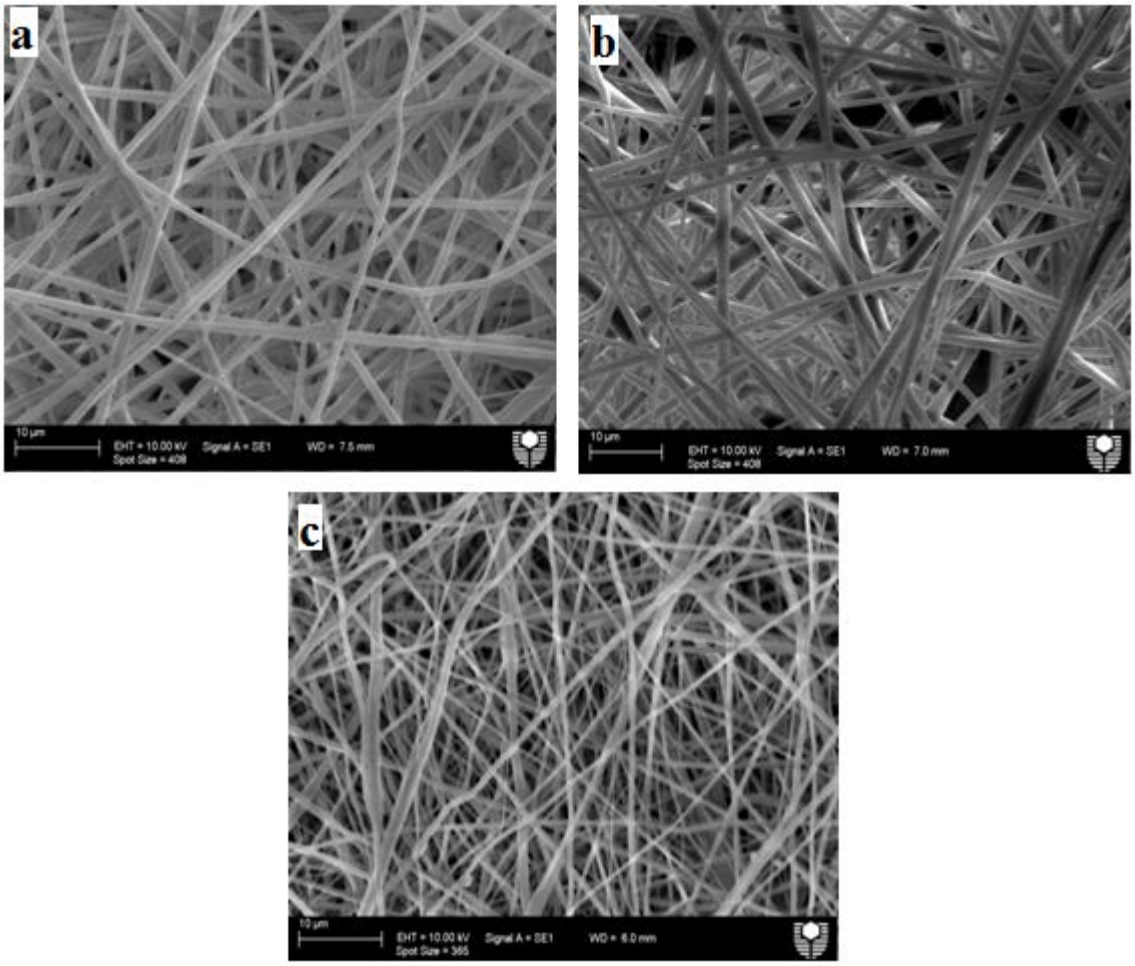

Figure 7-3: SEM micrographs of electrospun PLA: 15% PCL: (a) without drug, (b) with 5 wt% IMC, and (c) with 5 wt% TCH.

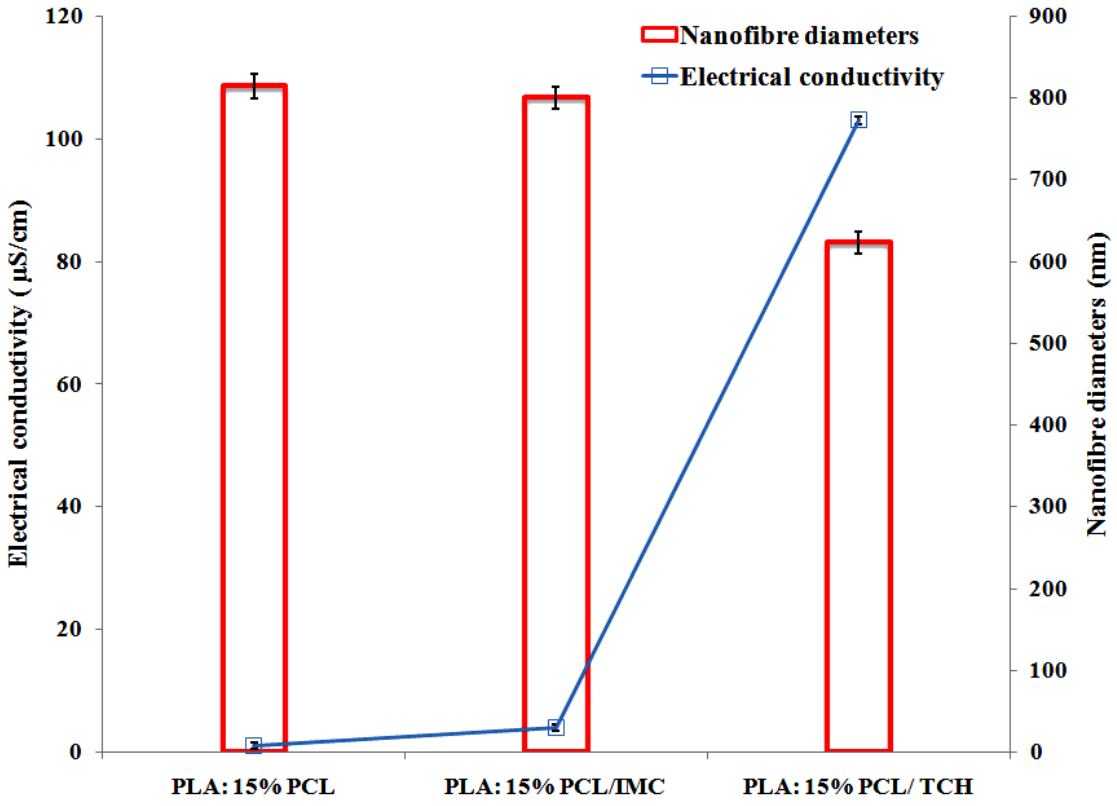

Figure 7-4: Effect of drug type (5 wt% of IMC and TCH) on average nanofibre diameters of PLA: 15% PCL blend solution (mix ratio: 1:1) and solution electrical conductivity.

7.2.3 Effect of MPs and TCH

To investigate the effect of TCH on MP nanocomposites, the addition of 5 wt% TCH into PLA: 15% PCL based composites with 0, 0.1 and 1 wt%/v MPs was undertaken. TCH facilitates the reduction of fibre diameter from 623 to 491 nm, as compared to their counterparts without TCH, Figures 7-5 and 7-6. In terms of the effect of electrical conductivity, an increase in the MP concentration led to an increase in the conductivity, apparently due to the addition of iron ions from the MPs, as shown in Figure 7-6. More prominently, the use of the drug TCH can further enhance the electrical conductivity of the electrospun composites especially at MP concentrations of 0.1 wt%/v. The additional amphoteric molecules of TCH, having several ionisable functional groups (Sassman and Lee, 2005), further increases the solution conductivity as compared to that without TCH.

This implies that electrical conductivity plays a relatively dominant role in determining fibre morphology though the addition of MPs increases the viscosity of the solution.

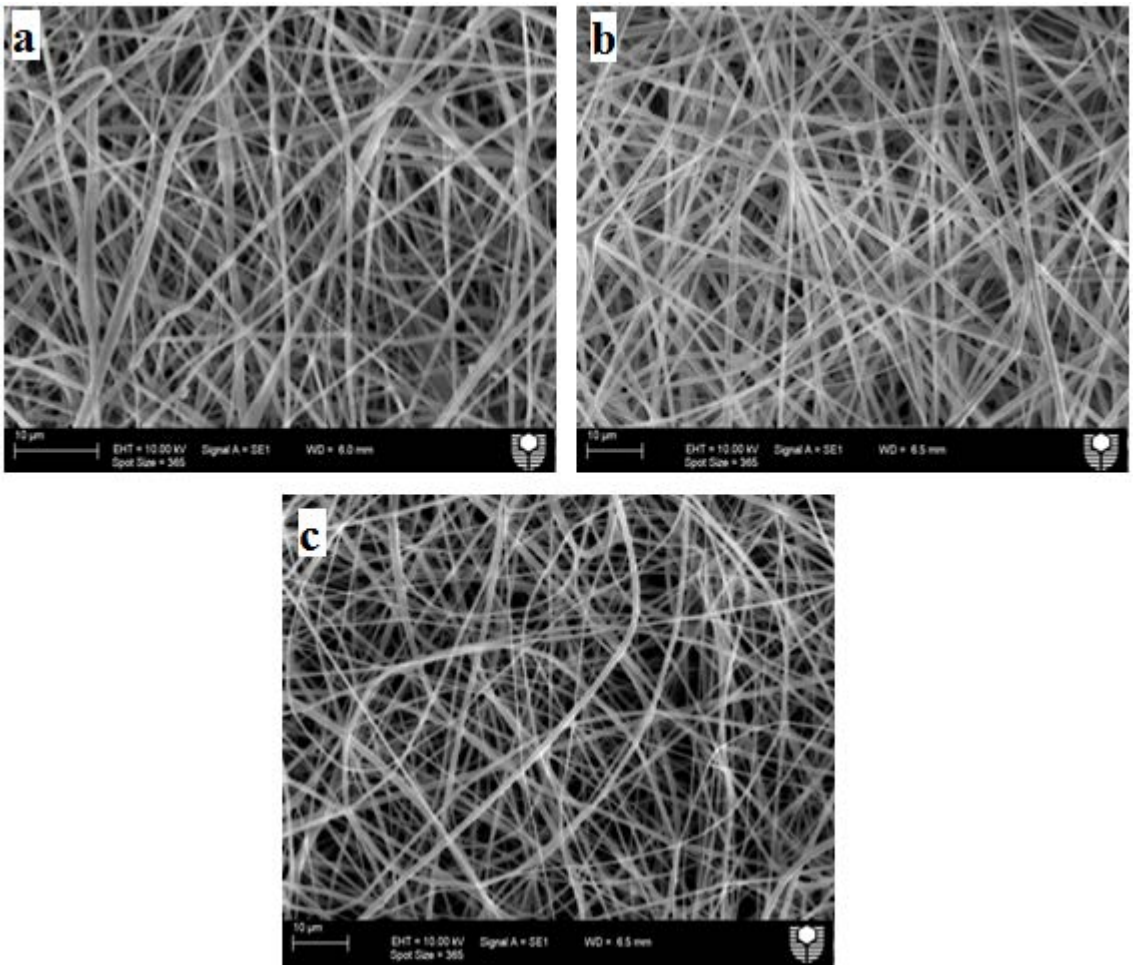

Figure 7-5: SEM micrographs of electrospun PLA: 15% PCL/ pure MP composites: (a) 0 wt%/v MPs and 5 wt% TCH, (b) 0.1 wt%/v MPs and 5 wt% TCH, and (c) 1wt%/v MPs and 5 wt% TCH.

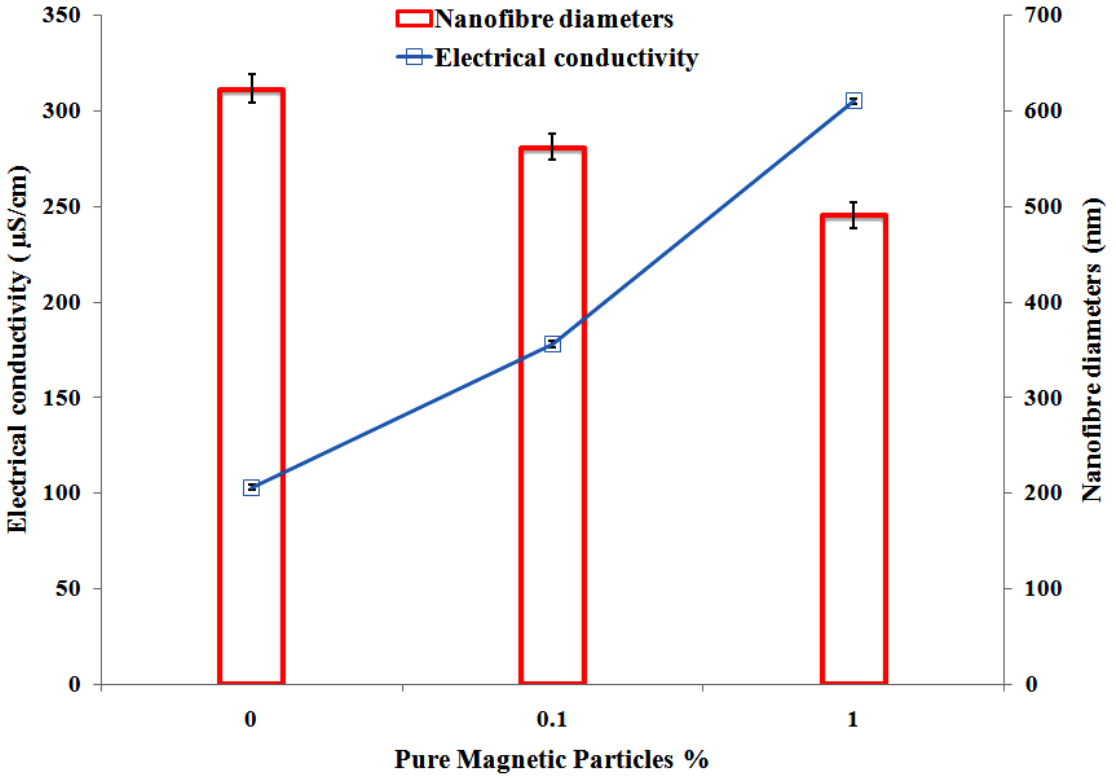

Figure 7-6: Effect of pure MP concentration on the average nanofibre diameters of PLA: 15% PCL blend solution (mix ratio: 1:1) and electrical conductivity of blend solution with 5 wt%/v TCH.

7.2.4 Effect of HNTs and TCH

PLA: PCL/ HNT-ASP/ TCH produced a uniform fibrous structure with a small average diameter of 716 nm, Figure 7-7, in contrast to the corresponding PLA: PCL and PLA: PCL/ HNT-ASP blends. The addition of TCH is associated with enhancement of the solution's electrical conductivity, which leads to the production of small nanofibre diameters. The use of HNT-ASP increases the average nanofibre diameter up to 905 nm relative to 814 nm for PLA: PCL blends. This result is ascribed to the dominant effect of material viscosity on the fibre morphological structure, compared with a slight increase in the electrical conductivity, Figure 7-8.

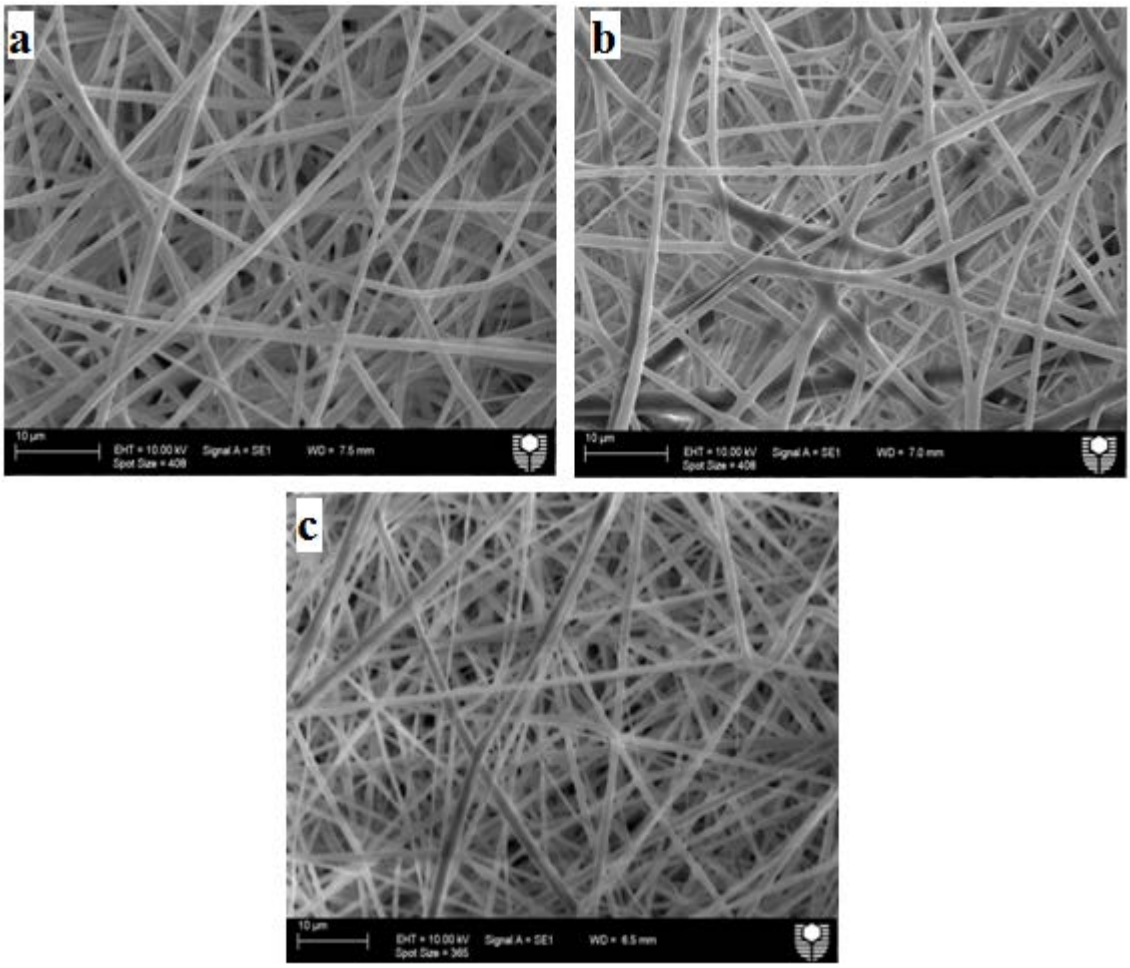

Figure 7-7: SEM micrographs of electrospun PLA: 15%PCL: (a) without HNT-ASP, (b) with 1 wt%/v HNT-ASP, and (c) with 1 wt%/v HNT-ASP / 5 wt% TCH.

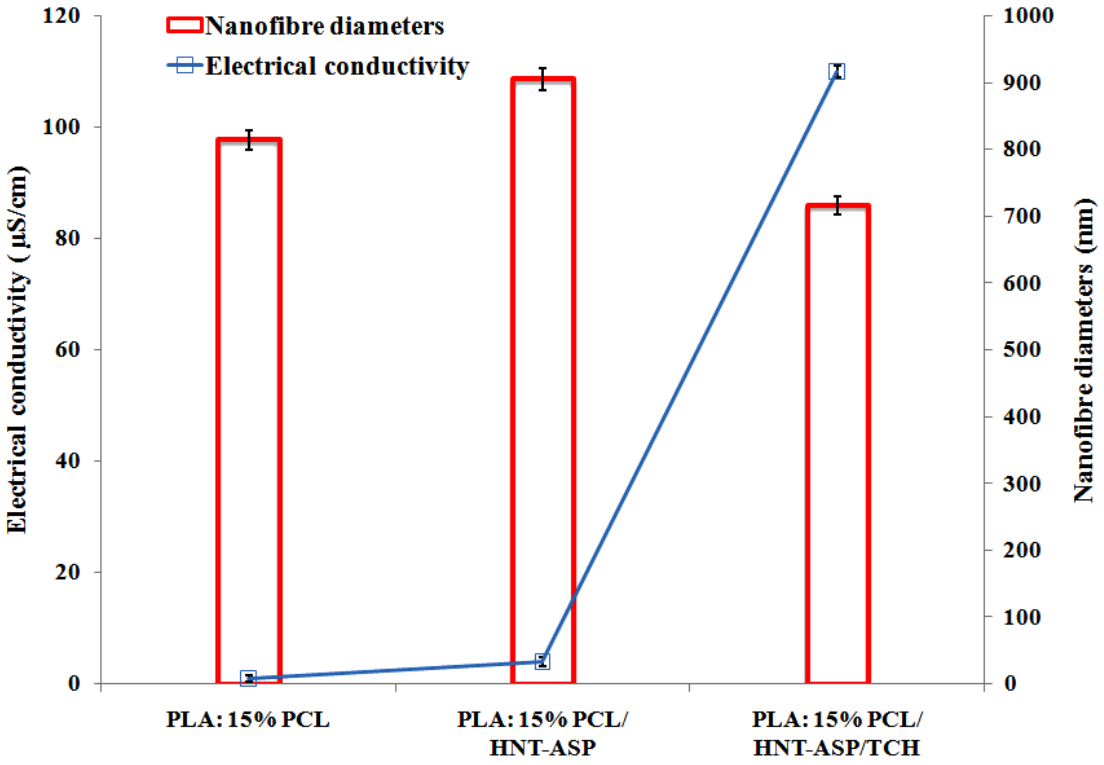

Figure 7-8: Effect of HNT-ASP and 5 wt% TCH on the average nanofibre diameters of PLA: 15% PCL blend solution (mix ratio: 1:1) and electrical conductivity of blend solution.

7.3 Crystallinity level and thermal properties

An XRD examination was carried out to investigate the changes in the TCH concentration and drug type on the degree of crystallinity and structure of electrospun nanocomposites. The peaks in the pattern were labelled for the XRD reflection and the crystal planes (*hkl*) corresponding to the main crystalline peaks were detected by the DICVOL program of the FullProf software. Figure 7-9 shows the XRD patterns for PLA: PCL blends and nanocomposite fibres with TCH and IMC. The XRD patterns possess two diffraction peaks at angles of 2θ = 20.11° and 23.2° corresponding to the planes (101) and (200), respectively. There was no significant difference in the peak positions for most samples, which indicates that the addition of TCH and IMC have a very minor effect on the crystalline structures of the composite fibres. This finding indicates that the TCH and IMC are most likely to be dispersed in an amorphous state in

the PLA: PCL nanofibre mat. In addition, the large surface area combined with small nanofibre diameters created through the electrospinning process can facilitate quick solvent evaporation, which could provide a short period for drug recrystallisation and formation of preferred configuration in amorphous state (Puppi et al., 2010).

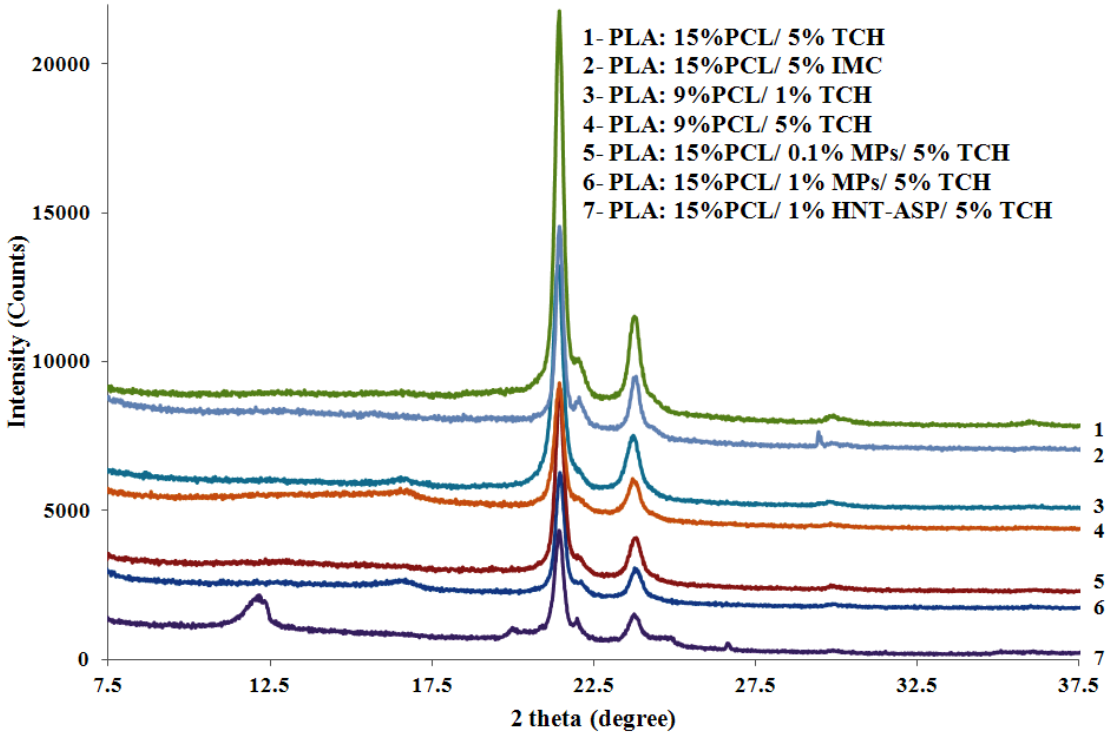

Figure 7-9: X-ray diffraction patterns for selected samples showing the relative position of the diffraction peaks due to the addition of the drugs TCH and IMC.

Figure 7-10 demonstrates that increasing the amount of TCH from 1 to 5 wt% in the PLA: 9% PCL nanofibres led to a moderate decrease of the degree of crystallinity. The crystallinity is reduced more remarkably when 5 wt% of TCH is concurrently added as compared to the PLA: 15%PCL polymer blend. IMC dispersed in the PLA: 15%PCL blend had a more significant impact on the degree of crystallinity than TCH did. The presence of both TCH and IMC appears to greatly accelerate the nucleation process. Accordingly, this phenomenon allows a shorter period for the disentanglement of the molecular chains because the resulting degree of crystallinity is influenced by the restricted mobility of the polymer chains, which hinders good crystal growth.

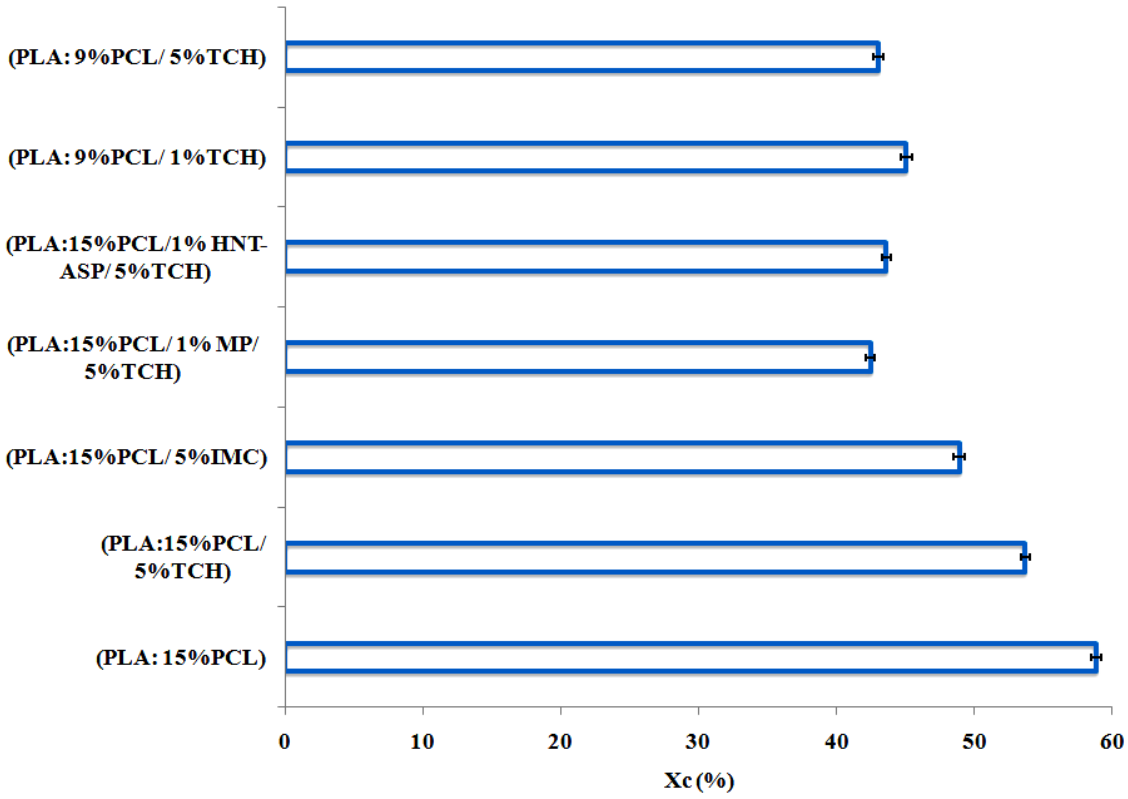

Figure 7-10: Degree of crystallinity results for adding drugs TCH and IMC.

The DSC thermal properties of electrospun composite fibres with IMC and TCH drugs are shown in Figure 7-11 and Table 7-1. The glass transition temperature (T_g) of PCL within the fibre composites decreases remarkably, and there was a slight decline in melting temperature (T_m) values of both PLA and PCL when increasing the MP concentration from 0 wt%/v to 1 wt%/v, as well as using HNT-ASP and 5% TCH. The decrease of T_g is attributed to the dual effect of incorporation of magnetite particles with anisotropic character, in good accordance with the previous work (Kumar et al., 2000), and blending of the drug TCH, which has a low molecular weight. The TCH molecules have short chains, which results in decreased packing density of the polymer chains, and thus facilitates chain mobility, leading to the lower T_g. Conversely, the use of TCH within composite fibres shows the significant increase of T_c at over 106ºC as opposed to 84ºC for PLA in PLA: PCL blends. This phenomenon implies that low molecular weight TCH can hinder the cold crystallisation process of PLA, acting as an anti-nucleating agent, which, however, maybe in opposition to the role of MPs. Increasing the

concentration of the drug TCH from 1 to 5 wt% leads to a decrease in the T_g of PCL with a significant increase in the T_c of PLA within the blend. On the other hand, changing the type of drug also had a remarkable impact on the values of T_m and T_c of PLA within the fibre composites. Adding IMC led to a drop in the T_m value, while there was a slight decrease in T_c, which could be explained by the fact that the interaction between the blend polymers and IMC was somewhat better compared with TCH.

Table 7-1: DSC results for PLA: PCL composite fibres embedded with MPs, HNTs, IMC and TCH[a].

Sample	T_g (°C) PCL	T_m (°C) PCL	T_c (°C) PLA	T_m (°C) PLA
PLA: 15% PCL	–52.2	63.8	84.0	152.5
PLA: 15% PCL/ 5% IMC	–58.6	54.6	82.0	149.0
PLA: 15% PCL/ 5% TCH	–58.5	59.6	105.8	151.9
PLA: 15% PCL / 1%MPs / 5% TCH	–62.0	59.6	100.1	149.3
PLA: 15% PCL/ 0.1% MPs/ 5% TCH	–60.5	59.2	101.8	149.4
PLA: 15% PCL/ 1% HNT-ASP/ 5% TCH	–61.4	59.2	102.8	149.1
PLA: 9% PCL/ 5% TCH	–60.5	60.6	99.3	151.0
PLA: 9% PCL/ 1%TCH	–58.4	60.4	80.4	151.6

[a]Calculations were repeated for three sets of samples. The standard deviation for the T_g, T_c and T_m values was less than 0.5°C.

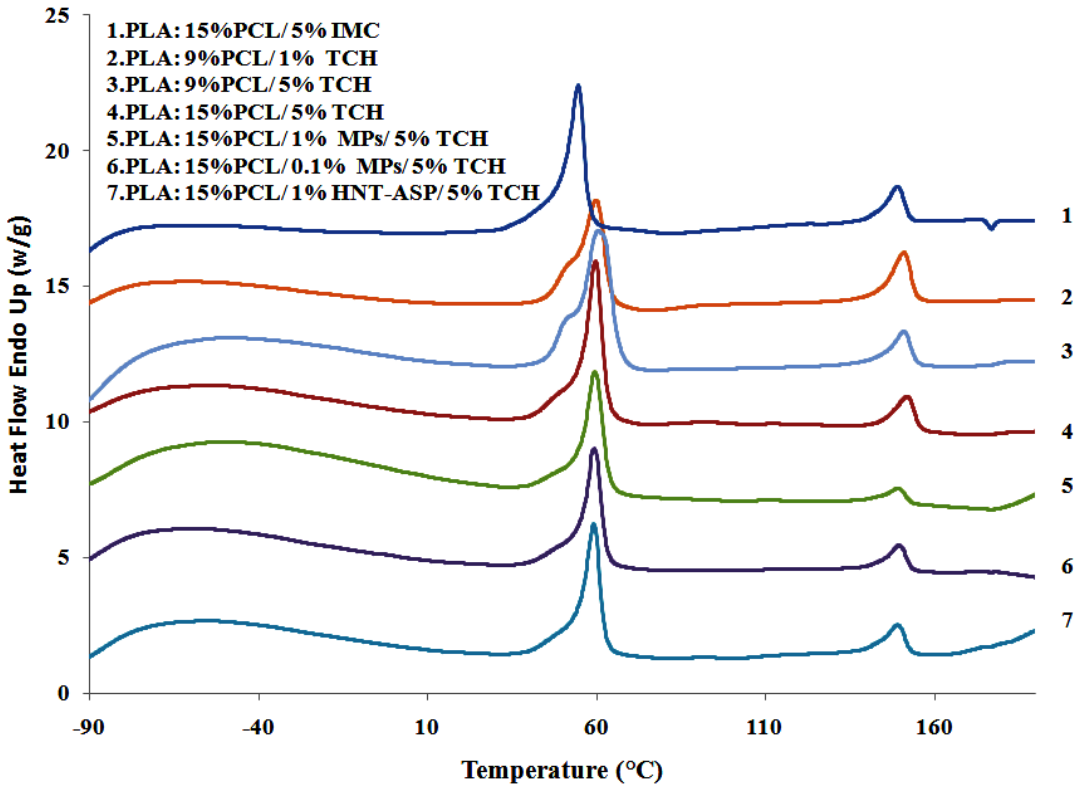

Figure 7-11: DSC thermograms for selected material samples.

7.4 Intermolecular interactions

Figure 7-12 shows the FTIR spectra of PLA: PCL/ TCH in various nanocomposites and the PLA: PCL/ IMC system. The spectra of 1 wt%/v and 5wt%/v TCH in PLA: PCL blends and nanocomposites, were difficult to interpret due to band shifting. However, the major distinguishable change in the infrared spectra is that the bands of TCH at 1614 and 1581 cm^{-1} were observed in the nanocomposites, and these were allocated to C=O stretching in ring A and C=O stretching in ring C, respectively. This observation confirms the successful encapsulation of TCH into the nanocomposites. It was hard to allocate bands for the spectrum of 1 wt%/v TCH in the PLA: PCL blends. The FTIR spectrum of the PLA: PCL/ 5 wt%/v IMC blend demonstrated that the bonds existing at 1560 cm^{-1} were associated with the ionization of carboxyl groups in the IMC, which shows that the IMC was intercalated in the anionic structure (Mi et al., 2001; Mohanambe and Vasudevan, 2005).

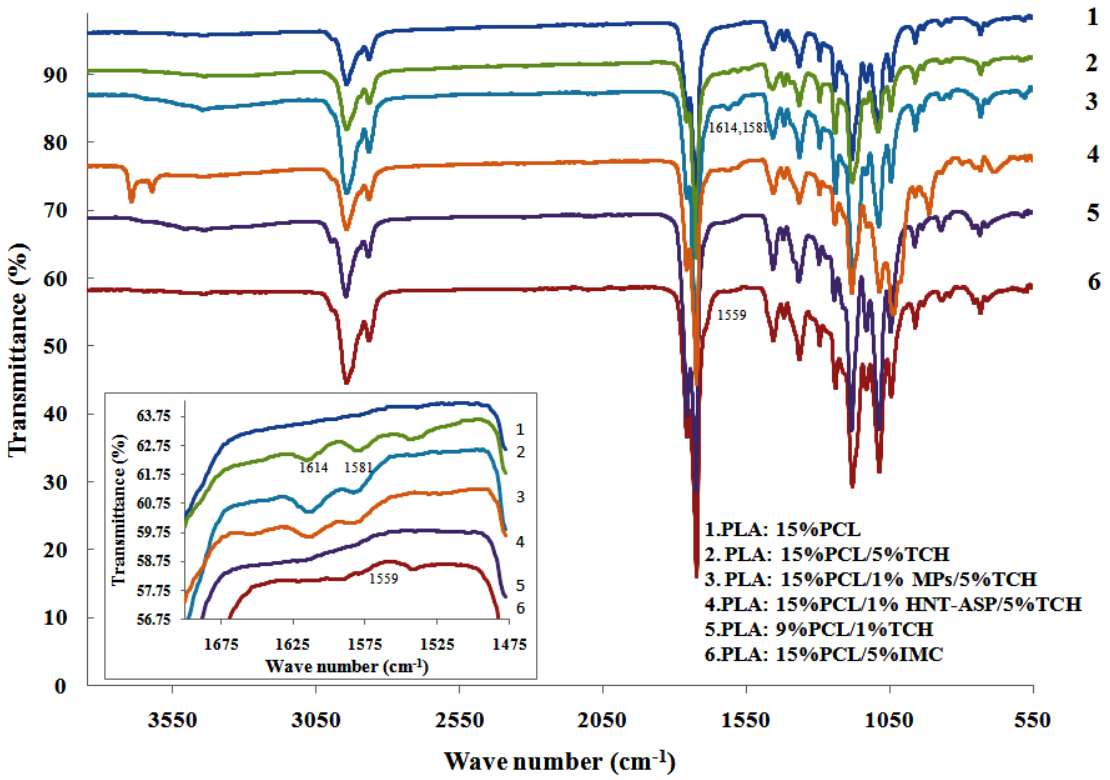

Figure 7-12: FTIR spectra for selected material samples showing the effect of drugs on the relative FTIR peaks.

7.5 In vitro drug release

7.5.1 Effect of TCH concentration

TCH release profiles from electrospun PLA: 9% PCL with 1 wt%/v and 5 wt%/v TCH are reported in Figure 7-13. Both samples have been found to have fast drug release performance. In the first 20 minutes, 44% of the drug was released for PLA: PCL/ 1% TCH samples compared to 56% for PLA: PCL/5% TCH samples. Within the first 2 h, this increased to 59% for the PLA: PCL/ 1% TCH samples and 64 % for PLA: PCL/ 5% TCH samples. This was followed by a steady release over the remainder of the 10 day release tests. The fast release is associated with the electrospinning process, which includes fast evaporation of the solvent and high ionic interactions leading to the drug being located on the surfaces of the electrospun fibres. It was found that TCH was released more quickly when 5 wt%/v TCH was added to the polymer blend. At higher concentrations of TCH, the dissolved TCH in the PLA: PCL solution has a greater

tendency to move to the nanofibre surface throughout the electrospinning period, which accelerates the drug release rate compared to that for a low TCH concentration. In addition, drug release took place initially from the amorphous regions (Luong-Van et al., 2006). Accordingly, increasing the TCH concentration in PLA: PCL nanofibres led to a decrease of the crystallinity for the PLA: PCL blends as shown in Figure 7-10. It is also possible to say that TCH accumulated in the amorphous regions because there was no change in the structure of PLA: PCL as shown by the XRD data. Consequently, the higher quantity of TCH supports a faster drug release rate from these regions.

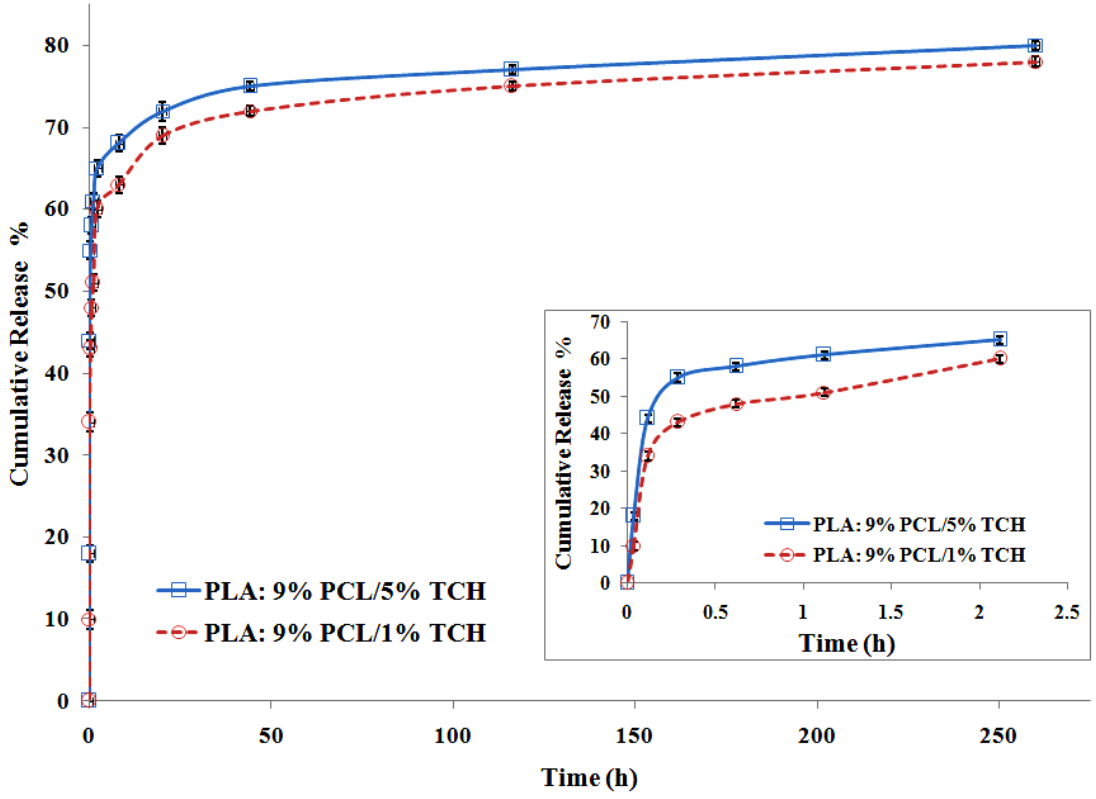

Figure 7-13: TCH release profiles from PLA: 9%PCL with 1 and 5 wt %/v TCH.

7.5.2 Effect of drug interaction

The drug particles within polymer nanofibres have a tendency to be attached to the fibre surface due to quick solvent evaporation from the PLA: PCL blend solution during the electrospinning process and also due to the highly ionic interactions. Accordingly, a considerable burst release of the drug may initially take place. The burst release

becomes faster when the drug and the PLA: PCL solution are not compatible; that is, when there is weak interaction between them.

A high PCL concentration in the PLA: 15% PCL fibres, as seen from Figure 7-14, leads to a slower drug release rate compared to low PCL concentration PLA: 9% PCL nanofibres. This is attributed to the lower porosity of the nanofibres produced from the higher concentration polymer solutions, which decreases the overall desorption of TCH molecules from the porous surfaces.

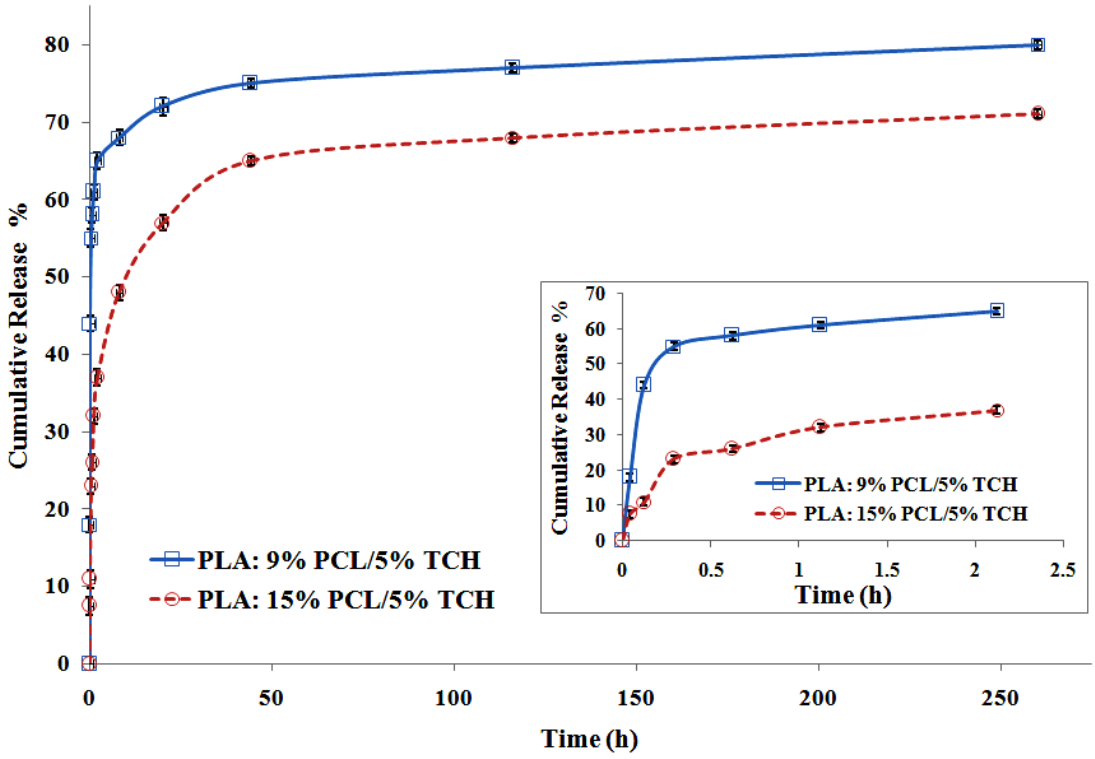

Figure 7-14: TCH release profiles from PLA: 9% PCL and PLA: 15% PCL.

The interaction between the drug and the PLA: PCL blend solution is an important factor for controlling drug release. The release kinetics of the hydrophilic drug TCH in the hydrophobic PLA: PCL solution were faster than for the hydrophobic drug IMC in the hydrophobic PLA: PCL solution. It can be seen from Figure 7-15 for the drug release within the first 5 h, 42% was released for PLA: PCL/ 5% TCH versus 30% for PLA: PCL/ 5% IMC. This could be ascribed to better interaction and compatibility between

IMC and the polymer blend compared with TCH. Furthermore, chemical interaction between drug and its carrier can impede drug crystallisation within the carrier, which may cause more sustained release of the drug in the crystalline state (Natu et al., 2010).

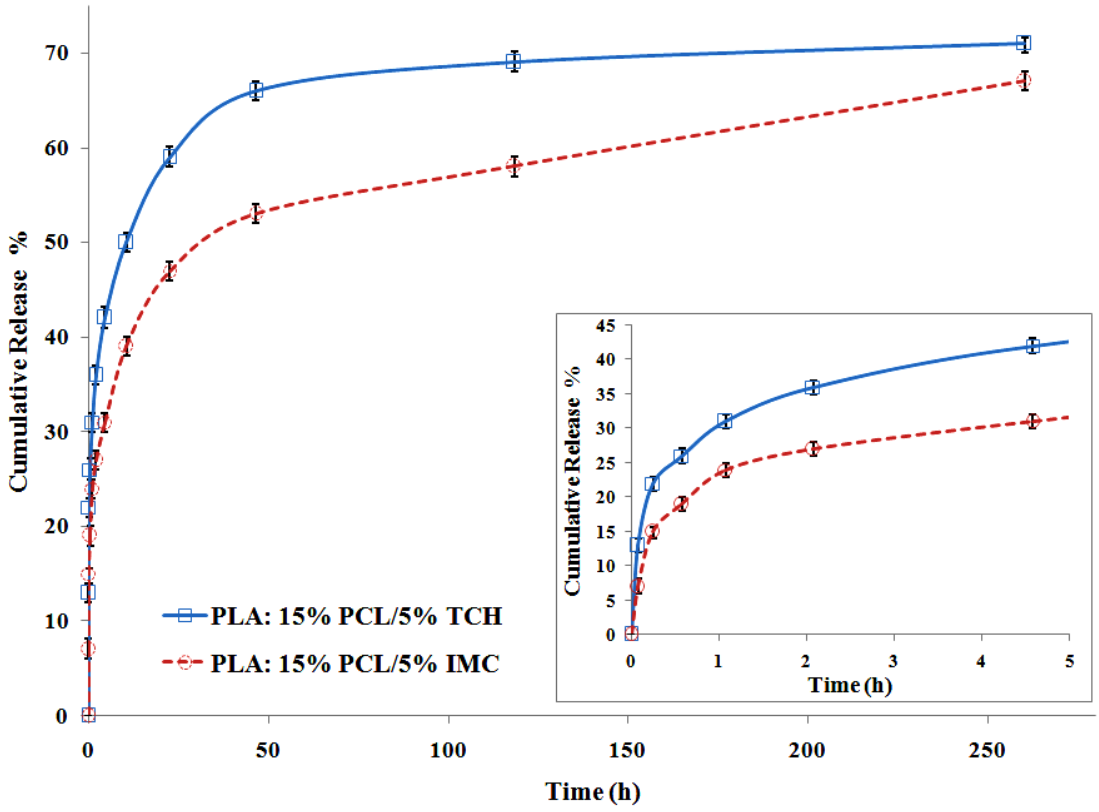

Figure 7-15: Drug release profiles from PLA: 15% PCL for 5 wt %/v IMC and 5 wt%/v TCH.

7.5.3 Effect of nanoparticles

TCH release profiles from electrospun composite fibre mats with and without pure MPs are reported in Figure 7-16. Nanocomposite mats have been shown to offer sustained drug release performance though a certain degree of fast drug release was found within the first 5 h (62% for PLA: 15% PCL/ 1 wt%/v MPs, 46% for PLA: 15% PCL/ 0.1 wt%/v MPs and 42% for PLA: 15% PCL samples). Whilst the addition of 1 wt% HNT-ASP into PLA: PCL not only reduces the initial bust release to 30% after 5 h with reference to the initial 42% for PLA: PCL, but it also has a similar release trend over the duration of the steady release period from 50 h to 250 h. This implies that robust control

of drug release for both short and long evaluation periods can be achieved by the use of HNT-ASP. As explained previously, fast release is associated with the electrospinning process, which includes fast solvent evaporation and highly ionic interactions leading to the location of the drug on the surfaces of the electrospun fibres. It was found that TCH was released more rapidly when adding MPs to the polymer blend and the difference in cumulative release (%) when adding 1 wt%/v MPs becomes fairly large compared to those composites without MPs while for 0.1 wt%/v MPs it becomes large after 50 h. This finding suggests that TCH release was due to many factors, such as drug diffusion through the pores, biodegradation of the electrospun fibres and the interaction between TCH and the PLA: PCL/ MP nanofibre mats. The incorporation of MPs, due to their nanoscale size, leads to increased fibre porosity (Mikołajczyk and Olejnik, 2006) and the porosity increases with increasing MP concentration from 0.1 to 1 wt%/v, which is then capable of accelerating the TCH release. In addition, the small diameters of the PLA: PCL/ MP composite fibrous structures compared with their PLA: PCL counterparts certainly increase the surface area, which leads to short diffusion distances and fast TCH release. Moreover, the low crystallinity of the PLA: PCL/ MP composites can also assist in the enhancement of fibre degradability, which affects long term TCH release. The release of TCH from PLA: PCL/ HNT-ASP nanocomposites is much slower than for PLA: PCL and PLA: PCL/ MP nanocomposites. HNTs are negatively charged on their outer surface and positively charged on their inner surface (Vergaro et al., 2010). Such charges on the HNT-ASP may permit electrostatic interaction between TCH and the surface and lumen of HNT-ASP, resulting in reduced TCH drug release from PLA: PCL/ HNT-ASP nanocomposites.

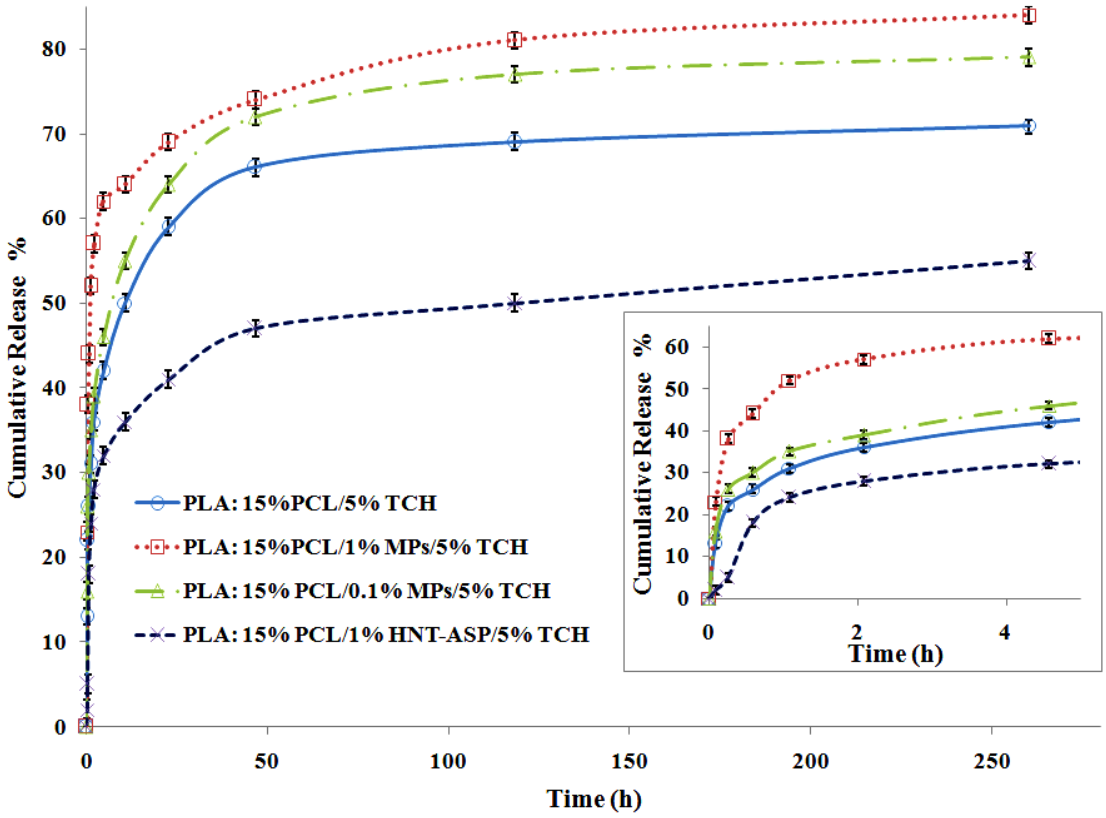

Figure 7-16: TCH release profiles from PLA: 15% PCL and its nanocomposites containing MPs and HNT-ASP for 5%TCH.

7.6 In vitro biodegradation studies

The biodegradation behaviour of the nanofibres mats is shown in Figure 7-17. After the degradation in PBS for the first 3 to 12 hours, the weight of all nanofibres mats remained approximately unchanged within a standard error, especially for PLA: 15% PCL, PLA: 15% PCL/ 0.1% MPs and PLA: 15% PCL/ HNT-ASP nanofibres as detected in the Figure 7-17. There was a high initial mass loss at 24 h for some nanofibre mats (1.13% for PLA: 15% PCL/ 1% MPs and 1.37% for PLA: 9% PCL), while the other nanofibres mats demonstrated very little mass loss (0.36% for PLA: 15% PCL). Mass loss for PLA: 15% PCL started after 72 h, and the mass loss increased over the degradation time of 336 h to reach 2.91% for PLA: 15% PCL, 3.44% for PLA: 15% PCL/ 1% HNT-ASP, 4.73% for PLA: 15% PCL/ 0.1% MPs, 6.10% for PLA: 15% PCL/ 1% MPs and 6.26% for PLA: 9% PCL. The possible explanation for this behaviour is that increasing the PCL concentration within the blends may hinder water penetration inside the nanofibres

and the absorption of water occurs slowly due to PCL being hydrophobic and semi-crystalline. That means the samples with 15% PCL had a higher degree of crystallinity than those with 9% PCL. The amorphous regions are easily degraded when compared with the crystalline regions due to the random and less tightly packed arrangement of the molecular chains. In addition, when a hydrophilic drug is released from the nanofibre mat, it may accelerate the degradation of the hydrophobic nanofibres due to its increased wettability (Huang et al., 2006).

The biodegradation rate of the PLA: 15% PCL/ MP nanocomposites are considerably accelerated in comparison with the PLA: 15%PCL blend. The difference in terms of the mass loss increases with increasing MP concentration. This may be due to the decrease in nanofibre diameter and also the increase of the porosity at the nanofibre surface when MPs are added. Moreover, it is noted that adding HNT-ASP to the nanofibres does not significantly affect the biodegradation rate and mass loss compared with adding MPs. This is related to the surface area exposed to the PBS being larger in the case of embedding MPs due to the creation of small diameter nanofibres.

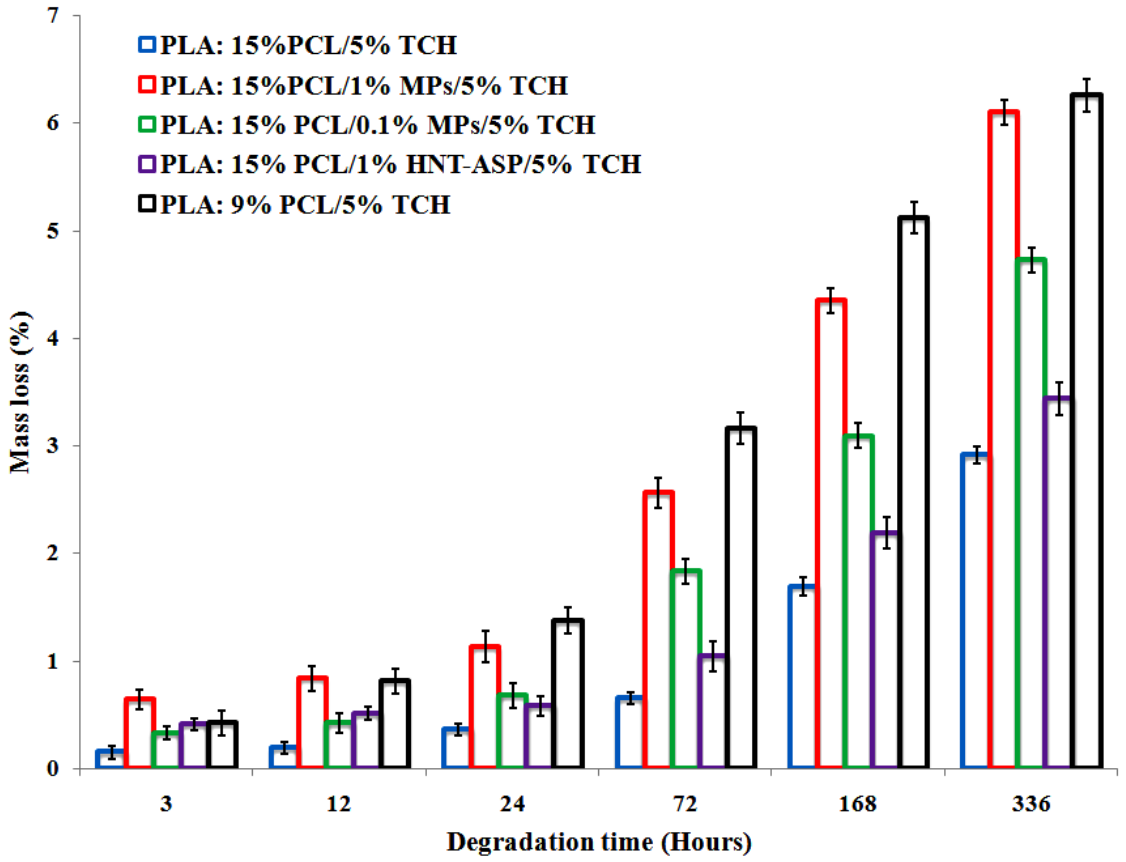

Figure 7-17: Mass loss of electrospun nanofibre mats during the degradation time.

Figure 7-18 shows the morphological changes in the fibres after immersion in PBS over a two week period. It was found that different morphologies appeared for nanofibre mats with different nanocomposite contents and PCL concentrations. The nanofibre diameters increased and the space between the nanofibres decreased after seven days, especially for PLA: 15% PCL/ 1% MP and PLA: 15% PCL/ 1% HNT-ASP nanocomposites. The nanofibres showed more wrinkled structures after 7 days compared with those for the 3 h degradation. The degradation initially took place in the amorphous area of the blend nanofibres, and then occurred in the crystalline area (Huang et al., 2004; Stefani et al., 2006). The degradation of the nanofibres in the solution is heterogeneous and the degradation at the nanofibre surface could be slower than in the nanofibre core due to the carboxylic acid groups existing in the fibre core areas by ester hydrolysis (Maquet et al., 2004). Moreover, the large diameters and swelling behaviour of the degraded nanofibres for PLA: 15% PCL/ 1% MP and PLA: 15% PCL/ 1% HNT-ASP

nanocomposite mats were more evident than for the PLA: 15% PCL nanofibre mats, indicating that the nanoparticles increased PBS absorption.

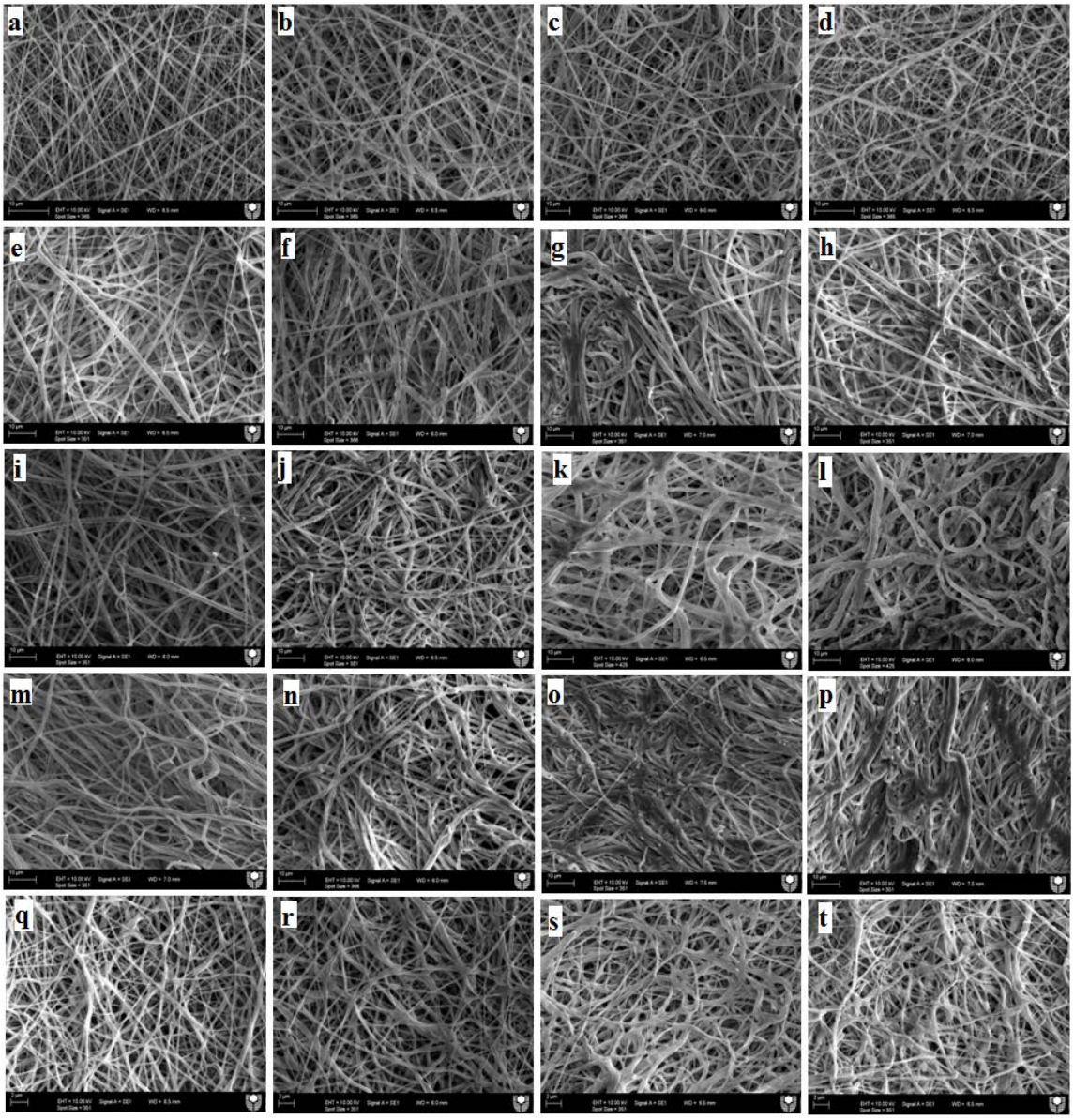

Figure 7-18: SEM micrographs of in vitro degradation of nanofibre mats: (a) to (d) PLA: 15%PCL/ TCH, (e) to (h) PLA: 15%PCL/ 0.1% MPs/ TCH, (i) to (l) PLA: 15%PCL/ 1% MPs/ TCH, (m) to (p) PLA: 15%PCL/ 1% HNT-ASP/ TCH, and (q) to (t) PLA: 9%PCL/ TCH, for periods of 3 h, 24 h, 7 days and 14 days, respectively.

7.7 Release kinetics and mechanistic interpretation

The release kinetics were examined by fitting five mathematical models, which are categorized as zero order, first order, Higuchi, Ritger-Peppas (Cai et al., 2011) and Zeng (Zeng et al., 2011) models, to the drug release data using a least squares objective function. Comparisons between the release data and the best-fit predictions for these five models are shown in Appendix I. The equations of each model and their reported best-fit parameters are listed in Table 7-2. The R^2 value was highest when fitting the experimental data to the first order, Ritger-Peppas and Zeng models compared to the other models. The first order model illustrates that drug release rate mainly depends on drug concentration and its carrier. According to the n values of the Ritger-Peppas model, the drug release mechanism follows Fickian transport phenomenon (Cai et al., 2011) with a dominant diffusion process. On the other hand, according to Zeng's model, the diffusion process and interaction between PLA: PCL and TCH has significant impact on the drug release. In the Zeng model, ΔG is the difference in the free energies of the free and bound states of the drug in the nanofibres. The addition of 0.1 wt%/v MPs to PLA: PCL led to a little decrease in ΔG values from -2.0×10^{-22} J to -2.6×10^{-22} J, which means that there is slightly improvement in the interaction between the drug carrier and TCH. Nevertheless, such improvement did not adjust the TCH release, and the fast release from PLA: PCL/ 0.1% MPs was higher than PLA: PCL/ TCH release. This observation could be due to the creation of small fibre diameters by adding MPs, which leads to the acceleration of TCH release. The fast release is also due to increasing the fibre pore size with the addition of MPs, which is reflected in increased values of K_s. On the other hand, incorporating 1wt%/v MPs suggests a weaker interaction while the number and size of fibre pores are suggested to grow. The TCH release kinetics are not completely described by these models because they do not take into account the erosion/biodegradation and dimensional alteration of the drug carrier. The big difference in ΔG, 1.47×10^{-21} J versus -2.2×10^{-21} J for PLA: 15% PCL/ 1% MPs and PLA: 15% PCL/ 1% HNT-ASP, respectively, suggests a better interaction between TCH and the larger HNT-ASP particles than the smaller MPs. The Zeng model suggests that due to embedding HNT-ASP into the nanofibres there was a small change in K_S. However, ΔG decreased from -2.0×10^{-22} J to-2.2×10^{-21} J. Such a result indicates that embedding HNT-

ASP enhances steady drug release and overcomes the fast release due to interaction between the TCH molecules and HNT-ASP from hydrogen bonding with the silanol groups on the HNT-ASP.

The Zeng model demonstrates the effect of drug concentration on drug release. When the drug concentration increases from 1 wt% to 5 wt%, ΔG also increases from 1.47×10^{-21} J to 2.49×10^{-21} J, which reveals to increase TCH release and diffusivity due to increase amount of free TCH on the PLA: 9% PCL nanofibre surface. Furthermore, K_S increased from 5.127 to 8.343 h^{-1}, indicating the pore size increases when the TCH concentration increases.

The Zeng model detected the effect of interaction between both drugs (TCH and IMC) and the carrier (PLA: 15% PCL nanofibres) on the release rate. IMC exhibits a much lower ΔG than TCH (-2.1×10^{-21} J for IMC against -2.0×10^{-22} J for TCH), suggesting that PLA: 15% PCL can decrease the release of hydrophobic IMC, but not hydrophilic TCH, due to the interaction enhancement between the drug and polymer. Furthermore, the decrease in K_{off} values of TCH (0.0033 h^{-1}) and IMC (0.0025 h^{-1}) implies a stronger interaction between IMC and carrier.

In addition, the Zeng model shows the effect polymer concentration on drug release. When the PCL concentration within a blend decreased from 15 to 9 wt%/v, the release rates of TCH from the nanofibre mat increased significantly. The Zeng model shows an increase in ΔG, from -2.0×10^{-22} J to 2.49×10^{-21} J, on account of a reduction of PCL concentration for the same amount of drug. Moreover, big pores increase diffusivity and TCH release from the nanofibres, and correspondingly K_S increased from 1.160 to 8.343 h^{-1}, which reflects increased pore size. The variations in the fitted model parameters, especially ΔG and K_S, are consistent with the previous interpretations of the experimental results.

Table 7-2: Parameters obtained by fitting five different models for drug release kinetics to the drug release data.

Model	Zero order	First order	Higuchi	Ritger-Peppas	Zeng
Equation	$M_t/M_\infty = K_0 t$	$M_t/M_\infty = 1 - e^{-K_1 t}$	$M_t/M_\infty = K_H t^{1/2}$	$M_t/M_\infty = K_R t^n$	**
PLA:15%PCL/ 5%IMC	K_0=0.002 h^{-1} R^2=0.564	K_1=0.436 h^{-1} R^2=0.822	K_H=0.037 $h^{-1/2}$ R^2= 0.801	K_R=1.618 h^{-n} n=0.251 R^2=0.938	K_{on}=0.0049 h^{-1} K_{off}=0.0025 h^{-1} K_s=1.006 h^{-1} *ΔG=–2.1×10^{-21}J R^2= 0.945
PLA:15%PCL/ 5%TCH	K_0=0.002 h^{-1} R^2=0.434	K_1=0.582 h^{-1} R^2=0.839	K_H=0.038 $h^{-1/2}$ R^2= 0.691	K_R=1.262 h^{-n} n=0.204 R^2=0.927	K_{on}=0.0034 h^{-1} K_{off}=0.0033 h^{-1} K_s=1.160 h^{-1} *ΔG=–2.0×10^{-22}J R^2=0.920
PLA:15%PCL/ 0.1%MPs/ 5%TCH	K_0=0.0022 h^{-1} R^2=0.451	K_1=0.625 h^{-1} R^2= 0.808	K_H=0.042 $h^{-1/2}$ R^2=0.705	K_R=1.127 h^{-n} n=0.193 R^2=0.950	K_{on}=0.0069 h^{-1} K_{off}=0.0065 h^{-1} K_s=1.864 h^{-1} *ΔG= –2.6×10^{-22}J R^2=0.923
PLA:15%PCL/ 1%MPs / 5%TCH	K_0=0.0019 h^{-1} R^2=0.348	K_1=2.097 h^{-1} R^2=0.856	K_H=0.037 $h^{-1/2}$ R^2=0.560	K_R=0.806 h^{-n} n=0.138 R^2=0.938	K_{on}=0.0041 h^{-1} K_{off}=0.0059 h^{-1} K_s=3.764 h^{-1} *ΔG=1.47×10^{-21}J R^2=0.956
PLA:15%PCL/ 1%HNT-ASP /5%TCH	K_0=0.0012 h^{-1} R^2=0.314	K_1=0.857 h^{-1} R^2=0.961	K_H=0.024 $h^{-1/2}$ R^2=0.534	K_R=2.025 h^{-n} n=0.323 R^2=0.684	K_{on}=0.0012 h^{-1} K_{off}=0.00068 h^{-1} K_s=1.025 h^{-1} *ΔG= –2.2×10^{-21}J R^2=0.986
PLA:9%PCL/ 1%TCH	K_0=0.0017 h^{-1} R^2=0.291	K_1=3.372 h^{-1} R^2=0.889	K_H=0.035 $h^{-1/2}$ R^2=0.489	K_R=0.912 h^{-n} n=0.167 R^2=0.779	K_{on}=0.0025 h^{-1} K_{off}=0.0036 h^{-1} K_s=5.127 h^{-1} *ΔG=1.47×10^{-21}J R^2=0.948
PLA:9%PCL/ 5%TCH	K_0=0.0015 h^{-1} R^2=0.224	K_1=6.899 h^{-1} R^2=0.930	K_H=0.030 $h^{-1/2}$ R^2=0.387	K_R=0.692 h^{-n} n=0.117 R^2=0.828	K_{on}=0.0017 h^{-1} K_{off}=0.0031 h^{-1} K_s=8.343 h^{-1} *ΔG=2.49×10^{-21}J R^2=0.975

**$M_t/M_\infty = (K_{off}/(K_{on} + K_{off}))(1 - e^{-K_S t}) + (K_{on}/(K_{on} + K_{off}))(1 - e^{-K_{off} t})$.

*$\Delta G = -k_B T \ln(K_{on}/K_{off})$ where k_B is Boltzmann's constant and T is absolute temperature (300 K).

7.8 Summary

This Chapter demonstrated that increasing the concentration of TCH appears to increase the electrical conductivity of solution thus considerably decreasing the average nanofibre diameters. However, when adding IMC, there was no noticeable change in the nanofibre diameters. TCH and IMC loading can contribute to decreased crystallinity levels, and decreased T_g and T_m values for PCL within the blend. The biodegradation rate was accelerated when blending 9% PCL with PLA and adding MPs to the solution in comparison with blending 15% PCL and loading HNT-ASP. The TCH release was found to be accelerated by adding pure MPs to PLA: PCL blended polymers. Loading a hydrophilic drug (TCH) into HNT-ASP and hydrophobic polymers (PLA: PCL) was shown to decrease drug release and overcome the weakness of the interaction between the polymer and drug. This typical characteristic was clearly revealed with excellent agreements obtained between the experimental data and the Ritger-Peppas and Zeng models for drug release kinetics.

Chapter 8
Conclusions and Future Work

8.1 Conclusions

This work has created several novel electrospun hybrid nanocomposite systems (PLA: PCL, PLA: PCL/ HNT-ASP and PLA: PCL/ MPs) with the aim of achieving sustained release of a hydrophilic drug (TCH) from the hydrophobic PLA: PCL composite system. This thesis examined the effects of the solvent system, solution electrical conductivity, solution viscosity, PCL concentration and PCL molecular weight on the nanofibre diameters, porosity and degree of crystallinity, which are considered to be significant parameters in the control of drug release. Furthermore, the work studied the effect of the embedded HNT and MPs on nanofibre morphology, crystallinity, thermal properties, connecting bonds and drug release kinetics of these hybrid nanocomposites. The impact of interactions between the drugs (TCH and IMC) and the PLA: PCL polymer blend on the drug release rate was examined. The study also investigated the drug release kinetics by fitting the release data to five mathematical models, including the zero order, first order, Higuchi, Ritger-Peppas and more recent Zeng models to help understand the mechanism of drug release. The following main conclusions were drawn from this work.

- Blending PLA with PCL alleviated the negative individual aspects of each polymer in terms of its crystallinity or formation of an acidic environment. There was a noticeable increase in the solution viscosity when the molecular weight and concentration of the PCL were increased. That improvement in viscosity leads to well-structured and bead-free nanofibrous networks, particularly at a PLA: PCL blending ratio of 1:1. The nanofibres created from co-solvents chloroform: methanol for all blend ratios of PLA: PCL had larger fibre diameters as compared to those based on DCM: DMF co-solvents. Chloroform: methanol was also found to facilitate better aligned fibrous structures than DCM: DMF or chloroform: acetone co-solvents.

- PLA: 15% high molecular weight PCL solution at blend ratio of 1:1 produced a higher degree of crystallinity (X_c) compared to PLA: 9% PCL at a blend ratio of 1:1 or PLA: 15% PCL at a blend ratio of 3:1. There was a sharp decline in X_c and melting temperature (T_m) of PCL within the blends when PLA was mixed with low molecular weight PCL compared to high molecular weight PCL. However, there was a noticeable increase in the crystallization temperature (T_c) of PLA due to the low molecular weight PCL. In addition, the fast evaporation of methanol in the chloroform: methanol solvent system led to moderate decreases in X_c and T_c relative to the DCM: DMF co-solvent system. Increasing the PCL concentration from 9 to 15 wt%/v increased the glass transition temperature (T_g) of PCL within the blends. Additionally, the shift of the carbonyl stretching band to higher wave numbers and the variations in T_g, T_m and T_c for nanofibres produced from blending, compared to pure PLA or PCL nanofibres, demonstrate the good miscibility of PLA and PCL within the blends. The miscibility was quite high for PLA: 15%PCL at a blend ratio of 1:1 dissolved in the chloroform: methanol system.

- When HNTs were incorporated into a PLA: low molecular weight PCL blend the non-uniform dispersion of HNT resulted and also HNT sedimentation increased during the electrospinning process. Furthermore, an increase of HNT concentration from 1 to 2 wt%/v did not substantially influence the nanofibre diameters due to the low viscosity of the blend solution. On the other hand, the embedding of HNT into PLA: high molecular weight PCL blends produced homogeneous fibres owing to the increase of the solution viscosity. For both concentrations of high molecular weight PCL within the blend, the average fibre diameters decreased with reduction in the HNT concentration. For 15 wt%/v PCL embedded with HNT, the average fibre diameters were found to be considerably smaller for HNT-ASP compared with unmodified HNT. Moreover, the PLA: PCL composites embedded with HNT-ASP showed slightly better HNT dispersion and less agglomeration compared to unmodified HNT. The high

solution viscosity for 15 wt%/v PCL compared with 9 wt%/v PCL promoted the formation of a HNT suspension and led to decreased sedimentation of HNT.

- There was a small decrease in the value of T_g of PCL, the T_c and T_m values of PLA when embedding HNT-ASP into the polymer blends, while there was a moderate decline in the degree of crystallinity. The addition of HNT-ASP into PLA: PCL nanofibres reduced HNT agglomeration compared to unmodified HNT as evidenced by the infrared spectra of the samples.

- The addition of pure MPs appears to increase the solution viscosity and thus facilitates better MP dispersion inside the electrospun composite fibrous networks, as compared to impure MPs, which result in a significant viscosity reduction. However, considerably decreased average fibre diameters were shown to result from impure MPs. The addition of impure MPs creates unique cell structures that are reported for the first time in this study.

- The incorporation of pure and impure MPs also led to quite different thermal properties. The former led to a decreasing crystallinity level and T_g of PCL, as well as decreasing T_c of PLA. In contrast, the latter caused overall increases of the aforementioned thermal parameters, except for the unidentified T_m of PLA. The infrared spectra of the electrospun composite nanofibres confirmed the successful embedding of MPs into the structure. In particular, impure MPs significantly affect the carbonyl stretching C=O and C–O stretch bonds.

- The average nanofibre diameters were significantly reduced when increasing the TCH concentration due to the increase of the solution electrical conductivity in contrast to the addition of IMC, there was no noticeable change in the nanofibre diameters. The addition of both TCH and IMC drugs to the PLA: PCL blends reduced the crystallinity level, T_g and T_m values of PCL within the blend.

- The nanofibre biodegradation rate was found to be greater for low concentration (9%) PCL blends and for embedding MPs compared to high concentration (15%) PCL blends and for embedding HNT-ASP. Embedding pure MPs into the PLA: PCL blend solution was found to increase the TCH release rate. Loading a hydrophilic drug (TCH) into HNT-ASP and then to hydrophobic polymer blends (PLA: PCL) was detected to decrease drug release and overcome the weak interaction between the PLA: PCL blends and TCH drug. Excellent agreement was obtained between the experimental data and the Ritger-Peppasand Zeng models for drug release kinetics.

8.2 Future work

Based on the outcomes of the work contained within this thesis, several possibilities for further studies concerning the improvement of the performance for hybrid composite nanofibre mats and drug release were identified as follows.

- Tailoring the mechanical properties of electrospun nanofibres may perhaps be achieved by embedding MPs and HNTs. It is important to study the possibility of using the nanofibre mats created by the current research for tissue engineering applications; that is, to further investigate their mechanical properties, dimensional shrinkage and surface erosion. Nanofibre mats must have very controllable mechanical properties related to physical handling, facilitating the process of tissue regeneration and their degradation.

- Depending on the best conditions and mix ratios obtained from this study, it can attain the benefit from the core-shell structure based electrospinning method to control or reduce the fast drug release. TCH could be mixed with a hydrophilic polymer and embedded HNTs, and this mixture could be made into the core of a fibre, while the shell of the fibre could be made from a PLA: PCL blend. The effect of drug release could then be studied.

- Develop a model to predict nanofibre diameter and beads formation as a function of solution composition.

- As the porosity affects the drug release, so it is substantial to study the relationship between nanofibre diameters and the porosity that exist on the nanofibres surface as well as that formed from nanofibers entanglement with each other.

- Develop a new mathematical model, or modify the Zeng model, to better describe the most important behaviour of the TCH and IMC release kinetics by taking into account the change in the nanofibre diameters and the mat's erosion/biodegradation.

- Intermolecular interactions are vital to the material morphology and the performance in drug delivery. It is important to understand the potential drug–polymer interactions that rely on the actual drug–polymer miscibility. In addition, it can further assist in developing a new molecular modelling study to indicate intermolecular interactions between drug and polymer molecules.

REFERENCES

ABDUL RAHMAN, N., GIZDAVIC-NIKOLAIDIS, M., RAY, S., EASTEAL, A. & TRAVAS-SEJDIC, J. 2010. Functional electrospun nanofibres of poly (lactic acid) blends with polyaniline or poly(aniline-co-benzoic acid). *Synthetic Metals,* 160**,** 2015-2022.

AGARWAL, S., WENDORFF, J. & GREINER, A. 2008. Use of electrospinning technique for biomedical applications. *Polymer,* 49**,** 5603-5621.

ALIPOUR, S., NOURI, M., MOKHTARI, J. & BAHRAMI, S. 2009. Electrospinning of poly(vinyl alcohol)-water-soluble quaternized chitosan derivative blend. *Carbohydrate research,* 344**,** 2496-2501.

ARAYANARAKUL, K., CHOKTAWEESAP, N., AHT ONG, D., MEECHAISUE, C. & SUPAPHOL, P. 2006. Effects of poly(ethylene glycol), inorganic salt, sodium dodecyl sulfate, and solvent system on electrospinning of poly(ethylene oxide). *Macromolecular Materials and Engineering,* 291**,** 581-591.

ARUMUGAM, G., KHAN, S. & HEIDEN, P. 2009. Comparison of the Effects of an Ionic Liquid and Other Salts on the Properties of Electrospun Fibers, 2-Poly(vinyl alcohol). *Macromolecular Materials and Engineering,* 294**,** 45-53.

BAYAT, M., YANG, H. & KO, F. 2011. Electromagnetic properties of electrospun Fe_3O_4/carbon composite nanofibers. *Polymer,* 52**,** 1645–1653.

BEACHLEY, V. & WEN, X. 2009. Effect of electrospinning parameters on the nanofiber diameter and length. *Materials Science and Engineering: C,* 29**,** 663-668.

BERMUDEZ, J. & GRAU, R. 2011. Thermosensitive poloxamer-based injectables as controlled drug release platforms for veterinary use: Development and in-vitro evaluation. *International Research Journal of Pharmacy and Pharmacology,* 1**,** 109-118.

BHARDWAJ, N. & KUNDU, S. 2010. Electrospinning: A fascinating fiber fabrication technique. *Biotechnology advances,* 28**,** 325-347.

BHATIA, A., GUPTA, R. K., BHATTACHARYA, S. N. & CHOI, H. 2007. Compatibility of biodegradable poly(lactic acid)(PLA) and poly(butylene succinate)(PBS) blends for packaging application. *Korea-Australia Rheology Journal,* 19**,** 125-131.

BIBER, E., GÜNDÜZ, G., MAVIS, B. & COLAK, U. 2010. Effects of electrospinning process parameters on nanofibers obtained from Nylon 6 and poly(ethylene-n-butyl acrylate-maleic anhydride) elastomer blends using Johnson S B statistical distribution function. *Applied Physics A: Materials Science & Processing,* 99**,** 477-487.

BOSWORTH, L. A. & DOWNES, S. 2012. Acetone, a Sustainable Solvent for Electrospinning Poly(ε-caprolactone) Fibres: Effect of Varying Parameters and Solution Concentrations on Fibre Diameter. *Journal of Polymers and the Environment,* 20**,** 879-886.

BOTTINO, M. C., YASSEN, G. H., PLATT, J. A., LABBAN, N., WINDSOR, L. J., SPOLNIK, K. J. & BRESSIANI, A. H. 2013. A novel three-dimensional scaffold for regenerative endodontics: materials and biological characterizations. *Journal of Tissue Engineering and Regenerative Medicine***,** doi: 10.1002/term.1712.

BOULTIF, A. & LOUER, D. 2004. Powder pattern indexing with the dichotomy method. *Journal of applied crystallography,* 37**,** 724-731.

BOZZOLA, J. J. 1992. *Electron microscopy,* Wiley Online Library.

BUSCHLE-DILLER, G., COOPER, J., XIE, Z., WU, Y., WALDRUP, J. & REN, X. 2007. Release of antibiotics from electrospun bicomponent fibers. *Cellulose,* 14**,** 553-562.

CAI, X., LUAN, Y., DONG, Q., SHAO, W., LI, Z. & ZHAO, Z. 2011. Sustained release of 5-fluorouracil by incorporation into sodium carboxymethylcellulose sub-micron fibers. *International journal of pharmaceutics,* 419**,** 240– 246.

CANTÓN, I., MCKEAN, R., CHARNLEY, M., BLACKWOOD, K., FIORICA, C., RYAN, A. & MACNEIL, S. 2010. Development of an Ibuprofen-releasing biodegradable PLA/PGA electrospun scaffold for tissue regeneration. *Biotechnology and bioengineering,* 105**,** 396-408.

CAO, H., JIANG, X., CHAI, C. & CHEW, S. 2010. RNA interference by nanofiber-based siRNA delivery system. *Journal of Controlled Release,* 144**,** 203-212.

CARLI, L. N., CRESPO, J. S. & MAULER, R. S. 2011. PHBV nanocomposites based on organomodified montmorillonite and halloysite: the effect of clay type on the morphology and thermal and mechanical properties. *Composites Part A: Applied Science and Manufacturing,* 42**,** 1601–1608.

CHARERNSRIWILAIWAT, N., OPANASOPIT, P., ROJANARATA, T., NGAWHIRUNPAT, T. & SUPAPHOL, P. 2010. Preparation and characterization of chitosan-hydroxybenzotriazole/polyvinyl alcohol blend nanofibers by the electrospinning technique. *Carbohydrate Polymers,* 81**,** 675–680.

CHEN, R., HUANG, C., KE, Q., HE, C., WANG, H. & MO, X. 2010. Preparation and Characterization of Coaxial Electrospun Thermoplastic Polyurethane/Collagen Compound Nanofibers for Tissue Engineering Applications. *Colloids and Surfaces B: Biointerfaces,* 79**,** 315-325.

CHEN, Z., WEI, B., MO, X. & CUI, F. 2009. Diameter control of electrospun chitosan collagen fibers. *Journal of Polymer Science Part B: Polymer Physics,* 47**,** 1949-1955.

CHENNAMANENI, S., ZHONG, B., LAMA, R. & SU, B. 2012. COX inhibitors Indomethacin and Sulindac derivatives as antiproliferative agents: synthesis, biological evaluation, and mechanism investigation. *European Journal of Medicinal Chemistry,* 56**,** 17–29.

CHEW, S., WEN, Y., DZENIS, Y. & LEONG, K. 2006. The role of electrospinning in the emerging field of nanomedicine. *Current pharmaceutical design,* 12**,** 4751–4770.

CHITTUR, K. K. 1998. FTIR/ATR for protein adsorption to biomaterial surfaces. *Biomaterials,* 19**,** 357-369.

CHOW, W., THAM, W. & SEOW, P. 2012. Effects of maleated-PLA compatibilizer on the properties of poly(lactic acid)/halloysite clay composites. *Journal of Thermoplastic Composite Materials.*

CHOWDHURY, M. & STYLIOS, G. 2011. Process optimization and alignment of PVA/$FeCl_3$ nano composite fibres by electrospinning. *Journal of materials science,* 46**,** 3378-3386.

CHUANGCHOTE, S., SAGAWA, T. & YOSHIKAWA, S. 2009. Electrospinning of poly(vinyl pyrrolidone): Effects of solvents on electrospinnability for the fabrication of poly (p phenylene vinylene) and TiO2 nanofibers. *Journal of Applied Polymer Science,* 114**,** 2777-2791.

CUI, W., LI, X., ZHU, X., YU, G., ZHOU, S. & WENG, J. 2006. Investigation of drug release and matrix degradation of electrospun poly(DL-lactide) fibers with paracetanol inoculation. *Biomacromolecules,* 7**,** 1623-1629.

CUI, W., ZHOU, Y. & CHANG, J. 2010. Electrospun nanofibrous materials for tissue engineering and drug delivery. *Science and Technology of Advanced Materials,* 11**,** 014108.

CUI, W., ZHU, X., YANG, Y., LI, X. & JIN, Y. 2009. Evaluation of electrospun fibrous scaffolds of poly(DL-lactide) and poly(ethylene glycol) for skin tissue engineering. *Materials Science and Engineering: C,* 29**,** 1869-1876.

DEITZEL, J., KLEINMEYER, J., HARRIS, D. & BECK TAN, N. 2001. The effect of processing variables on the morphology of electrospun nanofibers and textiles. *Polymer,* 42**,** 261-272.

DEMIR, M. M., YILGOR, I., YILGOR, E. & ERMAN, B. 2002. Electrospinning of polyurethane fibers. *Polymer,* 43**,** 3303-3309.

DENG, X. L., SUI, G., ZHAO, M. L., CHEN, G. Q. & YANG, X. P. 2007. Poly(L-lactic acid)/hydroxyapatite hybrid nanofibrous scaffolds prepared by electrospinning. *Journal of Biomaterials Science, Polymer Edition,* 18**,** 117-130.

DETREMBLEUR, C., TEYSSIE, P. & JÉRÔME, R. 2002. Control of the Radical Polymerization of t ert-Butyl Methacrylate in Water by a Novel Combination of Sodium Nitrite and Iron (II) Sulfate. *Macromolecules,* 35**,** 1611-1621.

DHAKATE, S. R., GUPTA, A., CHAUDHARI, A., TAWALE, J. & MATHUR, R. B. 2011. Morphology and thermal properties of PAN copolymer based electrospun nanofibers. *Synthetic Metals,* 161**,** 411-419.

DHANDAYUTHAPANI, B., KRISHNAN, U. & SETHURAMAN, S. 2010. Fabrication and characterization of chitosan gelatin blend nanofibers for skin tissue engineering. *Journal of Biomedical Materials Research Part B: Applied Biomaterials,* 94**,** 264-272.

DONG, Y., BICKFORD, T., HAROOSH, H. J., LAU, K.-T. & TAKAGI, H. 2013. Multi-response analysis in the material characterisation of electrospun poly (lactic acid)/halloysite nanotube composite fibres based on Taguchi design of experiments: fibre diameter, non-intercalation and nucleation effects. *Applied Physics A,* 112**,** 747-757.

DONG, Y., CHAUDHARY, D., HAROOSH, H. & BICKFORD, T. 2011. Development and characterisation of novel electrospun polylactic acid/tubular clay nanocomposites. *Journal of materials science,* 46**,** 6148-6153.

DONG, Y., GHATAURA, A., TAKAGI, H., HAROOSH, H. J., NAKAGAITO, A. N. & LAU, K.-T. 2014a. Polylactic acid (PLA) biocomposites reinforced with coir fibres: Evaluation of mechanical performance and multifunctional properties. *Composites Part A: Applied Science and Manufacturing,* 63**,** 76-84.

DONG, Y., MOSAVAL, T., HAROOSH, H. J., UMER, R., TAKAGI, H. & LAU, K. T. 2014b. The potential use of electrospun PLA nanofibers as alternative reinforcements in an epoxy composite system. *Journal of Polymer Science Part B: Polymer Physics,* 52**,** 618–623.

DU, M., GUO, B., LEI, Y., LIU, M. & JIA, D. 2008. Carboxylated butadiene-styrene rubber/halloysite nanotube nanocomposites: Interfacial interaction and performance. *Polymer,* 49**,** 4871-4876.

DUZYER, S., HOCKENBERGER, A. & ZUSSMAN, E. 2011. Characterization of solvent spun polyester nanofibers. *Journal of Applied Polymer Science,* 120**,** 759–769.

EVCIN, A. & KAYA, D. A. 2010. Effect of production parameters on the structure and morphology of aluminum titanate nanofibers produced using electrospinning technique. *Scientific Research and Essays,* 5**,** 3682-3686.

FOWLKS, A. C. & NARAYAN, R. 2010. The effect of maleated poly(lactic acid) (PLA) as an interfacial modifier in PLA-talc composites. *Journal of Applied Polymer Science,* 118**,** 2810-2820.

FRENOT, A. & CHRONAKIS, I. 2003. Polymer nanofibers assembled by electrospinning. *Current Opinion in Colloid & Interface Science,* 8**,** 64-75.

FU, Y. & KAO, W. 2010. Drug release kinetics and transport mechanisms of non-degradable and degradable polymeric delivery systems. *Expert opinion on drug delivery,* 7**,** 429-444.

GOLDBERG, M., LANGER, R. & JIA, X. 2007. Nanostructured materials for applications in drug delivery and tissue engineering. *Journal of Biomaterials Science, Polymer Edition,* 18**,** 241-268.

GU, S., WANG, Z., REN, J. & ZHANG, C. 2009. Electrospinning of gelatin and gelatin/poly(L-lactide) blend and its characteristics for wound dressing. *Materials Science and Engineering: C,* 29**,** 1822-1828.

GUO, B., ZOU, Q., LEI, Y., DU, M., LIU, M. & JIA, D. 2009a. Crystallization behavior of polyamide 6/halloysite nanotubes nanocomposites. *Thermochimica Acta,* 484**,** 48-56.

GUO, J., YE, X., LIU, W., WU, Q., SHEN, H. & SHU, K. 2009b. Preparation and characterization of poly(acrylonitrile-co-acrylic acid) nanofibrous composites with Fe_3O_4 magnetic nanoparticles. *Materials Letters,* 63**,** 1326-1328.

HADJIARGYROU, M. & CHIU, J. 2008. Enhanced composite electrospun nanofiber scaffolds for use in drug delivery. *Expert opinion on drug delivery,* 5**,** 1093-1106.

HAMOUDEH, M. & FESSI, H. 2006. Preparation, characterization and surface study of poly-epsilon caprolactone magnetic microparticles. *Journal of colloid and interface science,* 300**,** 584-590.

HAN, J., BRANFORD-WHITE, C. & ZHU, L. 2010. Preparation of poly(ε-caprolactone)/poly(trimethylene carbonate) blend nanofibers by electrospinning. *Carbohydrate Polymers,* 79**,** 214-218.

HAN, J., CHEN, T., BRANFORD-WHITE, C. & ZHU, L. 2009. Electrospun shikonin-loaded PCL/PTMC composite fiber mats with potential biomedical applications. *International journal of pharmaceutics,* 382**,** 215-221.

HAROOSH, H. J., CHAUDHARY, D. S. & INGRAM, G. D. 2011. Effect of solution concentration and co-solvent ratio on electrospun PEG fibers. *CHEMECA 2011: Engineering a Better World: Sydney Hilton Hotel, NSW, Australia, 18-21 September 2011***,** 1535.

HAROOSH, H. J., CHAUDHARY, D. S. & DONG, Y. 2012. Electrospun PLA/PCL fibers with tubular nanoclay: Morphological and structural analysis. *Journal of Applied Polymer Science,* 124**,** 3930-3939.

HAROOSH, H. J., DONG, Y., CHAUDHARY, D. S., INGRAM, G. D. & YUSA, S. 2013a. Electrospun PLA: PCL composites embedded with unmodified and 3-aminopropyltriethoxysilane (ASP) modified halloysite nanotubes (HNT). *Applied Physics A: Materials Science & Processing,* 110**,** 433-442.

HAROOSH, H. J., DONG, Y. & INGRAM, G. D. 2013b. Synthesis, Morphological Structures, and Material Characterization of Electrospun PLA: PCL/Magnetic Nanoparticle Composites for Drug Delivery. *Journal of Polymer Science Part B: Polymer Physics,* 51**,** 1607-1617.

HAROOSH, H. J., DONG, Y. & LAU, K.-T. 2014. Tetracycline hydrochloride (TCH)-loaded drug carrier based on PLA: PCL nanofibre mats: experimental characterisation and release kinetics modelling. *Journal of Materials Science,* 49**,** 6270-6281.

HE, C., HUANG, Z., HAN, X., LIU, L., ZHANG, H. & CHEN, L. 2006. Coaxial electrospun poly(l-lactic acid) ultrafine fibers for sustained drug delivery. *Journal of Macromolecular Science, Part B,* 45**,** 515-524.

HEYDARKHAN-HAGVALL, S., SCHENKE-LAYLAND, K., DHANASOPON, A., ROFAIL, F., SMITH, H., WU, B., SHEMIN, R., BEYGUI, R. & MACLELLAN, W. 2008. Three-dimensional electrospun ECM-based hybrid scaffolds for cardiovascular tissue engineering. *Biomaterials,* 29**,** 2907-2914.

HOMAYONI, H., RAVANDI, S. & VALIZADEH, M. 2009. Electrospinning of chitosan nanofibers: processing optimization. *Carbohydrate Polymers,* 77**,** 656-661.

HSU, F., HUNG, Y., LIOU, H. & SHEN, C. 2010. Electrospun hyaluronate-collagen nanofibrous matrix and the effects of varying the concentration of hyaluronate on the characteristics of foreskin fibroblast cells. *Acta biomaterialia,* 6**,** 2140-2147.

HUANG, M. H., LI, S. & VERT, M. 2004. Synthesis and degradation of PLA–PCL–PLA triblock copolymer prepared by successive polymerization of ε-caprolactone and dl-lactide. *Polymer,* 45**,** 8675-8681.

HUANG, Z., HE, C., YANG, A., ZHANG, Y., HAN, X., YIN, J. & WU, Q. 2006. Encapsulating drugs in biodegradable ultrafine fibers through co axial electrospinning. *Journal of Biomedical Materials Research Part A,* 77**,** 169-179.

IGNATIOUS, F., SUN, L., LEE, C. & BALDONI, J. 2010. Electrospun nanofibers in oral drug delivery. *Pharmaceutical research,* 27**,** 576-588.

IM, J., BAI, B. & LEE, Y. 2010. The effect of carbon nanotubes on drug delivery in an electro-sensitive transdermal drug delivery system. *Biomaterials,* 31**,** 1414-1419.

INAI, R., KOTAKI, M. & RAMAKRISHNA, S. 2005. Structure and properties of electrospun PLLA single nanofibres. *Nanotechnology,* 16**,** 208.

ISLAM, M. 2010. Fabrication and characterization of poly(vinyl alcohol)/alginate blend nanofibers by electrospinning method. *Colloids and Surfaces A: Physicochemical and Engineering Aspects,* 366**,** 135–140.

ISMAIL, H., PASBAKHSH, P., FAUZI, M. & ABU BAKAR, A. 2008. Morphological, thermal and tensile properties of halloysite nanotubes filled ethylene propylene diene monomer (EPDM) nanocomposites. *Polymer Testing,* 27**,** 841-850.

JANDAS, P., MOHANTY, S., NAYAK, S. & SRIVASTAVA, H. 2011. Effect of surface treatments of banana fiber on mechanical, thermal, and biodegradability properties of PLA/banana fiber biocomposites. *Polymer Composites,* 32**,** 1689–1700.

JANNESARI, M., VARSHOSAZ, J., MORSHED, M. & ZAMANI, M. 2011. Composite poly(vinyl alcohol)/poly(vinyl acetate) electrospun nanofibrous mats as a novel wound dressing matrix for controlled release of drugs. *International journal of nanomedicine,* 6**,** 993–1003.

JEONG, S., KREBS, M., BONINO, C., SAMOREZOV, J., KHAN, S. & ALSBERG, E. 2010. Electrospun chitosan–alginate nanofibers with in situ polyelectrolyte complexation for use as tissue engineering scaffolds. *Tissue Engineering Part A***,** 999.

JI, Y., GHOSH, K., LI, B., SOKOLOV, J., CLARK, R. & RAFAILOVICH, M. 2006a. Dual syringe reactive electrospinning of cross linked hyaluronic acid hydrogel nanofibers for tissue engineering applications. *Macromolecular bioscience,* 6**,** 811-817.

JI, Y., GHOSH, K., SHU, X., LI, B., SOKOLOV, J., PRESTWICH, G., CLARK, R. & RAFAILOVICH, M. 2006b. Electrospun three-dimensional hyaluronic acid nanofibrous scaffolds. *Biomaterials,* 27**,** 3782-3792.

JIA, Z., LUO, Y., YANG, S., GUO, B., DU, M. & JIA, D. 2009. Morphology, interfacial interaction and properties of styrene-butadiene rubber/modified halloysite nanotube nanocomposites. *Chinese Journal of Polymer Science,* 27**,** 857-864.

JIAN, F., HAITAO, N., TONG, L. & XUN-GAI, W. 2008. Applications of electrospun nanofibers. *Chin. Sci. Bull,* 53**,** 2265-2286.

JIANG, H., FANG, D., HSIAO, B., CHU, B. & CHEN, W. 2004. Optimization and characterization of dextran membranes prepared by electrospinning. *Biomacromolecules,* 5**,** 326-333.

JIANG, H., HU, Y., LI, Y., ZHAO, P., ZHU, K. & CHEN, W. 2005. A facile technique to prepare biodegradable coaxial electrospun nanofibers for controlled release of bioactive agents. *Journal of Controlled Release,* 108**,** 237-243.

JIANG, H., HU, Y., ZHAO, P., LI, Y. & ZHU, K. 2006. Modulation of protein release from biodegradable core–shell structured fibers prepared by coaxial electrospinning. *Journal of Biomedical Materials Research Part B: Applied Biomaterials,* 79**,** 50-57.

KARIM, M. R. & YEUM, J. H. 2010. Poly(vinyl alcohol)-Fe_3O_4 nanocomposites prepared by the electrospinning technique. *Soft Materials,* 8**,** 197-206.

KENAWY, E., ABDEL-HAY, F., EL-NEWEHY, M. & WNEK, G. 2009. Processing of polymer nanofibers through electrospinning as drug delivery systems. *Materials Chemistry and Physics,* 113**,** 296-302.

KENAWY, E., BOWLIN, G., MANSFIELD, K., LAYMAN, J., SIMPSON, D., SANDERS, E. & WNEK, G. 2002. Release of tetracycline hydrochloride from electrospun poly(ethylene-co-vinylacetate), poly(lactic acid), and a blend. *Journal of Controlled Release,* 81**,** 57-64.

KHAN, A. 2008. Preparation and characterization of magnetic nanoparticles embedded in microgels. *Materials Letters,* 62**,** 898-902.

KIM, G., YOON, H. & PARK, Y. 2010. Drug release from various thicknesses of layered mats consisting of electrospun polycaprolactone and polyethylene oxide micro/nanofibers. *Applied Physics A: Materials Science & Processing,* 100**,** 1197-1204.

KIM, K., LUU, Y., CHANG, C., FANG, D., HSIAO, B., CHU, B. & HADJIARGYROU, M. 2004. Incorporation and controlled release of a hydrophilic antibiotic using poly(lactide-co-glycolide)-based electrospun nanofibrous scaffolds. *Journal of Controlled Release,* 98**,** 47-56.

KIM, K., YU, M., ZONG, X., CHIU, J., FANG, D., SEO, Y., HSIAO, B., CHU, B. & HADJIARGYROU, M. 2003. Control of degradation rate and hydrophilicity in electrospun non-woven poly(D,L--lactide) nanofiber scaffolds for biomedical applications. *Biomaterials,* 24**,** 4977-4985.

KIM, T., CHUNG, H. & PARK, T. 2008. Macroporous and nanofibrous hyaluronic acid/collagen hybrid scaffold fabricated by concurrent electrospinning and deposition/leaching of salt particles. *Acta biomaterialia,* 4**,** 1611-1619.

KONTOGIANNOPOULOS, K. N., ASSIMOPOULOU, A. N., TSIVINTZELIS, I., PANAYIOTOU, C. & PAPAGEORGIOU, V. P. 2011. Electrospun fiber mats containing shikonin and derivatives with potential biomedical applications. *International journal of pharmaceutics,* 409**,** 216–228.

KUMAR, R. V., KOLTYPIN, Y., COHEN, Y., COHEN, Y., AURBACH, D., PALCHIK, O., FELNER, I. & GEDANKEN, A. 2000. Preparation of amorphous magnetite nanoparticles embedded in polyvinyl alcohol using ultrasound radiation. *Journal of Materials Chemistry,* 10**,** 1125-1129.

KUMBAR, S., JAMES, R., NUKAVARAPU, S. & LAURENCIN, C. 2008. Electrospun nanofiber scaffolds: engineering soft tissues. *Biomedical Materials,* 3**,** 034002.

KWEON, H. Y., YOO, M. K., PARK, I. K., KIM, T. H., LEE, H. C., LEE, H. S., OH, J. S., AKAIKE, T. & CHO, C. S. 2003. A novel degradable polycaprolactone networks for tissue engineering. *Biomaterials,* 24**,** 801-808.

KYUNG SUNG, Y., WOOK AHN, B. & JIN KANG, T. 2011. Magnetic nanofibers with core (Fe_3O_4 nanoparticle suspension)/Sheath (Poly ethylene terephthalate) structure fabricated by coaxial electrospinning. *Journal of Magnetism and Magnetic Materials.*

LAPPAS, A., ZORKO, A., WORTHAM, E., DAS, R. N., GIANNELIS, E. P., CEVC, P. & ARČON, D. 2005. Low-energy magnetic excitations and morphology in layered hybrid perovskite-poly(dimethylsiloxane) nanocomposites. *Chemistry of materials,* 17**,** 1199-1207.

LEE, G., SONG, J. & YOON, K. 2010. Controlled wall thickness and porosity of polymeric hollow nanofibers by coaxial electrospinning. *Macromolecular Research,* 18**,** 571-576.

LEE, J. H., PARK, T. G., PARK, H. S., LEE, D. S., LEE, Y. K., YOON, S. C. & NAM, J. D. 2003a. Thermal and mechanical characteristics of poly(L-lactic acid) nanocomposite scaffold. *Biomaterials,* 24**,** 2773-2778.

LEE, K., KIM, H., KHIL, M., RA, Y. & LEE, D. 2003b. Characterization of nano-structured poly (ε-caprolactone) nonwoven mats via electrospinning. *Polymer,* 44**,** 1287-1294.

LEVIS, S. & DEASY, P. 2003. Use of coated microtubular halloysite for the sustained release of diltiazem hydrochloride and propranolol hydrochloride. *International journal of pharmaceutics,* 253**,** 145-157.

LI, H. Y., CHANG, C. M., HSU, K. Y. & LIU, Y. L. 2012. Poly(lactide)-functionalized and Fe_3O_4 nanoparticle-decorated multiwalled carbon nanotubes for preparation of electrically-conductive and magnetic poly(lactide) films and electrospun nanofibers. *J. Mater. Chem.,* 22**,** 4855-4860.

LI, J., HE, A., HAN, C., FANG, D., HSIAO, B. & CHU, B. 2006. Electrospinning of hyaluronic acid (HA) and HA/gelatin blends. *Macromolecular Rapid Communications,* 27**,** 114-120.

LI, Y., JIANG, H. & ZHU, K. 2008. Encapsulation and controlled release of lysozyme from electrospun poly(ε-caprolactone)/poly(ethylene glycol) non-woven membranes by formation of lysozyme–oleate complexes. *Journal of Materials Science: Materials in Medicine,* 19**,** 827-832.

LIANG, D., HSIAO, B. & CHU, B. 2007. Functional electrospun nanofibrous scaffolds for biomedical applications. *Advanced drug delivery reviews,* 59**,** 1392-1412.

LIAO, C. C., WANG, C. C., SHIH, K. C. & CHEN, C. Y. 2011. Electrospinning fabrication of partially crystalline bisphenol A polycarbonate nanofibers: Effects on conformation, crystallinity, and mechanical properties. *European Polymer Journal,* 47**,** 911–924.

LIM, L. T., AURAS, R. & RUBINO, M. 2008. Processing technologies for poly(lactic acid). *Progress in polymer science,* 33**,** 820-852.

LIN, C. R., TSAI, T. C., CHUNG, M. & LU, S. Z. 2009. Synthesis and characterization of magnetic nanoparticles embedded in polyvinyl pyrrolidone nanofiber film by electrospinning method. *Journal of Applied Physics,* 105**,** 07B509-07B509-3.

LIU, F., GUO, R., SHEN, M., WANG, S. & SHI, X. 2009a. Effect of Processing Variables on the Morphology of Electrospun Poly [(lactic acid) co (glycolic acid)] Nanofibers. *Macromolecular Materials and Engineering,* 294**,** 666-672.

LIU, H., WANG, G., WEXLER, D., WANG, J. & LIU, H. 2008a. Electrochemical performance of $LiFePO_4$ cathode material coated with ZrO_2 nanolayer. *Electrochemistry communications,* 10**,** 165-169.

LIU, H., WANG, S. & QI, N. 2012. Controllable structure, properties, and degradation of the electrospun PLGA/PLA-blended nanofibrous scaffolds. *Journal of Applied Polymer Science,* 125**,** E468–E476.

LIU, M., GUO, B., DU, M., CHEN, F. & JIA, D. 2009b. Halloysite nanotubes as a novel β-nucleating agent for isotactic polypropylene. *Polymer,* 50**,** 3022-3030.

LIU, M., GUO, B., DU, M. & JIA, D. 2007. Drying induced aggregation of halloysite nanotubes in polyvinyl alcohol/halloysite nanotubes solution and its effect on properties of composite film. *Applied Physics A: Materials Science & Processing,* 88**,** 391-395.

LIU, M., GUO, B., LEI, Y., DU, M. & JIA, D. 2009c. Benzothiazole sulfide compatibilized polypropylene/halloysite nanotubes composites. *Applied Surface Science,* 255**,** 4961-4969.

LIU, M., GUO, B., ZOU, Q., DU, M. & JIA, D. 2008b. Interactions between halloysite nanotubes and 2, 5-bis (2-benzoxazolyl) thiophene and their effects on reinforcement of polypropylene/halloysite nanocomposites. *Nanotechnology,* 19**,** 205709.

LIU, S., KAU, Y., CHOU, C., CHEN, J., WU, R. & YEH, W. 2010a. Electrospun PLGA/collagen nanofibrous membrane as early-stage wound dressing. *Journal of Membrane Science,* 355**,** 53-59.

LIU, S., ZHANG, L., ZHOU, J. & WU, R. 2008c. Structure and properties of cellulose/Fe_2O_3 nanocomposite fibers spun via an effective pathway. *The Journal of Physical Chemistry C,* 112**,** 4538-4544.

LIU, Y., MA, G., FANG, D., XU, J., ZHANG, H. & NIE, J. 2010b. Effects of solution properties and electric field on the electrospinning of hyaluronic acid. *Carbohydrate Polymers.*

LUONG-VAN, E., GRØNDAHL, L., CHUA, K., LEONG, K., NURCOMBE, V. & COOL, S. 2006a. Controlled release of heparin from poly(ε-caprolactone) electrospun fibers. *Biomaterials,* 27**,** 2042-2050.

LUONG-VAN, E., GRØNDAHL, L., CHUA, K. N., LEONG, K. W., NURCOMBE, V. & COOL, S. M. 2006b. Controlled release of heparin from poly(ε-caprolactone) electrospun fibers. *Biomaterials,* 27**,** 2042-2050.

LV, G., HE, F., WANG, X., GAO, F., ZHANG, G., WANG, T., JIANG, H., WU, C., GUO, D. & LI, X. 2008. Novel nanocomposite of nano Fe_3O_4 and polylactide nanofibers for application in drug uptake and induction of cell death of leukemia cancer cells. *Langmuir,* 24**,** 2151-2156.

MA, Z., KOTAKI, M., INAI, R. & RAMAKRISHNA, S. 2005. Potential of nanofiber matrix as tissue-engineering scaffolds. *Tissue engineering,* 11**,** 101-109.

MACOSSAY, J., MARRUFFO, A., RINCON, R., EUBANKS, T. & KUANG, A. 2007. Effect of needle diameter on nanofiber diameter and thermal properties of electrospun poly(methyl methacrylate). *Polymers for Advanced Technologies,* 18**,** 180-183.

MAKINO, K., OHSHIMA, H. & KONDO, T. 1986. Mechanism of hydrolytic degradation of poly(L-lactide) microcapsules: effects of pH, ionic strength and buffer concentration. *Journal of microencapsulation,* 3**,** 203-212.

MAO, S., SHUAI, X., UNGER, F., SIMON, M., BI, D. & KISSEL, T. 2004. The depolymerization of chitosan: effects on physicochemical and biological properties. *International Journal of Pharmaceutics,* 281**,** 45-54.

MAQUET, V., BOCCACCINI, A. R., PRAVATA, L., NOTINGHER, I. & JÉRÔME, R. 2004. Porous poly(α-hydroxyacid)/Bioglass® composite scaffolds for bone tissue engineering. I: preparation and in vitro characterisation. *Biomaterials,* 25**,** 4185-4194.

MATUSIK, J., STODOLAK, E. & BAHRANOWSKI, K. 2011. Synthesis of polylactide/clay composites using structurally different kaolinites and kaolinite nanotubes. *Applied Clay Science,* 51**,** 102-109.

MCCULLEN, S. D., STANO, K. L., STEVENS, D. R., ROBERTS, W. A., MONTEIRO-RIVIERE, N. A., CLARKE, L. I. & GORGA, R. E. 2007. Development, optimization, and characterization of electrospun poly(lactic acid) nanofibers containing multi-walled carbon nanotubes. *Journal of Applied Polymer Science,* 105**,** 1668-1678.

MCKEE, M. G., ELKINS, C. L. & LONG, T. E. 2004. Influence of self-complementary hydrogen bonding on solution rheology/electrospinning relationships. *Polymer,* 45**,** 8705-8715.

MENCZEL, J. D., JUDOVITS, L., PRIME, R. B., BAIR, H. E., READING, M. & SWIER, S. 2009. Differential scanning calorimetry (DSC). *Thermal Analysis of Polymers***,** 7-239.

MENG, F., ZHAN, Y., LEI, Y., ZHAO, R., ZHONG, J. & LIU, X. 2012. Electrospun magnetic fibrillar polyarylene ether nitriles nanocomposites reinforced with Fe-phthalocyanine/Fe_3O_4 hybrid microspheres. *Journal of Applied Polymer Science,* 123**,** 1732–1739.

MENG, Z., ZHENG, W., LI, L. & ZHENG, Y. 2010. Fabrication and Characterization of Three-Dimensional Nanofiber Membrance of PCL-MWCNTs by Electrospinning. *Materials Science and Engineering: C,* 30**,** 1014–1021.

MI, F. L., SUNG, H. W. & SHYU, S. S. 2001. Release of indomethacin from a novel chitosan microsphere prepared by a naturally occurring crosslinker: Examination of crosslinking and polycation–anionic drug interaction. *Journal of Applied Polymer Science,* 81**,** 1700-1711.

MIKOŁAJCZYK, T. & OLEJNIK, M. 2006. Effects of spinning conditions on structure and properties of multifunctional fibers of polyimidoamide nanocomposites. *Journal of Applied Polymer Science,* 100**,** 3323-3331.

MOHANAMBE, L. & VASUDEVAN, S. 2005. Anionic clays containing anti-inflammatory drug molecules: comparison of molecular dynamics simulation and measurements. *The Journal of Physical Chemistry B,* 109**,** 15651-15658.

NATU, M., DE SOUSA, H. & GIL, M. 2010. Effects of drug solubility, state and loading on controlled release in bicomponent electrospun fibers. *International journal of pharmaceutics,* 397**,** 50–58.

NING, N., YIN, Q., LUO, F., ZHANG, Q., DU, R. & FU, Q. 2007. Crystallization behavior and mechanical properties of polypropylene/halloysite composites. *Polymer,* 48**,** 7374-7384.

NOOR AZMAN, N., SIDDIQUI, S. A., HAROOSH, H. J., ALBETRAN, H. M., JOHANNESSEN, B., DONG, Y. & LOW, I. M. 2013. Characteristics of X-ray attenuation in electrospun bismuth oxide/polylactic acid nanofibre mats. *Journal of synchrotron radiation,* 20**,** 741–748.

NYSTRÖM, M., MURTOMAA, M. & SALONEN, J. 2010. Fabrication and characterization of drug particles produced by electrospraying into reduced pressure. *Journal of Electrostatics,* 68**,** 42-48.

PHAM, Q., SHARMA, U. & MIKOS, A. 2006. Electrospinning of polymeric nanofibers for tissue engineering applications: a review. *Tissue engineering,* 12**,** 1197-1211.

PICCIANI, P., MEDEIROS, E., PAN, Z., WOOD, D., ORTS, W., MATTOSO, L. & SOARES, B. 2010. Structural, Electrical, Mechanical, and Thermal Properties of Electrospun Poly(lactic acid)/Polyaniline Blend Fibers. *Macromolecular Materials and Engineering,* 295**,** 618-627.

PICCIANI, P. H. S., MEDEIROS, E. S., PAN, Z., ORTS, W. J., MATTOSO, L. H. C. & SOARES, B. G. 2009. Development of conducting polyaniline/poly(lactic acid) nanofibers by electrospinning. *Journal of Applied Polymer Science,* 112**,** 744-753.

PITT, G., GRATZL, M., KIMMEL, G., SURLES, J. & SOHINDLER, A. 1981. Aliphatic polyesters II. The degradation of poly(DL-lactide), poly(ε-caprolactone), and their copolymers in vivo. *Biomaterials,* 2**,** 215-220.

PUPPI, D., PIRAS, A., DETTA, N., DINUCCI, D. & CHIELLINI, F. 2010. Poly(lactic-co-glycolic acid) electrospun fibrous meshes for the controlled release of retinoic acid. *Acta Biomaterialia,* 6**,** 1258-1268.

QI, R., GUO, R., SHEN, M., CAO, X., ZHANG, L., XU, J., YU, J. & SHI, X. 2010. Electrospun poly(lactic-co-glycolic acid)/halloysite nanotube composite nanofibers for drug encapsulation and sustained release. *J. Mater. Chem.,* 20**,** 10622-10629.

QIAN, Y., SU, Y., LI, X., WANG, H. & HE, C. 2010. Electrospinning of polymethyl methacrylate nanofibres in different solvents. *Iranian Polymer Journal,* 19**,** 123-129.

QIN, X. & WU, D. 2012. Effect of different solvents on poly(caprolactone)(PCL) electrospun nonwoven membranes. *Journal of Thermal Analysis and Calorimetry,* 107**,** 1388-6150.

RIBEIRO, C., SENCADAS, V., COSTA, C. M., GÓMEZ RIBELLES, J. L. & LANCEROS-MÉNDEZ, S. 2011. Tailoring the morphology and crystallinity of poly(L-lactide acid) electrospun membranes. *Science and Technology of Advanced Materials,* 12**,** 015001.

RIBEIRO, C., SENCADAS, V., RIBELLES, J. & LANCEROS-MÉNDEZ, S. 2010. Influence of processing conditions on polymorphism and nanofiber morphology of electroactive poly(vinylidene fluoride) electrospun membranes. *Soft Materials.* Taylor & Francis.

ROMERO-CANO, M. & VINCENT, B. 2002. Controlled release of 4-nitroanisole from poly(lactic acid) nanoparticles. *Journal of Controlled Release,* 82**,** 127-135.

ROOJ, S., DAS, A., THAKUR, V., MAHALING, R., BHOWMICK, A. K. & HEINRICH, G. 2010. Preparation and properties of natural nanocomposites based on natural rubber and naturally occurring halloysite nanotubes. *Materials & Design,* 31**,** 2151-2156.

SAMANI, F., KOKABI, M., SOLEIMANI, M. & VALOJERDI, M. 2010. Fabrication and characterization of electrospun fibrous nanocomposite scaffolds based on poly(lactide co glycolide)/poly(vinyl alcohol) blends. *Polymer International,* 59**,** 901-909.

SARAF, A., LOZIER, G., HAESSLEIN, A., KASPER, F., RAPHAEL, R., BAGGETT, L. & MIKOS, A. 2009. Fabrication of nonwoven coaxial fiber meshes by electrospinning. *Tissue Engineering Part C: Methods,* 15**,** 333-344.

SASSMAN, S. A. & LEE, L. S. 2005. Sorption of three tetracyclines by several soils: Assessing the role of pH and cation exchange. *Environmental science & technology,* 39**,** 7452-7459.

SCHLUETER, J., PARK, H., MANSON, J., NAKOTTE, H. & SCHULTZ, A. 2010. Effect of deuteration on the structural and magnetic properties of $CuF_2(H2O)_2$ (pyrazine). *Physica B: Condensed Matter,* 405**,** S324-S326.

SCHMIDT, A. M. 2005. The synthesis of magnetic core-shell nanoparticles by surface-initiated ring-opening polymerization of ε-caprolactone. *Macromolecular rapid communications,* 26**,** 93-97.

SHARMA, C., VASITA, R., UPADHYAY, D., SHARMA, A., KATTI, D. & VENKATARAGHAVAN, R. 2010a. Photoresist derived electrospun carbon nanofibers with tunable morphology and surface properties. *Industrial & Engineering Chemistry Research,* 49**,** 2731-2739.

SHARMA, N., JAFFARI, G. H., SHAH, S. I. & POCHAN, D. J. 2010b. Orientation-dependent magnetic behavior in aligned nanoparticle arrays constructed by coaxial electrospinning. *Nanotechnology,* 21**,** 085707.

SHEN, X., YU, D., ZHU, L., BRANFORD-WHITE, C., WHITE, K. & CHATTERTON, N. P. 2011. Electrospun diclofenac sodium loaded Eudragit® L 100-55 nanofibers for colon-targeted drug delivery. *International Journal of Pharmaceutics,* 408**,** 200–207.

SHIBATA, M., INOUE, Y. & MIYOSHI, M. 2006. Mechanical properties, morphology, and crystallization behavior of blends of poly(l-lactide) with poly(butylene succinate-co-L-lactate) and poly(butylene succinate). *Polymer,* 47**,** 3557-3564.

SIKAREEPAISAN, P., SUKSAMRARN, A. & SUPAPHOL, P. 2008. Electrospun gelatin fiber mats containing a herbal-Centella asiatica-extract and release characteristic of asiaticoside. *Nanotechnology,* 19**,** 015102.

SINGH, S., LAKSHMI, S. & VIJAYAKUMAR, M. 2009. Effect of process parameters on the microstructural characteristics of electrospun poly(vinyl alcohol) fiber mats. *NanoBioTechnology,* 5**,** 10-16.

SMITH, B. C. 2009. *Fundamentals of Fourier transform infrared spectroscopy,* CRC.

SONG, B., WU, C. & CHANG, J. 2012. Controllable delivery of hydrophilic and hydrophobic drugs from electrospun poly(lactic-co-glycolic acid)/mesoporous silica nanoparticles composite mats. *Journal of Biomedical Materials Research Part B: Applied Biomaterials,* 100B**,** 2178–2186.

SONSECA, A., PEPONI, L., SAHUQUILLO, O., KENNY, J. M. & GIMÉNEZ, E. 2012. Electrospinning of biodegradable polylactide/hydroxyapatite nanofibers: Study on the morphology, crystallinity structure and thermal stability. *Polymer Degradation and Stability,* 97**,** 2052–2059.

SPASOVA, M., STOILOVA, O., MANOLOVA, N., RASHKOV, I. & ALTANKOV, G. 2007. Preparation of PLLA/PEG nanofibers by electrospinning and potential applications. *Journal of Bioactive and Compatible Polymers,* 22**,** 62-76.

SRIKAR, R., YARIN, A., MEGARIDIS, C., BAZILEVSKY, A. & KELLEY, E. 2008. Desorption-limited mechanism of release from polymer nanofibers. *Langmuir,* 24**,** 965-974.

STEFANI, M., COUDANE, J. & VERT, M. 2006. In vitro ageing and degradation of PEG–PLA diblock copolymer-based nanoparticles. *Polymer Degradation and Stability,* 91**,** 2554-2559.

SUBBIAH, T., BHAT, G., TOCK, R., PARAMESWARAN, S. & RAMKUMAR, S. 2005. Electrospinning of nanofibers. *Journal of Applied Polymer Science,* 96**,** 557-569.

SUN, M. & DOWNES, S. 2009. Physicochemical characterisation of novel ultra-thin biodegradable scaffolds for peripheral nerve repair. *Journal of Materials Science: Materials in Medicine,* 20**,** 1181-1192.

SUNG, Y. K., AHN, B. W. & KANG, T. J. 2012. Magnetic nanofibers with core (Fe_3O_4 nanoparticle suspension)/sheath (poly ethylene terephthalate) structure fabricated by coaxial electrospinning. *Journal of magnetism and magnetic materials,* 324**,** 916-922.

SUWA, T., TAKEHISA, M. & MACHI, S. 1973. Melting and crystallization behavior of poly (tetrafluoroethylene). New method for molecular weight measurement of poly (tetrafluoroethylene) using a differential scanning calorimeter. *Journal of Applied Polymer Science,* 17**,** 3253-3257.

THOMPSON, C., CHASE, G., YARIN, A. & RENEKER, D. 2007. Effects of parameters on nanofiber diameter determined from electrospinning model. *Polymer,* 48**,** 6913-6922.

TIMKO, M., KONERACKÁ, M. & KOPČANSKÝ, P. 2006. Magnetite polymer nanospheres loaded by Indomethacin for anti-inflammatory therapy. *Journal of magnetism and magnetic materials,* 300**,** e191-e194.

TIWARI, S., TZEZANA, R., ZUSSMAN, E. & VENKATRAMAN, S. 2010. Optimizing partition-controlled drug release from electrospun core-shell fibers. *International Journal of Pharmaceutics,* 392**,** 209–217.

TOUNY, A., LAWRENCE, J., JONES, A. & BHADURI, S. 2010. Effect of electrospinning parameters on the characterization of PLA/HNT nanocomposite fibers. *Journal of Materials Research,* 25**,** 857-865.

TSIOPTSIAS, C., SAKELLARIOU, K. G., TSIVINTZELIS, I., PAPADOPOULOU, L. & PANAYIOTOU, C. 2010. Preparation and characterization of cellulose acetate-Fe_2O_3 composite nanofibrous materials. *Carbohydrate Polymers,* 81**,** 925-930.

TUNGPRAPA, S., JANGCHUD, I. & SUPAPHOL, P. 2007. Release characteristics of four model drugs from drug-loaded electrospun cellulose acetate fiber mats. *Polymer,* 48**,** 5030-5041.

UM, I., FANG, D., HSIAO, B., OKAMOTO, A. & CHU, B. 2004. Electro-spinning and electro-blowing of hyaluronic acid. *Biomacromolecules,* 5**,** 1428-1436.

VERGARO, V., ABDULLAYEV, E., LVOV, Y. M., ZEITOUN, A., CINGOLANI, R., RINALDI, R. & LEPORATTI, S. 2010. Cytocompatibility and uptake of halloysite clay nanotubes. *Biomacromolecules,* 11**,** 820-826.

VERRECK, G., CHUN, I., PEETERS, J., ROSENBLATT, J. & BREWSTER, M. E. 2003a. Preparation and characterization of nanofibers containing amorphous drug dispersions generated by electrostatic spinning. *Pharmaceutical research,* 20**,** 810-817.

VERRECK, G., CHUN, I., ROSENBLATT, J., PEETERS, J., DIJCK, A., MENSCH, J., NOPPE, M. & BREWSTER, M. 2003b. Incorporation of drugs in an amorphous state into electrospun nanofibers composed of a water-insoluble, nonbiodegradable polymer. *Journal of Controlled Release,* 92**,** 349-360.

WANG, B., SUN, Y. & WANG, H. 2010a. Preparation and properties of electrospun PAN/Fe_3O_4 magnetic nanofibers. *Journal of Applied Polymer Science,* 115**,** 1781-1786.

WANG, B. Y., FU, S. Z., NI, P. Y., PENG, J. R., ZHENG, L., LUO, F., LIU, H. & QIAN, Z. Y. 2012. Electrospun polylactide/poly (ethylene glycol) hybrid fibrous scaffolds for tissue engineering. *Journal of Biomedical Materials Research Part A,* 100A**,** 441–449.

WANG, C., HSU, C. H. & LIN, J. H. 2006a. Scaling laws in electrospinning of polystyrene solutions. *Macromolecules,* 39**,** 7662-7672.

WANG, C., YAN, K. W., LIN, Y. D. & HSIEH, P. C. H. 2010b. Biodegradable core/shell fibers by coaxial electrospinning: processing, fiber characterization, and its application in sustained drug release. *Macromolecules,* 43**,** 6389–6397.

WANG, H., FANG, M., SHI, T., ZHAI, L. & TANG, C. 2006b. Preparation of porous poly(lactic acid)/SiO_2 hybrid microspheres. *Journal of Applied Polymer Science,* 102**,** 679-683.

WANG, H., SONG, H., CHEN, X. & DENG, Y. 2010c. Release of ibuprofen from PEG-PLLA electrospun fibers containing poly(ethylene glycol)-b-poly(hydroxy octanoic acid) as an additive. *Chinese Journal of Polymer Science,* 28**,** 417-425.

WANG, M., YU, J., HSIEH, A. & RUTLEDGE, G. 2010d. Effect of tethering chemistry of cationic surfactants on clay exfoliation, electrospinning and diameter of PMMA/clay nanocomposite fibers. *Polymer,* 51**,** 6295–6302.

WANG, X., UM, I., FANG, D., OKAMOTO, A., HSIAO, B. & CHU, B. 2005. Formation of water-resistant hyaluronic acid nanofibers by blowing-assisted electro-spinning and non-toxic post treatments. *Polymer,* 46**,** 4853-4867.

WEI, A., WANG, J., WANG, X., WEI, Q., GE, M. & HOU, D. 2010. Preparation and characterization of the electrospun nanofibers loaded with clarithromycin. *Journal of Applied Polymer Science,* 118**,** 346-352.

WILLIAMS, D. B. & CARTER, C. B. 2009. The Transmission Electron Microscope. *Transmission Electron Microscopy***,** 3-22.

XIE, C., LI, X., LUO, X., YANG, Y., CUI, W., ZOU, J. & ZHOU, S. 2010. Release modulation and cytotoxicity of hydroxycamptothecin-loaded electrospun fibers with 2-hydroxypropyl-(beta)-cyclodextrin inoculations. *International Journal of Pharmaceutics,* 391**,** 55-64.

XIE, Z. & BUSCHLE DILLER, G. 2010. Electrospun poly(D, L lactide) fibers for drug delivery: The influence of cosolvent and the mechanism of drug release. *Journal of Applied Polymer Science,* 115**,** 1-8.

XU, S., LI, J., HE, A., LIU, W., JIANG, X., ZHENG, J., HAN, C., HSIAO, B., CHU, B. & FANG, D. 2009. Chemical crosslinking and biophysical properties of electrospun hyaluronic acid based ultra-thin fibrous membranes. *Polymer,* 50**,** 3762-3769.

XU, X., CHEN, X., MA, P., WANG, X. & JING, X. 2008. The release behavior of doxorubicin hydrochloride from medicated fibers prepared by emulsion-electrospinning. *European Journal of Pharmaceutics and Biopharmaceutics,* 70**,** 165-170.

XU, X., ZHONG, W., ZHOU, S., TRAJTMAN, A. & ALFA, M. 2010. Electrospun PEG–PLA nanofibrous membrane for sustained release of hydrophilic antibiotics. *Journal of Applied Polymer Science,* 118**,** 588-595.

YAN, N., ZHANG, X., CAI, Q., YANG, X., ZHOU, X., WANG, B. & DENG, X. 2012. The Effects of Lactidyl/Glycolidyl Ratio and Molecular Weight of Poly(D, L-Lactide-co-Glycolide) on the Tetracycline Entrapment and Release Kinetics of Drug-Loaded Nanofibers. *Journal of Biomaterials Science, Polymer Edition,* 23**,** 1005-1019.

YANG, D., LI, Y. & NIE, J. 2007a. Preparation of gelatin/PVA nanofibers and their potential application in controlled release of drugs. *Carbohydrate Polymers,* 69**,** 538-543.

YANG, D., LU, B., ZHAO, Y. & JIANG, X. 2007b. Fabrication of aligned fibrous arrays by magnetic electrospinning. *Advanced Materials,* 19**,** 3702-3706.

YANG, J., PARK, S. B., YOON, H. G., HUH, Y. M. & HAAM, S. 2006. Preparation of poly-caprolactone nanoparticles containing magnetite for magnetic drug carrier. *International journal of pharmaceutics,* 324**,** 185-190.

YAO, C., LI, X. & SONG, T. 2007. Fabrication of zein/hyaluronic acid fibrous membranes by electrospinning. *Journal of Biomaterials Science, Polymer Edition,* 18**,** 731-742.

YU, D., BRANFORD-WHITE, C., SHEN, X., ZHANG, X. & ZHU, L. 2010. Solid dispersions of ketoprofen in drug-loaded electrospun nanofibers. *Journal of Dispersion Science and Technology,* 31**,** 902-908.

YU, H., GUO, J., ZHU, S., LI, Y., ZHANG, Q. & ZHU, M. 2012. Preparation of continuous alumina nanofibers via electrospinning of PAN/DMF solution. *Materials Letters,* 74**,** 247–249.

YUAN, P., SOUTHON, P. D., LIU, Z., GREEN, M. E. R., HOOK, J. M., ANTILL, S. J. & KEPERT, C. J. 2008. Functionalization of halloysite clay nanotubes by grafting with γ-aminopropyltriethoxysilane. *The Journal of Physical Chemistry C,* 112**,** 15742-15751.

ZAMANI, M., MORSHED, M., VARSHOSAZ, J. & JANNESARI, M. 2010. Controlled release of metronidazole benzoate from poly(ε-caprolactone) electrospun nanofibers for periodontal diseases. *European Journal of Pharmaceutics and Biopharmaceutics,* 75**,** 179-185.

ZAVISOVA, V., KONERACKA, M., STRBAK, O., TOMASOVICOVA, N., KOPCANSKY, P., TIMKO, M. & VAVRA, I. 2007. Encapsulation of indomethacin in magnetic biodegradable polymer nanoparticles. *Journal of magnetism and magnetic materials,* 311**,** 379-382.

ZENG, L., AN, L. & WU, X. 2011. Modeling drug-carrier interaction in the drug release from nanocarriers. *Journal of Drug Delivery,* 2011.

ZHANG, D., KARKI, A. B., RUTMAN, D., YOUNG, D. P., WANG, A., COCKE, D., HO, T. H. & GUO, Z. 2009. Electrospun polyacrylonitrile nanocomposite fibers reinforced with Fe_3O_4 nanoparticles: Fabrication and property analysis. *Polymer,* 50**,** 4189-4198.

ZHANG, L., WANG, T. & LIU, P. 2008. Polyaniline-coated halloysite nanotubes via in-situ chemical polymerization. *Applied Surface Science,* 255**,** 2091-2097.

ZHANG, Q., ZHANG, H., XIE, G. & ZHANG, J. 2007a. Effect of surface treatment of magnetic particles on the preparation of magnetic polymer microspheres by miniemulsion polymerization. *Journal of magnetism and magnetic materials,* 311**,** 140-144.

ZHANG, X., NAKAGAWA, R., CHAN, K. H. K. & KOTAKI, M. 2012. Mechanical property enhancement of polylactide nanofibers through optimization of molecular weight, electrospinning conditions, and stereocomplexation. *Macromolecules,* 45**,** 5494–5500.

ZHANG, Y., OUYANG, H., LIM, C., RAMAKRISHNA, S. & HUANG, Z. 2005. Electrospinning of gelatin fibers and gelatin/PCL composite fibrous scaffolds. *Journal of Biomedical Materials Research Part B: Applied Biomaterials,* 72**,** 156-165.

ZHANG, Y., SU, B., VENUGOPAL, J., RAMAKRISHNA, S. & LIM, C. 2007b. Biomimetic and bioactive nanofibrous scaffolds from electrospun composite nanofibers. *International Journal of Nanomedicine,* 2**,** 623–638.

ZHANG, Y., WANG, X., FENG, Y., LI, J., LIM, C. & RAMAKRISHNA, S. 2006. Coaxial electrospinning of (fluorescein isothiocyanate-conjugated bovine serum albumin)-encapsulated poly(ε-caprolactone) nanofibers for sustained release. *Biomacromolecules,* 7**,** 1049-1057.

ZONG, X., KIM, K., FANG, D., RAN, S., HSIAO, B. & CHU, B. 2002a. Structure and process relationship of electrospun bioabsorbable nanofiber membranes. *Polymer,* 43**,** 4403-4412.

ZONG, X., KIM, K., FANG, D., RAN, S., HSIAO, B. S. & CHU, B. 2002b. Structure and process relationship of electrospun bioabsorbable nanofiber membranes. *Polymer,* 43**,** 4403-4412.

Appendix I
Model fitting to drug release data

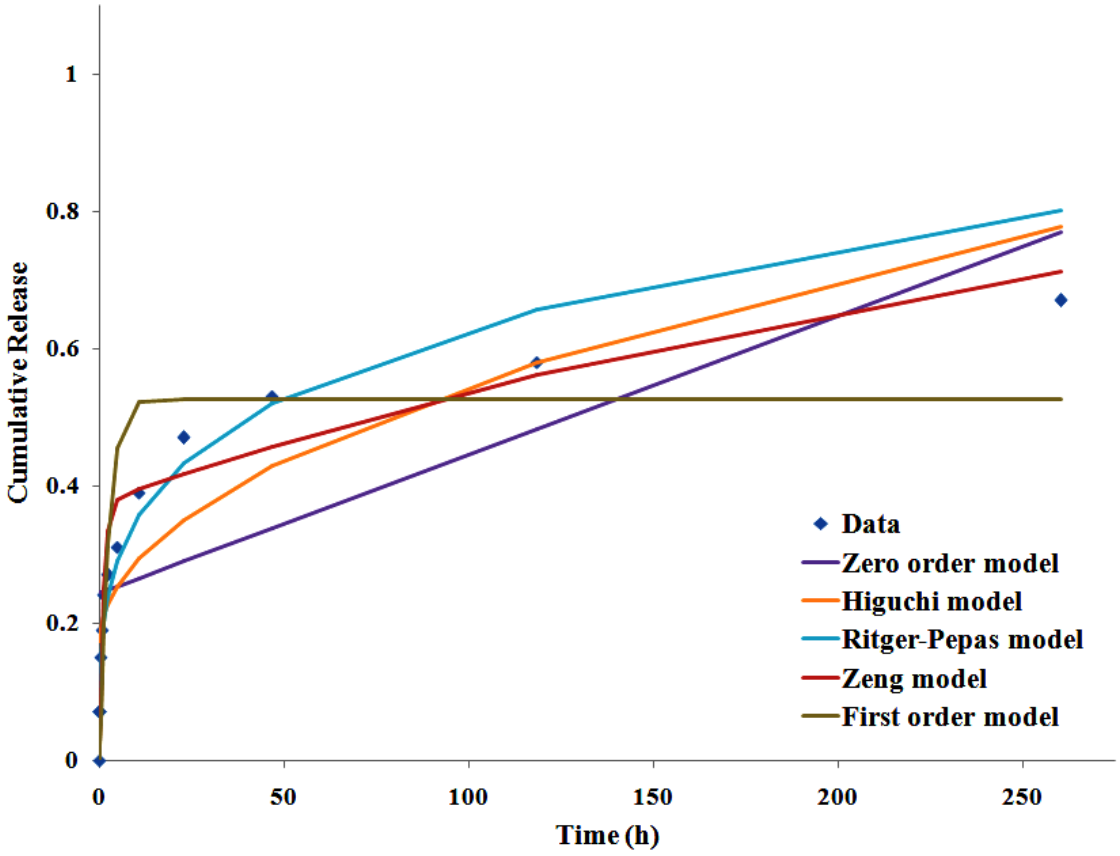

Figure I-1: Model fittings to the drug release data for PLA: 15% PCL/ 5 wt%/v IMC nanofibres.

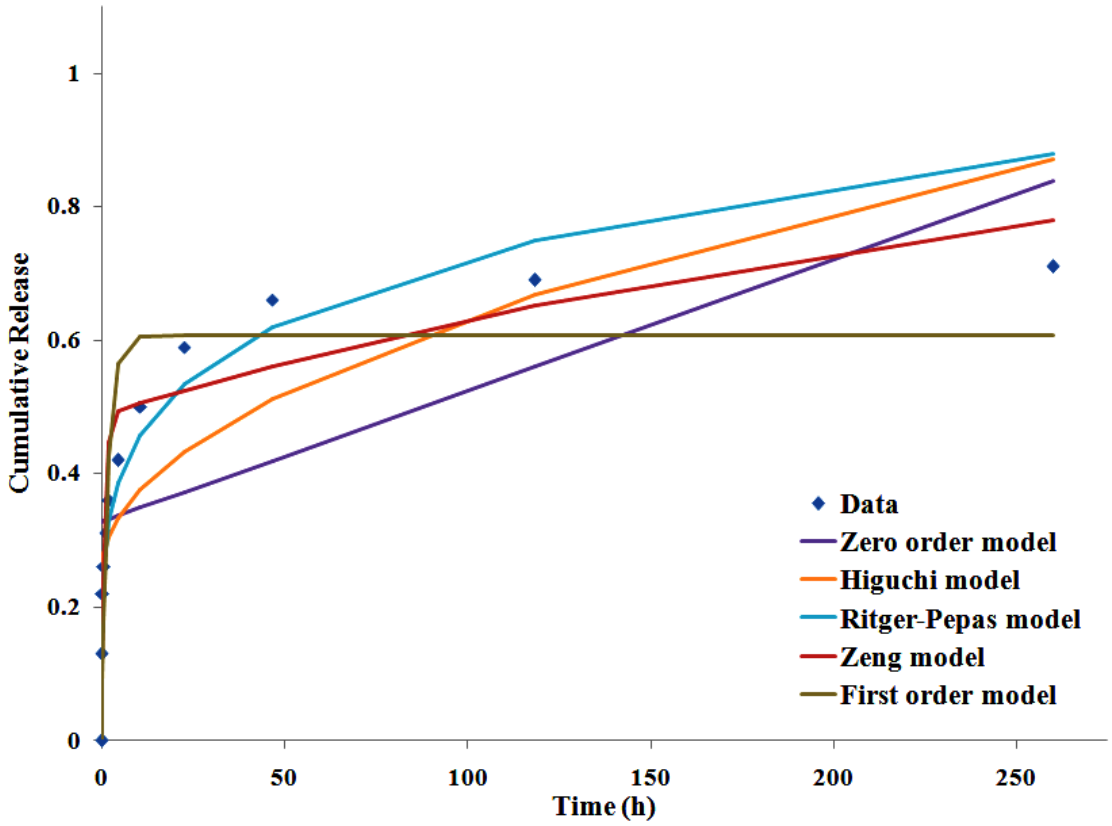

Figure I-2: Models fittings to the drug release data for PLA: 15% PCL/ 5 wt%/v TCH nanofibres.

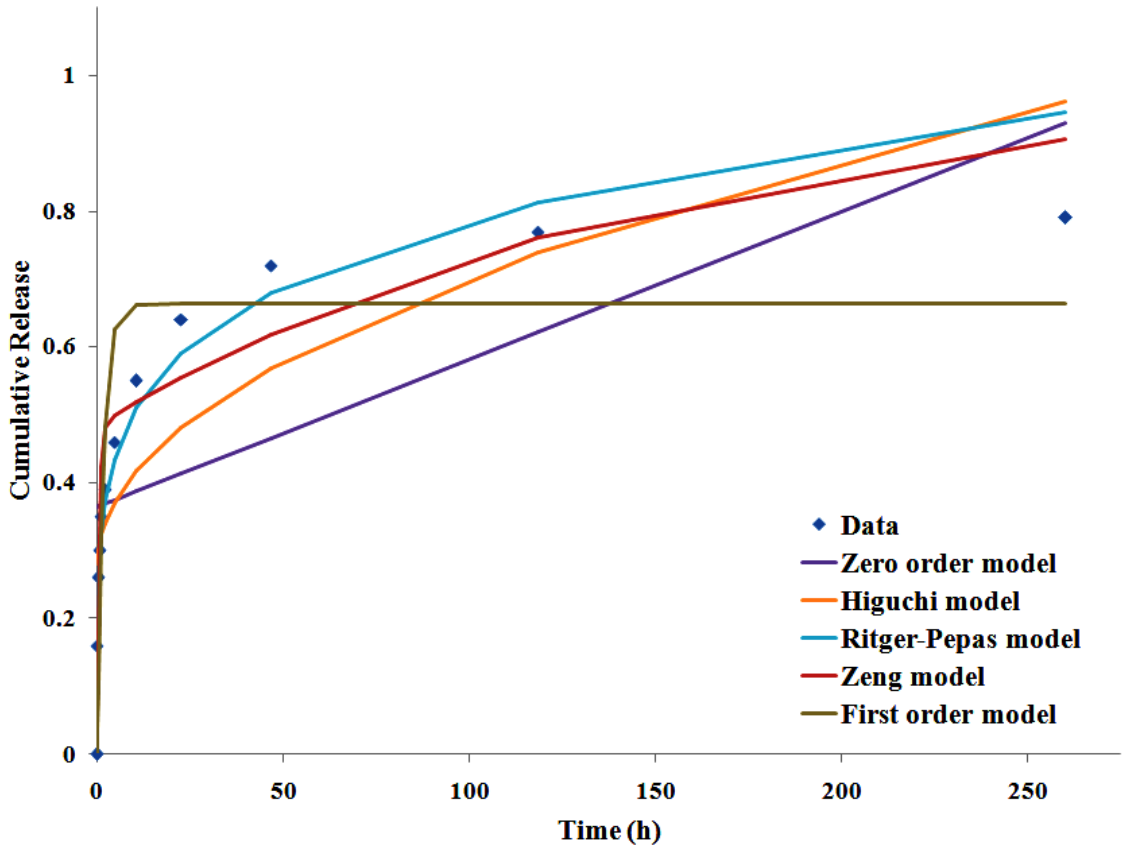

Figure I-3: Model fittings to the drug release data for PLA: 15% PCL/ 0.1 wt%/v MPs/ 5wt/v % TCH nanofibres.

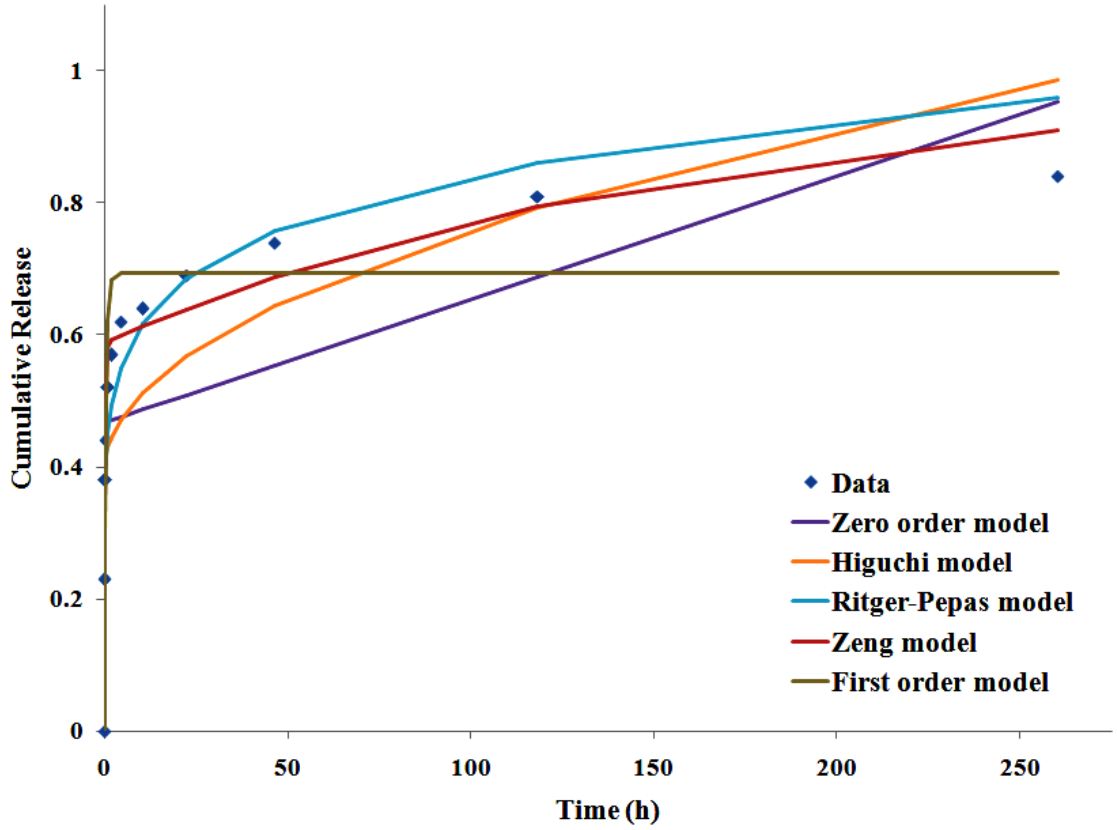

Figure I-4: Model fittings to the drug release data for PLA: 15% PCL/ 1% MPs/ 5 wt%/v TCH nanofibres.

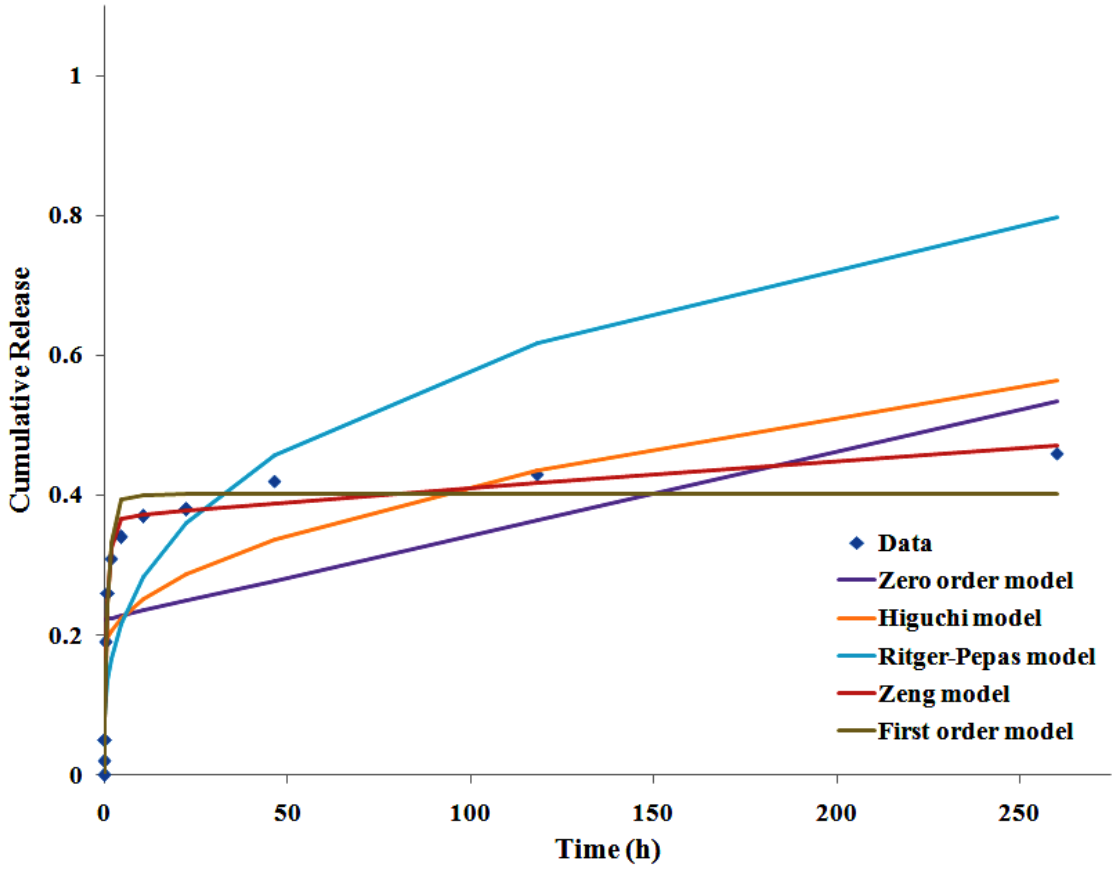

Figure I-5: Model fittings to drug release data for PLA: 15% PCL/ 1% HNT-ASP/ 5 wt%/v TCH nanofibres.

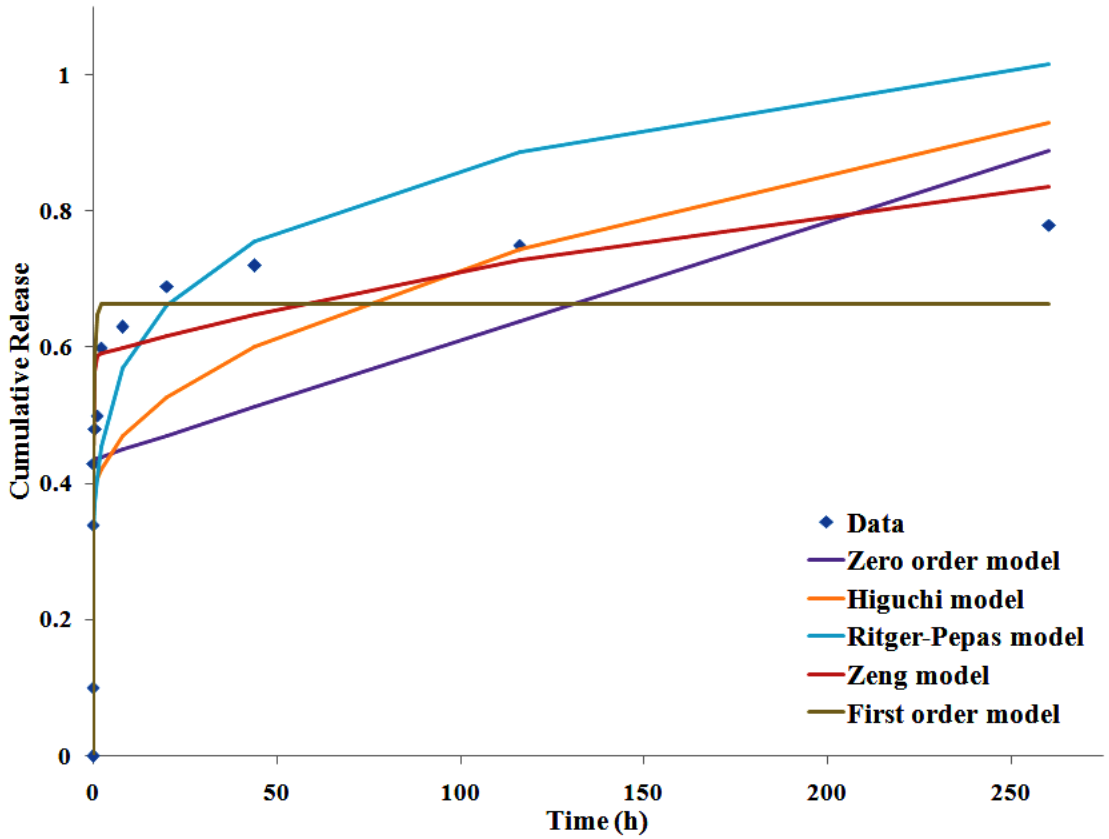

Figure I-6: Model fittings to drug release data for PLA: 9% PCL/ 1wt%/v TCH nanofibres.

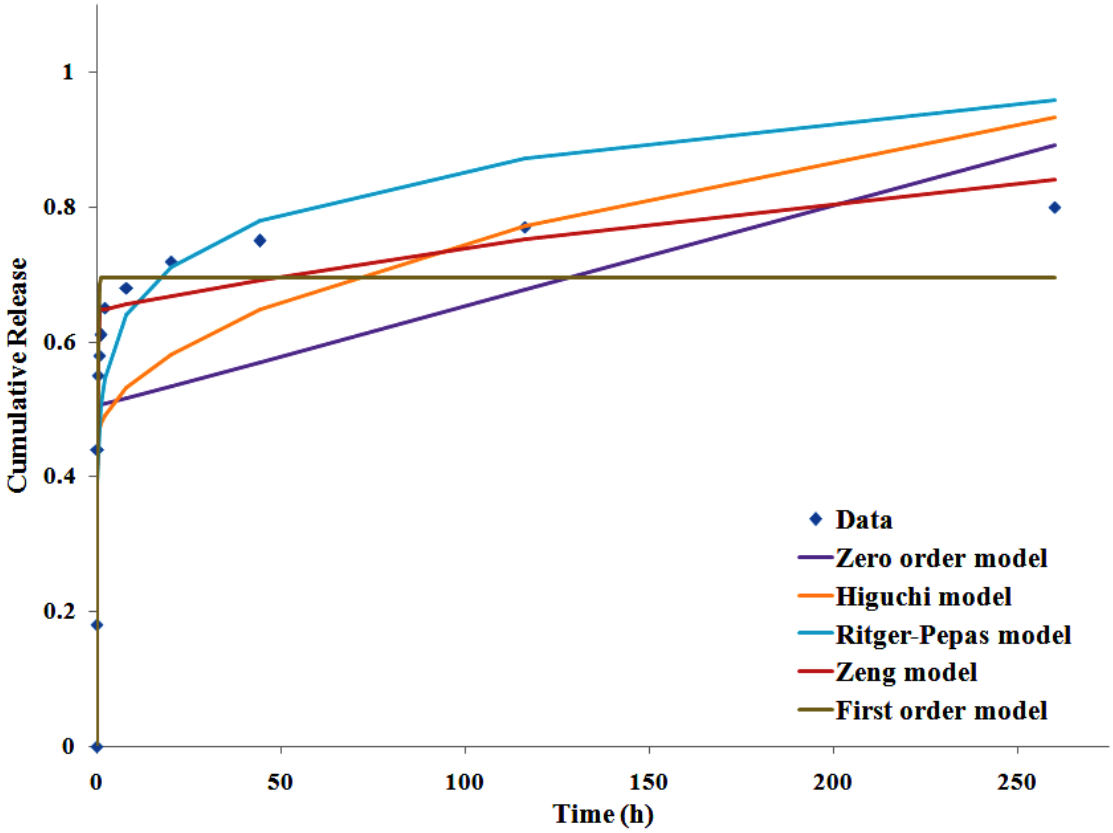

Figure I-7: Model fittings to drug release data for PLA: 9% PCL/ 5wt%v TCH nanofibres.